

3S'22

SYMPOSIUM ON SURFACE SCIENCE 2022

**St. Christoph am Arlberg, Austria
March 13 - 19, 2022**

CONTRIBUTIONS

EDITORS

Friedrich Aumayr, Ulrike Diebold and Christoph Lemell
TU Wien



**SCIENCE
RESEARCH & DEVELOPMENT
B2B SERVICES**

CEST
www.cest.at

20 years' experience with 45 researchers for outstanding research and delivering solutions to our customers.

- Electrochemistry and bioelectrochemistry
- Functional interfaces and surfaces
- Adhesive bonding and corrosion science and research
- Hydrogen degradation and technology
- Surface and interface analysis

Join us, visit us

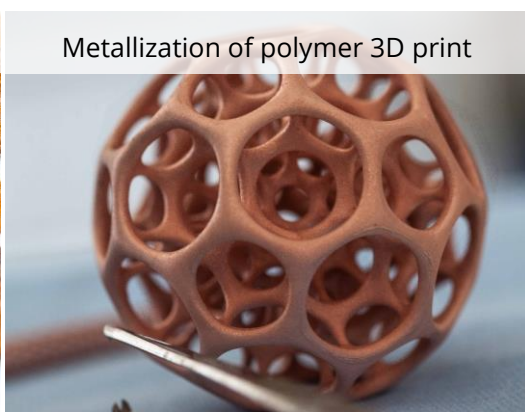
For job opportunities also master / PhD theses and more information visit our homepage: www.cest.at

CEST Centre for Electrochemistry and Surface Technology

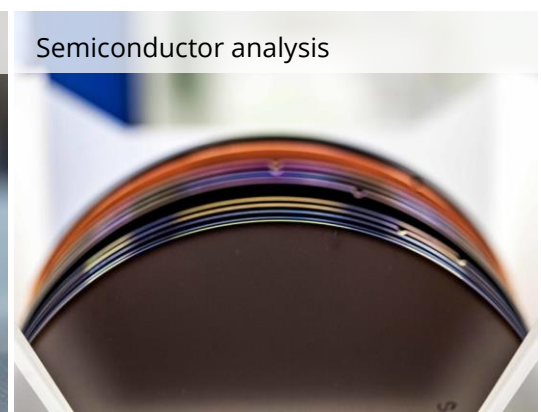
Viktor-Kaplan-Straße 2, 2700 Wr. Neustadt, Austria
Phone: +43 (0) 2622/22266, Mail: office@cest.at



Customized material testing



Metallization of polymer 3D print



Semiconductor analysis

HAXPES Lab

A Window to the Bulk

Scienta Omicron's HAXPES Lab brings hard X-ray photoelectron spectroscopy (HAXPES) capability directly to the local laboratory environment. This novel system probes bulk sample properties and accesses deep core level electrons via photoelectron spectroscopy (XPS) without the need for a synchrotron end station. Using world class technology and expert engineering, the HAXPES Lab sets the standard for laboratory based high energy photoelectron spectroscopy.

Photoelectron spectroscopy is a well-established tool for analyzing a wide range of chemical and material properties. Traditional photoelectron spectroscopy instruments employ low energy X-ray sources, limiting the kinetic energy of the photo-emitted electrons. Low kinetic energy electrons have short inelastic mean free paths (IMFP), confining analysis by traditional instrument to the top several nanometers of a material's surface. HAXPES, using higher kinetic energies, greatly extends the analysis depth.

While HAXPES measurements have been successfully deployed at synchrotrons, obtaining access to the required end stations is a significant challenge. The HAXPES Lab solves this problem and serves as a complete analytical tool by bringing cutting edge HAXPES directly to the end user's laboratory. Comparison (shown below) between different lab sources highlights the information depth advantage the

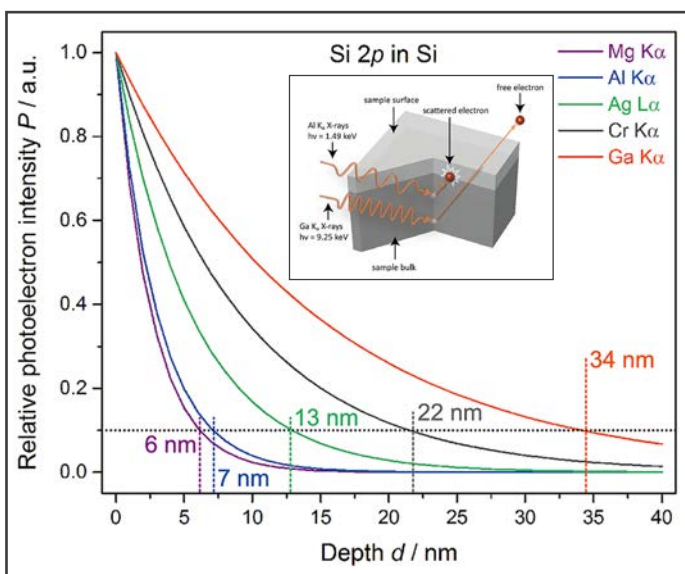


Figure 1. HAXPES using the Ga source offers 5x greater information depth, providing bulk sensitivity that is unavailable using conventional XPS.

High Flux Monochromated Ga K α Source

- Excillium Metal Jet Technology
- High flux $h\nu = 9.25$ keV for productive measurement times
- HAX9-5 Monochromator with <0.5 eV instrument resolution
- Easy crystal alignment
- Temperature stabilised crystals

4-axis Manipulator

- Software automation
- High precision

Monochromated Al K α Source

- Al K α @ $h\nu = 1.49$ keV
- Surface sensitive
- Probing with different excitation energies

Dual anode X-ray source (Mg/Al)

- Charge neutraliser

EW4000 Analyser

- High energy analyser
- Resolution $\Delta E < 100$ meV @ 10 keV
- 60 degrees acceptance angle

System Solution

- Fully integrated
- Ease-of-use & throughput
- Full safety interlocks

Ga source provides. Information depth is defined as the region in which 90 % of the total signal originates. Beyond this advantage, the monochromated Ga X-ray source provides higher flux than alternative hard X-ray lab sources.

HAXPES Lab:

- Practical laboratory based HAXPES measurements on synchrotron time scales
- Sensitive to surface and bulk chemical and electrical properties
- Proven state-of-the-art technology ensures staying at the forefront of materials research
- Increased information depth capabilities provide unparalleled opportunities to explore new physics and produce high impact science

How to contact us:

www.ScientaOmicron.com
info@ScientaOmicron.com

For more information on HAXPES Lab, please visit: <https://scientaomicron.com/en/products-solutions/electron-spectroscopy/HAXPES-Lab>



3S'22

SYMPOSIUM ON SURFACE SCIENCE 2022

**St. Christoph am Arlberg, Austria
March 13 - 19, 2022**

CONTRIBUTIONS

EDITORS

Friedrich Aumayr, Ulrike Diebold and Christoph Lemell
TU Wien

This symposium is organized by

Friedrich Aumayr, Ulrike Diebold & Markus Valtiner

TU Wien, Institute of Applied Physics (IAP)

Wiedner Hauptstr. 8-10/E134

1040 Vienna, Austria

<http://www.iap.tuwien.ac.at/www/3s22/>

International Scientific Committee

A. Arnau, Donostia, ES

F. Aumayr, Vienna, AT

H. Daimon, Nara, JP

U. Diebold, Vienna, AT

C. Draxl, Berlin, DE

P. M. Echenique, Donostia, ES

R. Fasel, Dübendorf, CH

T. Koshikawa, Osaka, JP

E. Lundgren, Lund, SE

D. Menzel, Berlin/Munich, DE

M. Messing, Lund, SE

K. Morgenstern, Bochum, DE

P. Müller, Marseille, FR

F. Netzer, Graz, AT

K. Reuter, Munich, DE

M. Rocca, Genova, IT

W. D. Schneider, Lausanne/Berlin, CH/DE

G. Thornton, London, GB

Organizing Committee

F. Aumayr (IAP, TU Wien)

U. Diebold (IAP, TU Wien)

C. Lemell (ITP, TU Wien)

M. Valtiner (IAP, TU Wien)

Venue

Ski Austria Academy, St. Christoph 10,

6580 St. Anton a. Arlberg, Austria

www.skiakademie.at

Medieninhaber: F. Aumayr, U. Diebold, M. Valtiner, Institut für Angewandte Physik,

Technische Universität Wien, Adresse: Wiedner Hauptstr. 8-10/E134, A-1040 Wien

Druck: R. & W. Smutny OEG, A-1110 Wien

PREFACE

We welcome all participants and accompanying persons to the 34th Symposium on Surface Science (3S). The 3S was founded in 1983 as a winter school by members of the Institute of Applied Physics of the Vienna University of Technology (TU Wien). The conference seeks to promote the growth of scientific knowledge and its effective exchange among scientists in the field of surface physics and chemistry and related areas, including applied topics. Its format is similar to that of Gordon Conferences, with ample time for discussions and joint outdoor activities. Attendance is kept below 100 to ensure active communication among all participants.

Originally, the 3S was held exclusively in Austria and took place every other year. It became an annual event in 1990, and the site started to alternate between locations in France and Austria. In 1998 the 3S evolved into a truly global conference, with venues in the US, Canada, Bulgaria, Japan, Switzerland, Spain, France and Sweden, always returning to Austria in alternate years.

Unfortunately, last year's 3S (2021) had to be cancelled due to the Covid-19 pandemic. Holding the 3S as an online meeting was obviously out of the question. Therefore, we are even more pleased this year that the 3S can once again be held as an in-person event. Of course, the risk for us as organizers but also for all participants is higher than in pre-pandemic times. However, we have taken all possible protective measures to keep the risk to our participants as low as possible. We therefore ask for your understanding for, and cooperation with, the measures we have taken (participation only for fully vaccinated attendees, mandatory wearing of masks in the lecture hall, etc.).

We hope that, after two years of the pandemic, participants will again experience a lively and successful in-person meeting in this beautiful mountain region of Austria.

Fritz Aumayr

Ulrike Diebold

Markus Valtiner

Dates and locations of 3S conferences:

1983	(31.01.-04.02.)	Obertraun	AT
1985	(27.01.-02.02.)	Obertraun	AT
1988	(22.05.-28.05.)	Kaprun	AT
1990	(11.03.-17.03.)	La Plagne	FR
1991	(10.02.-16.02.)	Obertraun	AT
1992	(15.03.-21.03.)	La Plagne	FR
1993	(09.05.-15.05.)	Kaprun	AT
1994	(06.03.-12.03.)	Les Arcs	FR
1995	(23.04.-29.04.)	Kaprun	AT
1997	(26.01.-31.01.)	Aussois	FR
1998	(29.03.-04.04.)	Park City	US
1999	(21.02.-27.02)	Pamporova	BG
2000	(15.02.-18.02.)	Kananaskis	CA
2001	(07.01.-13.01.)	Furano	JP
2002	(03.03.-09.03.)	St.Christoph/Arlberg	AT
2003	(30.03.-05.04.)	La Plagne	FR
2004	(29.02.-06.03.)	St.Christoph/Arlberg	AT
2005	(13.03.-19.03.)	Les Arcs 1800	FR
2006	(05.03.-11.03.)	St. Christoph/Arlberg	AT
2007	(11.03.-17.03.)	Les Arcs 2000	FR
2008	(02.03.-08.03.)	St. Christoph/Arlberg	AT
2009	(08.03.-14.03.)	St. Moritz	CH
2010	(07.03.-13.03.)	St. Christoph/Arlberg	AT
2011	(06.03.-12.03.)	Baqueira Beret	ES
2012	(11.03.-17.03.)	St. Christoph/Arlberg	AT
2013	(03.03.-09.03.)	Åre	SE
2014	(09.03.-15.03.)	St. Christoph/Arlberg	AT
2015	(22.03.-28.03.)	Les Arcs 1800	FR
2016	(21.02.-27.02.)	St. Christoph/Arlberg	AT
2017	(05.03.-10.03.)	St. Moritz	CH
2018	(25.02.-03.03.)	St. Christoph/Arlberg	AT
2019	(10.03.-16.03.)	Baqueira Beret	ES
2020	(01.03.-07.03.)	St. Christoph/Arlberg	AT
2021	Cancelled due to Covid-19 pandemic		
2022	(13.03.-19.03.)	St. Christoph/Arlberg	AT

Peter Varga 3S-Poster Prize

In memory of one of the founding fathers of the 3S workshop series, Peter Varga (1946 – 2018), the *Peter Varga 3S-Poster Prize* is awarded every year starting with 3S*19.

List of prize winners

- 3S*19 Ales Cahlik (CAS, Praha, Czech Republic)
 3S*20 Anna Niggas (TU Wien, Vienna, Austria)

3S'22

SYMPOSIUM ON SURFACE SCIENCE 2022

**St. Christoph am Arlberg, Austria
March 13 – March 18, 2022**

Time Schedule

Sunday, 13 March 2022

16:00 – 18:30 **Registration**

20:00 – 20:20 **Opening**

20:25 – 20:45 *Chair: F. Aumayr*

A. Stierle

Single Alloy Nanoparticle X-Ray Imaging during a Catalytic Reaction

20:45 – 21:05

F. J. Giessibl

Very Weak Bonds to Artificial Atoms Formed by Quantum Corrals

21:05 – 21:25

A. Götzhäuser

Imaging of SARS-CoV-2 infected Vero E6 Cells by Helium Ion Microscopy

Monday, 14 March 2022

- 08:00 – 08:20 *Chair: T. Sikola*
M. Sterrer
Charging and metalation of porphyrins on ultrathin oxide films
- 08:20 – 08:40 **S. Maier**
Tuning of binding-motifs and chirality in cyano-porphyrin self-assemblies: from metal to bulk insulator on surfaces
- 16:40 – 17:00 *Chair: W.-D. Schneider*
K. Morgenstern
On-surface synthesis of a carbanion by electrophilic activation of water at a carbene-metal interface
- 17:00 – 17:20 **J. V. Barth**
Navigate flying molecular elephants safely to the ground: mass-selective soft landing up to the mega-Dalton range by electrospray controlled ion-beam deposition and its use for molecular engineering at surfaces
- 17:20 – 17:40 **J. Doležal**
Real Space Visualization of Entangled Excitonic States in Charged Molecular Assemblies
- 17:40 – 18:00 **G. B. Vonbun-Feldbauer**
Atomistic Modelling of Surfaces and Interfaces for Magnetite-based Nanocomposites
- 18:00 – 18:20 **K.-H. Ernst**
Planarization of non-planar aromatic hydrocarbons: Dehydrogenation versus hydrogenation
- 19:30 – 19:50 *Chair: A. Enders*
S. Auras
CO₂ adsorption and dissociation on kinked Cu surfaces at (near-) ambient pressure
- 19:50 – 20:10 **P. Bábor**
Real Time Monitoring of Catalytic Oxidation of CO to CO₂ Over Platinum Surfaces
- 20:10 – 20:30 **H. Edström**
Reaction driven ordering of the surface of a PtRh alloy model catalyst
- 20:30 – 20:50 **D. Borodin**
Recombination of hydrogen atoms at metal surfaces – A step towards predictive surface chemistry

Tuesday, 15 March 2022

- 08:00 – 08:20 *Chair: J. Berger*
E. Lundgren
2D surface optical reflectance for surface studies in harsh environments
- 08:20 – 08:40 **P. Jelinek**
Real-space imaging of anisotropic atomic charges by means of Kelvin probe force microscopy
- 16:40 – 17:00 *Chair: U. Diebold*
T. Berghaus
A New Cryogen-Free UHV Scanning Probe Microscope with 5K Base Temperature
- 17:00 – 17:20 **P. Amann**
Laboratory based hard X-ray photoemission spectroscopy
- 17:20 – 17:40 **T. Stempel**
All-round improved: Innovations for photoexcitation, electron detection and sample handling in high-performance ARPES systems
- 17:40 – 18:00 **M. Rebarz**
Versatile Experimental Platform for Broadband Femtosecond Ellipsometry at ELI Beamlines Facility
- 18:00 – 18:20 **M. Valtiner**
Visualization of Ion-Surface Binding, binding energy quantification, and charge regulation in slit geometries
- 19:30 – 19:50 *Chair: G. Franceschi*
H. Dil
Magnetic switching driven by stochastic resonance in multiferroic (Ge,Mn)Te
- 19:50 – 20:10 **M. A. Schneider**
From tellurized surfaces towards telluride films: Te on Cu(111) and Pt(111)
- 20:10 – 20:30 **G. Renaud**
Decoupling of TaS₂ single-layer from its Au(111) substrate by alkali intercalation
- 20:30 – 20:50 **H. Biber**
Modeling the sputtering processes on the surface of Mercury in the laboratory

Wednesday, 16 March 2022

- 08:00 – 08:20 *Chair: J. Pavelec*
K. Reuter
First-Principles based Modelling of Electrocatalysis Beyond the Potential of Zero Charge
- 08:20 – 08:40 **J. Kunze-Liebhäuser**
Cu(111) reconstruction and oxidation in oxygen free alkaline media imaged with electrochemical STM
- 16:40 – 17:00 *Chair: J. Balajka*
J. Libuda
Catalysis at liquid interfaces: New SCILLs in ultrahigh vacuum and at the electrified interface
- 17:00 – 17:20 **V. Vonk**
Electrochemical and Thermal Oxidation of Pt(111)
- 17:25 – 18:20 *Chair: J. Kunze-Liebhäuser*
Poster Introduction
- J. Balajka**
Structure of Anatase TiO₂(001) in Aqueous Environment
- J. Berger**
On-surface and tip induced synthesis of carbon-based macrocycle polyradicaloids
- J. Brötzner**
An optimised Quartz Crystal Microbalance setup to investigate the sputtering behaviour of bulk targets
- C. Cupak**
Sputtering of highly corrugated surfaces
- F.-F. Delatowski**
Probing photo-induced dynamics of organic molecules on surfaces by time resolved spectroscopic ellipsometry
- U. Diebold**
Water and Hydroxyls at In₂O₃(111)
- S. Espinoza**
Time-resolved spectroscopic ellipsometry applied to ellagic acid thin films
- J. Fingerhut**
Investigation of the interaction of formic acid with flat and stepped palladium surfaces
- G. Franceschi**
Nc-AFM and XPS studies of UHV-cleaved and hydrated mica
- L. Hammer**
No telluride formation on Ir(111), Ir(100), and Au(100) - just

repelling adatoms

J. Hütner

Surface investigations of zirconia films on Rh(111)

A. M. Imre

Introducing ViPErLEED: The Vienna Package for TensErLEED

Z. Jakub

Stable metal-organic networks on a weakly-interacting substrate: Fe-, Ni-, and Mn-TCNQ on graphene

A. Jelínková

Our Unity in Their Own Code

L. Kalchgruber

Characterisation and comparison of model and industrial steel samples

L. Lezuo

Design and Testing of a Home-Built UHV Suitcase

P. Müller

Surface electromigration of 2D confined islands

M. Olgıati

Combined spectro-electrochemical methods to investigate electrochemical corrosion in real-time

J. Pavelec

Design of apparatus for surface tension measurement of pure water in vacuum

W.-D. Schneider

Mesoscopic structures in ultrathin silica films

M. Schwarzer

Towards Elementary Rate Constants of Water Formation from the Reaction of Hydrogen and Oxygen on Palladium.

T. Šikola

Single-layer graphene on epitaxial FeRh thin films

V. M. Silkin

Image-potential states in graphene

S. Vazquez-Miranda

Charge Accumulation and Reactions Dynamics on Copper Electrodes Surfaces study by Electrochemical and Optical Polarization Techniques

R. A. Wilhelm

Ion charge exchange spectroscopy with 2D materials

M. Wolf

Multiple-pump system for combinatorial thin-film deposition by ultrasonic spray pyrolysis

Thursday, 17 March 2022

- 08:00 – 08:20 *Chair: P. Müller*
U. Starke
Epitaxial Graphene Nanoribbons: One-dimensional confinement and pn-junction array
- 08:20 – 08:40 **H. Brune**
Transfer of Graphene under Ultra-High-Vacuum
- 16:40 – 17:00 *Chair: R. A. Wilhelm*
D. Sánchez-Portal
Boron Substitution in Graphene Nanoribbons: Onedimensional Spin Chains with Tuneable Interactions
- 17:00 – 17:20 **J. Ibañez-Azpiroz**
Dimensionality effects in the nonlinear optical properties of TMD nanotubes
- 17:20 – 17:40 **F. Mittendorfer**
Growth of supported boron-based monolayers: h-BN and borophene on Pt(110)
- 17:40 – 18:00 **A. Niggas**
Energy distribution of electrons emitted from atomically thin materials due to highly charged ion impact
- 18:00 – 18:20 **M. Ostermann**
Reduced graphene oxide: From industrialisable production to de-icing application
- 19:30 – 19:50 *Chair: V.M. Silkin*
U. Ramach
A novel membrane-on-a-chip setup demonstrates in-plane conductivity of Q-lipid membranes
- 19:50 – 20:10 **P. Bilotto**
Competition at crowded interfaces
- 20:10 – 20:30 **R. Meißner**
Getting control over magnesium corrosion
- 20:30 – 20:50 **H. E. Hoster**
Order and disorder in Li-ion batteries: a Surface-Science perspective

Friday, 18 March 2022

- 08:00 – 08:20 *Chair: Z. Jakub*
A. Arnau
Nature of Interfacial Dzyaloshinskii-Moriya Interactions in Graphene/Co/Pt(111) Multilayer Heterostructures
- 08:20 – 08:40 **Z. Novotny**
An intercalated Cu_{2-x}O thin film confined underneath hexagonal boron nitride on top of Cu(111)
- 16:30 – 16:50 *Chair: L. Hammer*
F. P. Netzer
How stable are 2-D oxide lattices against doping?
- 16:50 – 17:10 **L. Haager**
Comparison of single Rh and Ir adatoms on $\alpha\text{-Fe}_2\text{O}_3(1\bar{1}02)$ – stabilization with and without water
- 17:10 – 17:30 **P. Kocán**
Polaronic Diffusion in Doped Hematite – experiment vs. Kinetic Monte Carlo simulations
- 17:30 – 17:50 **M. Riva**
The link between surface diffusion and surface reconstructions on oxides
- 17:50 – 18:10 **S. Goetz**
Stability investigations of sputtered molybdenum oxide thin films in the presence of water
- 18:30 – 18:50 *Chair: C. Cupak*
R. Bliem
Tuning the surface properties of thin films via disorder
- 18:50 – 19:10 **M. Rocca**
Prominence of Terahertz Acoustic Surface Plasmon excitation in Gas-Surface interaction with Metals
- 19:10 – 19:40 **Giant Slalom Race Award Ceremony**
- 20:00 **Conference Dinner**

CONTRIBUTIONS

Content

Single Alloy Nanoparticle X-Ray Imaging during a Catalytic Reaction	27
<i>Y.Y. Kim, T.F. Keller, T.J. Goncalves, M. Abuin, H. Runge, L. Gelisio, J.Carnis, V. Vonk, P.N. Plessow, I.A. Vartanyants, A. Stierle</i>	
Very Weak Bonds to Artificial Atoms Formed by Quantum Corrals	29
<i>F. Stilp, J. Berwanger, N. Mundigl, A. Bereczuk, K. Richter, F.J. Giessibl</i>	
Imaging of SARS-CoV-2 infected Vero E6 Cells by Helium Ion Microscopy	31
<i>N. Frese, P. Schmerer, M. Wortmann, M. Schürmann, M. König, M. Westphal, F. Weber, H. Sudhoff, A. Götzhäuser</i>	
Charging and metalation of porphyrins on ultrathin oxide films	35
<i>M. Sterrer, F. Presel, F. Schwarz, T. Bone, G. Koller, M. Ramsey, C. Kern, P.Puschnig</i>	
Tuning of binding-motifs and chirality in cyano-porphyrin self-assemblies: From metal to bulk insulator on surfaces	37
<i>M. Ammon, M. Devarajulu, Y. Liu, C. Steiner, T. Sander, M. Gurrath, D.Lungerich, N. Jux, B. Meyer, S. Maier</i>	
On-surface synthesis of a carbanion by electrophilic activation of water at a carbene-metal interface	39
<i>Y.-J. Cao, J. Mieres-Perez, J.F. Rowen, E. Sanchez-Garcia, W. Sander, K.Morgenstern</i>	
Navigate flying molecular elephants safely to the ground: mass-selective soft landing up to the mega-Dalton range by electrospray controlled ion-beam deposition and its use for molecular engineering at surfaces	41
<i>A. Walz, K. Stoiber, W. Ran, P. Knecht, H. Xu, A.C. Papageorgiou, A. Huettig, D. Cortizo-Lacalle, J.P. Mora-Fuentes, A. Mateo-Alonso, J. Reichert, H.Schlichting, J.V. Barth</i>	
Real Space Visualization of Entangled Excitonic States in Charged Molecular Assemblies	43
<i>J. Doležal, S. Canola, P. Hapala, R.C. de C. Ferreira, P. Merino, M. Švec</i>	
Atomistic Modelling of Surfaces and Interfaces for Magnetite-based Nanocomposites	45
<i>K. Sellschopp, W. Mayr-Schmölzer, S. Banerjee, S. Müller, G.B. Vonbun-Feldbauer</i>	

Planarization of non-planar aromatic hydrocarbons: Dehydrogenation versus hydrogenation	47
<i>B. Irziqat, A. Cebat, M. Baljuzović, K. Martin, M. Parschau, N. Avarvari, K.-H. Ernst</i>	
CO₂ adsorption and dissociation on kinked Cu surfaces at (near-)ambient pressure	49
<i>S.V. Auras, F. Garcia-Martinez, F. Schiller, J.E. Ortega</i>	
Real Time Monitoring of Catalytic Oxidation of CO to CO₂ Over Platinum Surfaces	51
<i>M. Janák, A. Jaroš, D. Hruza, M. Kolíbal, T. Šíkola, P. Bátor</i>	
Reaction driven ordering of the surface of a PtRh alloy model catalyst	53
<i>H. Edström, U. Hejral, S. Albertin, K. von Allmen, B. Hagman, E. Lundgren, A.Schaefer, A. Stierle, V. Vonk, L. Jacobse, X. Deng, C. Seitz, S. Geile, U. Lienert, T. Müller, Z. Hegedüs, S. Gutschmidt, J. Gustafson</i>	
Recombination of hydrogen atoms at metal surfaces – A step towards predictive surface chemistry	55
<i>D. Borodin, N. Hertl, F. Nitz, M. Schwarzer, J. Fingerhut, T.N. Kitsopoulos, A.M. Wodtke</i>	
2D surface optical reflectance for surface studies in harsh environments	61
<i>E. Lundgren, A. Larsson, G. Abbondanza, L. Rämisch, S. Pfaff, S. Gericke, J.Zetterberg</i>	
Real-space imaging of anisotropic atomic charges by means of Kelvin probe force microscopy	63
<i>B. Mallada, A. Gallardo, B. de la Torre, P. Jelinek</i>	
A New Cryogen-Free UHV Scanning Probe Microscope with 5K Base Temperature	65
<i>T. Berghaus, J. Kasai, T. Koyama, M. Yokota, K. Iwaya</i>	
Laboratory based hard X-ray photoemission spectroscopy	67
<i>P. Amann, M. Schmid, S. Eriksson, P. Palmgren, T. Wiell, M. Lundwall</i>	
All-round improved: Innovations for photoexcitation, electron detection and sample handling in high-performance ARPES systems	69
<i>T. Stempel, S. Böttcher, S. Mähl, M. Meyer, O. Schaff, T. Kampen</i>	
Versatile Experimental Platform for Broadband Femtosecond Ellipsometry at ELI Beamlines Facility	71
<i>M. Rebarz, S. Espinoza, S. Richter, O. Herrfurth, M. Zahradnik, J. Andreasson</i>	

- Visualization of Ion-Surface Binding, binding energy quantification, and charge regulation in slit geometries** 73
J. Lee, J. Dziadkowiec, V. Wieser, A.M. Imre, H.-W. Cheng, P.-L. Bilotto, M. Valtiner
- Magnetic switching driven by stochastic resonance in multiferroic (Ge,Mn)Te** 75
J. Krempasky, J. Minar, M. Gmitra, G. Springholz, H. Dil
- From tellurized surfaces towards telluride films: Te on Cu(111) and Pt(111)** 77
M.A. Schneider, T. Kießlinger, A. Schewski, A. Raabgrund, L. Hammer
- Decoupling of TaS₂ single-layer from its Au(111) substrate by alkali intercalation** 79
X. Weng, P. David, V. Guisset, O. Geaymond, L. Martinelli, J. Coraux, G. Renaud
- Modeling the sputtering processes on the surface of Mercury in the laboratory** 81
H. Biber, P.S. Szabo, N. Jäggi, C. Cupak, J. Brötzner, A. Nening, A. Galli, P. Wurz, F. Aumayr
- First-Principles based Modelling of Electrocatalysis Beyond the Potential of Zero Charge** 85
K. Reuter
- Cu(111) reconstruction and oxidation in oxygen free alkaline media imaged with electrochemical STM** 87
A. Auer, T. Moser, J. Kunze-Liebhäuser
- Catalysis at liquid interfaces: New SCILLs in ultrahigh vacuum and at the electrified interface** 89
J. Libuda
- Electrochemical and Thermal Oxidation of Pt(111)** 91
S. Volkov, L. Jacobse, V. Vonk, T.F. Keller, J. Fleig, A. Stierle
- Structure of Anatase TiO₂(001) in Aqueous Environment** 97
J. Balajka, G. Franceschi, M. Riva, J. Pavelec, M. Schmid, U. Diebold
- On-surface and tip induced synthesis of carbon-based macrocycle polyradicaloids** 99
J. Berger, A. P. Solé, A.G. Sanchez, D. Mildner, A. Matej, D. Soler, F. Romero, J.M. Carvajal, A. Campana, P. Jelínek

An optimised Quartz Crystal Microbalance setup to investigate the sputtering behaviour of bulk targets	101
<i>J. Brötzner, H. Biber, P.S. Szabo, N. Jäggi, C. Cupak, A. Nenning, B. Cserveny, A. Galli, P. Wurz, F. Aumayr</i>	
Sputtering of highly corrugated surfaces	103
<i>C. Cupak, M. Fellinger, H. Biber, A. Redl, A. Lopez-Cazalilla, R. Gonzalez-Arrabal, F. Aumayr</i>	
Probing photo-induced dynamics of organic molecules on surfaces by time-resolved spectroscopic ellipsometry	105
<i>F.-F. Delatowski, K. Khakurel, J. Rappich, S. Espinoza, M. Rebarz, M.Zahradnik, J. Andreasson</i>	
Water and Hydroxyls at In₂O₃(111)	107
<i>U. Diebold, M. Schmid, B. Meyer, M. Wagner</i>	
Time-resolved spectroscopic ellipsometry applied to ellagic acid thin films	109
<i>S. Espinoza, M. Zahradník, M. Rebarz, J. Andreasson, E. Bittrich</i>	
Investigation of the interaction of formic acid with flat and stepped palladium surfaces	111
<i>J. Fingerhut, L. Lecroart, D. Borodin, M. Schwarzer, A. Kandratsenka, T.N.Kitsopoulos, A.M. Wodtke</i>	
Nc-AFM and XPS studies of UHV-cleaved and hydrated mica	113
<i>G. Franceschi, J. Balajka, S. Brandstetter, I. Sokolović, J. Pavelec, M. Schmid, M. Setvin, U. Diebold</i>	
No telluride formation on Ir(111), Ir(100), and Au(100) - just repelling adatoms	115
<i>L. Hammer, T. Kießlinger, A. Schewski, A. Raabgrund, M.A. Schneider</i>	
Surface investigations of zirconia films on Rh(111)	117
<i>J. Hütner, J. Balajka, P. Lackner, J. Pavelec, M. Schmid, U. Diebold</i>	
Introducing ViPerLEED: The Vienna Package for TensErLEED	119
<i>A.M. Imre, F. Kraushofer, F. Doerr, M. Schmid, T. Kießlinger, U. Diebold, L.Hammer, M. Riva</i>	
Stable metal-organic networks on a weakly-interacting substrate: Fe-, Ni-, and Mn-TCNQ on graphene	121
<i>Z. Jakub, A. Kurowská, O. Herich, L. Černá, P. Procházka, L. Kormoš, A.Shahsavari, J. Čechal</i>	

Our Unity in Their Own Code	123
<i>A. Jelínková</i>	
Characterisation and comparison of model and industrial steel samples	125
<i>L. Kalchgruber, M. Hahn, J. Pavelec, M. Valtiner</i>	
Design and Testing of a Home-Built UHV Suitcase	127
<i>L. Lezuo, L. Dockalová, J. Pavelec, G. Parkinson, U. Diebold</i>	
Surface electromigration of 2D confined islands	129
<i>S. Curiotto, F. Cheynis, P. Müller, F. Leroy</i>	
Combined spectro-electrochemical methods to investigate electrochemical corrosion in real-time	131
<i>M. Olgiati, M. Valtiner</i>	
Design of apparatus for surface tension measurement of pure water in vacuum	133
<i>J. Pavelec, P. Ryan, J. Balajka, U. Diebold</i>	
Mesoscopic structures in ultrathin silica films	135
<i>K.M. Burson, H.J. Yang, D.S. Wall, T. Marsh, Z. Yang, D. Kuhness, M. Brinker, L. Gura, M. Heyde, W.-D. Schneider, H.-J. Freund</i>	
Towards Elementary Rate Constants of Water Formation from the Reaction of Hydrogen and Oxygen on Palladium	137
<i>M. Schwarzer, N. Hertl, D. Borodin, J. Fingerhut, T.N. Kitsopoulos, A.M. Wodtke</i>	
Single-layer graphene on epitaxial FeRh thin films	139
<i>V. Uhlíř, F. Pressacco, J.A. Arregi, P. Procházka, S. Průša, M. Potoček, T. Šikola, J. Čechal, A. Bendounan, F. Sirotti</i>	
Image-potential states in graphene	141
<i>V. M. Silkin, E. Kogan, G. Gumbs</i>	
Charge Accumulation and Reactions Dynamics on Copper Electrodes Surfaces study by Electrochemical and Optical Polarization Techniques	143
<i>S. Vazquez-Miranda, R.E. Balderas Navarro, S. Espinoza, J. Andreasson, K.Hingerl, C. Cobet</i>	
Ion charge exchange spectroscopy with 2D materials	145
<i>R.A. Wilhelm, A. Niggas, M. Werl, F. Aumayr</i>	
Multiple-pump system for combinatorial thin-film deposition by ultrasonic spray pyrolysis	147
<i>M. Wolf, G.K.H. Madsen, T. Dimopoulos</i>	

Epitaxial Graphene Nanoribbons: One-dimensional confinement and pn-junction array	151
<i>U. Starke, H. Karakachian, P. Rosenzweig, B. Matta, T.T.N. Nguyen, J. Aprojanz, A.A. Zakharov, R. Yakimova, T. Balasubramanian, Z. Mamiyev, S.R.Power, C. Tegenkamp, C.M. Polley</i>	
Transfer of Graphene under Ultra-High-Vacuum	153
<i>D. Merk, S. Rusponi, H. Brune</i>	
Boron Substitution in Graphene Nanoribbons: Onedimensional Spin Chains with Tuneable Interactions	155
<i>N. Friedrich, P. Brandimarte, J. Li, S. Saito, S. Yamaguchi, I. Pozo, D. Peña, T.Frederiksen, A. García-Lekue, J.I. Pascual, D. Sánchez-Portal</i>	
Dimensionality effects in the nonlinear optical properties of TMD nanotubes	157
<i>J. Krishna, J. Ibañez-Azpiroz</i>	
Growth of supported boron-based monolayers: h-BN and borophene on Pt(110)	159
<i>F. Mittendorfer, M. Thaler, D. Steiner, A. Menzel, E. Bertel</i>	
Energy distribution of electrons emitted from atomically thin materials due to highly charged ion impact	161
<i>A. Niggas, D. Weichselbaum, F. Aumayr, R.A. Wilhelm</i>	
Reduced graphene oxide: From industrialisable production to de-icing application	163
<i>M. Ostermann, P. Bilotto, P. Lieberzeit, J. Schodl</i>	
A novel membrane-on-a-chip setup demonstrates in-plane conductivity of Q-lipid membranes	165
<i>U. Ramach, J. Andersson, M. Valtiner</i>	
Competition at crowded interfaces	167
<i>P. Bilotto, A.M. Imre, D. Dworschak, L.L.E. Mears, M. Valtiner</i>	
Getting control over magnesium corrosion	169
<i>T. Würger, C. Feiler, R. Meißner</i>	
Order and disorder in Li-ion batteries: a Surface-Science perspective	171
<i>H.E. Hoster, D. Kramer, E.P.M. Leiva, M.P. Mercer</i>	
Nature of Interfacial Dzyaloshinskii-Moriya Interactions in Graphene/Co/Pt(111) Multilayer Heterostructures	177
<i>M. Blanco-Rey, G. Bihlmayer, A. Arnau, J.I. Cerdá</i>	

An intercalated Cu_{2-x}O thin film confined underneath hexagonal boron nitride on top of Cu(111)	179
<i>Z. Novotny, J.T. Diulus, N. Comini, J. Beckord, M. Muntwiler, M. Hengsberger, J. Osterwalder</i>	
How stable are 2-D oxide lattices against doping?	181
<i>M. Mohammadi, F.R. Negreiros, S. Surnev, F.P. Netzer</i>	
Comparison of single Rh and Ir adatoms on α-Fe₂O₃(1$\bar{1}$02) – stabilization with and without water	183
<i>L. Haager, F. Kraushofer, M. Eder, A. Rafsanjani-Abbasi, G. Franceschi, M.Riva, G. Franceschi, M. Schmid, U. Diebold, G.S. Parkinson</i>	
Polaronic Diffusion in Doped Hematite – experiment vs. Kinetic Monte Carlo simulations	185
<i>P. Kocán, V. Gabriel, J. Redondo, D. Wrana, G. Franceschi, E. Rheinfrank, I.Sokolovic, G.S. Parkinson, U. Diebold, M. Riva, M. Setvín</i>	
The link between surface diffusion and surface reconstructions on oxides	187
<i>G. Franceschi, M. Schmid, U. Diebold, M. Riva</i>	
Stability investigations of sputtered molybdenum oxide thin films in the presence of water	189
<i>S. Goetz, R.A. Wibowo, E. Franzke, C. Linke, J. Winkler, M. Valtiner, T.Dimopoulos</i>	
Tuning the surface properties of thin films via disorder	191
<i>A. Troglia, S. van Vliet, R. Bliem</i>	
Prominence of Terahertz Acoustic Surface Plasmon excitation in Gas-Surface interaction with Metals	193
<i>G. Bracco, L. Vattuone, M. Smerieri, G. Carraro, L. Savio, G. Paolini, G.Benedek, P.M. Echenique, M. Rocca</i>	
Obituary: Stefan Müller	197
Post-deadline posters:	
Exploring Percolation in Nanocluster Assemblies for Neuromorphic Computing	201
<i>M. Baljzović, Y. Niu, J. McCormack, T. Slater, R.E. Palmer, R.J. Coble</i>	

USM1200-XHT low He loss LT-SPM

USM1400 UHV LT-SPM & Optics

USM1500 2K & affordable magnets

USM1300 400mK high field magnets

USM1600 the milli Kelvin SPM

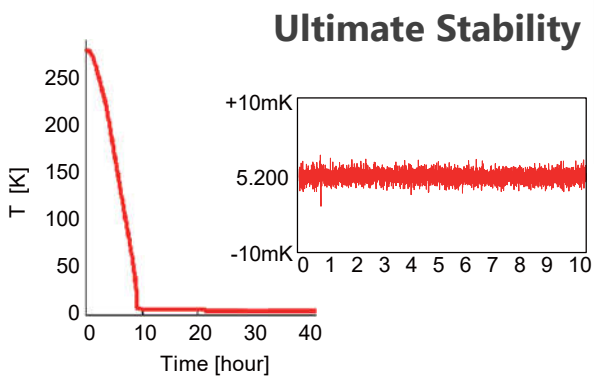
USM1800 *EasyCool* dry-cooled SPM

NEW

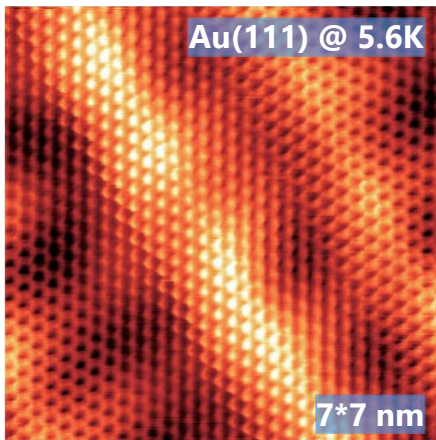
UNISOKU
TII Group



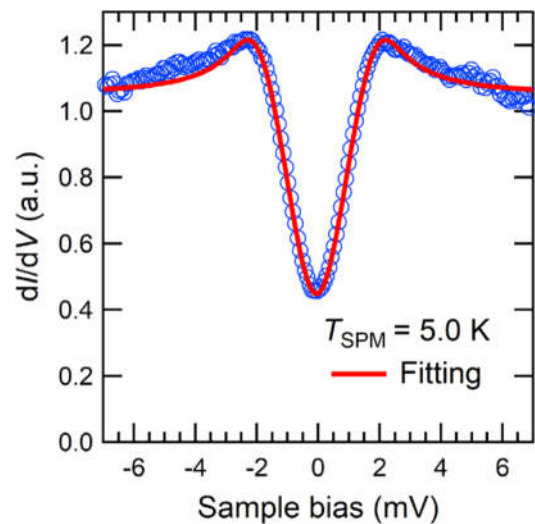
Quick and Easy Cool Down



Ultimate STM Resolution



Proven 5K Performance SC gap of Pb



Sunday

Single Alloy Nanoparticle X-Ray Imaging during a Catalytic Reaction

Young Yong Kim¹, Thomas F. Keller^{1,2}, Tiago J. Goncalves³, Manuel Abuin¹, Henning Runge¹, Luca Gelisio¹, Jerome Carnis¹, Vedran Vonk¹, Philipp N. Plessow³, Ivan A. Vartanyants¹, Andreas Stierle^{1,2}

¹*Deutsches Elektronen-Synchrotron (DESY), D-22607 Hamburg, Germany (corresponding author: Andreas Stierle, e-mail: andreas.stierle@desy.de)*

²*University of Hamburg, Physics Department, D-20355 Hamburg, Germany*

³*Institute of Catalysis Research and Technology, Karlsruhe Institute of Technology, D-76344 Eggenstein-Leopoldshafen, Germany*

The imaging of active nanoparticles represents a milestone in decoding heterogeneous catalysts' dynamics. We report the facet resolved, surface strain state of a single PtRh alloy nanoparticle on SrTiO₃ determined by coherent x-ray diffraction imaging under catalytic reaction conditions [1]. Density functional theory calculations allow us to correlate the facet surface strain state to its reaction environment dependent chemical composition. We find that the initially Pt terminated nanoparticle surface gets Rh enriched under CO oxidation reaction conditions. The local composition is facet orientation dependent and the Rh enrichment is non-reversible under subsequent CO reduction. Tracking facet resolved strain and composition under operando conditions is crucial for a rational design of more efficient heterogeneous catalysts with tailored activity, selectivity and lifetime.

Funding from the European Union H2020 project "Nanoscience Foundries and Fine Analysis" (NFFA), and from DFG SFB 1441 pre-funding is acknowledged. This work was supported by state of Baden-Württemberg through bwHPC (bwUniCluster and JUSTUS, RV bw17D011).

- [1] Young Yong Kim, Thomas F. Keller, Tiago J. Goncalves, Manuel Abuin, Henning Runge, Luca Gelisio, Jerome Carnis, Vedran Vonk, Philipp N. Plessow, Ivan A. Vartanyants, Andreas Stierle; „Science Advances“, 2021; 10.1126/sciadv.abh0757

Very Weak Bonds to Artificial Atoms Formed by Quantum Corrals

Fabian Stilp,¹ Julian Berwanger,¹ Nadine Mundigl,¹ Andreas Bereczuk,² Klaus Richter,² Franz J. Giessibl¹

¹*Institute of Experimental and Applied Physics, University of Regensburg, D-93053 Regensburg, Germany*

²*Institute of Theoretical Physics, University of Regensburg, D-93053 Regensburg, Germany*

e-mail: Franz.Giessibl@ur.de

We explored the bonding properties of the quantum corral (a circle of 48 iron atoms placed on a copper surface) reported by Crommie et al. in 1993 [1], along with variants, as an artificial atom using an atomic force microscope (AFM). The original corral geometry confines 102 electrons to 28 discrete energy states, and we found that these states can form a bond to the front atom of the AFM with an energy of about 5 millielectron volts. The measured forces are about 1/1000 of typical forces in atomically resolved AFM. The confined electrons showed covalent attraction to metal tips and Pauli repulsion to CO-terminated tips as shown in Fig. 1.

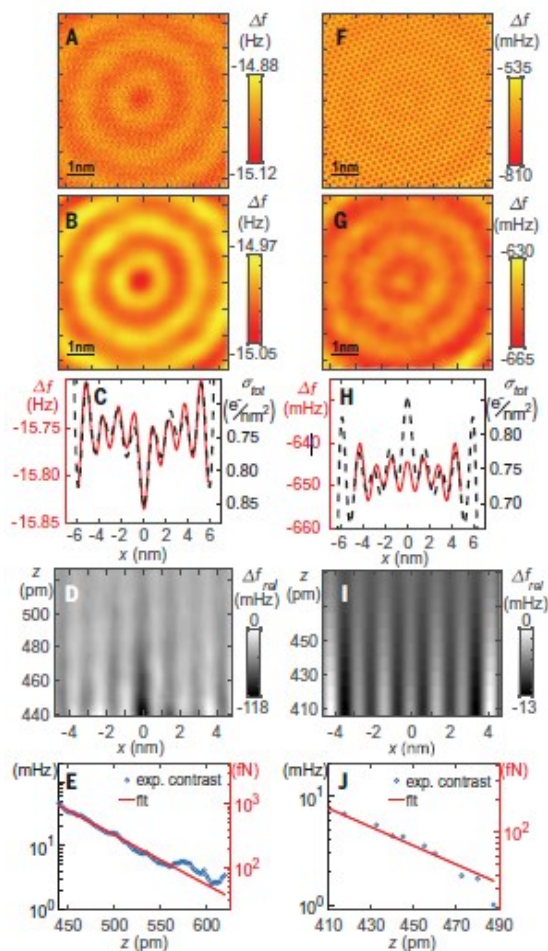


Fig. 1. AFM data inside the quantum corral for a single-atom metal tip (left column) and a CO-terminated tip (right column). (A) Frequency shift data $\Delta f(x, y, z = \text{const.})$ with an attractive interaction between the probe tip and the Bessel-type eigenstates. (B) Lowpass-filtered version of (A). (C) Profile line through the center of (B) and re-versed total surface charge density of the corral. (D) Grayscale representation of offset and slope-corrected frequency shift $\Delta f_{\text{rel}}(x, 0, z)$. (E) Distance dependence of the contrast, defined as the difference between the average of the first and second maxima and the minimum in between. (F) Frequency shift data $\Delta f(x, y, z = \text{const.})$ showing attraction to the Cu surface atoms and repulsion to the Bessel-type eigenstates. (G) Low-pass-filtered version of (F) showing only the repulsion to the Bessel-type eigenstates. (H) Profile line through the center of (G) compared with total charge density. (I) Grayscale presentation of offset and slope-corrected frequency shift $\Delta f_{\text{rel}}(x, 0, z)$. (J) Contrast, defined by the difference between the first maximum at $x \approx \pm 1.3$ nm and the average between the first and second minimum, evolution as a function of vertical distance z .

The 102 electrons that are held in the corral occupy states ψ_{nl} characterized by two quantum numbers: the number of radial nodes n and angular momentum l . The energy of the state $\psi_{n=5,l=0}$ is directly at the Fermi level, and the filling of this state can be modified by electrons flowing into or out of the bulk states of the Cu substrate. Therefore, the filling of the $\psi_{n=5,l=0}$ state changes when the tip approaches to the corral. Attractive interaction by a metal tip leads to an energetic lowering of states and thus increased filling, while repulsive interaction empties the state.

Natural atoms repel each other for very small distances. When approaching the metal tip to the corral, tip instabilities at very close distances prevent to check if a metal tip would also repel the corral states for extremely small distances.

However, placing an additional metal atom inside the corral shows that repulsive interaction occurs for very small distances. The $\psi_{n=2,l=7}$ state has a local maximum for a distance from the center of 4 nm. Placing an atom there lifts the degeneracy of the $\cos(7\phi)$ and $\sin(7\phi)$ states with azimuthal angle ϕ – the $\cos(7\phi)$ is shifted upwards in energy and partially emptied, leading to azimuthal ripples that can be observed by STM as shown in Figure 2.

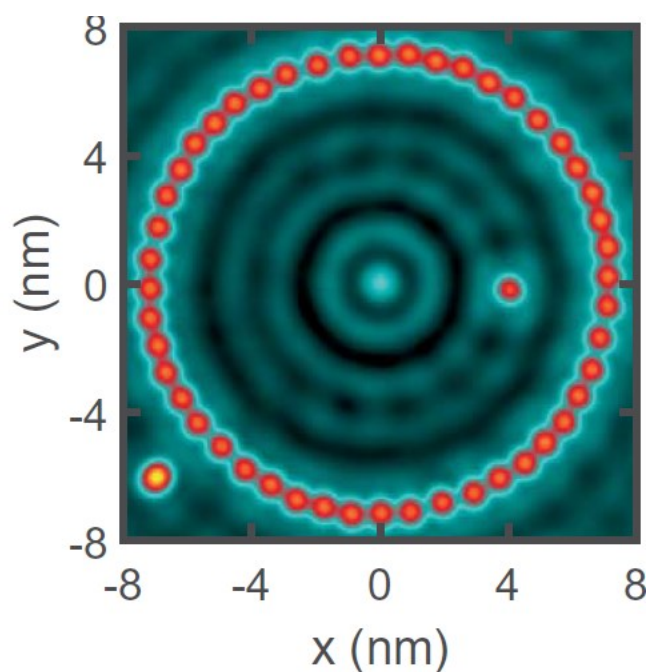


Fig. 2. STM data of a quantum corral that has a single metal adatom inside at $x = 4$ nm. The metal adatom leads to a repulsive interaction and 14 azimuthal ripples proportional to $\sin^2(7\phi)$.

Support by the Deutsche Forschungsgemeinschaft under grant SFB 1277 project A02 is gratefully acknowledged.

- [1] M. F. Crommie, C. P. Lutz and D. M. Eigler, Confinement of Electrons to Quantum Corrals on a Metal Surface, *Science* 262, 218 (1993).
- [2] Fabian Stilp, Julian Berwanger, Nadine Mundigl, Andreas Berezuk, Klaus Richter, Franz J. Giessibl, Very Weak Bonds to Artificial Atoms Formed by Quantum Corrals, *Science* 372, 1172 (2021).

Imaging of SARS-CoV-2 infected Vero E6 Cells by Helium Ion Microscopy

Natalie Frese, Patrick Schmerer², Martin Wortmann,
Matthias Schürmann¹, Matthias König², Michael Westphal,
Friedemann Weber², Holger Sudhoff¹ and Armin Götzhäuser

Physics of Supramolecular Physics and Surfaces, Bielefeld University, Germany
(corresponding author: ag@uni-bielefeld.de)

¹*Faculty of Medicine, Bielefeld University, Germany*

²*Institute for Virology, Justus-Liebig-University Giessen, Germany*

The Helium Ion Microscope (HIM) utilizes a focused beam of helium ions to image and modify materials with high spatial resolution, large depth of field, and chemical sensitivity [1]. HIM images show stronger chemical and topographical contrasts than images from the related scanning electron microscope, and the HIM is capable to resolve sub-nanometer features. Due to its charge compensation capability, the HIM can image insulating biological samples without additional conductive coatings [2]. In this contribution, the first HIM images of uncoated SARS-CoV-2 infected Vero E6 cells are presented. Interactions between cells and virus particles, as well as among virus particles, could be imaged [3]. The HIM pictures show the three-dimensional appearance of SARS-CoV-2 and the surface of Vero E6 cells at a multiplicity of infection (MOI) of approximately 1 with great morphological detail. The absence of a conductive coating allows a distinction between virus particles bound to the cell membrane and virus particles lying on top of the membrane.

[1] G. Hlawacek and A. Götzhäuser (Ed.): *Helium Ion Microscopy*, Springer-International (2016).

[2] M. Schürmann, N. Frese, A. Beyer, P. Heimann, D. Widera, V. Mönkemöller, T. Huser, B. Kaltschmidt, C. Kaltschmidt and A. Götzhäuser: *Helium Ion Microscopy Visualizes Lipid Nanodomains in Mammalian Cells*, *Small* 43, 5781 (2015).

[3] N. Frese, P. Schmerer, M. Wortmann, M. Schürmann, M. König, M. Westphal, F. Weber, H. Sudhoff and A. Götzhäuser: *Imaging of SARS-CoV-2 infected Vero E6 Cells by Helium Ion Microscopy*, *Beilstein J. Nanotechnol.* 12, 172 (2021).

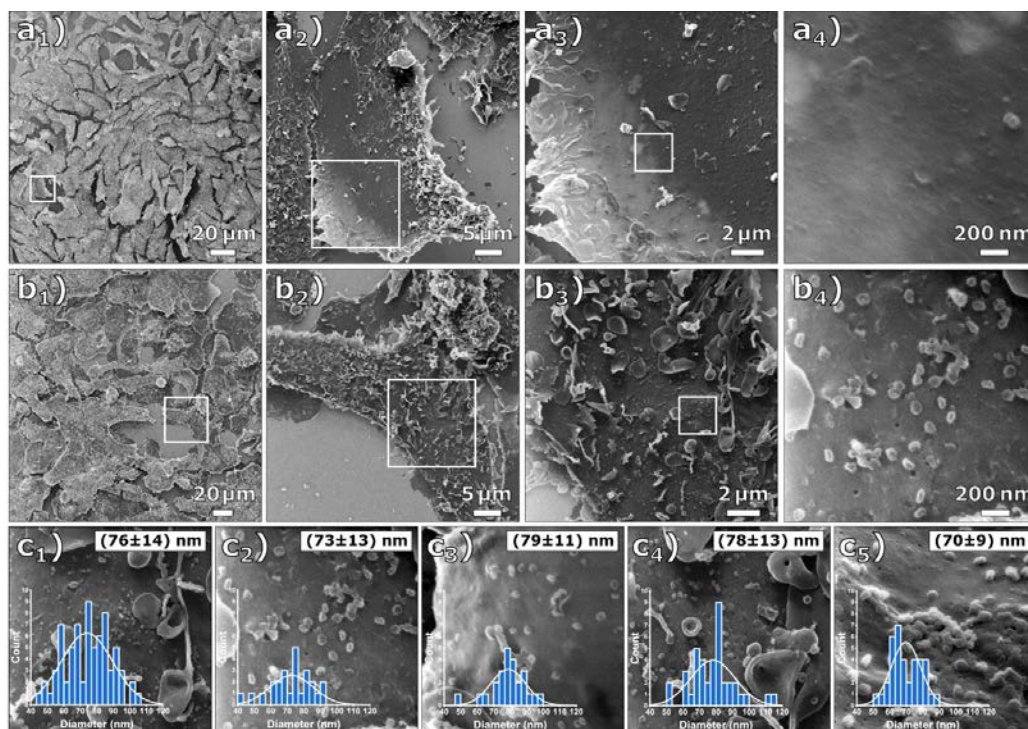


Fig. 1: Comparative HIM images of non-infected and infected Vero E6 cells: a₁₋₄) Non-infected cell at different magnifications (FOV 200 μm , 45 μm , 15 μm , 1.7 μm) and b₁₋₄) MOI 1 infected cells at different magnifications (FOV 250 μm , 45 μm , 15 μm , 1.7 μm). The cell membrane is covered with the virus particles. c₁₋₅) Virus particle diameter distributions determined. The inserted histograms show the respective image evaluation, the average particle diameter of all evaluated images is 75 ± 13 nm.

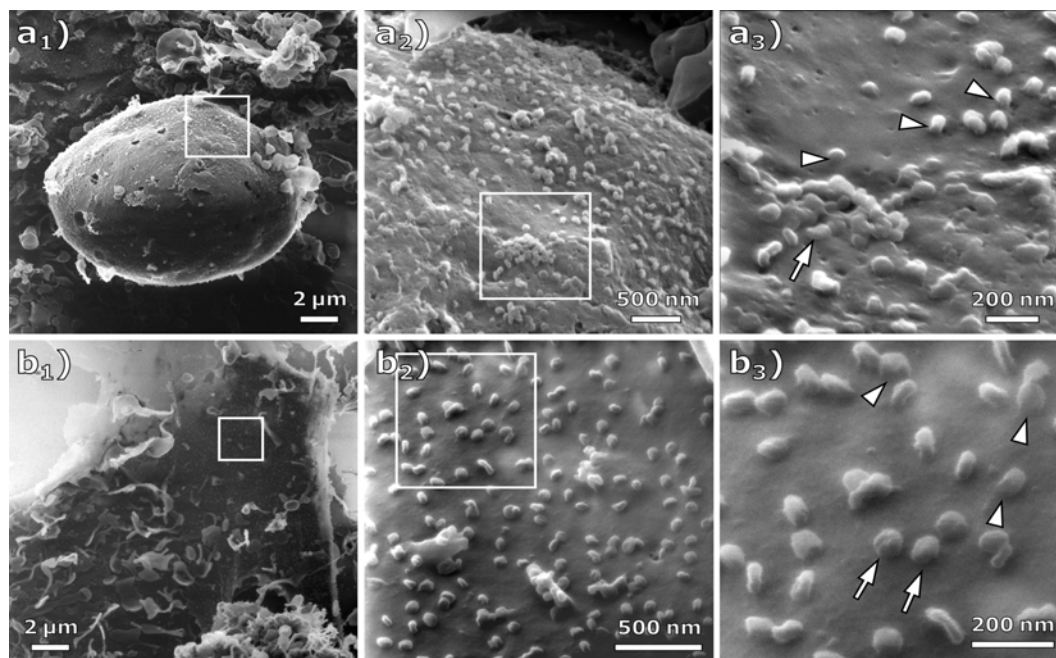


Fig. 2: HIM images of infected cells imaged with charge compensation. a₁₋₃) Different magnifications of a MOI 1 infected cell (FOV 17 μm , 3.5 μm , 1.3 μm). At high magnification clusters of virus particles (arrow) and junctions (arrowheads) between virus particles and the cell membrane become visible. b₁₋₃) Different magnifications of a MOI 1 infected cell (FOV 18 μm , 2 μm , 850 nm). While some of the virus particles appear to be bound to the cell membrane (arrowheads), others seem to just lie on top (arrow).

Monday

Charging and metalation of porphyrins on ultrathin oxide films

M. Sterrer, F. Presel, F. Schwarz, T. Bone, G. Koller, M. Ramsey, C. Kern, P. Puschnig

Institut für Physik, Universität Graz, A-8010 Graz, Austria

(corresponding author: M. Sterrer, e-mail: martin.sterrer@uni-graz.at)

Porphyrins and metalloporphyrins are versatile molecules, which offer a large variability of their properties due to the possibility to attach different ligands or metal atoms to the porphyrin macrocycle. The surface-confined self-metalation reaction describes the replacement of two aminic protons in the macrocycle of the porphyrin molecule by a metal atom of the substrate. This reaction was first observed on metal surfaces, but more recent investigations show that it also occurs on oxides such as magnesium oxide (MgO). Previous work has shown that the self-metalation of 2H-tetraphenyl porphyrin (2H-TPP) on MgO is strongly dependent on the morphology of the material and occurs only on surface irregularities but not on a perfect planar surface.

By a combination of results obtained with scanning tunneling microscopy, photoemission spectroscopy, and DFT computations, we show that the self-metalation reaction on MgO can also be induced on planar MgO surfaces [1]. The key to this is the use of only few atomic layers thin MgO films, which are grown on a metallic substrate. Because of the reduction of the work function of the silver substrate by the MgO film, electron transfer occurs into adsorbed 2H-TPP molecules, which then leads to the self-metalation reaction. By chemical tuning of the work function we could furthermore show that states where the molecules are charged and metalated or uncharged and non-metalated can deliberately be generated. These results suggest a method to control the electronic and chemical properties of porphyrins on surfaces, which opens the way for selective surface functionalization.

To understand the role of charging, we compare the self-metalation of 2H-TPP and 2H-porphine on ultrathin MgO films. Our results suggest that charging helps to bring the macrocycle closer to the MgO surface, which facilitates the transfer of an Mg ion from the oxide lattice into the molecule.

We have recently extended these studies to ultrathin FeO(111)/Pt(111) and FeO(111)/Au(111) films and will present first STM results for the adsorption of 2H-TPP and 2H-P on these substrates.

- [1] L. Egger, M. Hollerer, C. Kern, H. Herrmann, P. Hurdax, A. Haags, X. Yang, A. Gottwald, M. Richter, S. Soubatch, F. S. Tautz, G. Koller, P. Puschnig, M. G. Ramsey, M. Sterrer, *Angew. Chem. Int. Ed.*, 2021, 60, 5078 (2021)

Tuning of binding-motifs and chirality in cyano-porphyrin self-assemblies: from metal to bulk insulator on surfaces

M. Ammon, M. Devarajulu, Y. Liu, C. Steiner, T. Sander, M. Gurrath¹, D. Lungerich²,
N. Jux², B. Meyer¹, S. Maier

*Department of Physics, Friedrich-Alexander-Universität Erlangen-Nürnberg,
Erlangen, Germany*

(corresponding author: Sabine Maier, e-mail: sabine.maier@fau.de)

¹ *Interdisciplinary Center for Molecular Materials (ICMM) and Computer Chemistry Center (CCC),
Friedrich-Alexander-Universität Erlangen-Nürnberg, Erlangen, Germany*

² *Lehrstuhl für Organische Chemie II, Friedrich-Alexander-Universität Erlangen-Nürnberg,
Erlangen, Germany*

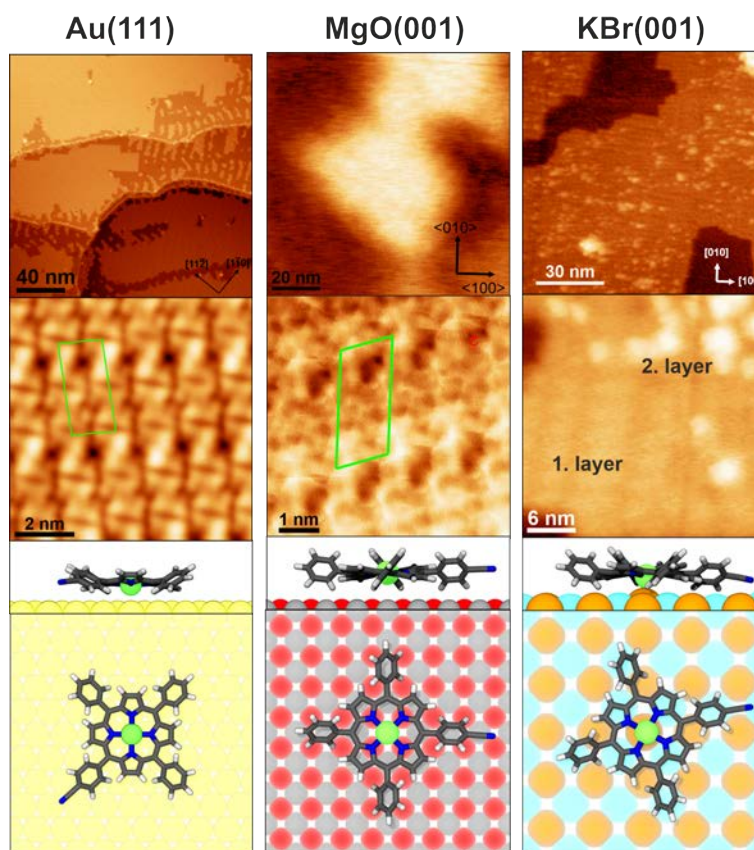
Molecular self-assemblies on surfaces have emerged as a highly efficient strategy for creating tailor-made surface structures with dedicated functionality. Thereby, porphyrins are versatile molecular building blocks because their macrocycle can be decorated with different substituents and metal centers, which offers excellent opportunities to tune intermolecular and molecule-surface interactions. Moreover, porphyrins adapt their conformation by deformation of the macrocycle and reorientation of the substituents upon adsorption on the surface, which affects intermolecular interactions in self-assemblies. Despite the importance of porphyrin structures on surfaces, the effect of the molecule-surface interaction on the adsorption geometry and self-assembly was in ultra-high vacuum up to now mostly focused to studies on metal surfaces [1,2]. In contrast on (weaker) interacting bulk-insulating ionic crystals, the adsorption and self-assembly of porphyrins is not well understood.

Here we discuss the adsorption, binding motifs, and organizational chirality in self-assembled networks of cyanofunctionalized zinc-tetraphenylporphyrin derivatives (Zn-CNTPP) on Au(111), MgO(001), and KBr(001) at submonolayer coverage under ultrahigh vacuum conditions based on low-temperature scanning tunneling (STM) and noncontact atomic force microscopy (nc-AFM) data combined with detailed density functional theory calculations. We chose a TPP with one peripheral cyano group, as the asymmetric substitution allows us directly to unravel competing interactions between cyanophenyl and phenyl units.

We show that Zn-CNTPPs adopt a planar adsorption geometry with the macrocycle parallel to the surface on all three surfaces. However, while a global minimum structure is found on KBr due to a strong CN \cdots K interaction, multiple and energetically nearly equivalent adsorption sites occur on MgO and Au.[3] Therefore, commensurate adsorption is suggested on KBr

while optimizing the molecule-molecule interactions over molecule-surface interactions is more important on MgO and Au, which the STM and nc-AFM data experimentally evidence.

On MgO(001) and Au(111), the T-stacking of phenyl rings determines the structure of the well-ordered self-assemblies. However, since the interaction of porphyrins with Au(111) is stronger than on MgO(001), the phenyl rings are more inclined toward the surface. [4] This leads to larger unit cells on Au(111) than on MgO, and on the other hand, the binding motif of the cyanophenyl groups changes from dominantly parallel stacked on MgO(001) to T-stacked on Au(111). Moreover, we found that, depending on the interaction of the cyanophenyl groups, the organizational chirality in the phenyl T-stacking can be preserved or switched.



In conclusion, we demonstrate that the distortion of the macrocycle and the rotation and bending of the substituents triggered by the molecule-substrate interaction upon adsorption represent an effective way to tune the intermolecular interactions and organizational chirality in the porphyrin networks.

Support by the German Research Foundation (DFG) through Research Unit FOR~1878 (funCOS), the Collaborative Research Center SFB~953 (project number 182849149), and the Research Training Group GRK~1896 at the Friedrich-Alexander-Universität Erlangen-Nürnberg is gratefully acknowledged.

- [1] W. Auwärter, D. Eciija, F. Klappenberger, J. V. Barth, *Nat. Chem.* 7 (2) 105-20, (2015)
- [2] J. M. Gottfried, *Surf. Sci. Rep.* 70 (3), 259- 379, (2015)
- [3] M. Ammon et al., submitted (2022)
- [4] M. Ammon et al., in preparation (2022)

On-surface synthesis of a carbanion by electrophilic activation of water at a carbene-metal interface

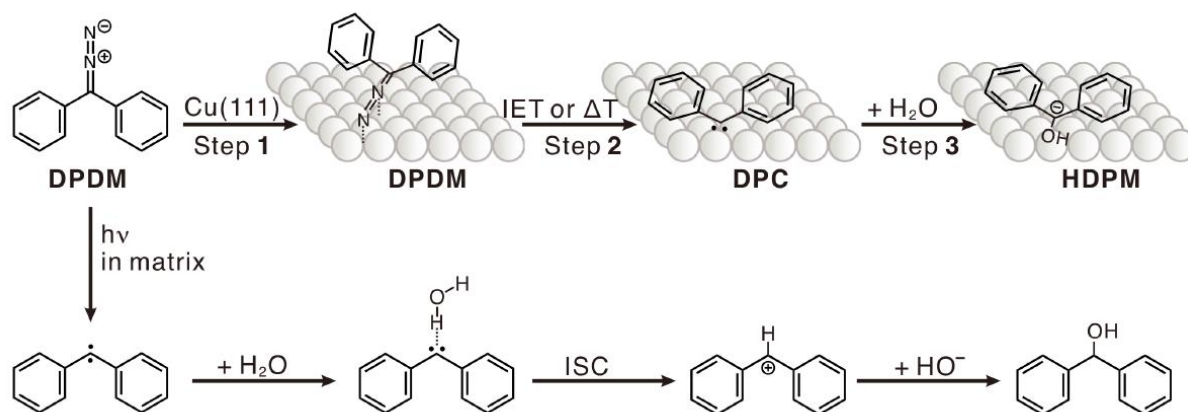
Yun-Jun Cao¹, Joel Mieres-Perez², Julien Frederic Rowen³, Elsa Sanchez-Garcia²,
Wolfram Sander³, and Karina Morgenstern¹

¹ *Physical Chemistry I, Ruhr-Universität Bochum, Universitätsstr. 150, D-44801 Bochum, Germany
(corresponding author: K. Morgenstern, e-mail: karina.morgenstern@rub.de)*

² *Computational Biochemistry, Universität Duisburg-Essen, Universitätsstr. 2, D-45141 Essen, Germany*

³ *Organic Chemistry II, Ruhr-Universität Bochum, Universitätsstr. 150, D-44801 Bochum, Germany*

Carbene, a reactive intermediate processing lone pair electrons and vacant orbitals, exhibits multifaceted reactivity towards small molecules such as oxygen, hydrogen, and water. Though water activation by carbenes is of synthetic importance, the product is limited to carbenium ions in conventionally employed environments such as solutions or cryogenic matrices. In such environments, only the lone pair electrons of carbonyl carbons are involved.



Scheme 1: Reaction pathways of DPC with water in cryogenic matrices [4] and on the Cu(111) surface. **DPDM**: diphenyldiazomethane. **HDPM**: hydroxy-diphenylmethanide. **IET**: inelastic tunneling manipulation. **ISC**: intersystem crossing.

Here, we tune the coordination number of an aryl carbene on a metal surface by introducing two-dimensional confinement, making the vacant orbitals of carbenes accessible to an electrophilic activation of water (Scheme 1). An unprecedented type of reactive intermediate, the hydroxy-diphenylmethanide carbanion is unambiguously identified by combining scanning tunneling microscopy and infrared reflection absorption spectroscopy.

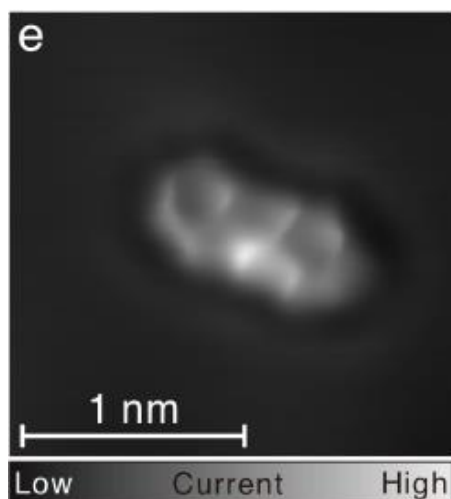


Figure 1: High resolution images of HDPM acquired with a modified tip in constant height mode, $I_t = 10$ pA, $V_b = 5$ mV, $\Delta z = -50$ pm.

In particular, the advantages of combining bond-resolution images acquired by a carbene-modified tip (Figure 1) with the chemical information gained in isotopically-labelled vibrational IRRAS experiments (Figure 2) in following an on-surface reaction will be discussed.

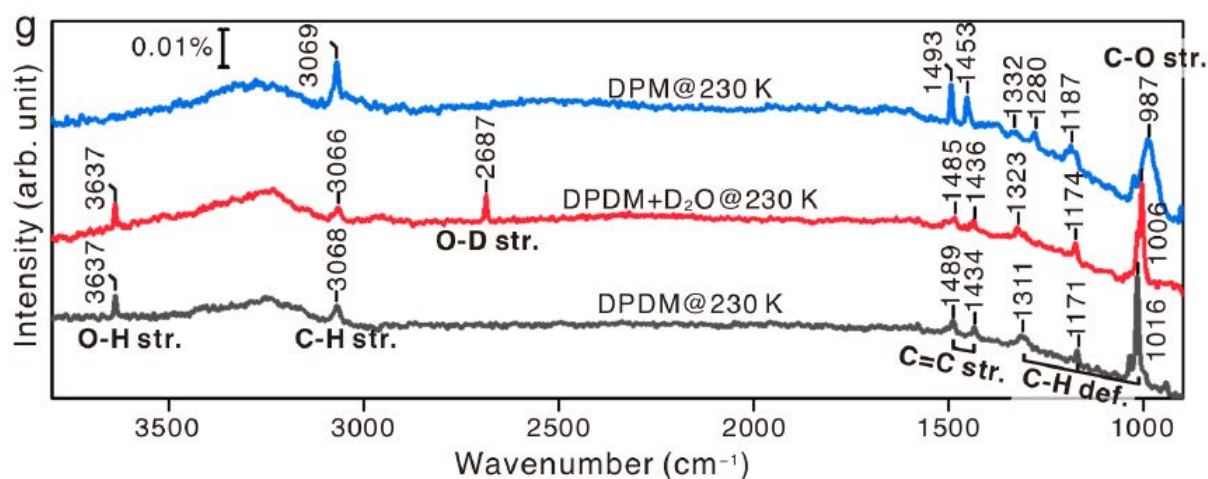


Figure 2: IRRAS spectra after deposition of DPDM (black), DPDM + D₂O (red), and DPM (blue) on Cu(111) at 230 K with wavenumbers.

These findings open up a new avenue to tame the reactivity of carbenes for selective synthesis of reactive intermediates that are inaccessible in conventionally employed environments, by controlling the coordination number of carbenic carbons with transition metals.

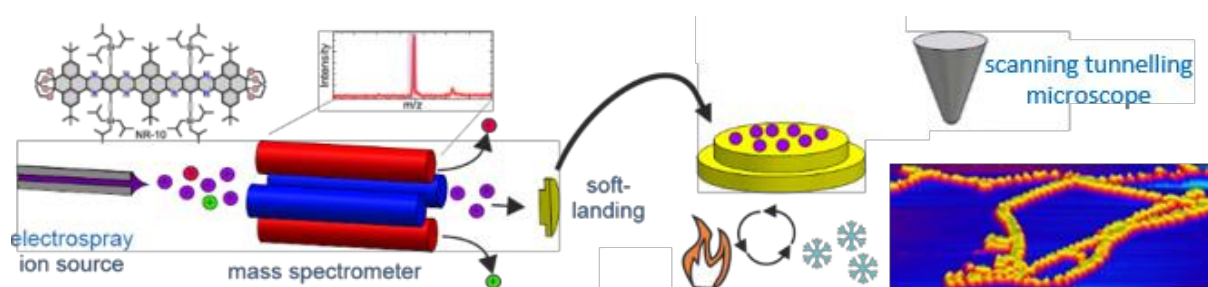
This work was funded by the Deutsche Forschungsgemeinschaft (DFG, German Research Foundation) under Germany's Excellence Strategy-EXC-2033-390677874 RESOLV. Y.J. Cao acknowledges the Alexander-von-Humboldt Foundation for a Humboldt Research Fellowship.

Navigate flying molecular elephants safely to the ground: mass-selective soft landing up to the mega-Dalton range by electrospray controlled ion-beam deposition and its use for molecular engineering at surfaces

Andreas Walz, Karolina Stoiber, Wei Ran, Peter Knecht, Hongxiang Xu, Anthoula C. Papageorgiou, Annette Huettig, Diego Cortizo-Lacalle², Juan P. Mora-Fuentes², Aurelio Mateo-Alonso², Joachim Reichert, Hartmut Schlichting, and Johannes V. Barth*

*Physics Department E20, Technical University of Munich, James Franck Straße 1, 85748 Garching (Germany); ²POLYMAT, University of the Basque Country UPV/EHU, Avenida de Tolosa 72, 20018 Donostia-San Sebastian, Spain | (*corresponding author - jvb@tum.de)*

The prototype of a highly versatile and efficient preparative mass spectrometry system used for the deposition of complex molecular species in ultra-high vacuum (UHV) is presented, along with encouraging performance data obtained with several model species which are thermolabile or not sublimable. The test panel comprises small organic compounds, proteins, and large DNA units covering a 4-log mass range up to 1.7 MDa providing a broad spectrum of analyte species evaluated to date. Three designs of innovative ion guides, a novel digital mass-selective quadrupole (dQMS) and a standard electrospray ionization (ESI) source are combined to an integrated device, designated Electrospray Controlled Ion Beam Deposition (ES-CIBD) [1].



Herein we notably apply this methodology for interfacial molecular engineering by combining multistep solution synthesis of N-doped molecular graphene nanoribbons (GNRs) with controlled ion beam deposition and real-space visualisation by scanning tunnelling microscopy [2]. We demonstrate how this method yields exclusively a controllable amount of specific, otherwise unsublimable, GNRs of 2.9 nm length on a planar Ag(111) surface, where they readily self-assemble at ambient temperature. Moreover, we achieved further processing by developing appropriate on-surface synthesis protocols and exploiting the reactivity of the substrate. Accordingly, following multiple chemical transformations, GNRs provide reactive building blocks engaging in the formation of extended, metal-organic coordination polymers.

This work was supported by the ERC Advanced Grant MolArt #247299, the ERC-PoC Grant Softbeam #780907, the FET Innovation Launchpad Grant MolShuttle #946223, and the FET-Open Grant 2D Ink # 664878. Further funding sources are the H2020-EU.1.2.1. - FET Open programme (no. 946223 and no. 899895), the German Research Foundation (DFG) through the TUM International Graduate School of Science and Engineering (IGSSE), Excellence Cluster e-conversion, and the priority programme 1928 COORNETs, the China Scholarship Council (CSC) and the European Research Council (ERC) (no. 722951). Part of this work was carried out with support from the Basque Science Foundation for Science (Ikerbasque), POLYMAT, the University of the Basque Country, Gobierno Vasco (BERC programme). Technical and human support provided by SGiker of UPV/EHU and European funding (ERDF and ESF) is acknowledged.

- [1] Andreas Walz, Karolina Stoiber, Annette Huettig, Hartmut Schlichting* and Johannes V. Barth*, *subm. Anal. Chem.* (2021), cf. chemrxiv.org/engage/chemrxiv/article-details/6152faf9aef99c32dd04d151. CIBD technology is based on three novel ion guides, which inventions have been filed for patents, cf. PCT WO2019193170A1, WO2019193171A1, WO2019193191A1.
- [2] Wei Ran, Andreas Walz, Karolina Stoiber, Peter Knecht, Hongxiang Xu, Anthoula C. Papageorgiou,* Annette Huettig, Diego Cortizo-Lacalle, Juan P. Mora-Fuentes, Aurelio Mateo-Alonso, Hartmut Schlichting, Joachim Reichert,* and Johannes V. Barth*, *subm. Angew. Chem. Int. Ed.* (2021).

Real Space Visualization of Entangled Excitonic States in Charged Molecular Assemblies

J. Doležal^{1,2}, S. Canola¹, P. Hapala¹, R. C. de C. Ferreira¹, P. Merino^{3,4}, and M. Švec¹

¹*Institute of Physics, Czech Academy of Sciences, CZ16200 Praha 6, Czech Republic*
(corresponding author: J. Dolezal, e-mail: dolezalj@fzu.cz)

²*Faculty of Mathematics and Physics, Charles University, CZ12116 Praha 2, Czech Republic*

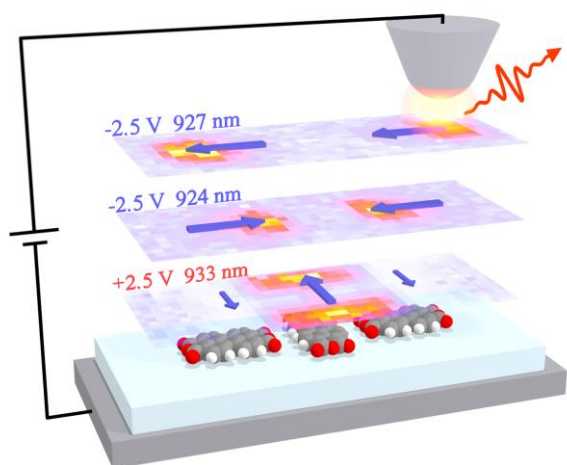
³*Instituto de Ciencia de Materiales de Madrid; CSIC, E28049 Madrid, Spain*

⁴*Instituto de Física Fundamental, CSIC, E28006 Madrid, Spain*

Optically active molecules offer key advantages as quantum emitters due to their very small dimensions, well-defined optical transitions and photostability [1]. They are also ideal transducers of electric currents into optical signals [2] and can host charged excitons when gated on thin insulating surfaces [3-5]. Coupling between the excited states of single molecular emitters leads to the formation of delocalized excitonic states, whose properties finely depend on the exact intermolecular arrangement at the nanoscale [6-8]. The entanglement between the molecular excited states, specific to molecular aggregates holds great promise for the future of quantum computing [9-11], which would use individual molecular dyes as building blocks of their circuitry.

Here, using thermally activated diffusion of perylenetetracarboxylic dianhydride (PTCDA) anions on ultrathin NaCl layers on Ag(111) we create small clusters that manifest exciton delocalization. Hyperspectral electroluminescence maps above the chromophore using the scanning tunneling microscopy-induced luminescence (STML) method show contrast corresponding to the intensity of the individual eigenmodes. With the help of atomic force microscopy (AFM) we were able to determine the exact geometry of each cluster. This was used as an input to time-dependent density functional theory (TD-DFT) calculations. Obtained transition density was produced with our photon maps simulation tool considering the coupling of the molecular excitation to the optical field of the laterally scanning nanocavity. Finally, theoretical photon maps were generated which are in very good agreement with the experimental photon maps.

We identified the dominant exciton coupling as the interaction between the first excited states D_1^- of the single-emitter PTCDA units. Additionally, we have found that a favorable interaction between D_1^- and the second excited D_2^- state, due to their low energy difference, enables exciton coupling between molecular units that are in a mutually perpendicular geometry, giving rise to delocalized eigenmodes. Finally, in a particular case of PTCDA trimer shown in Fig 1, we demonstrated control over the exciton coupling by switching the assembly charge states by the electric field.



with a shorter arrow along the short molecular axis.

Fig.1: Schematic of the STML photon mapping on a PTCDA trimer. At negative sample bias voltage, the central molecule has a different charge state (neutral) than the peripheral ones (anions) and does not act in exciton delocalization. Two delocalized eigenmodes on different energies (wavelengths) corresponding to the molecular transient dipoles in parallel and antiparallel configuration are observed. At positive bias voltage, all the molecules are in the anionic state. Longitudinal mode of the central PTCDA now weakly interacts with the transversal mode of the second excited state sketched

- [1] Toninelli, C.; Gerhardt, I.; Clark, A. S.; Reserbat-Plantey, A.; Götzinger, S.; Ristanović, Z.; Colautti, M.; Lombardi, P.; Major, K. D.; Deperasińska, I.; Pernice, W. H.; Koppens, F. H. L.; Kozankiewicz, B.; Gourdon, A.; Sandoghdar, V.; Orrit, M., *Nat. Mater.* **2021**
- [2] Kuhnke, K.; Große, C.; Merino, P.; Kern, K., *Chem. Rev.* **2017**, 117, 5174–5222.
- [3] Doležal, J.; Canola, S.; Merino, P.; Švec, M., *ACS Nano* **2021**, 15, 7694-7699.
- [4] Doppagne, B.; Chong, M. C.; Bulou, H.; Boeglin, A.; Scheurer, F.; Schull, G., *Science* **2018**, 361, 251-255.
- [5] Rai, V.; Gerhard, L.; Sun, Q.; Holzer, C.; Repän, T.; Krstić, M.; Yang, L.; Wegener, M.; Rockstuhl, C.; Wulfhekel, W., *Nano Lett.* **2020**, 20, 7600-7605.
- [6] Hettich, C.; Schmitt, C.; Zitzmann, J.; Kühn, S.; Gerhardt, I.; Sandoghdar, V., *Science* **2002**, 298, 385-389.
- [7] Nordén, B., *Q. Rev. Biophys.* **2016**, 49, E17.
- [8] Hestand, N.J.; Spano, F.C., *Acc. Chem. Res.* **2017**, 50, 341-350.
- [9] Castellanos, M. A.; Dodin, A.; Willard, A. P., *Phys. Chem. Chem. Phys.* **2020**, 22, 3048–3057.
- [10] Cho, M. *Two-Dimensional Optical Spectroscopy*, 1st Edition; CRC Press: Boca Raton, **2009**.
- [11] Nielsen, M.; Chuang, I. *Quantum Computation and Quantum Information*, 10th Anniversary Edition; Cambridge University Press: Cambridge, **2010**.

Atomistic Modelling of Surfaces and Interfaces for Magnetite-based Nanocomposites

Kai Sellschopp^{1,2}, Wernfried Mayr-Schmölzer¹, Somak Banerjee¹, Stefan Müller¹, and Gregor B. Vonbun-Feldbauer¹

¹ *Institute of Advanced Ceramics, Hamburg University of Technology
Denickestr. 15, D-21073 Hamburg, Germany
(corresponding author: G. Vonbun-Feldbauer, e-mail: gregor.feldbauer@tuhh.de)*

² *Institute of Hydrogen Technology, Helmholtz-Zentrum hereon
Max-Planck-Straße 1, D-21502 Geesthacht, Germany*

Novel hybrid materials from nano-building blocks promise excellent properties and diverse functions [1]. Inspired by nature, supercrystalline nanocomposites are a particularly interesting class of materials with a broad range of potential applications including bio-inspired structural materials, bioimplants, optoelectronics, batteries, and catalysis. One realization are inorganic ceramic nanoparticles (NP) from transition-metal oxides like magnetite or titania which are functionalized with organic ligands. Those nanoscale functional units assemble in periodic structures on a first level of hierarchy (see figure 1). Even macroscale structures can be achieved using advanced manufacturing methods [2]. After further processing such crystals can be arranged via complex polymers on an additional level of hierarchy to achieve hierarchical materials. The structural integrity and mechanical properties of such materials is important for many applications. Tailoring the composition and structure of the nanocomposites allows improving their strength, stiffness, hardness, and toughness [3]. For optimized results a detailed understanding of all relevant contributions from the different levels of hierarchy and scales is crucial, but has not been achieved yet. In this contribution atomistic modeling is used to shed light on the lowest level of hierarchy, mainly the surfaces and interfaces of the NP.

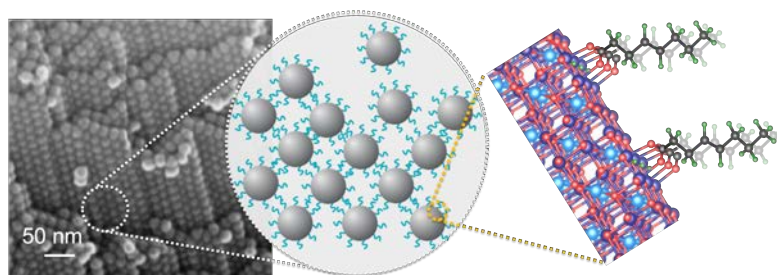


Figure 1: Schematic zoom into a nanocomposite hybrid material from magnetite NP linked via carboxylic acid molecules. Left and center image courtesy of project A6, SFB986.

At the lowest relevant level of hierarchy various contributions are essential including the shape of the NP [7, 4], the interactions and interfacial properties between different ligands and the exposed NP surfaces [5, 6], and effects in the interphase between the NP. Those aspects are also essential in other fields such as heterogeneous catalysis.

At first, the magnetite (111) surface which is one of the major facets of magnetite NP and the adsorption of organic ligands, mainly formic acid as a simple probe molecule, will be discussed [6]. We present results from density functional theory (DFT) calculations and DFT-based analysis in comparison to experiments from the DESY Nanolab employing a range of surface science techniques (SXR, STM, LEED, FT-IRRAS). The program CodeRed (Configuration space determination and Reduction) [8] is presented which allows to sample the adsorption configuration space and to select configurations as input for DFT calculations using unsupervised machine learning approaches like dimensionality reduction and clustering algorithms. The structure search for formic acid on magnetite (111) reveals two stable adsorption modes, a chelating and a quasi-bi-dentate mode. Both modes are observed on real (111) surfaces according to the comparison of calculated vibrational spectra with experimental data. This is in difference to the (001) surface where a bi-dentate mode is favorable [5]. Further, a stabilization of iron vacancies on the surface is indicated and effects on the electronic structure are highlighted.

Secondly, approaches for further facilitating the presented results are sketched and an outlook is given. For example, mechanical tests on coupled surface slabs or whole NP can simulate the effect of different surface facets, deformation modes, and interphase configurations. Using DFT, however, only properties of strongly simplified model systems can be calculated. Multi-scale modeling combining various tools for different scales can help here. To this end, the transfer of DFT results into a newly parametrized empirical force field for molecular dynamics simulations is presented [9]. This is achieved by using partial point charges derived from ab initio Bader charge analyses and allows for an accurate description of the investigated magnetite interfaces in larger and more complex systems.

Supported by the Deutsche Forschungsgemeinschaft (DFG),
Projektnummer 192346071 - SFB 986 "M³".

References

- [1] Boles *et al.*, Chem. Rev. **116** 11220 (2016).
- [2] Domènech *et al.*, Adv. Eng. Mater. **22** 2000352 (2020).
- [3] Clancy *et al.*, ACS Appl. Mater. Interfaces **12** 15955 (2020).
- [4] Sellschopp *et al.*, J. Chem. Phys. **152** 064702 (2020).
- [5] Arndt/Sellschopp *et al.*, Comm. Chem. **2** 92 (2019).
- [6] Creutzburg/Sellschopp *et al.*, J. Phys. Chem. Lett. **12** 3847 (2021).
- [7] Feld *et al.*, ACS Nano **13** 152 (2018).
- [8] CodeRed: <https://collaborating.tuhh.de/groups/m-9/commod/-/shared>
- [9] Konuk *et al.*, J. Phys. Chem. C **125** 4794 (2021).

Planarization of non-planar aromatic hydrocarbons: Dehydrogenation *versus* hydrogenation

Bahaaeddin Irziqat, Aleksandra Cebrat, Miloš Baljuzović, Kevin Martin,¹ Manfred Parschau, Narcis Avarvari,¹ and Karl-Heinz Ernst^{2,3}

Empa, Swiss Federal Laboratories for Materials Science and Technology, Überlandstrasse 129, 8600 Dübendorf, Switzerland

¹ *Laboratoire Moltech-Anjou, CNRS-Université d'Angers, 49045 Angers, France*

² *Department of Chemistry, University of Zurich, 8057 Zürich, Switzerland*

³ *Nanosurf Laboratory, Institute of Physics, Czech Academy of Sciences*

Besides their interest for potential organic electronic devices, 2D chiral crystallization of carbohelicenes on metal surfaces is of paramount importance for light sensors or for electron-spin filters. Here, we report the 2D chiral crystallization of 2,2'-bis[5]helicene on a Au(111) surface and its thermally-induced cyclodehydrogenation studied with scanning tunneling microscopy (STM). The low coverage deposition of bis[5]helicenes on Au(111) kept at 400 K, leads to formation of heterochiral zigzag chains of the (*M,M*)- and (*P,P*)-enantiomers growing along the herringbone reconstruction pattern. In the closed-packed monolayer, both enantiomers self-assemble into a racemate phase and rotational and mirror domains can be differentiated. Due to its strong steric overcrowding in its adsorbate state, the (*P,M*)-meso form was not observed.

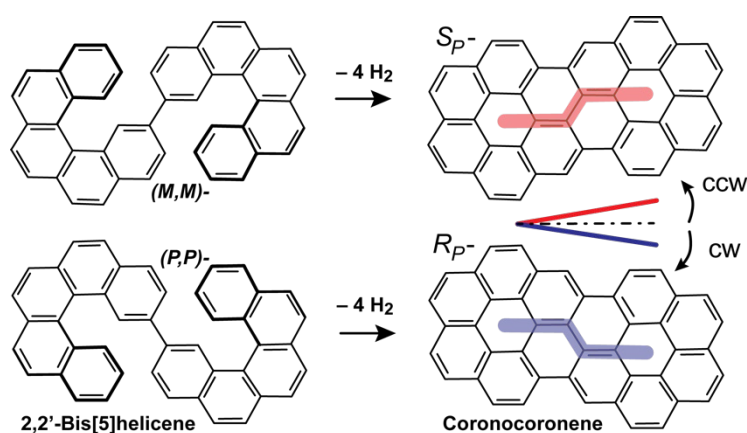


Figure 1. Cyclodehydrogenation bis[5]helicene proceeds stereoselectively to planar coronacoronene which is chiral if confined onto a surface.

Upon annealing the substrate to approximately 670 K and subsequent cooling to 50 K, the characteristic twisted shape of the bis[5]helicenes with protrusions is no longer observed and two-dimensional homochiral domains of planar coronacoronene molecular species can be distinguished. The transformation from helical to planar chiral molecules via dehydrogenation and loss of eight hydrogen atoms

was confirmed by secondary ion mass spectrometry (ToF-SIMS). Further STM measurements at 7.5 K affirmed the formation of mirror and rotational 2D homochiral conglomerate domains of planar *S_P*- and *R_P*-coronacoronene (Fig. 1).

CO₂ adsorption and dissociation on kinked Cu surfaces at (near-)ambient pressure

S.V. Auras, F. Garcia-Martinez, F. Schiller, and J.E. Ortega

Centro de Física de Materiales, Universidad del País Vasco, 20018 Donostia – San Sebastian, Spain

(corresponding author: S.V. Auras, e-mail: sabine.auras@ehu.eus)

Rising CO₂ concentrations in the atmosphere and the resulting consequences on the earth's climate are a major global challenge. CO₂ is emitted in the majority of industrial processes, e.g. through the use of fossil fuels as an energy source, or as a chemical by-product. In this context, capturing CO₂ and converting it to other chemicals presents an attractive alternative to emitting it into the atmosphere. However, the thermodynamic stability and chemical inertness of CO₂ as a molecule pose inherent challenges realizing this goal.

The reverse water-gas shift reaction ($\text{CO}_2 + \text{H}_2 \rightarrow \text{CO} + \text{H}_2\text{O}$) or conversion to methanol ($\text{CO}_2 + 3\text{H}_2 \rightarrow \text{CH}_3\text{OH} + \text{H}_2\text{O}$) are considered promising pathways to recycle CO₂ in a gas-phase process.^[1] Both processes require breaking the stable C=O double bond. Industrially, Cu based materials are most frequently employed as catalysts for these reactions. Nonetheless, high pressures are necessary to compensate for otherwise slow reaction rates. A fundamental understanding of the necessary reaction steps, however, is still limited.^[2-5]

Pure Cu-surfaces are suitable model catalysts for fundamental studies on this type of reaction. At near-ambient pressure, they have been found to catalyze CO₂ reduction by first adsorbing CO₂ in a chemisorbed state, thus facilitating subsequent dissociation to CO and adsorbed O.^[6,7] While CO desorbs from the surface as a gas, the O-covered Cu surface has been found to be inactive towards CO₂ adsorption and thus prevent further dissociation.^[8] Even though surface defects in the form of steps may improve this process,^[9] most studies only consider a few, typically high symmetry, Cu surfaces and a narrow pressure range. Consequently, a considerable materials and pressure gap remains to industrially relevant conditions.

To address this, here we employ a curved Cu-sample with variable surface structures (ranging from (111) via (645) to (312)) to study CO₂ dissociation at near ambient pressures (0.01 – 100 mbar). This enables us to independently vary surface orientation, temperature, and pressure over a wide range. We show the presence of different reaction regimes by observing the influence of these parameters on adsorption and dissociation rates. Furthermore, we find changes in how the surface (partially) oxidizes, and identify differently adsorbed CO₂ species. Our efforts provide a novel approach to closing the gap between fundamental research and industrial applications in a controlled and systematic manner.

- [1] E. C. Ra et al., *ACS Catal.*, **10** (2020) 11318.
- [2] L. C. Grabow, M. Mavrikakis, *ACS Catal.*, **1** (2011) 365.
- [3] M. Behrens et al., *Science*, **336** (2012) 893.
- [4] R. M. Palomino et al., *J. Phys. Chem. B*, **122** (2018) 794.
- [5] S. Kattel et al., *Science*, **355** (2017) 1296.
- [6] B. Eren et al., *J. Am. Chem. Soc.*, **138** (2016) 8207.
- [7] M. Favaro et al., *PNAS*, **114** (2017) 6706.
- [8] P. B. Rasmussen et al., *Surf. Sci.*, **269–270** (1992) 352.
- [9] B. Hagmann et al., *J. Am. Chem. Soc.*, **140** (2018) 12974.

Real Time Monitoring of Catalytic Oxidation of CO to CO₂ Over Platinum Surfaces

Marcel Janák¹, Antonín Jaroš¹, Dominik Hruža¹, Miroslav Kolíbal^{1,2}, Tomáš Šikola^{1,2},
Petr Bátor^{1,2}

¹ *Institute of Physical Engineering, Faculty of Mechanical Engineering, Brno University of Technology, Technická 2896/2, Brno, 616 69, Czech Republic*
(corresponding author: P. Bátor, e-mail: bator@fme.vutbr.cz)

² *CEITEC - Central European Institute of Technology, Brno University of Technology, Brno, 616 00, Czech Republic*

Industrial development in recent decades has raised the importance of CO elimination from various gas product streams. Incomplete fossil fuel combustion in the production and transportation sector is the primary sources of atmospheric CO. Increased CO concentrations in living environments cause oxygen deprivation of the human body vital organs [1]. CO molecules are also an unwanted by-product of hydrogen production from natural gas or other carbon feedstocks (e.g., methanol). Excessive CO feeds to hydrogen fuel cells may cause decay in their electro-generation performance. [2-4]

Platinum group metals (Ru, Rh, Pd, Ir, Pt) are the most widespread catalysts for CO oxidation by O₂. The role of the catalyst is to increase the reaction rate by lowering activation barriers. Although the catalyst remains throughout the reaction unconsumed, structural changes like catalyst sintering, surface faceting, or surface poisoning in long-term runs lead to the catalytic activity lowering. Therefore, reaction mechanism and deactivation mechanism understanding is crucial for designing stable CO catalytic converters with high CO conversion rates.

Many conventional surface science techniques may be employed for heterogeneous catalysis research but not all of them offer sufficient chemical, spatial and temporal resolution. The selection of proper techniques is based on the research objectives. Our study's objective is the dynamics of catalytic CO oxidation over platinum polycrystalline microstructures at high vacuum pressures (10⁻⁵ mbar). In-situ scanning electron microscopy (SEM) and in-situ static secondary ion mass spectrometry (SSIMS) were employed for the real-time observation of gas-phase- and temperature-induced processes on platinum surfaces. Elemental composition changes observed by in-situ SSIMS were compared with work function changes observed by in-situ SEM. Our research demonstrates the abilities of in-situ SSIMS as a powerful technique for the real-time chemical monitoring of surface composition in a flow reactor under fixed conditions. Spatio-temporal patterns of varying surface coverages were observed during distinct catalyst regimes in both instruments (see Figure 1 and Figure 2).

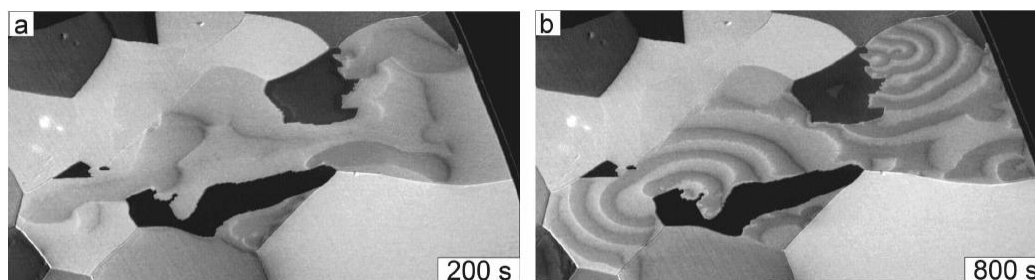


Figure 1 Temporal evolution of rotating spirals on Pt(4,1,10) surface at $T = 170\text{ }^{\circ}\text{C}$ observed by UHV-SEM TESCAN, $p_{\text{CO}} = 3.0 \cdot 10^{-4}\text{ Pa}$, $p_{\text{O}_2} = 1.5 \cdot 10^{-3}\text{ Pa}$. Bright areas are covered by CO; dark areas are covered by oxygen. The figure a) shows the evolution of the waves at the beginning of the experiment and formation of the spiral waves is on the figure b).

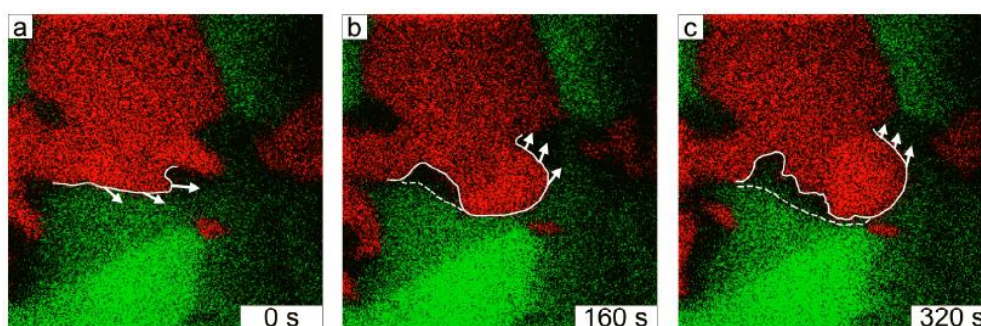


Figure 2 Temporal evolution of patterns observed on an active Pt(4,1,10) grain at $T = 170^{\circ}\text{C}$, $p_{\text{CO}} = 3.0 \cdot 10^{-4}\text{ Pa}$, $p_{\text{O}_2} = 1.5 \cdot 10^{-3}\text{ Pa}$ measured by TOF-SIMS5 IONTOF on the same Pt grain line in the Figure 1. A full white line highlights the moving wavefront; white arrows indicate the direction in which the wave proceeds between frames; a dashed white line delimits the area without chemisorbed reactants.

CzechNanoLab project LM2018110 funded by MEYS CR is gratefully acknowledged for the financial support of the measurements at CEITEC Nano Research Infrastructure.

- [1] Kinoshita, H.; Türkan, H.; Vucinic, S.; Naqvi, S.; Bedair, R.; Rezaee, R.; Tsatsakis, Toxicol. Rep. 2020; 7, 169-173.
- [2] Garzia, G.; Koper, M. T. M., ChemPhysChem 2011; 12 (11), 2064-2072.
- [3] Oh, S. H., Sinkevitch, R. M., J. Catal. 1993; 142 (1), 254-262.
- [4] Holton, O. T.; Stevenson, J. W., Platinum Metals Rev. 2013; 57 (4), 259-271.

Reaction driven ordering of the surface of a PtRh alloy model catalyst

H. Edström,¹ U. Hejral,¹ S. Albertin,¹ K. von Allmen,¹ B. Hagman,¹ E. Lundgren,¹
A. Schaefer,² A. Stierle,³ V. Vonk,³ L. Jacobse,³ X. Deng,³ C. Seitz,³ S. Geile,³
U. Lienert,³ T. Müller,³ Z. Hegedűs,³ S. Gutschmidt,³ and J. Gustafson¹

¹*Synchrotron Radiation Research, Lund University, Box 118, SE-221 00 Lund, Sweden*
(corresponding author: H. Edström, email: helen.edstrom@sljus.lu.se)

²*Department of Physics and Competence Centre for Catalysis,*

Chalmers University of Technology, SE-412 96 Gothenburg, Sweden

³*Deutsches Elektronen-Synchrotron (DESY), D-226 03 Hamburg, Germany*

During an X-ray diffraction study of CO oxidation over a Pt₂₅Rh₇₅(100) single crystal, an unexpected c(2 × 2) structure emerged, indicating that not only the adsorbate is important, but also the near-surface layers.

It has been shown that platinum group metals, such as Pt and Rh, are efficient oxidation catalysts [1, 2]. These two metals can with advantage be combined in a bimetallic alloy to improve the catalytic activity and selectivity, thermal stability, and make it more poison resistant compared to the pure metals [3]. Previous studies on PtRh(100) single crystals have shown that mildly oxidizing conditions cause a p(3 × 1) reconstruction with chemisorbed O to form [1, 4–8], while strongly oxidizing conditions entail a c(8 × 2) surface oxide [1, 4, 9]. Despite being well-studied, the PtRh system is not fully understood.

To gain a better understanding of this alloy system, we have studied CO oxidation over a Pt₂₅Rh₇₅(100) single crystal using high-energy surface X-ray diffraction (HESXRD) under reaction conditions. The study was performed at the beamline P21.2 at PETRA III, DESY, in Hamburg, Germany. Under oxidizing conditions, we found the two Rh–O structures mentioned in the previous paragraph. However, under reducing conditions and elevated temperature, we found an unexpected c(2 × 2) structure, see Figure 1a where the superstructure rods are indicated with white rings. This structure remained even when changing to more oxidizing conditions (up to CO:O₂ = 5 : 40).

CO adsorbs in a c(2 × 2) pattern on both Pt(100) [10] and Rh(100) [11], and thus we expect CO to adsorb in a c(2 × 2) pattern on Pt₂₅Rh₇₅(100). However, our analysis indicates that not only the adsorbate is contributing to the c(2 × 2) structure, but also the metal atoms in the surface or near-surface layers. There are undulations along the superstructure rods, as seen in Figure 1b, suggesting that more than one layer contributes to the c(2 × 2) structure. The first peak appears at $q_{\perp} \approx 1 \text{ \AA}^{-1}$, which corresponds to a maximum out-of-plane distance of atoms contributing to the c(2 × 2) structure of $\frac{2\pi}{1 \text{ \AA}^{-1}} \approx 6 \text{ \AA}$. This would approximately correspond to the distance between the O atom of the adsorbed CO and the third metal layer, as illustrated in Figure 1c.

The ongoing quantitative analysis, together with DFT calculations, however, suggests that the structure is more complex than this. In this presentation we will provide an update of the current status of the analysis and interpretation.

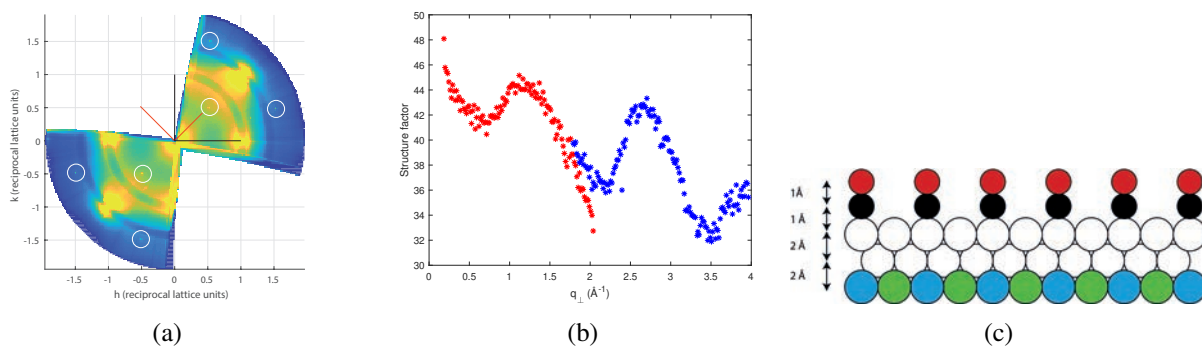


FIG. 1: (a) The HESXRD intensity shown as a projection in the h - k plane. The $c(2 \times 2)$ structure is revealed by the reflections marked with white rings. The black and red lines in the center of the plot mark the (1×1) substrate unit cell and the $c(2 \times 2)$ unit cell, respectively. (b) The structure factor as a function of q_{\perp} value for the $(0.5, 0.5)$ (blue) and $(0.5, 1.5)$ (red) rods. (c) Side view of the first three metal layers and the adsorbed CO.

Support by the Swedish Research Council and the Knut and Alice Wallenberg Foundation is gratefully acknowledged.

-
- [1] J. Gustafson et al., Structure of a thin oxide film on Rh(100), *Phys. Rev. B*, **71**, 1 (2005)
 - [2] J. Gustafson et al., Sensitivity of catalysis to surface structure: The example of CO oxidation on Rh under realistic conditions, *Phys. Rev. B*, **78**, 1 (2008)
 - [3] S. H. Oh and J. E. Carpenter, Platinum-rhodium synergism in three-way automotive catalysts, *J. Cat.*, **98**, 178 (1986)
 - [4] R. Westerström et al., Structure and reactivity of a model catalyst alloy under realistic conditions, *J. Phys. Cond. Mat.*, **20**, 6 (2008)
 - [5] Y. Matsumoto et al., STM studies of a catalytically active $p(3 \times 1)$ Pt-Rh(100) alloy surface, *Surf. Sci.*, **355**, 109 (1996)
 - [6] J. Gustafson et al., The Rh(100)- (3×1) -2O structure, *J. Phys. Condens. Matter*, **24** (2012)
 - [7] J. Gustafson et al., A high pressure x-ray photoelectron spectroscopy study of CO oxidation over Rh(100), *J. Phys. Condens. Matter*, **26** (2014)
 - [8] M. Sporn et al., A quantitative LEED analysis of the oxygen-induced $p(3 \times 1)$ reconstruction of Pt₂₅Rh₇₅(100), *Surf. Sci.*, **416**, 384 (1998)
 - [9] J. Gustafson et al., Structure and catalytic reactivity of Rh oxides, *Cat. Tod.*, **145**, 227 (2009)
 - [10] R. J. Behm et al., The interaction of CO and Pt(100). I. Mechanism of adsorption and Pt phase transition, *J. Chem. Phys.*, **78**, 7437, (1983)
 - [11] A. Baraldi et al., CO adsorption and CO oxidation on Rh(100), *Appl. Surf. Sci.*, **99**, 1 (1996)

Recombination of hydrogen atoms at metal surfaces – A step towards predictive surface chemistry

Dmitriy Borodin¹, Nils Hertl², Florian Nitz¹, Michael Schwarzer¹, Jan Fingerhut¹, Theofanis N. Kitsopoulos^{1,2}, Alec M. Wodtke^{1,2}.

¹ *Institute of Physical Chemistry, Georg-August University Göttingen, 37077 Göttingen, Germany
(corresponding author: Dmitriy Borodin, e-mail: dborodi@gwdg.de)*

² *Max-Planck Institute for Biophysical Chemistry, 37077 Göttingen, Germany*

Transition state theory (TST) is the leading tool for the description of chemical reaction rates. Predictive surface chemistry is limited by the inaccuracy of electronic structure theory and simplifications within TST. For reactions at metal surfaces, which are so important to heterogeneous catalysis, there are few tests of its accuracy against elementary rate constants from experiments. This is mostly because highly accurate experimental data is absent. For example, previously reported rate constants for hydrogen atom recombination at Pt(111) have uncertainties of 3 orders of magnitude[1-4].

Here, we report accurate experimental rate constants for hydrogen atom recombination on Pt(111) and Pt(332) derived from the Velocity Resolved Kinetics[5] method (VRK). VRK combines molecular beam-surface scattering with out-of-plane ion imaging of reaction products, which enables independent determination of reaction kinetics and dynamics.

We also introduce a TST-based model which reproduces experiments with no adjustable parameters over a broad temperature range. The model's key to success is a fully quantum mechanical partition function for the adsorbed H atoms. It accounts for nuclear quantum effects, associated with the light mass of the atom, and electronic quantum effects, associated with the hydrogen atoms electron spin. We note that conventional models for adsorbate partition functions like Harmonic Approximation or Complete Potential Energy Sampling[6] introduce errors of more than one order of magnitude between 300 and 1000 K.

Our modelling efforts are extended to other single crystal metal surfaces and catalytic nanoparticles and we find a general applicability for the model prediction of hydrogen atom recombination rates and adsorbate entropies.

[1]: M. Salmeron, R. J. Gale and G. A. Somorjai, *J. Chem. Phys.* 1979, **70**, 2807.

[2]: G. E. Gdowski, J. A. Fair and R. J. Madix, *Surf. Sci.* 1983, **127**, 541.

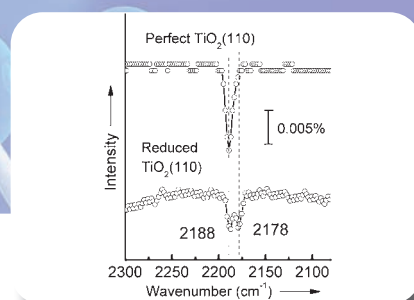
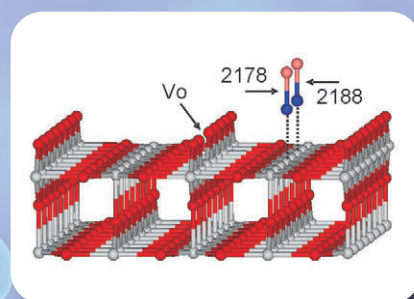
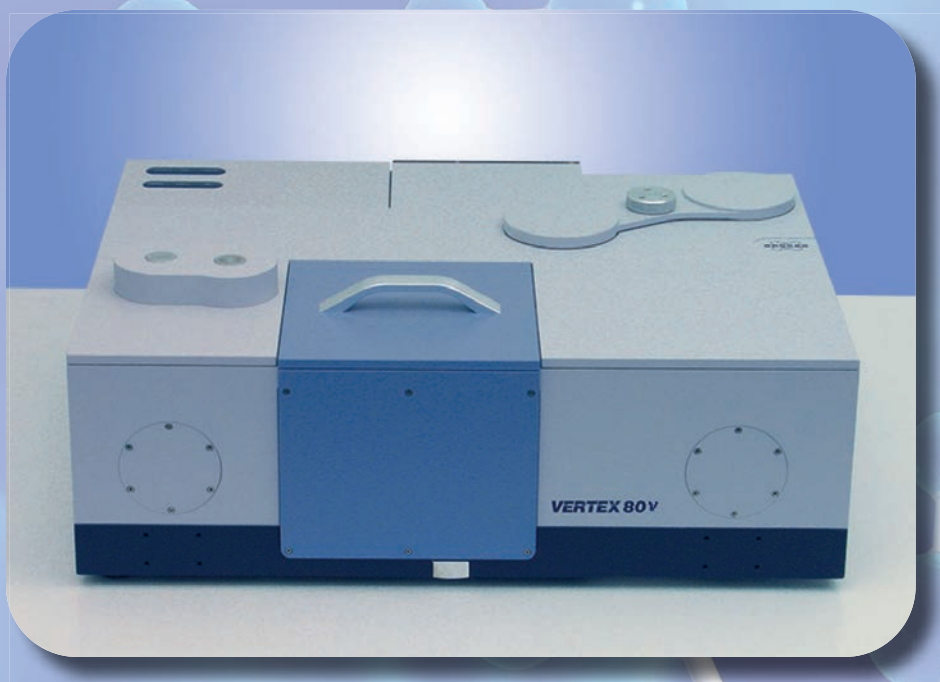
[3]: K. Christman, G. Ertl and T. Pignet, *Surf. Sci.* 1976, **54**, 365.

[4]: van der Niet *et al.*, *J. Chem. Phys.* 2010, **132**, 174705.

[5]: Neugeboren *et al.*, *Nature* 2018, **558**, 280.

[6]: M. Jørgensen and H. Grönbeck, *J. Phys. Chem. C* 2017, **121**, 7199.

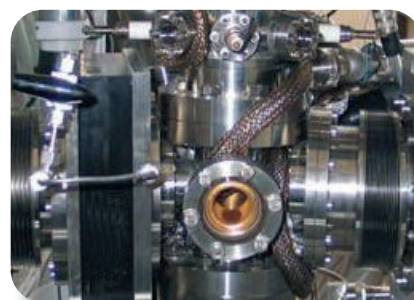
VERTEX 80v



FT-IR in Ultrahigh Vacuum

Bruker's solution for UHV FT-IR combined analysis technique with VERTEX series vacuum spectrometers and customized sample chambers

- Atomic layer deposition
- Investigations of heterogeneous catalysts
- In-situ reaction monitoring under defined conditions with model systems
- Nano- or micro-scale surface modification and functionalization
- Material development



Contact us for more details: www.bruker.com/optics

Bruker Austria GmbH

Lemböckgasse 47b
1230 Wien

Phone: +43 1 804 78 81-0

Fax: +43 1 804 78 81-99

optics.at@bruker.com

Tuesday

2D surface optical reflectance for surface studies in harsh environments

E. Lundgren¹, A. Larsson¹, G. Abbondanza¹,
L. Rämisch², S. Pfaff², S. Gericke², J. Zetterberg²

¹Division of synchrotron radiation research, Lund University, Lund, Sweden,

²Division of combustion physics, Lund University, Lund, Sweden

Edvin.Lundgren@sljus.lu.se

During recent years, 2D Surface Optical Reflectance (2D-SOR) [1,2] microscopy [3] has emerged as a valuable surface characterization tool for model catalysts or electrodes [4] when performing operando investigations in harsh environments. In particular, 2D-SOR microscopy is favorably used as a complementary technique to other photon-in-photon-out techniques which do not carry direct information on the surface 2D morphology. In this presentation we will present the development and examples of 2D-SOR investigations from single and polycrystalline samples in combination with Planar Laser Induced Fluorescence (PLIF) [2, 3], High Energy Surface X-Ray Diffraction (HESXRD) [5,6,7] and Polarization Modulation-Infrared Reflection Absorption Spectroscopy (PM-IRRAS) [8] coupled to Mass Spectrometry (MS) and Cyclic Voltammetry (CV) in thermal catalysis, electrocatalysis and corrosion.

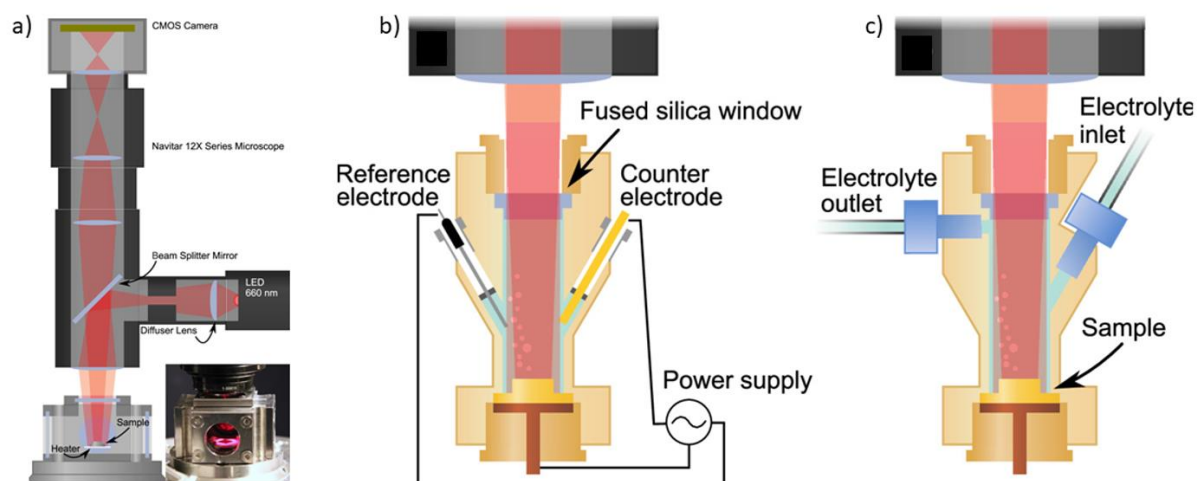


Figure 1: a) The 2D-SOR experimental setup for thermal catalysis. b) Side view of the electrochemical flow-cell showing the electrode configuration. c) Same as b) but rotated 90° to show the inlet and outlets for the electrolyte.

- [1] W. G. Onderwaater et al *Rev. Sci. Instrum.*, **88** (2017) 023704.
- [2] J. Zhou et al, *J. Phys. Chem. C* **121** (2017) 23511.
- [3] S. Pfaff et al, *ACS Appl. Mater. Interfaces* **13** (2021) 19530.
- [4] W. Linpe, et al, E. Lundgren, *Rev. Sci. Instrum.*, **91** (2020) 044101.
- [5] S. Pfaff, et al *Rev. Sci. Instrum.* **90** (2019) 033703.
- [6] S. Albertin, et al, *J. Phys. D: Appl. Phys.* **53** (2020) 224001.
- [7] W. Linpé, et al *J. Electrochem. Soc.* **168** (2021) 096511.
- [8] L. Rämisch et al, *Appl. Surf. Sci.* **578** (2022) 152048.

Real-space imaging of anisotropic atomic charges by means of Kelvin probe force microscopy

B. Mallada¹, A. Gallardo¹, B. de la Torre¹, P. Jelinek¹

*Institute of Physics of the Czech Academy of Sciences, Prague, Czech
(corresponding author: P. Jelinek, e-mail: pavel.jelinek@fzu.cz)*

¹ *Institute of Physics of the Czech Academy of Sciences, Prague, Czech*

An anisotropic charge distribution on individual atoms, such as e.g. σ -hole [1], may strongly affect material and structural properties of systems. Nevertheless, subatomic resolution of such anisotropic charge distributions represents a long-standing experimental challenge. In particular, the existence of the σ -hole on halogen atoms has been demonstrated only indirectly through determination of crystal structures of organic molecules containing halogens or via theoretical calculations [2]. Nevertheless, its direct experimental visualization has not been reported yet. We demonstrate that Kelvin probe force microscopy [3], with a properly functionalized probe, can reach subatomic resolution imaging the σ -hole, as well as a quadrupolar charge of carbon monoxide molecule [4]. This achievement opens new way to characterize biological and chemical systems where anisotropic atomic charges play decisive role.

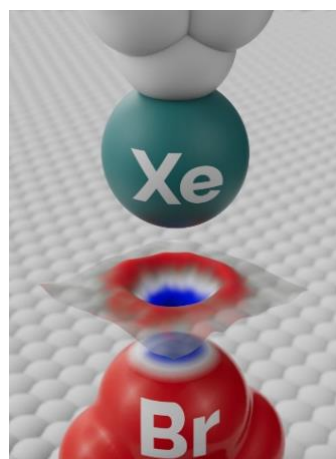


Fig. 1 Schematic view showing the principle of the experiment that made it possible to visualize the sigma-hole on a bromine (Br) atom in a molecule using a specially modified tip of a scanning microscope functionalized with a single xenon (Xe) atom. Top: schematic view of the tip of the scanning microscope with single xenon (Xe) atom. Center: an experimental illustration of the sigma-hole acquired by means of a scanning microscope using the Kelvin probe principle. Bottom: electrostatic potential map depicting the sigma-hole (inhomogeneous atomic charge distribution on a bromine atom), which is formed by a positive charge on top of the atom (blue crown) surrounded by a negative electron plume (red field).

[1] T. Clark, M. Hennemann, J. S. Murray, P. Politzer, *Journal of molecular modeling*, **13**, 291–6 (2007).

[2] L. C. Gilday, et al, *Chemical Reviews*, **115**, 7118–7195 (2015).

[3] T. Glatzel, S. Sadewasser, Eds., *Kelvin Probe Force Microscopy* (Springer International Publishing, 2018), vol. 65.

[4] B. Mallada, et al, *Science* 374 863 – 867 (2021).

A New Cryogen-Free UHV Scanning Probe Microscope with 5K Base Temperature

T. Berghaus¹, Jun Kasai², Tomoki Koyama², Munenori Yokota², and Katsuya Iwaya²

¹ *nanoscore gmbh, Maisebachstr. 3, 61479 Glashütten, Germany*
(corresponding author: T. Berghaus, e-mail: t.berghaus@nanoscore.de)

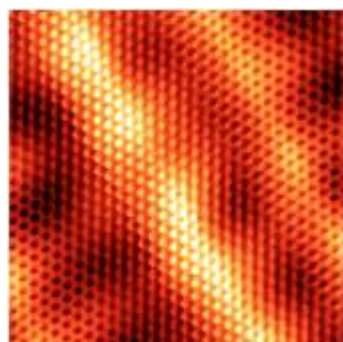
² *UNISOKU Co., Ltd. Hirakata, Osaka 573-0131, Japan*

We present the design of a cryogen-free scanning probe microscopy (SPM) system. Extensive tests have proven the routine capability of high resolution SPM measurements and uninterrupted operation at a base temperature of ~5K. This 5K base temperature paired with a performance comparable to liquid Helium based LT-SPMs is unique and marks the 'step beyond' over the state of the art [1,2,3,4,5,6,7,8].

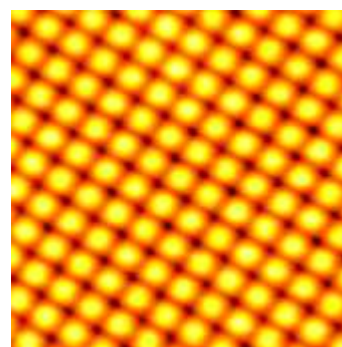
The crucial point of any cryogen-free SPM design is the trade-off between ultimate vibration isolation and most efficient thermal coupling to the cryo cooler. Here we use a pulse tube refrigerator (PTR) [9] with a cooling power of 0.9W at 4.2K. The PTR is split into the cold head and the valve unit, which are interconnected by high pressure tubes and hoses. The valve unit is mounted on a separate, rigid frame. The cold head is mounted on top of the SPMs UHV chamber. Vibration decoupling is realised by a two stage bellows design, and a spring suspension with eddy current damping.

The thermal coupling between the cold head and the SPM head is purely realised by means of He contact gas in series with copper braids. A gas-handling system controls the He exchange gas pressure, facilitating both the fast cool down and maintaining a stable base temperature at the STM stage of 5.2K.

Extensive tests have verified the performance with respect to (i) speed cool down and stability of temperature, (ii) SPM resolution and noise level, (iii) drift stability and spectroscopic performance. The noise level and the resolution capability are comparable to liquid LHe base LT-SPMs:



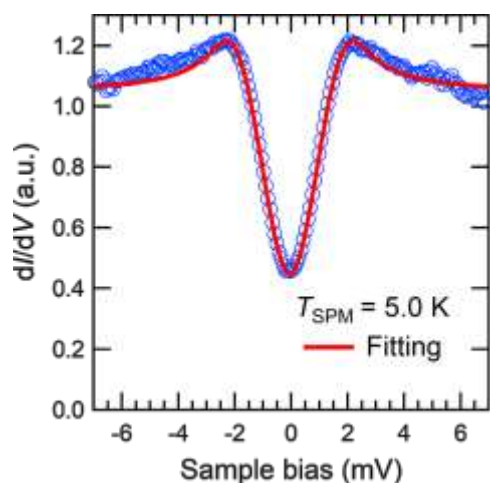
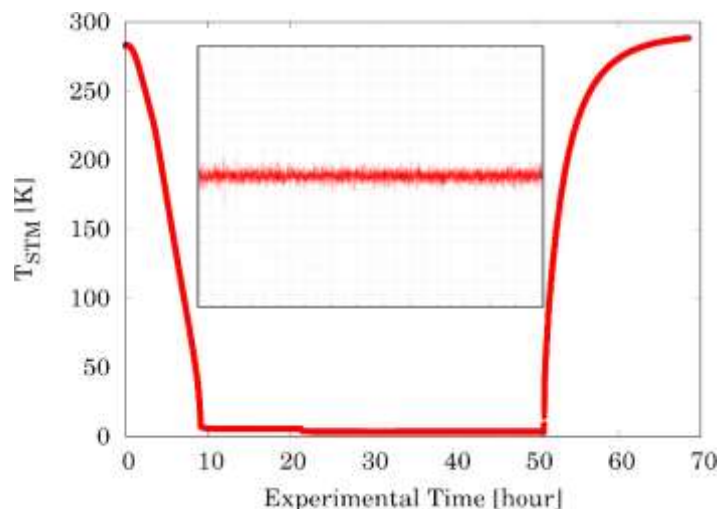
The STM image (left) shows the topography of Au (111) / mica at 5.6K (7nm x 7nm, $V_B = +5\text{mV}$, Tunnel current 1nA).



The AFM image (right) shows the surface of cleaved NaCl (100) detected with q-plus™ sensor ($\Delta f = -13\text{Hz}$, 200pm, $V_B = +1,7\text{V}$).

The corrugation is ~10pm_{pp}. The noise is less than 1pm.

Cool down from RT to stable condition at $\sim 5\text{K}$ is achieved within 12h. The insert shows a remarkable stability of the temperature with a variation of less than 1mK_{rms} over 13h at 5.2K at the STM stage.



The ultimate proof of the true sample temperature is provided by the measurement of a superconducting gap by tunneling spectroscopy. The spectrum (left) was taken on a polycrystalline Pb sample. The fit corresponds to an electronic temperature of 5.7K .

We conclude that the new cryogen-free UHV SPM is a unique instrument with unsurpassed low temperature *and* STM performance. It is manufactured and marketed by UNISOKU as USM1800 *EasyCool* [10].

-
- [1] A. M. J. den Haan, G. H. C. J. Wijts, F. Galli, O. Usenko, G. J. C. van Baarle, D. J. van der Zalm, and T. H. Oosterkamp, *Rev. Sci. Instrum.* 85, 035112 (2014)
 - [2] J. D. Hackley, D. A. Kislitsyn, D. K. Beaman, S. Ulrich, and G. V. Nazin, *Rev. Sci. Instrum.* 85, 103704 (2014)
 - [3] S. Zhang, D. Huang, and S. Wu, *Rev. Sci. Instrum.* 87, 063701 (2016)
 - [4] L. Pabbi, A. R. Binion, R. Banerjee, B. Dusch, C. B. Shoop, and E. W. Hudson, *Rev. Sci. Instrum.* 89, 063703 (2018)
 - [5] W. Meng, J. Wang, Y. Hou, M. Sui, J. Wang, G. Wu, J. Li, and Q. Lu, *Ultramicroscopy* 205, 20 (2019)
 - [6] S. Chaudhary, J. Panda, S. Mundlia, S. Mathimalar, A. Ahmedof, and K. Raman, *Rev. Sci. Instrum.* 92, 023906 (2021)
 - [7] PanScan Freedom, RHK Technology, Inc. USA
 - [8] INFINITY SPM Lab, Scienta Omicron GmbH, Germany
 - [9] RP-082B2S, Sumitomo Heavy Industries, Japan
 - [10] UNISOKU Co., Ltd., Japan, <http://www.unisoku.com/products/usm1800.html>

Laboratory based hard X-ray photoemission spectroscopy

P. Amann^{1,2}, M. Schmid², S. Eriksson¹, P. Palmgren¹, T. Wiell¹, M. Lundwall¹

¹ Scienta Omicron AB, Danmarksgratan 22, 75323 Uppsala, Sweden
(corresponding author: P. Amann, e-mail: peter.amann@scientaomicron.com)

² Scienta Omicron GmbH, Limburger Strasse 75, 65232 Taunusstein, Germany

X-ray photoemission spectroscopy (XPS) is a powerful method to investigate the chemical nature of surfaces. However, the investigation of buried interfaces occurring in, e.g., device electronics is difficult as the energy of the created photoelectrons is not high enough and scattering inside the material bulk limit the detected signal intensity.

During the past decade, increased attention has been shown to hard X-rays in the photoelectron spectroscopy field [1]. This is mainly due to the increased information depth enabled by the higher photon energies. Such bulk sensitive measurements could previously only be performed at dedicated synchrotron radiation facilities. The beam lines providing this type of radiation are heavily booked, so access to the experimental setups is thus limited.

We present a novel product featuring a monochromatized X-ray source creating Ga $K\alpha$ radiation at 9.25 keV and a +/- 30 degrees wide acceptance angle hemispherical electron analyzer, both combined on a simple to use vacuum system (figure 1) [2]. The base system can easily be customized by adding separate modules such as a preparation chamber or a glove box. With this novel base system, a new set of possible experiments opens in the home laboratory: investigations of buried interfaces, in operando devices, real world samples, etc. [3] Such samples or conditions have previously been unattainable with the limited information depth of traditional XPS.

At the heart of the system is a liquid jet of a molten Ga-rich alloy. Electrons which are accelerated into this jet generate an intense Ga $K\alpha$ radiation. These X-rays are monochromatized and refocused using an ellipsoidal mirror in a Rowland geometry. The small spot size of 20 μm provided by the liquid jet source is maintained throughout the passing of the monochromator and only slightly broadened to about 30 x 45 μm^2 . The photon energy width is targeted at 0.45 eV, suitable for the typical intrinsic core level width at the relatively high photon energy. To allow for easy adjustment of the X-ray focal point relative to the electron analyzer, the entire assembly of monochromator and source can be moved down to a precision of a few micrometers. The hemispherical electron analyzer is configured for high kinetic energies allowing for detection of the full energy range the source provides. For increased signal intensity, the Ga X-ray source is positioned at 90° with respect to the analyser length axis and with a grazing incidence- normal emission geometry. Using the

angular mode in combination with the 2D detector, continuous depth information can be obtained. [4]

We present example data taken from polycrystalline gold and silicon wafers as well as from device electronics using bias applied spectroscopy. Examples are further extended towards ambient pressure XPS using HAXPES [5].

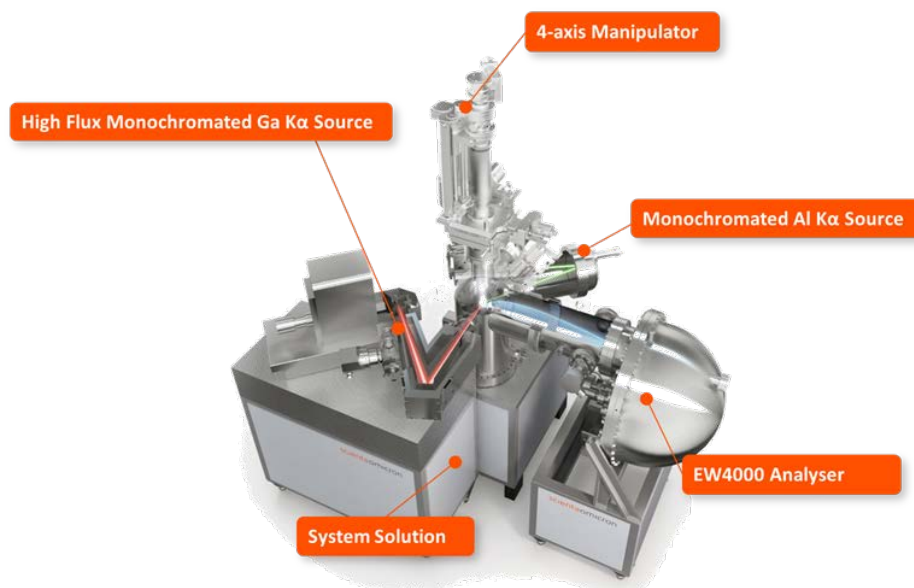


Figure 1: Schematic of the HAXPES Lab including the Ga $K\alpha$ X-ray source, a 4-axis manipulator, the wide acceptance angle analyser EW 4000 and a monochromated Al $K\alpha$ X-ray source.

- [1] C. Kalha, N.K. Fernando, P. Bhatt, F.O.L. Johansson, A. Lindblad, H. Rensmo, L.Z. Medina, R. Lindblad, S. Siol, L.P.H. Jeurgens, C. Cancellieri, K. Rossnagel, K. Medjanik, G. Schonhense, M. Simon, A.X. Gray, S. Nemsak, P. Lomker, C. Schlueter, A. Regoutz, *J. Phys. Condens. Matter* 33 (2021) 233001.
- [2] A. Regoutz, M. Mascheck, T. Wiell, S.K. Eriksson, C. Liljenberg, K. Tetzner, B.A.D. Williamson, D.O. Scanlon, P. Palmgren, *Rev. Sci. Instrum.* 89 (2018).
- [3] T. Hashimoto, P. Amann, A. Regoutz, N. Barrett, L.F.J. Piper, W. Hamouda, O. Renault, M. Lundwall, M. Masatake, *Vac. Surf. Sci.* 64 (2021) 493–498.
- [4] B.F. Spencer, S. Maniyarasu, B.P. Reed, D.J.H. Cant, R. Ahumada-Lazo, A.G. Thomas, C.A. Muryn, M. Maschek, S.K. Eriksson, T. Wiell, T.L. Lee, S. Tougaard, A.G. Shard, W.R. Flavell, *Appl. Surf. Sci.* 541 (2021) 148635.
- [5] P. Amann, D. Degerman, M.-T. Lee, J.D. Alexander, M. Shipilin, H.-Y. Wang, F. Cavalca, M. Weston, J. Gladh, M. Blom, M. Björkhage, P. Löfgren, C. Schlueter, P. Loemker, K. Ederer, W. Drube, H. Noei, J. Zehetner, H. Wentzel, J. Åhlund, A. Nilsson, *Rev. Sci. Instrum.* 90 (2019) 103102.

All-round improved: Innovations for photoexcitation, electron detection and sample handling in high-performance ARPES systems.

T. Stempel, S. Böttcher, S. Mähl, M. Meyer, O. Schaff, and T. Kampen

SPECS Surface Nano Analysis GmbH, Voltastr. 5, 13355 Berlin, Germany

ARPES spectrometers have recently taken a quantum leap in functionality and ease of use due to novel concepts in electron lens systems and more powerful data processing capabilities, massively cutting down the required time of effort of band structure observation and therefore increasing material screening capability. In this contribution we will present our newest development in ARPES spectrometer and high flux UV sources with small spot: The ASTRAIOS 190. This is a 2D momentum mapping electron analyzer with a revolutionary direct k-mapping single spot shifting lens with a virtual entrance slit for ultimate k- and energy resolution.

One of the most important design aspects of the ASTRAIOS is the parallel momentum imaging: the divergent beam of electrons coming from the sample is converted into a perfect parallel bundle of electrons in the entrance plane of the analyzer. This is achieved by focusing the electrons into a sharp spot in the first real space image. A single shifting electrode assembly in this plane can shift the momentum image such that the full momentum space mapping can be performed on the full acceptance cone of the accepted electrons.

With improved detection capabilities, the influence of the excitation source on data quality increases. Reduced spot size with increased photon density becomes a requirement when measuring on small structures and with high k-resolution. With the new μ SIRIUS UV source, we now offer a new laboratory UV source with spot sizes down to 100 μ m and unrivaled photon flux. Together with the possibility of multi line excitation (He, Xe, Kr), the μ SIRIUS source is an excellent alternative to hard-fought synchrotron beam times.

Finally, our new ARPES portfolio is rounded off by the Ganymed sample manipulator series, offering 5-axis precision movement for temperatures from as low as 7K to as high as 1100K even with closed cycle He cooling. This way, SPECS can offer state cutting-edge ARPES performance, which is largely independent of extensive infrastructure.

In this talk, we will introduce the concept, design and performance of the above mentioned equipment, along with exemplary experimental results from installed systems.

SPECS would like to thank Prof. Gerd Schönhense for his contribution to the electron optical design of the ASTRAIOS 190 analyzer.

A Versatile Experimental Platform for Broadband Femtosecond Ellipsometry at ELI Beamlines Facility

M. Rebarz, S. Espinoza, S. Richter¹, O. Herrfurth², M. Zahradnik, J. Andreasson

*ELI Beamlines, Institute of Physics, Czech Academy of Sciences, Prague, Czech Republic
(corresponding author: M. Rebarz, e-mail: mateusz.rebarz@eli-beams.eu)*

¹ *Institutionen för fysik, Linköpings universitet, Linköping, Sweden*

² *Felix-Bloch-Institut für Festkörperphysik, Universität Leipzig, Leipzig, Germany*

Spectroscopic ellipsometry is the method that allows characterization of thin films, surfaces and interfaces. As an optical technique it is contactless and destruction-free and can be used in vacuum, atmospheric or liquid environments. Employment of ultrashort laser pulses in ellipsometry makes this technique suitable to follow ultrafast changes in optical and dielectric constants of the studied materials induced by external electromagnetic excitation. Ellipsometric approach outclasses conventional time-resolved reflectance and transmittance experiments giving unambiguous distinction between the real (refraction) and imaginary (absorption) part of the dielectric function. However, propagation of ultrashort and ultrabroadband pulses through polarizing optics requires special care due to dispersive and chromatic effects. In consequence, obtaining high quality ellipsometric data with fs resolution is challenging and many technical as well as methodological issues have to be addressed.

Here, we present the current status of a versatile experimental platform, located in ELI Beamlines facility in Czech Republic, dedicated to ultrafast pump-probe ellipsometry with time resolution about 100 fs [1]. The whole system is based on 1 kHz Ti:Saph laser which produces fundamental ultrashort (20-35 fs) NIR (800 nm) pulses subsequently transformed into desired pump and probe beams. The setup is devoted to UV-VIS-NIR spectral range and the broadband probe pulses obtained by supercontinuum generation cover 350-1300 nm region. The narrowband pump pulses are produced by optical parametric amplification and can be tuned from 190 nm to 20 μ m. The current capabilities and experimental details of this cutting edge ellipsometric platform will be presented with the example results obtained on the excited semiconductors [2,3,4].

ELI is thought as a user facility open to all scientists. Details of how to submit a proposal to carry on experiments using ELI Beamlines capabilities will be also provided.

Support by the projects Structural dynamics of biomolecular systems (CZ.02.1.01/0.0/0.0/15-003/0000447) and Advanced research using high intensity laser produced photons and particles (CZ.02.1.01/0.0/0.0/16-019/0000789) from the European Regional Development Fund is gratefully acknowledged.

- [1] S. Richter, M. Rebarz, O. Herrfurth, S. Espinoza, R. Schmidt-Grund, J. Andreasson, *Rev. Sci. Instrum.* 92, 033104 (2021)
- [2] S. Richter, O. Herrfurth, S. Espinoza, M. Rebarz, M. Kloz, J.A. Leveillee, A. Schleife, S. Zollner, M. Grundmann, J. Andreasson, R. Schmidt-Grund, *New J. Phys.* 22, 083066 (2020)
- [3] S. Espinoza, S. Richter, M. Rebarz, O. Herrfurth, R. Schmidt-Grund, J. Andreasson, S. Zollner, *Appl. Phys. Lett.* 115, 052105 (2019)
- [4] O. Herrfurth, S. Richter, M. Rebarz, S. Espinoza, J. Zuniga-Perez, C. DeParis, J. Leveillee, A. Schleife, M. Grundmann, J. Andreasson, R. Schmidt-Grund: *Phys. Rev. Res.* 3, 013246 (2021)

Visualization of Ion|Surface Binding, binding energy quantification, and charge regulation in slit geometries

Jinhoon Lee, J. Dziadkowiec, V. Wieser, A.M. Imre, H.-W. Cheng,
P.-L. Bilotto² and M. Valtiner

Institut für Allgemeine Physik, Technische Universität Wien, A-1040 Wien, Austria

(corresponding author: M. Valtiner, e-mail: valtiner@iap.tuwien.ac.at)

²CEST Centre for Electro chemistry and Surface Technology, A-2700 Wienerneustadt, Austria

Function and properties at biologic as well as technological interfaces are controlled by a complex and concerted competition of specific and unspecific binding with ions and water in the electrolyte. It is not possible to date to directly estimate by experiment the interfacial binding energies of involved species in a consistent approach, thus limiting our understanding of how interactions in complex (physiologic) media are moderated. Further, ion binding has a string influence on transport of ions in molecular-scale confined spaces is central to all aspects of life and technology: into a crack, it may break steel within days; through a membrane separator, it determines the efficiency of electrochemical energy conversion devices; or through lipid membranes, it steers neural communication. Yet, the direct observation of ion mobility and structuring in sub-nanometer confinement is experimentally challenging and, so far, solely accessible to molecular simulations.

Here, we will first discuss a model system utilizing polymers with end grafted amines interacting with a negatively charged mica surface and will show how ion interactions can be quantified.[1] Therefore, we measure interaction forces as a function of the molecule density and ion concentration in NaCl solutions and demonstrate by molecular resolution imaging how ions increasingly populate the binding surface at elevated concentrations, and are effectively competing with the functional group for a binding site. We demonstrate that a competing Langmuir isotherm model can describe this concentration-dependent competition. Further, based on this model we can quantitatively estimate ion binding energies, as well as binding energy relationships at a complex solidliquid interface. Our approach enables the extraction of thermodynamic interaction energies and kinetic parameters of ionic species during monolayer level interactions at a solidliquid interface, which to-date is impossible with other techniques.

Second, we discuss quantitative, 3D molecularly-resolved ion transportation of aqueous ionic liquid and s-block metal ion solutions, confined to electrochemically-modulated, molecular-sized slits.[2] Our analysis of atomically resolved solid/liquid interface unveils generic rules of how enthalpic ion-ion and ion-surface interactions and entropic confinement effects determine the charge regulation mechanism. We demonstrate that confined charge regulation

can proceed via fast, kinetically favoured, metastable pathways, followed by slow diffusive thermodynamic ion reorganization, which has important implications for all charge-regulated systems.

[1] *ACS Phys. Chem Au* 2021, 1, 1, 45–53, August 23, 2021

[2] <https://arxiv.org/abs/2104.01157>

Magnetic switching driven by stochastic resonance in multiferroic (Ge,Mn)Te

Juraj Krempasky¹, Jan Minar², Martin Gmitra³, Gunther Springholz⁴, and Hugo Dil^{1,5}

¹Photon Science Division, Paul Scherrer Institut, Villigen, Switzerland

²New Technologies-Research Center, University of West Bohemia, Plzeň, Czech Republic

³Institute of Physics, P. J. Šafárik University in Košice, Slovakia

⁴Institut für Halbleiter-und Festkörperphysik, Johannes Kepler Universität, Linz, Austria

⁵Institute of Physics, Ecole Polytechnique Fédérale de Lausanne, Switzerland

(corresponding author: H. Dil, e-mail: hugo.dil@epfl.ch)

The interplay between spin-orbit interaction (SOI) and magnetic order is currently one of the most active research fields in condensed matter physics. In a basic sense one can say that SOI adds dynamics to the static real space spin order determined by exchange interaction, or that magnetism adds a real space component and stability to the reciprocal space spin structures induced by SOI. Famous examples of this interplay are skyrmions and spin waves, but also the search for Majorana zero modes and magnetic topological insulators fit directly in this field and have gained much attention in recent years. Furthermore, the ultrafast magnetic switching observed in simple magnets is suggested to be driven by the presence of spin-orbit interaction.

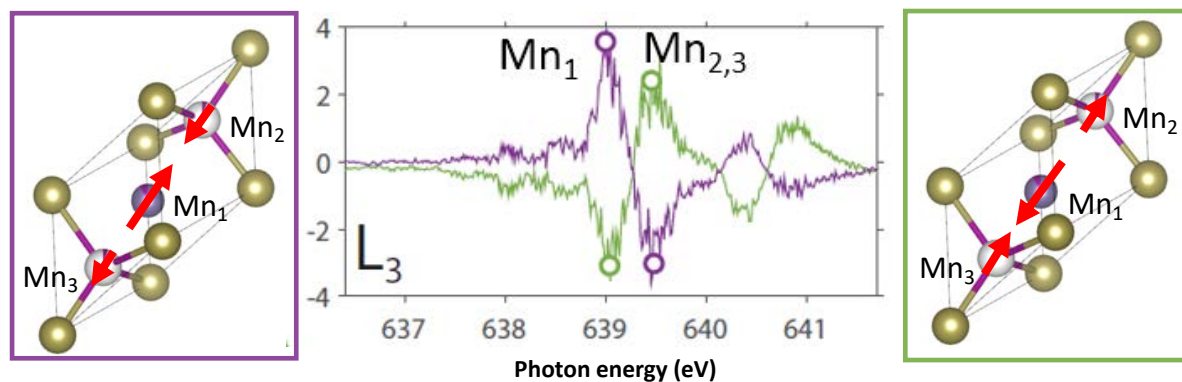
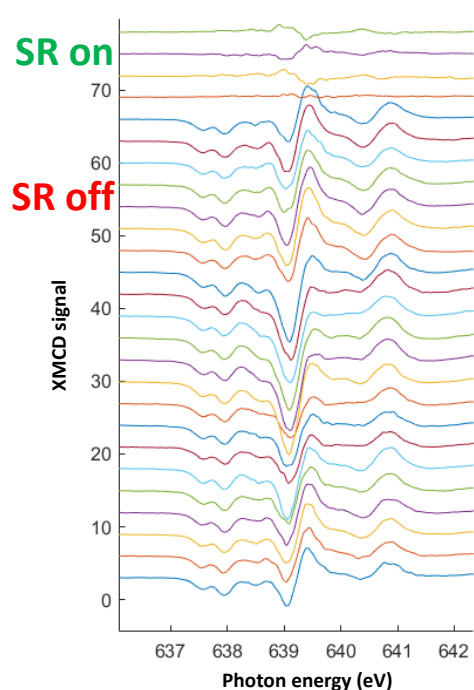


Figure 1 XMCD signal on the Mn L3 edge and ferrimagnetic atomic configuration for two switched states indicated by different colours.

The full spectrum of possibilities is unleashed in combination with breaking the symmetry of the system, either at interfaces or in the crystal structure itself. This makes multiferroic materials, where symmetry breaking in the form of ferroelectric order and magnetic order coexist, a promising playground to look for functional properties combining SOI and magnetism. Here we will show that starting from a ferroelectric system with strong spin orbit interaction and doping this with magnetic impurities is indeed a promising pathway to achieve magnetic order with tuneable dynamics. Furthermore, the switching mechanism in the resulting ferrimagnetic system will be explained based on stochastic resonance (SR).

With only two atoms per unit cell α -GeTe is arguably the simplest room temperature ferroelectric semiconductor. The combination of the ferroelectric order and large SOI yields a switchable Rashba-type spin structure of the bulk states [1, 2], whereby the states are fully spin polarised around the valance band maximum [3]. When doped with up to 20% Mn a magnetic order is induced while the ferroelectric order remains present, rendering it a multiferroic material [4]. Moreover, the strong magnetoelectric coupling in the system [2] ensures a colinear alignment of the magnetisation and polarisation axes, resulting in the opening of a Zeeman gap in the Rashba split bands around the Brillouin zone centre [5]. This unique combination of properties creates a large bulk Rashba-Edelstein effect and allows for current driven magnetisation switching [6].



Here we will present X-ray magnetic circular dichroism (XMCD) results supported by SPR-KKR-CPA and magnetic cluster calculations. In accordance with our previous resonant ARPES results [5] we find that the Mn atoms occupy two distinct lattice sites; substituting Ge (site 1) and interstitial positions (2 and 3). As illustrated in Figure 1 these sites are antiferromagnetically coupled, but with slightly different magnetic moments, resulting in a ferrimagnetic order for the full system.

One of the astonishing results is that the system spontaneously switches its magnetisation direction without changing any of the typical external parameters, as shown by the different colours in Figure 1. This switching occurs independent of whether the light helicity is alternated, of applied magnetic field (up to 4 T), of temperature (up to 65 K), and of previous treatments like field cooling. This switching can be explained by stochastic resonance as evidenced by the fact that the switching stops when the resonance conditions are turned off, as illustrated in Figure 2. It will be shown that the occurrence of this SR is closely related to the formation of topological spin textures in the films. Finally the nature of the SR and its use in magnetic switching in a correlated spin glass like (Ge,Mn)Te will be discussed.

- [1] D. Di Sante, P. Barone, R. Bertacco, and S. Picozzi, *Advanced Materials* 25, 509 (2013).
- [2] J. Krempasky et al. *Physical Review X* 8, 021067 (2018).
- [3] J. Krempasky et al. *Physical Review Research* 2, 013107 (2020).
- [4] H. Przybylinska, G. Springholz, et al. *Phys. Rev. Lett.* 112, 047202 (2014).
- [5] J. Krempasky et al. *Nature Communications* 7, 13071 (2016).
- [6] R. Yoshimi et al. *Science Advances* 4 (2018) 10.1126/sciadv.aat9989

From tellurized surfaces towards telluride films: Te on Cu(111) and Pt(111)

M. A. Schneider, T. Kießlinger, A. Schewski, A. Raabgrund, and L. Hammer

*Lehrstuhl für Festkörperphysik, Friedrich-Alexander Universität Erlangen-Nürnberg (FAU), Germany
(corresponding author: M. A. Schneider, e-mail: alexander.schneider@fau.de)*

Transition metal chalcogenides (TMCs) are a fascinating class of materials which received a lot of attention as 2D solids “beyond graphene”. The transition metal tellurides are no exception. They are used as phase-change materials in rewritable DVDs, as thermoelectric materials with a high figure of merit, and as high-efficiency solar cells, etc. In the thin film limit of the materials, effects induced by the topology of the electronic states are of interest. Particularly the dichalcogenides are promising as they form van der Waals stacked crystals with a natural two-dimensionality when exfoliated.

Similarly to the growth of oxide films, the tellurization of metal surfaces or thin metal films on suitable substrates in ultra-high vacuum is a way forward to make the tellurides accessible to surface science methods and maybe even provide scalable production methods. Hence, the stakes are high and the fruits seem low-hanging. However, Te is an element with very variable bonding configurations and therefore it is paramount that the grown films are properly characterized in terms of their crystalline (surface) structure. We demonstrate that a structural analysis solely based on STM imaging and DFT calculations can be misleading and – not surprisingly – this is healed by the inclusion of quantitative LEED-IV into a powerful triple.

We formed surface tellurides by depositing Te on the Cu(111) surface and subsequent annealing. We find (depending on Te content) chain like $(3 \times \sqrt{3})_{\text{rect}}$ and $(5 \times \sqrt{3})_{\text{rect}}$ phases [1, 2]. The structure of these is determined by LEED-IV analyses with Pendry R-factors of $R_P = 0.10$ ($(3 \times \sqrt{3})_{\text{rect}}$) and $R_P = 0.17$ ($(5 \times \sqrt{3})_{\text{rect}}$). The latter is a complex structure (dubbed ad-chain-and-trough model, Fig. 1 (a) and (b)) that involves a missing-row substrate reconstruction and sheds light to some limitations of the LEED-IV model calculations. Nevertheless, other potential models can be clearly discarded and the structural parameters, perfectly confirmed by DFT calculations, are determined with accuracy better than 5 pm. Experiment and theory show that these structures are neither a CuTe_2 honeycomb layer [3] nor a Te_2 ad-chain structure [4] as inferred from STM and DFT alone.

On Pt(111) at a Te coverage $\theta = 4/9$ ML a surface telluride (3×3) structure is formed (Fig. 1 (c)). This structure is a buckled, hexagonal Te overlayer which however is formed by severe reconstructions of the Pt surface. Therefore it is not a simple adatom structure. Again LEED-IV ($R_P = 0.14$) and DFT agree perfectly on the parameters of the crystal structure with single picometer accuracy, alternative models can clearly be discarded based on their much larger R_P values. Particularly, this surface structure is not a “patterned” PtTe_2 film as claimed

[5]. Here, the fallacy of a structural analysis based on STM and DFT becomes very obvious. By DFT structural relaxation the model of [5] is found to be a stable (local) minimal energy structure that also reproduces the appearance in STM images. Without a cross-check with an independent (diffraction) method and a careful characterization of the Te content in the film, the true surface structure could not be detected.

These complex surface tellurides set the scene for the growth of thicker telluride films. With increasing Te coverage, homogeneous nanometer thick films can be prepared on Cu(111) and Pt(111) by simple annealing in UHV. However, the thicker films are not di-telluride films as maybe anticipated, and show various surface reconstructions. I will report of the ongoing quest to unravel the structure of the thicker telluride films on Cu(111) and Pt(111).

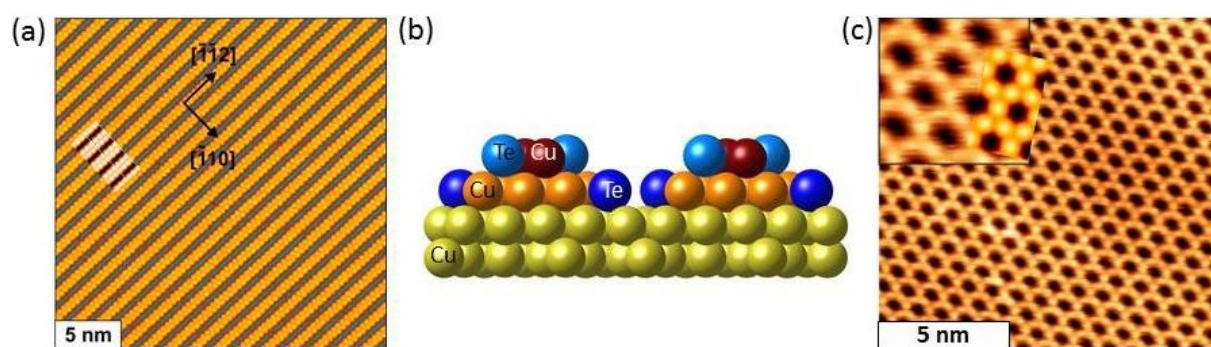


Figure 1: (a) STM image and DFT simulation and (b) structural model of the ad-chain-and-trough structure $\text{Cu}(111)-(5 \times \sqrt{3})_{\text{rect}}$ at $\theta = 0.4$ ML Te coverage. (c) The $\text{Pt}(111)-(3 \times 3)4\text{Te}$ Kagome network: STM and DFT simulation.

We gratefully acknowledge supply of computing resources and support provided by the Erlangen Regional Computing Center (RRZE).

- [1] T. Kißlinger, et al., Phys. Rev. B **102**, 155422 (2020)
- [2] T. Kißlinger, M.A. Schneider, L. Hammer, Phys. Rev. B **104**, 155426 (2021)
- [3] Y. Tong, et al., 2D Materials **7**, 035010 (2020).
- [4] D. Zhou, et al., Appl. Phys. Lett. **116**, 061602 (2020)
- [5] L. Liu et al., 2D Mater. **8** 045033 (2021)

Decoupling of TaS₂ single-layer from its Au(111) substrate by alkali intercalation

X. Weng, P. David¹, V. Guisset¹, O. Geaymond¹, L. Martinelli¹, J. Coraux¹, and G. Renaud

Université Grenoble Alpes & IRIG/DEPHY/MEM/NRS CEA, Grenoble, France

(Corresponding author: G. Renaud, e-mail: gilles.renaud@cea.fr)

¹*Université Grenoble Alpes & Institut NEEL CNRS/UGA UPR2940, Grenoble, France*

2D transition-metal dichalcogenides (TMDCs) such as TaS₂ have many potential applications in *e.g.* electronics, optoelectronics and spintronics. Bulk TaS₂ undergoes electronic instabilities towards charge density waves and superconductivity, whose persistence at the 2D limit, where the substrate can play a role^[1], is an open question. Here, we focus on the growth of a TaS₂ single layer (SL) on a metallic substrate, Au(111). The material can be grown using a Ta atomic beam in a few 10⁻⁶ mbar H₂S partial pressure. Yet several phases, TaS and TaS₂, which may have similar appearance with Scanning Tunneling Microscopy (STM), can coexist on the surface^[2]. Therefore it is insightful to finely characterize the structure of the material, which has been done already with using a variety of techniques^[1,2], among which X-ray standing waves, angle-resolved photoemission spectroscopy, STM and *ab initio* simulations.

Here we present a high-resolution grazing incidence X-ray diffraction (GIXRD) study, that allows to map the reciprocal space and analyze the strain state of the monolayer Ta-S compounds. We analyze how one compound transforms into the other (TaS vs TaS₂), and the relationship between the composition and the decoupling / recoupling with the Au substrate respectively induced by intercalation / de-intercalation of monolayer alkali atoms (Cs and Li)

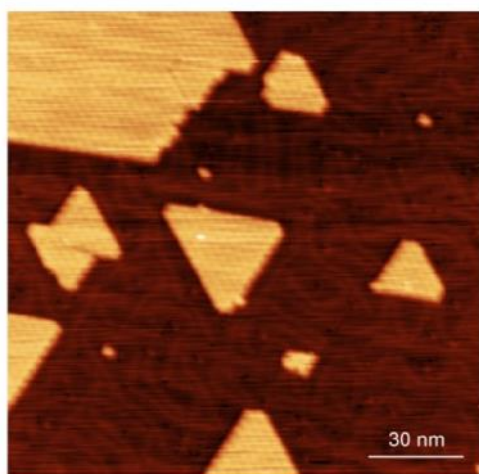


Fig.1: STM of TaS_x grown on an Au(111) substrate. TaS_x flakes are in yellow with the moiré appearing as darker hexagonally arranged dots. The substrate is dark, with the herringbone reconstruction appearing lighter.

STM (Fig. 1) evidence triangular sulfide 2D flakes the Au(111) surface, and the herringbone reconstruction in between. A moiré is evidenced both by STM and reflection high-energy

electron diffraction (RHEED). Grazing Incidence high-resolution X-Ray Diffraction (GIXRD) performed at the European Synchrotron (ESRF, BM32 beamline) provides more detailed structural information. In Fig.2, radial scans along the (100) direction show the structural evolution before, during and after intercalation using Cs. They evidence a highly oriented epitaxy of the tantalum sulfide(s) layer on Au(111) together with satellites that sign the presence of a moiré due to a strong coupling between the 2D layer and Au. These satellites disappear upon intercalation, demonstrating a decoupling between the 2D layer and its substrate. Meanwhile, the herringbone structure becomes more intense and less ordered. The sulfide diffraction peaks evolution upon Cs intercalation shows that the its lattice becomes more regular and is expanded. An analysis of the lineshape of the sulfide Bragg peaks informs on the fraction of the material that is decoupled from Au *via* intercalation. Remarkably, the decoupling can be reversed during annealing under H₂S, which leads to a re-appearance of the moiré diffraction pattern. With several cycles of intercalation and de-intercalation, the evolution of the sulfide lattice parameter is interpreted as being related to the co-existence of TaS and TaS₂ and the transition between these two phases. We will discuss the appearance, under adequate conditions, of an additional 2D super-lattice, which might be interpreted as a charge density wave like modulation of the moiré that was not mentioned in any previous study.

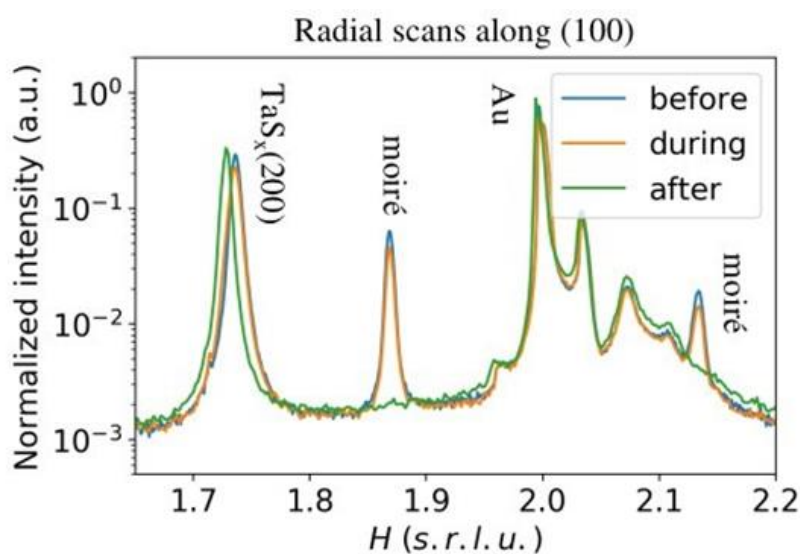


Fig.2: GIXRD radial scan measurements around the (200) Au peak of a TaS_x layer on Au(111) before (blue line), during (orange) and after (green) the Cs intercalation. The scattering intensities are plotted v.s. h in Au(111) surface reciprocal lattice units.

- [1] Sanders *et.al.* Phys. Rev. B. **94** 081404(R) (2016)
- [2] Caio C. Silva *et.al.* Phys. Rev. B. **104**, 205414 (2021)

Modeling the sputtering processes on the surface of Mercury in the laboratory

H. Biber, P. S. Szabo*, N. Jäggi¹, C. Cupak, J. Brötzner, A. Nenning², A. Galli¹, P. Wurzl¹, and F. Aumayr

*Institute of Applied Physics, TU Wien, A-1040 Vienna, Austria
(corresponding author: H. Biber, email: biber@iap.tuwien.ac.at)*

¹ *Physics Institute, University of Bern, CH-3012 Bern, Switzerland*

² *Institute of Chemical Technologies and Analytics, TU Wien, A-1040 Vienna, Austria*

* *Current address: Space Sciences Laboratory, University of California, CA 94720 Berkeley, USA*

Our solar system is a harsh environment. Planets and other objects are continuously exposed to energetic radiation. Micro-meteorites and ions originating from the Sun - the solar wind - impinge on the surfaces of celestial bodies' while sunlight leads to thermal and photon-stimulated desorption. The term space weathering [1] sums up those effects, which constantly alter the bodies' surfaces if not protected by an atmosphere. In addition to this alteration, emitted particles lead to the formation of a layer with increased particle density around planets and moons, the so-called exosphere [2]. Its exact properties are heavily dependent on the characteristics of the emission processes. The contribution of sputtering by the solar wind to the exosphere formation is expected to be significant. Its modeling therefore relies on correct sputtering data as input. With the high complexity of a planet's surface, costly experiments are not feasible for all expected scenarios. Therefore, numerical simulations have to be used to determine the effect of sputtering on rocky bodies in space. Often, two different types of simulations are used. Molecular Dynamic (MD) simulations can deliver precise results, but are tedious to implement and computationally demanding. In contrast, Binary Collision Approximation (BCA) codes are simpler to carry out and much faster in execution. Experimental investigations however have shown that input parameters like the surface binding energy of oxygen have to be adapted to get reasonable agreement between simulations and experimental results (see Figure 1) [3]. Benchmarking of simulation results with experiments is therefore required.

When investigating dynamic effects in the laboratory, thin films deposited on Quartz Crystal Microbalances (QCM) are of advantage, as they allow real time measurements of mass changes during irradiations [4]. Furthermore, they can be used to determine mass changes during Temperature Programmed Desorption (TPD) measurements after ion beam experiments in situ [5]. Mineral based samples used for studying the interaction of ions with the hermean surface are usually transferred onto QCMs by means of Pulsed Laser Deposition (PLD), forming an amorphous layer [3][6]. We have recently upgraded our experimental setup at TU Wien to compare the sputtering of thin films and bulk samples. This is done by placing a second QCM, called catcher QCM (C-QCM), in the direct vicinity of the irradiated sample. It faces the primary sample holder and can be moved in a circular arc around it. During ion beam irradiations, sputtered material is deposited on the C-QCM, which can be measured again in situ and in real time.

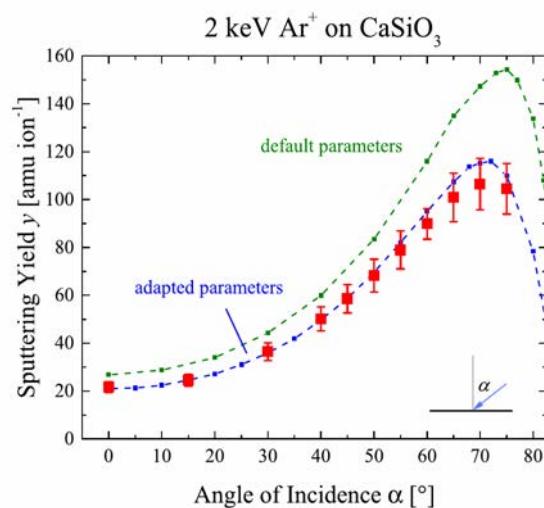


Figure 1: Comparison of different SDTrimSP simulations with experimental results (red) for 2 keV Ar^+ sputtering yields. Default parameters (green) overestimate the measured yields, while the adapted parameters (blue) give a better agreement. Figure taken from [3].

Measurements are performed with the silicates wollastonite (CaSiO_3) and enstatite (MgSiO_3) as analogs for the surface of the planet Mercury. In both cases ion beam analysis shows that the stoichiometry of the minerals is preserved in the thin films. Furthermore, pressed mineral pellets are mounted in the same sample holder as a system more representative for the surface of a rocky planet [7]. This setup allows C-QCM measurements of both samples alternately. The absolute sputter yields can be directly measured for the irradiated films on the primary QCM. Due to the same stoichiometry of the pellet and the thin film, this can be used as a reference to also calculate sputter yields of the pressed pellets together with the C-QCM signal. To evaluate the sputtering of the different sample types from these data, the contribution of surface roughness has to be taken into account. This property is known to influence the sputtering properties upon ion impact significantly [8]. We therefore perform Atomic Force Microscopy (AFM) and combine it with 3D sputtering simulations to evaluate this effect [9]. By doing so, it is possible to untangle the influence of roughness and evaluate the intrinsic sputtering yield of the pressed mineral samples.

This work was funded by the Austrian Science Fund FWF (Project No. I 4101-N36) as well as the Swiss National Science Foundation Fund (200021L_182771/1).

- [1] Hapke B.: *J. Geophys. Res. Planet.*, 106, 10039, (2001)
- [2] Wurz P., et al.: *Planet. Space Sci.*, 58, 1599, (2010)
- [3] Szabo P. S., et al.: *Astrophys. J.*, 891, 100, (2020)
- [4] Hayderer G., et al.: *Rev. Sci. Instrum.*, 70, 3696, (1999)
- [5] Biber H., et al.: *Nucl. Instrum. Methods Phys. Res. B*, 480, 10, (2020)
- [6] Hijazi H., et al.: *J. Geophys. Res. Planets*, 122, 1597, (2017)
- [7] Jäggi N., et al.: *Icarus*, 365, 114492, (2021)
- [8] Küstner M., et al.: *Nucl. Instrum. Methods Phys. Res. B*, 145, 320, (1998)
- [9] Cupak C., et al.: *Appl. Surf. Sci.*, 570, 151204, (2021)

Wednesday

First-Principles based Modelling of Electrocatalysis Beyond the Potential of Zero Charge

K. Reuter

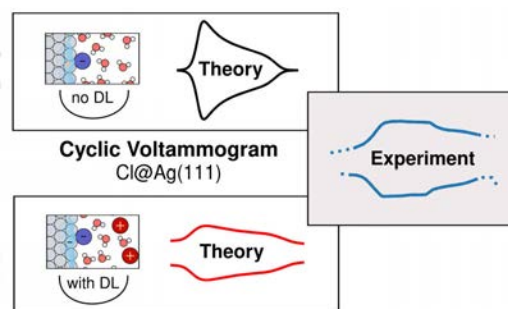
*Fritz-Haber-Institut der Max-Planck-Gesellschaft, Faradayweg 4-6, D-14195 Berlin, Germany
(corresponding author: K. Reuter, e-mail: reuter@fhi.mpg.de)*

Electrocatalytic processes gain an ever-increasing importance for a future sustainable energy system. Electrolytic generation of hydrogen, electroreduction of CO₂ to synthetic fuels or the reverse fuel cell processes are key components for the required storage, transport and provision of energy on a global scale. Unfortunately, the transition to corresponding energy technologies is still largely impeded by insufficient efficiencies or stabilities of hitherto employed materials or devices. Many of these limitations arise at the involved solid-liquid interfaces, which often undergo strong structural and compositional changes in the operating device. Such operando evolution presents already a severe challenge to the predictive-quality modeling and simulation of working thermal catalysts [1]. In interfacial electrocatalysis, this is further aggravated by the simultaneous need to reliably capture solvent dynamics and the long-range electrostatics in the diffuse double layer (DL). The present state-of-the-art is therefore largely characterized by harsh approximations. Operando evolution is generally not treated, solvation effects are often ignored and the applied bias at best considered through thermodynamic potentials. In particular, the prevalent computational hydrogen electrode (CHE) approach considers the surface electronic structure to constantly remain at the potential of zero charge (PZC) and therefore precludes capacitive charging effects by construction.

In recent years, implicit solvation approaches have experienced a renaissance in the context of interfacial electrochemistry [2]. Originating in molecular chemistry with finite solutes, implicit solvation is a most efficient, highly coarse-grained ansatz that accounts for a surrounding liquid electrolyte on the level of a continuous polarizable medium. In the context of first-principles modeling of electrochemistry and electrocatalysis at extended (often metallic) electrodes it primarily allows to introduce counter charges in the electrolyte and therefore enables an explicit charging of the surface slab, while maintaining the overall charge neutrality of the periodic boundary condition supercell. Notably, implicit solvation thus opens the door to mimic a polarization of the electrode's electronic density under the applied potential and the concomitant capacitive charging of the entire double layer beyond the limitations of the employed density-functional theory supercell.

In this talk, I will tutorially introduce the concept of such fully-grand canonical (FGC) calculations [3], highlighting in particular its use in the widespread *ab initio* thermodynamics approach to surface catalysis. Specifically, I will discuss the application to compute

thermodynamic cyclic voltammograms (CVs) and demonstrate that only FGC calculations are able to capture non-Nernstian peak shifts and other DL-effects on the CV shape [4]. Relevant for catalysis is in particular the ability to predict potential-induced variations of adsorption energies and concomitant changes of preferred adsorption sites under applied bias.



Financial support through the EuroTech Postdoc Programme and through the Deutsche Forschungsgemeinschaft (DFG, German Research Foundation) under Germany's Excellence Strategy - EXC 2089/1- 390776260 is gratefully acknowledged. Computing time was provided through the John von Neumann Institute for Computing (NIC) on the GCS Supercomputer JUWELS at Jülich Supercomputing Centre (JSC).

- [1] A. Bruix, J.T. Margraf, M. Andersen, and K. Reuter, *Nature Catal.* 2, 659 (2019).
- [2] S. Ringe, N.G. Hörmann, H. Oberhofer, and K. Reuter, *Chem. Rev.* (in press); <https://pubs.acs.org/doi/abs/10.1021/acs.chemrev.1c00675>
- [3] N.G. Hoermann, N. Marzari, and K. Reuter, *npj Comp. Mat.* 6, 136 (2020).
- [4] N.G. Hörmann and K. Reuter, *J. Chem. Theory Comput.* 17, 1782 (2021); *J. Phys. Condens. Matter* 33, 264004 (2021).

Cu(111) reconstruction and oxidation in oxygen free alkaline media imaged with electrochemical STM

Andrea Auer, Toni Moser, and Julia Kunze-Liebhäuser

*Institute of Physical Chemistry, University of Innsbruck, Innrain 52c, Innsbruck, 6020, Austria
(corresponding author: J. Kunze-Liebhäuser, e-mail: Julia.kunze@uibk.ac.at)*

Cu has recently gained considerable attention due to its capability to efficiently oxidize CO at low overpotentials.^[1] The Cu(111) surface structure, under CO oxidation conditions, shows extremely high and reversible dynamics, featuring the formation of Cu nanostructures that are effectively stabilized through the presence of CO. Therefore, CO itself activates the (111) surface of Cu and enhances its own oxidation.

Inspired by this interesting behavior, we revisited the anodic oxidation of Cu(111) under the exact same conditions without CO in solution, in order to investigate its reversibility. In earlier studies of the Cu(111) oxidation, oxygen was often present in the electrolyte. Also, in most of the works, contaminations from the glassware have not been avoided, which leads to differences in the shapes and positions of all the peaks in the cyclo-voltammograms (CVs). When oxygen is present, the formation of crystalline, several monolayers thick Cu₂O was observed at potentials ≤ 0.57 V versus the reversible hydrogen electrode (RHE).^[2] The reduction of this oxide did not lead to a recovery of the pristine Cu(111) surface structure.

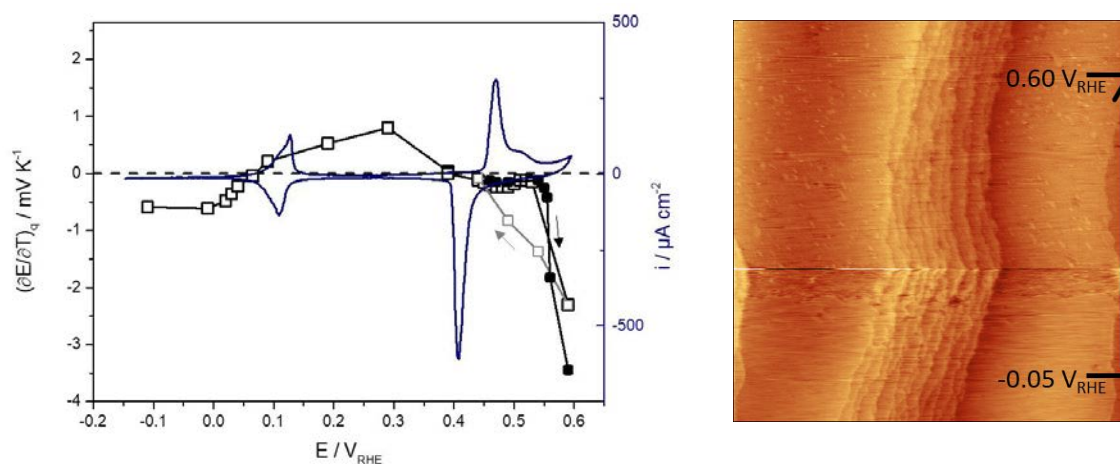


Figure 1: Cyclo-voltammogram (CV, blue curve) with electric field (black curves), and electrochemical scanning tunneling microscopy (EC-STM) image, during a potential sweep from -0.10 to 0.60 V_{RHE} , towards anodic oxide formation of Cu(111) in 0.1 M NaOH.

By conducting all electrochemical scanning tunneling microscopy (EC-STM) experiments inside an Ar filled glove box, and through avoidance of glassware, the presence of atmospheric oxygen and of contaminations can be excluded. Under these conditions, and by combining EC-STM with cyclo-voltammetry and laser induced potential transients (LIPT), we could now gain new insight in the surface structure and charge evolution under anodic polarization conditions, and in the oxidation behavior of Cu(111) in general.

Figure 1 shows the CV of Cu(111) in 0.1 M NaOH, with its typical OH adsorption/desorption feature at around 0.12 V_{RHE} and a sharp anodic peak at $\sim 0.43 V_{\text{RHE}}$ that has been recently assigned to O-adsorption.^[3] The electric field at the solid/liquid interface is measured via LIPT and represented through the thermal coefficient. It reveals negative values at low potentials ($< 0.06 V_{\text{RHE}}$), positive values in an intermediate potential region, a range between 0.39 and 0.54 V_{RHE} where the effective double layer charge is close to zero, and a steep decrease of the field to negative values at anodic potentials $> 0.54 V_{\text{RHE}}$, due to surface oxide formation. This non-monotonic charging behavior has been described earlier for Pt electrodes^[4,5] and can be explained by an electrostatic model of the double layer^[5].

In completely deaerated alkaline electrolyte, we find a much delayed formation of an amorphous oxide layer at potentials $\geq 0.54 V_{\text{RHE}}$, where the electric field strength pronouncedly decreases to high negative values. This confirms the hypothesis^[3] that the anodic peak at 0.43 V_{RHE} is really related to an adsorption process at the surface and not to bulk oxidation. No crystalline or three-dimensional Cu(I) oxide is formed under the applied conditions in the potential range shown in Figure 1, which clearly differs from the studies where oxygen was present. Subsequent reduction processes of the anodic amorphous oxide grown at potentials up to 0.60 V_{RHE} lead to a smoothening of the surface and a quasi-reversible recovery of the pristine surface morphology and structure.

Therefore, it can be concluded that the presence of oxygen in the electrolyte changes the oxidation behavior of Cu(111) tremendously. The new insights into surface structure and electric field evolution of Cu(111) at anodic potentials are of utmost importance to fundamentally understand the behavior of this material under potential control at the solid/liquid interface. This, in turn, enables its technologically efficient use in important electrocatalytic reactions, such as the CO oxidation and the CO₂ reduction.

References:

- [1] A. Auer, M. Andersen, E.-M. Wernig, N. G. Hörmann, N. Buller, K. Reuter & J. Kunze-Liebhäuser, *Nature Catal.* 3 (2020) 797-803.
- [2] J. Kunze-Liebhäuser, Reference Module in Chemistry, Molecular Sciences and Chemical Engineering, *Encyclopedia of Interfacial Chemistry - Surface Science and Electrochemistry*, (2018) 107-120.
- [3] S.J. Raaijman, N. Arulmozhi, A.H.M. da Silva, M.T.M. Koper, *J. Electrochem. Soc.* 168 (2021) 096510.
- [4] N. Garcia-Araez, V. Climent, J. Feliu, *J. Phys. Chem. C* 113 (2009) 9290-9304.
- [5] J. Huang, A. Malek, J. Zhang, M.H. Eikerling, *J. Phys. Chem. C* 120 (2016) 13587-13595.

Catalysis at liquid interfaces: New SCILLs in ultrahigh vacuum and at the electrified interface

J. Libuda

Interface Research and Catalysis, ECRC,

Friedrich-Alexander-Universität Erlangen-Nürnberg, 91058 Erlangen, Germany

(corresponding author: J. Libuda, e-mail: joerg.libuda@fau.de)

In catalyst development, it is a commonly accepted guiding principle to first design and then synthesize an active site for optimized activity and selectivity. However, catalysts are highly dynamic materials and quite often such tailor-made sites are lost rapidly under operation conditions. In this presentation, we introduce the research concept of the new Collaborative Research Center “Catalysis at Liquid Interfaces” [1] in which we follow a new paradigm to tackle the challenges associated with the structural dynamics of catalytic materials. We use the highly dynamic environment at the interface of liquid phases to self-assemble catalytically active sites with unique reactivity and robustness.

In the present contribution, we focus on one particular materials concept explored in the above-mentioned Collaborative Research Center, namely the “Solid Catalysts with Ionic Liquid Layer” (SCILL).[1] In the SCILL approach, a conventional supported catalyst is coated with an ionic liquid (IL) film to improve the selectivity. The concept has been shown to be extremely successful and, recently, first SCILL systems have been introduced at industrial scale for selective hydrogenation. The great success of SCILLs in heterogeneous catalysis raises the question whether we can use the same concept in electrocatalysis. To explore the mechanism and potential of SCILLs in electrocatalytic transformations, we proceed in two steps. In the first step, we investigate the interaction of ILs with atomically defined single crystal surfaces in ultrahigh vacuum (UHV). In the second step, we perform in-situ studies at the electrified solid-liquid interface using ILs as catalytic modifiers to explore potential effects on activity and selectivity.

For the UHV studies, we deposit thin films of ILs (e.g. $[\text{C}_n\text{C}_m\text{Pyr}][\text{NTf}_2]$, $[\text{C}_n\text{C}_m\text{Im}][\text{NTf}_2]$, $[\text{C}_n\text{C}_m\text{Im}][\text{OTf}]$) by physical vapor deposition (PVD) onto metal single crystal surfaces (Pd(111), Pt(111)) and onto supported model catalysts (Pd and Pt nanoparticles on HOPG).[2-5] The molecular interactions with the model surfaces and the molecular orientation at the interface are monitored by time-

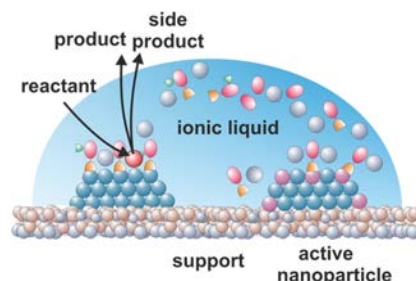


Fig. 1: Solid catalyst with ionic liquid layer.

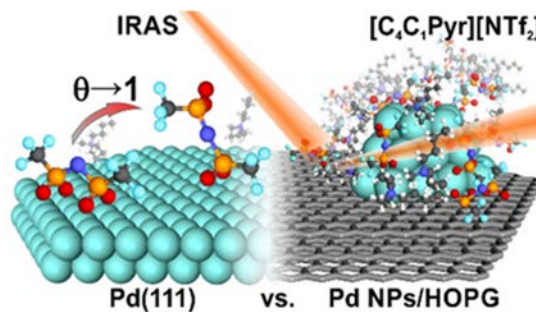


Fig. 2: Model SCILL systems prepared in UHV.

resolved and temperature-programmed infrared reflection absorption spectroscopy (IRAS). We combine the spectroscopic studies with theoretical modelling by density functional theory (DFT) and molecular dynamics (MD) calculations performed by cooperation partners in the Collaborative Research Center.[2] Based on the experimental and the modelling data, we identify the adsorption motifs of the IL ions as a function of coverage and temperature. In particular, we show that the preferred adsorption motif changes as a function of layer thickness. In addition, we investigate the effect of ILs on coadsorbates and compare the interaction strength of different ILs with the catalytically active surface.[4]

To probe the effect of the ILs on electrocatalytic activity, we scrutinize the electrooxidation of secondary alcohols as a test reaction. We follow both, the formation of products in solution and the adsorption of IL ions at the electrode in-situ by polarization dependent electrochemical infrared reflection absorption spectroscopy (EC-IRRAS).[6] For the oxidation of 2,3-butanediol, two products are formed — acetoin and diacetyl — in the potential range from 0.3 V_{RHE} to 0.7 V_{RHE}. In the absence of ILs, acetoin is

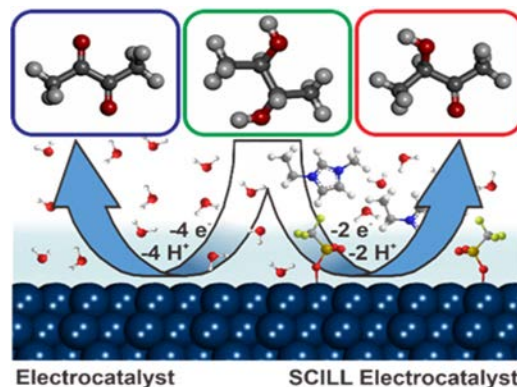


Fig.3: Model SCILL electrocatalyst.

formed first and then rapidly converted to diacetyl. In the presence of the [C_nC_mIm][OTf] as a catalytic modifier, the activity decreases and the conversion to diacetyl is very efficiently suppressed. As a result, the selectivity to the partial oxidation product acetoin increases drastically. We show that the effect of the IL on the activity and selectivity is associated with the specific adsorption of the [OTf]⁻ anion at the Pt(111) electrode in the potential region of interest. The [OTf]⁻ anion suppresses the formation of surface OH, which has a particular strong effect on the conversion of acetoin to diacetyl. Our results demonstrate the potential of electrochemical SCILLs for selective electrooxidation which opens up a plethora of new possibilities to tailor electrocatalysts for energy conversion and electrosynthesis.

Supported by the Deutsche Forschungsgemeinschaft (DFG) via Collaborative Research Centre SFB 1452 – Catalysis at Liquid Interfaces (project 431791331). Additional financial support is acknowledged by the German Federal ministry of Education and Research (BMBF, Project Combined Infrared and X-Ray Analytics of Energy Materials, CIXenergy 05K19WE1) and by the Bavarian ministry of Economic Affairs, Regional Development and Energy.

- [1] CRC 1452 – CLINT – Catalysis at Liquid Interfaces, www.clint.fau.eu
- [2] C. Schuschke, L. Fromm, J. Träg, C. Stumm, C. Hohner, R. Eschenbacher, S. Grau, D. Zahn, A. Görling, T. Bauer, J. Libuda, *Journal of Physical Chemistry C* 125, 13264 (2021)
- [3] D. Blaumeiser, C. Schuschke, L. Fromm, N. Taccardi, S. Schötz, R. Eschenbacher, H. Bühlmeier, T. Xu, T. Bauer, P. Wasserscheid, A. Görling, J. Libuda, *Journal of Physical Chemistry C* 125, 15301 (2021)
- [4] R. Eschenbacher, C. Schuschke, H. Bühlmeier, N. Taccardi, P. Wasserscheid, T. Bauer, T. Xu, J. Libuda, *Journal of Physical Chemistry Letters* 12, 10079 (2021)
- [5] C. Hohner, L. Fromm, C. Schuschke, N. Taccardi, T. Xu, P. Wasserscheid, A. Görling, J. Libuda, *Langmuir* 37, 12596 (2021)
- [6] T. Yang, J. Yang, X. Deng, E. Franz, L. Fromm, Z. Liu, A. Görling, P. Wasserscheid, O. Brummel, J. Libuda, submitted.

Electrochemical and Thermal Oxidation of Pt(111)

S. Volkov¹, L. Jacobse², V. Vonk², T.F. Keller², J. Fleig³ and A. Stierle^{2,3}

¹Photon Science, Petra III, Deutsches Elektronen-Synchrotron (DESY), D-22607 Hamburg

²Centre for X-ray and Nanoscience, Deutsches Elektronen-Synchrotron (DESY), D-22607 Hamburg

³Institute of Chemical Technologies and Analytics, TU Wien, A-1060 Vienna

⁴Physics Department, University of Hamburg, D-20355 Hamburg

(corresponding author: V. Vonk, e-mail: vonk@desy.de)

Considered a noble metal with catalytic activity, platinum is an attractive stable electrode material in various electrochemical applications. In general, for electrocatalysis, which has become ever more important in view of a sustainably green economy, platinum-based electrodes play an important role. In such applications, the electrodes typically undergo redox cycles and the long-term stability is problematic [1]. It is discussed that platinum oxide formation is involved in various mass transport phenomena leading to electrode failure [2], which calls for detailed mechanistic studies of the oxidation (and reduction) process. Although platinum is relatively stable under thermal oxidation conditions [3], its use under more harsh electrochemical conditions can lead to severe degradation [4].

Here we present the results of several in-situ x-ray experiments under controlled electrochemical potential, addressing the Pt(111) atomic interface structure evolution. First, experiments of a model solid state electrochemical interface: a 100nm Pt(111) epitaxial film on a YSZ(111) substrate, are discussed. The YSZ is a solid state electrolyte, with enhanced oxygen conductivity at elevated temperatures and this interface is encountered in oxygen sensors. At an anodic potential of approx. +100 mV, a temperature of 623 K and ambient conditions, oxygen is pumped through the YSZ towards the Pt metal. Detailed x-ray measurements show that at the buried interface an ultrathin Pt-oxide forms, which is reduced at cathodic potentials (see Fig. 1).

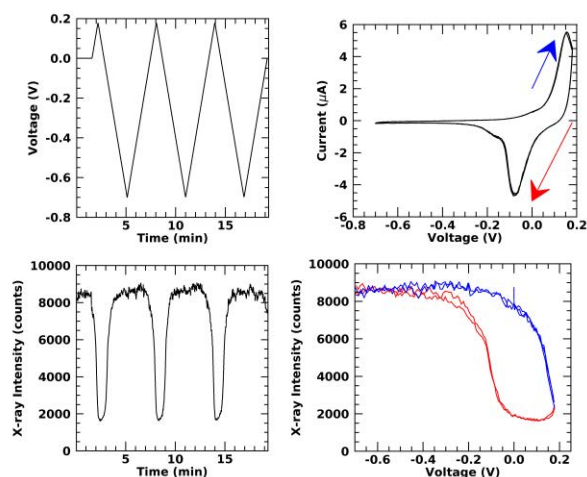


Fig 1. Cyclic Voltammetry (CV) curves measured during the operando x-ray measurements and corresponding reflected intensity. a) Voltage vs. time. b) CV measurements during 3 cycles. The arrows indicate the positive voltage increase direction (blue) and negative (red). c,d) Reflected intensity at a $Q=0.61 \text{ \AA}^{-1}$. The XRR intensity cycles between two values, which is a direct evidence for the reversible formation of an ultrathin PtOx layer at the deeply buried interface.

After many cycles, the outermost Pt surface shows first signs of delamination. This process is understood to start locally at defects, where oxygen gas accumulates in voids and starts to build up pressure. Fig 2. Shows an AFM image of pyramids, which formed in this way [6].

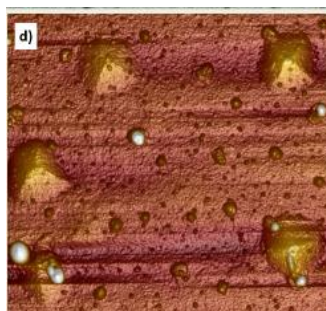


Fig 2. AFM image showing surface topography after many CV cycles whereby typical pyramids (and bubbles) have formed during the onset of delamination.

At the same time, the outermost Pt surface (in between the pyramids and bubbles), remains oxidized in a manner as known from thermal oxidation: it shows to consist of an 1-2 ML thin Pt-oxide with an in-plane lattice constant of 0.315 nm. X-ray measurements whereby the angle of incidence is chosen such to illuminate only the topmost surface or the entire film, including the buried interface, allow to prove that this particular oxide only forms at the topmost surface, see Fig. 3 [5].

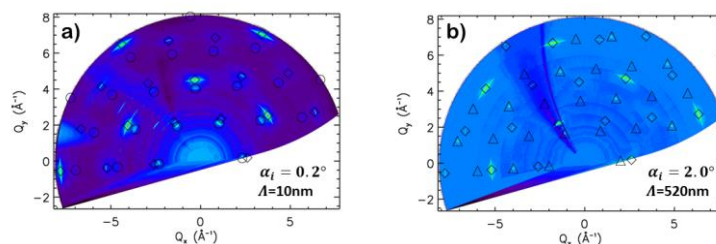
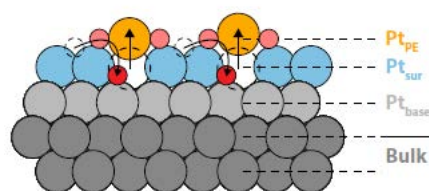


Fig 3 In-plane Reciprocal Space Maps (similar to LEED measurements) of Pt/YSZ showing reflections from the top Pt surface only (a) and also from the buried interface (b). Shown are reflections from the Pt metal (diamonds), PtOx (circles) and YSZ (triangles). These measurements show that the surface PtOx is always present under these conditions, irrespective of the electrochemical potential.

The results of the oxidation at the two interfaces encountered in the Pt/YSZ system are compared with the results of a Pt(111) surface in contact with a liquid electrolyte (0.5M H₂SO₄) under electrochemical conditions. Here, by choosing a particularly low potential sweep rates, an apparently commensurate thin oxide layer is formed with relatively high in-plane order. This oxide formation is discussed in terms of the place exchange mechanism (Fig. 4) and its relation to the so-called spoke-wheel reconstruction [7,8].

Fig. 4 Schematic ball model of the place-exchange mechanism occurring during the oxidation of Pt(111) in a liquid electrolyte. Large balls: Pt, small balls: oxygen.



- [1] S. Zhang et al. , J. of Power Sources **194**, 588-600 (2009)
- [2] Y-F. Huang and T.M. Koper, J. Phys. Chem. Lett. **8**, 1152-1156 (2017)
- [3] C. Ellinger, A. Stierle et al. J. Phys: Cond Mat. **20**, (2008).
- [4] L. Jacobse et al. Nature Materials **17**, 277 (2018).
- [5] S. Volkov, T. Keller, A. Hutterer, P. Lakner, A. Stierle, F. Bertram, J. Fleig. V. Vonk (in preparation).
- [6] T.F. Keller, S. Volkov, V.Vonk. A. Stierle et al. Sol. State Ionics **330**, 17 (2019)
- [7] M.A. van Spronsen, J.W.M. Frenken, I.M.N. Groot, Nature Communications **8**, 429 (2017)
- [8] L. Jacobse, V. Vonk, I.T. McCrum, C. Seitz, M.T.M. Koper, M.J. Rost, A. Stierle Electrochim. Acta (2022) (accepted).

Instruments for Advanced Science

Mass spectrometers for vacuum, gas, plasma and surface science

Residual Gas Analysis

Perform RGA at UHV/XHV . Our RGA configurations include systems for UHV science applications including temperature-programmed desorption and electron/photon stimulated desorption.



Thin Film Surface Analysis

Conduct both static and dynamic SIMS analysis with a choice of primary ions for full chemical composition and depth profiling. Our SIMS solutions include complete workstations and bolt-on modules.



Plasma Characterization

Fully characterise a range of plasmas: RF, DC, ECR and pulsed plasmas, including neutrals and neutral radicals. Extend your analyses to atmospheric pressure processes using the HPR-60, with time-resolved mass/energy analysis.



Postersession

Structure of Anatase TiO₂(001) in Aqueous Environment

J. Balajka, G. Franceschi, M. Riva, J. Pavelec, M. Schmid, U. Diebold

Institute of Applied Physics, TU Wien, A-1040 Wien, Austria

(Corresponding author: J. Balajka, e-mail: balajka@iap.tuwien.ac.at)

Anatase is commonly regarded as the more active phase of titania, and it is a major component of the TiO₂ powder photocatalyst Degussa P25. In particular, the minority (001) termination of anatase is expected to be reactive due to a high density of undersaturated cations and strained configuration of surface atoms [1]. The (001) surface undergoes a stress-driven (1×4) reconstruction when prepared by standard methods in ultrahigh vacuum (UHV), which stabilizes the surface and reduces its reactivity [2]. The reconstructed surface, however, has been theoretically predicted to be unstable in water and aqueous solutions [3–5], and experimental evidence indicates lifting of the (1×4) reconstruction in carboxylic acid solutions [6].

We explored the stability of anatase TiO₂(001)-(1×4) reconstructed surface in an aqueous environment using a dispenser of ultrapure liquid water under UHV-compatible conditions [7,8] in combination with noncontact AFM and STM imaging in UHV. With this method, we deposit a droplet of liquid water onto a sample prepared under ultrahigh vacuum without exposing the sample to air or other possible sources of spurious contamination. Atomically resolved SPM images evidence the retention of the (1×4) reconstruction upon immersion in ultrapure water. The stability of anatase (001)-(1×4) in pure water is in agreement with recent theoretical work [9]. However, it might not be the case in more reactive aqueous solutions, as suggested in ref. [9]. I will discuss strategies for using aqueous solutions that may lead to the lifting of the reconstruction and increase the surface reactivity.

Despite the importance of this material, pure anatase samples of suitable size for surface science investigations are mostly unavailable. Anatase is often found in the form of nanoparticles, whereas larger TiO₂ crystals are usually in the thermodynamically stable rutile phase. This challenge was overcome by using epitaxial anatase TiO₂(001) films grown with pulsed laser deposition (PLD) on a SrTiO₃(001) substrate, similar to ref. [10].

Support by the European Research Council (ERC) under the European Union's Horizon 2020 research and innovation program (grant agreement No. 883395, Advanced Research Grant 'WatFun') is gratefully acknowledged.

References

- [1] A. Selloni, *Nat. Mater.* **7**, 613 (2008).
- [2] M. Lazzeri and A. Selloni, *Phys. Rev. Lett.* **87**, 266105 (2001).
- [3] F. De Angelis *et al.*, *Chem. Rev.* **114**, 9708 (2014).
- [4] S. Selçuk and A. Selloni, *Nat. Mater.* **15**, 1107 (2016).
- [5] S. Selçuk and A. Selloni, *J. Phys. Chem. C* **117**, 6358 (2013).

- [6] W. J. I. DeBenedetti *et al.*, J. Phys. Chem. C **122**, 4307 (2018).
- [7] J. Balajka *et al.*, Rev. Sci. Instrum. **89**, 083906 (2018).
- [8] J. Balajka *et al.*, Science **361**, 786 (2018).
- [9] G. Zeng, B. Wen, and A. Selloni, J. Phys. Chem. C [acs.jpcc.1c03623](https://doi.org/10.1021/acs.jpcc.1c03623) (2021).
- [10] M. Radović *et al.*, J. Chem. Phys. **135**, 034705 (2011).

On-surface and tip induced synthesis of carbon-based macrocycle polyradicaloids

J. Berger^{1,2}, A. P. Solé¹, A.G. Sanchez¹, D. Mildner^{1,2}, A. Matej^{1,2}, D. Soler¹,
F. Romero³, J. M. Carvajal³, A. Campana³, and P. Jelínek^{1,2}
(corresponding author: J. Berger, e-mail: bergerj@fzu.cz)

¹ FZU - Institute of Physics of the Czech Academy of Sciences
Cukrovarnická 10/112 162 00 Prague 6, Czech Republic

² CATRIN-Czech Advanced Technology and Research Institute,
Šlechtitelů 241/27, 783 71, Olomouc – Holice, Czech Republic

³ Department of Organic Chemistry, Faculty of Sciences, University of Granada
Avda. Fuentenueva, s/n, 18071, Granada (Spain)

Since their early discovery at the turn of the 20th century, radicaloid polyaromatic hydrocarbon (PAH) molecules with open-shell ground state have attracted continued interest. The high reactivity and/or low solubility of such radicaloid PAH compounds make them challenging to obtain in conventional solution chemistry. Therefore, new strategies have been developed to overcome such limitations. One of the promising strategies is on-surface synthesis in ultra-high vacuum conditions [1]. This method complemented with high-resolution scanning probe imaging provides the unique opportunity to explore novel multiradical PAH systems with the unprecedented spatial resolution.

Here, we present on-surface synthesis of PAH multiradical macrocycles consisting of benzene units connected by pentadiene bridges (see Figure 1), on Au(111) substrate. Namely, we employ two step synthesis consisting of thermally activated cyclodehydrogenation and subsequent selective dehydrogenation by tip manipulation to form multiradical PAH compounds. Moreover, choice of slightly different precursors enables us to synthesize macrocycles of different size. These multiradical systems represent an interesting playground for testing different concepts of global/local (anti)aromaticity [2] and competing multiradical ground states with different π -resonant forms.

In order to understand their electronic properties, π -conjugation topology and (anti)aromaticity, we have combined scanning tunnelling microscopy/spectroscopy (STM/STS) and non-contact atomic force microscopy (nc-AFM) investigations rationalized by DFT and many-body complete active space (CAS) calculations.

In conclusion, we present the novel synthesis of multiradical PAH macrocycles using the two-step synthetic process based on annealing and tip-induced manipulation (see Figure 2). Our results open new strategies for the synthesis of novel polyradicaloid open-shell PAH macrocycles.

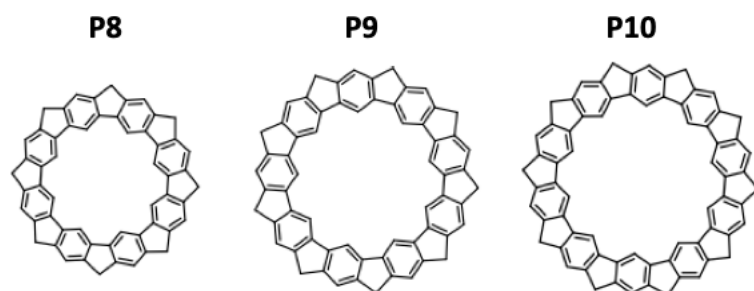


Figure 1 Schematic images of P8, P9 and P10 molecule. They are composed from 8 benzene and 8 pentadiene rings, 9 benzene and 9 pentadiene and 10 benzene and 10 pentadiene rings.

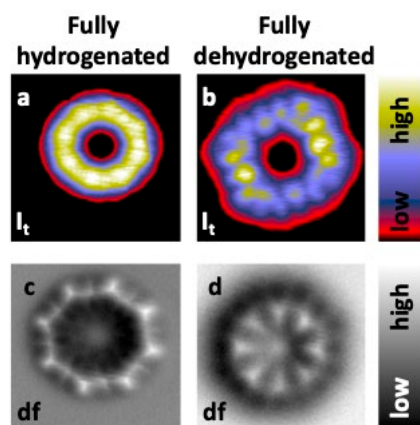


Figure 2 (a) and (c) Simultaneously taken constant height df and I_t image of fully hydrogenated P8 molecule. (b) and (d) Simultaneously taken constant height df and I_t image of fully dehydrogenated P8 molecule. All images are $2.5 \times 2.5 \text{ nm}^2$, bias voltage $U = 2 \text{ mV}$.

- [1] S. Clair, D.G. de Oteyza, *Chem. Rev.* 2019, 119, 7, 4717–4776
 [2] Ch. Liu, Y. Ni, X. Lu, G. Li, J. Wu, *Acc. Chem. Res.* 2019, 52, 8, 2309–2321

An optimised Quartz Crystal Microbalance setup to investigate the sputtering behaviour of bulk targets

J. Brötzner, H. Biber, P. S. Szabo*, N. Jäggi¹, C. Cupak, A. Nenning², B. Cserveny, A. Galli¹, P. Wurz¹, and F. Aumayr

*Institute of Applied Physics, TU Wien, A-1040 Vienna, Austria
(corresponding author: J. Brötzner, email: broetzner@iap.tuwien.ac.at)*

¹ *Physics Institute, University of Bern, CH-3012 Bern, Switzerland*

² *Institute of Chemical Technologies and Analytics, TU Wien, A-1040 Vienna, Austria*

* *Current address: Space Sciences Laboratory, University of California, CA 94720 Berkeley, USA*

In modelling the exosphere formation of atmosphere-less planetary objects [1], the sputtering contributions is often calculated using Monte-Carlo style simulations like SRIM [2]. However, input parameters of these codes often need to be adapted to successfully describe experimental data [3]. To provide such experimental data, we perform sputter measurements in which we irradiate mineral samples relevant for modelling the surfaces of Mercury or the Moon. Usually, such experiments are performed using thin sample films deposited onto a Quartz Crystal Microbalance (QCM), allowing to determine mass changes in real time and in situ [4, 5]. Advancing on this technique, we conduct measurements using a previously presented setup with a second QCM facing the irradiated samples [6]. It collects particles liberated by sputtering and probes their angular distribution. This setup allows for experiments with bulk samples, including pellets made of mineral powders [7]. These are currently being used in addition to the aforementioned thin films on primary QCMs. The goal with these samples is to detect possible differences in sputtering behaviour between the amorphous films and the bulk specimens that might be explained by crystallinity [8]. A schematic of this setup is given in figure 1.

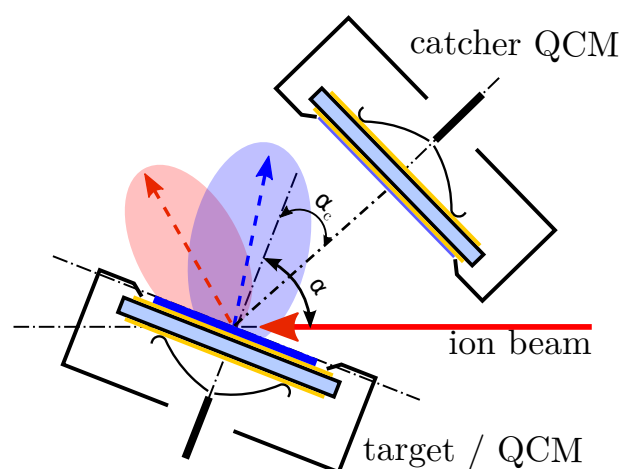


Figure 1: Sketch of the Catcher-QCM setup. Depicted is an ion beam impinging under the incidence angle α on a primary thin film coated QCM as sample in addition to the catching QCM. Adapted from [9].

Experiments with such an advanced setup require an optimisation of the measurement procedure. Due to the high sensitivity of the QCM technique, small fluctuations in the experimental conditions can lead to noticeably different catcher signals. We therefore adapted the setup geometry to ensure constant relative distances between all specimens. Additionally, sample preparation cycles were changed to minimise transient effects on the QCMs which can be caused by non-equilibrium sticking on the catcher QCM. Furthermore, data evaluation was adapted to focus on relative changes from thin film to pellet measurements, rather than absolute signals. We immediately irradiate both types of samples after each other at a fixed catcher angle. This allows us to neglect long-term changes in experimentation parameters at this chosen position. Using these procedures, we can reliably reproduce irradiation results. We are therefore capable of precisely measuring sputtering yields and angular distributions of atoms sputtered by solar wind ions for bulk samples.

- [1] Wurz P., et al.: *Icarus*, 191, 486, 2007.
- [2] Ziegler, J. F., et al.: *Nucl Instrum Methods Phys Res B*, 268, 1818, 2010.
- [3] Schaible, M. J., et al.: *J. Geophys. Res. Planets*, 122, 1968, 2017
- [4] Hayderer G., et al.: *Rev. Sci. Instrum.*, 70, 3696, 1999.
- [5] Szabo P. S., et al.: *Icarus*, 314, 98, 2018.
- [6] Biber H., et al.: EPSC2021, online, EPSC2021-526, 2021.
- [7] Jäggi N., et al.: *Icarus*, 365, 114492, 2021.
- [8] Schlueter, K., et al.: *Phys. Rev. Lett.*, 125.22, 225502, 2020.
- [9] Berger, B. M., et a.: *Nucl Instrum Methods Phys Res B*, 406, 533, 2017

Sputtering of highly corrugated surfaces

C. Cupak^{1*}, M. Fellingner¹, H. Biber¹, A. Redl¹, A. Lopez-Cazalilla²,
R. Gonzalez-Arrabal³, F. Aumayr¹

¹*Institute of Applied Physics, TU Wien, Fusion@ÖAW, 1040 Vienna, Austria*

²*Department of Physics, University of Helsinki, 00014 Helsinki, Finland*

³*Instituto de Fusión Nuclear/Departamento de Ingeniería Energética, Universidad Politécnica de Madrid, 28006 Madrid, Spain*

Ion-induced sputtering of surfaces is of importance in various scientific fields. In nuclear fusion research, erosion of first wall materials in reactor vessels due to sputtering by plasma ions is of major interest for lifetime estimations and plasma impurity assessment [1]. In space science, sputtering due to solar wind ions is known to occur also on celestial bodies that are not protected by a dense atmosphere [2]. Furthermore, physical vapour deposition (PVD) methods often rely on ion-induced sputtering for creating nm-thin coatings on substrates [3].

Dependencies of the sputter yield (i.e., the mean number of sputtered atoms per incoming projectile) on ion kinetic energy, incident angle and mass ratio between target and ion species are already well described by existing theoretical models [4] or numerical simulation codes, often based on the Binary Collision Approximation (BCA) [5]. However, surface roughness remains a challenging property for sputter yield calculation. Although modern 3D versions of BCA codes can cope with rough surface input already, the usage of large-scale topographies larger than several 100x100nm² is often too demanding for accessible computational infrastructure [6]. In addition, experimental methods, which can assess static sputtering properties of a rough surface, are scarce, since the erosion by ions itself usually modifies the surface during the experiment.

Recently, we have developed a new raytracing code called SPRAY [7] (SPuttering simulation via RAYtracing of particles), which is capable of quickly simulating sputter yields for rough topographies (as e.g., derived from Atomic Force Microscopy) without limitations in size. Using a precise Quartz Crystal Microbalance (QCM) in combination with a low-flux ion source, we benchmarked SPRAY with quasi-static experimental sputtering data of W samples and largely variable roughness obtained under 2keV Ar⁺ bombardment. On this basis, we have shown that the mean inclination angle δ_m is a much more reliable parameter than e.g., the root mean square roughness (RMS) for sputter yield predictions [7].

In our current work, we extend our studies from isotropically rough surfaces towards more corrugated and oriented structures. For this purpose, a dense assembly of vertical W nanopillars with a height of 500nm and a diameter of 50nm was deposited on our W sample surfaces in Madrid, so that direct investigations with our QCM experiment under Ar⁺ bombardment are possible in Vienna. In parallel, AFM images are used as input for SPRAY

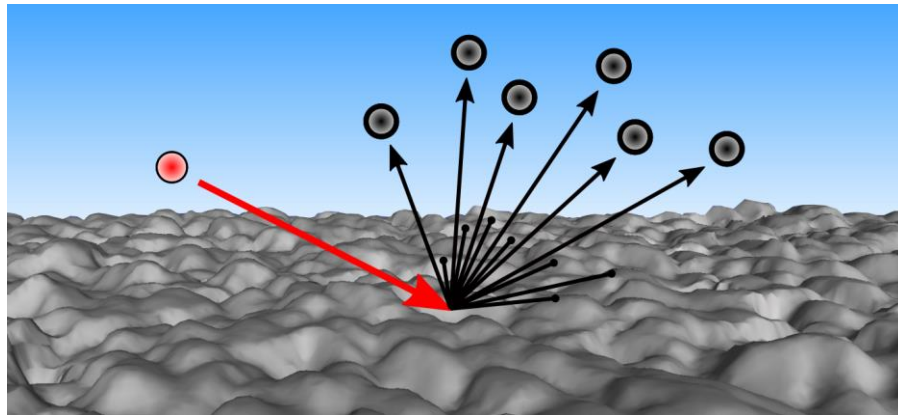


Fig 1 Surface roughness changes the local impact angles of the ions. Some areas of the surface can't be hit by ions at all (shadowing effect). In addition, some sputtered atoms may be redeposited on neighbouring slopes [7].

simulations of such complex structures. Since deviations due to AFM tip convolution effects are to be expected, also artificial topographies are created as input for SPRAY which mimic the appearance of the surface as observed by Scanning Electron Microscopy (SEM). As an important first result, we notice that the nanocolumnar W surfaces not only show a significant reduction in the sputter yield in comparison to a flat W surface, but also that the sputter yield is nearly independent on the ion's incidence angle.

- [1] S. Brezinsek et al., *Nucl. Fusion* **57**, 116041 (2017)
- [2] P.S. Szabo et al., *J. Geophys. Res.: Planets* **125**, e2020JE006583 (2020)
- [3] Y. Deng et al., *Appl. Surf. Sci.* **512**, 145508 (2020)
- [4] P. Sigmund, *Phys. Rev. Lett.*, **184**, 383-416 (1969)
- [5] H. Hofsäss et al., *Appl. Surf. Sci.* **310**, 134-141 (2014)
- [6] R. Stadlmayr et al., *J. Nucl. Mater.* **532**, 152019 (2020)
- [7] C. Cupak et al., *Appl. Surf. Sci.* **570**, 151204 (2021)

Probing photo-induced dynamics of organic molecules on surfaces by time-resolved spectroscopic ellipsometry

F.-F. Delatowski^{1,3}, K. Khakurel¹, J. Rappich², S. Espinoza¹, M. Rebarz¹, M. Zahradnik¹, and J. Andreasson¹

¹ELI Beamlines, Institute of Physics, Czech Academy of Sciences, Czech Republic
(corresponding author: F.-F. Delatowski, e-mail: delatowski@eli-beams.eu)

²Institute Silicon Photovoltaics, Helmholtz-Zentrum Berlin für Materialien und Energie, Germany

³Semiconductor Physics Group, Felix Bloch Institute for Solid State Physics, Universität Leipzig, Germany

Photo-induced dynamics of organic molecules on surfaces are extensively studied because of its potential applications as bio-sensors and ultrafast molecular switches [1-2]. Despite rich experimental studies, many of the fundamental questions, such as the structural dynamics of the molecules, charge transfer and relaxation processes, remain highly relevant. Time-resolved spectroscopic ellipsometry is a promising surface sensitive tool to investigate these phenomena. In this work, we explore the potential of this measurement technique, taking pyrimidine derivatives on gold surface as a test system.

We present preliminary experimental results of femtosecond pump-probe spectroscopic ellipsometry of organic molecules on gold surfaces. The measurements were performed at the time-resolved ellipsometry set-up at ELI Beamlines, described in detail in previous work [3]. The samples used for our studies consist of a thin film of pyrimidine derivatives, deposited on a ~200 nm Au layer on p-Si (100). The organic molecules, are attached to the substrate using electro-grafting technique [4]. A schematic model of the sample is shown in Fig 1 (a). The presence of the

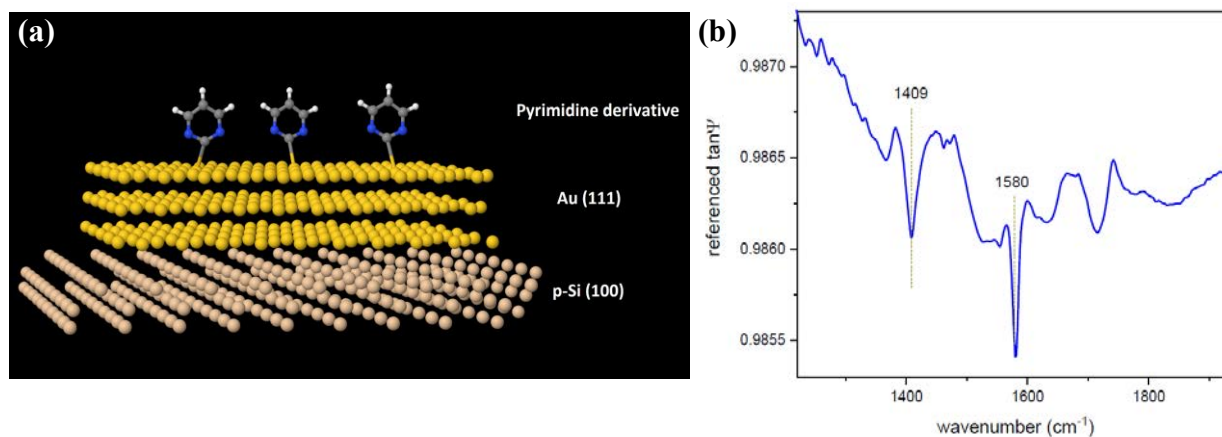


Figure 1: (a) Schematic of the composition of the sample (b) IR spectrum confirming the presence of the pyrimidine molecule on the substrate

pyrimidine molecule on the substrate is confirmed by IR spectroscopic ellipsometry which is shown in the Fig 1 (b).

In addition to the experimental observations, we also present an approach to predict the ellipsometry spectrum from the sample through *ab-initio* DFT calculations using the program SIESTA [5]. We discuss the benefits that the synergy of *ab-initio* based spectrum predictions and experiments bring in the interpretation of the dynamics in the sample.

ELI Beamlines authors acknowledge the support of the ELIBIO (No. CZ.02.1.01/0.0/0.0/15-003/0000447) and ADONIS (No. CZ.02.1.01/0.0/0.0/16-019/0000789) projects from the European Regional Development Fund.

[1] Wesley R. Browne and Ben L. Feringa, "Light Switching of Molecules on Surfaces", *Annual Review of Physical Chemistry* 60:1, 407-428 (2009).

[2] Oleg V. Prezhdo, Walter R. Duncan, and Victor V. Prezhdo, "Dynamics of the Photoexcited Electron at the Chromophore–Semiconductor Interface", *Acc. Chem. Res.* 41, 2, 339–348 (2008).

[3] Steffen Richter, Mateusz Rebarz, Oliver Herrfurth, Shirly Espinoza, Rüdiger Schmidt-Grund, and Jakob Andreasson, "Broadband femtosecond spectroscopic ellipsometry", *Review of Scientific Instruments* 92, 033104 (2021).

[4] Daniel Bélanger and Jean Pinson, "Electrografting: a powerful method for surface modification", *Chem. Soc. Rev.*, 40, 3995-4048 (2011).

[5] Alberto García et al., "Siesta: Recent developments and applications", *J. Chem. Phys.* 152, 204108 (2020)

Water and Hydroxyls at $\text{In}_2\text{O}_3(111)$

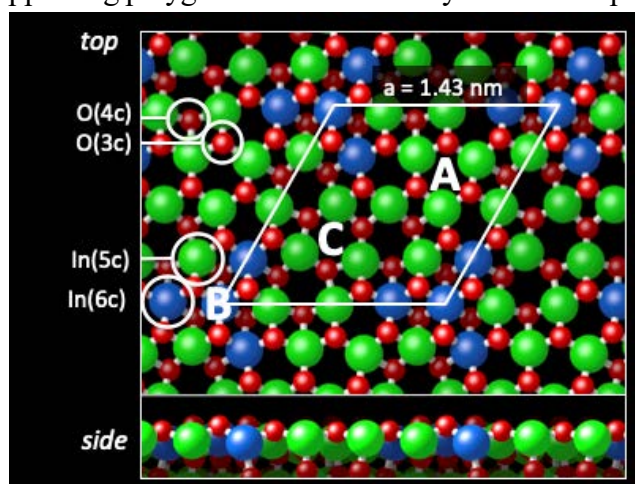
Ulrike Diebold, Michael Schmid, Bernd Meyer¹, and Margareta Wagner

*Institute for Applied Physics, TU Wien, A-1040 Vienna, Austria
(corresponding author: U. Diebold, e-mail: diebold@iap.tuwien.ac.at)*

¹*Interdisciplinary Center for Molecular Materials and Computer Chemistry Center,
Friedrich-Alexander-Universität Erlangen-Nürnberg, Erlangen, Germany*

In_2O_3 is a post-transition metal oxide with a wide band-gap. The material combines optical transparency with a high electrical conductivity that is sensitive to gas adsorption. Because of these attractive properties, In_2O_3 finds extensive use as a transparent conductive oxide and chemical sensor [1]. More recently, interesting catalytic properties were identified, e.g., efficient hydrogenation of CO_2 [2].

From a surface science perspective, In_2O_3 is peculiar because reduction does not result in oxygen vacancies [3] but in an ordered array of single indium adatoms [4]. Its most stable (111) surface has a simple (1×1) bulk termination but an unusually large unit cell that provides an appealing playground for atomically resolved experiments. The figure shows $\text{In}_2\text{O}_3(111)$ in top and side views, with bulk-like



and side views, with bulk-like $\text{In}(6c)/\text{O}(4c)$ and surface $\text{In}(5c)/\text{O}(3c)$ atoms. The surface has three-fold symmetry, and the areas around the high-symmetry points labelled A, B, and C show different chemical reactivity.

We have combined surface science techniques (ncAFM/STM, XPS, TPD, etc. in UHV) with DFT calculations to study the interaction with water. Single crystals are rare, small, and (to our knowledge) not

commercially available; we have perfected the growth of epitaxial thin films [5] and used both types of samples in our experiments.

Water dissociates at room temperature with saturation coverage of 3 mol/u.c. located around B [6]. This provided the basis for establishing a method to probe the proton affinity of individual surface hydroxyls [7]. At higher coverages, water accumulates around B and C, but A stays water-free; the unit cell exhibits both, hydrophobic and hydrophilic behaviour.

Support by the Austrian Science Fund (Richter Program, Project V773), and the European Research Council (Advanced Research Grant ‘WatFun’ (Grant Nr. 883395) is gratefully acknowledged.

- [1] Egdell, R. G., Dopant and Defect Induced Electronic States at In_2O_3 Surfaces. *In Defects at Oxide Surfaces*, Springer International Publishing: Cham, 2015; Vol. 58, pp 351-400.
- [2] Martin, O.; Martín, A. J.; Mondelli, C.; Mitchell, S.; Segawa, T. F.; Hauert, R.; Drouilly, C.; Curulla-Ferré, D.; Pérez-Ramírez, J., Indium Oxide as a Superior Catalyst for Methanol Synthesis by CO_2 Hydrogenation. *Angewandte Chemie* 2016, 128 (21), 6369-6373.
- [4] Setvin, M.; Wagner, M.; Schmid, M.; Parkinson, G. S.; Diebold, U., Surface point defects on bulk oxides: atomically-resolved scanning probe microscopy. *Chemical Society Reviews* 2017, 46, 1772-1784.
- [3] Wagner, M.; Seiler, S.; Meyer, B.; Boatner, L. A.; Schmid, M.; Diebold, U., Reducing the $\text{In}_2\text{O}_3(111)$ surface results in ordered Indium adatoms. *Advanced Materials Interfaces* **2014**, 1 (8), 1400289-6.
- [5] Franceschi, G.; Wagner, M.; Hofinger, J.; Krajňák, T.; Schmid, M.; Diebold, U.; Riva, M., Growth of $\text{In}_2\text{O}_3(111)$ thin films with optimized surfaces. *Physical Review B* **2019**, 3 (10), 103403.
- [6] Wagner, M.; Lackner, P.; Seiler, S.; Brunsch, A.; Bliem, R.; Gerhold, S.; Wang, Z.; Osiecki, J.; Schulte, K.; Boatner, L. A.; Schmid, M.; Meyer, B.; Diebold, U., Resolving the Structure of a Well-Ordered Hydroxyl Overlayer on $\text{In}_2\text{O}_3(111)$: Nanomanipulation and Theory. *ACS nano* **2017**, 11 (11), 11531-11541.
- [7] Wagner, M.; Meyer, B.; Setvin, M.; Schmid, M.; Diebold, U., Direct assessment of the acidity of individual surface hydroxyls. *Nature* **2021**, 592 (7856), 722-725.

Time-resolved spectroscopic ellipsometry applied to ellagic acid thin films

Shirly Espinoza¹, Martin Zahradník, Mateusz Rebarz, Jakob Andreasson, and Eva Bittrich²

¹*ELI Beamlines, Institute of Physics, Czech Academy of Science, Dolní Břežany, 252 41 Czechia*

²*Leibniz-Institut für Polymerforschung Dresden e.V., 01069 Dresden, Germany*

(Corresponding authors: Shirly Espinoza, e-mail: shirly.espinoza@eli-beams.eu; and Eva Bittrich, email: bittrich-eva@ipfdd.de)

Ellagic acid (EA) is a polyphenol present in numerous fruits like strawberries and pomegranates. It is well known in food research for its anticancer and antioxidant effects. It has recently evoked interest in the field of organic electronics because of its weak electron donor properties. In this work, we report on the ultra-fast optical behavior of uniaxial π -stacked EA films on gold surfaces prepared by thermal evaporation [1].

The samples were measured by time-resolved spectroscopic ellipsometry using a femtosecond pump-probe polarizer-sample-rotating-compensator-analyzer (PSC_{RA}) ellipsometer. Our home-built experimental setup is based on a 35 fs 800 nm Ti:sapphire laser with a 1 kHz repetition rate. This laser beam was used in a pump-probe scheme where the pump was a 400 nm beam generated by frequency doubling and the probe was white light super continuum generated in a CaF₂ window. The pump beam was chosen to be 400 nm, 3.1 eV, in order to excite with an energy higher than the gap energy of the ellagic acid, which was obtained from the steady-state ellipsometric spectra of the sample [2]. In order to investigate the polarization effect of the pump beam on the sample, the pump was kept at normal angle of incidence and measurements were taken at s- and p- polarization; the angle of incidence of the probe beam was 60°.

We aimed to examine the ultra-fast response of the aromatic π - π^* transitions to a pump signal looking for influences of the films morphology (e.g. the grain packing density, π -stacking orientation) or H-bonding interactions on the ultra-fast optical behavior. This study, together with tailoring of the photoactive film morphology [3] would likely lead to a better understanding of performance improvements of organic photovoltaic cells.

Preliminary results of the imaginary and real part of the pseudo-dielectric function show different behavior with pump polarization. At 2.8 eV (figure 1), there is an intensity lost in the real part of the dielectric function present only on the sample excited with s-polarization. The interpretation of this feature requires a modelling of the data to obtain the dielectric function and the calculation of the time constant associated with this transient signal

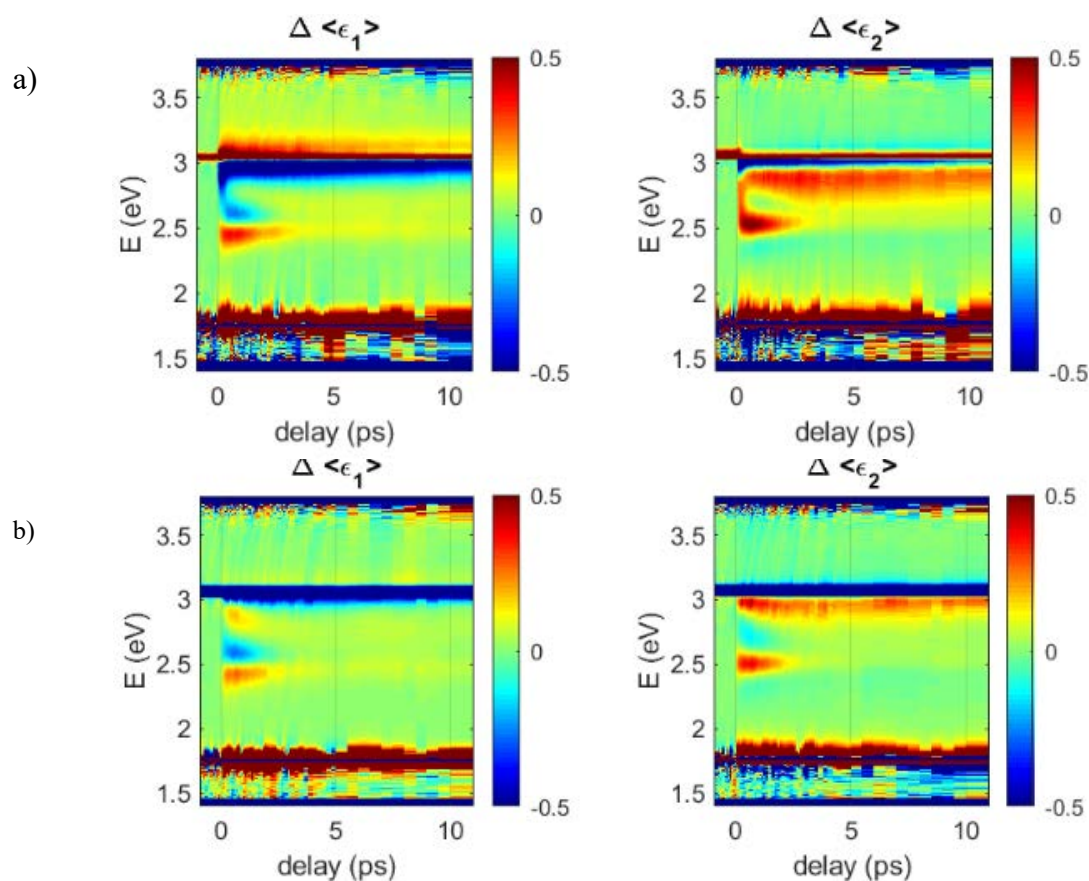


Figure 1. Time evolution of the pseudo-dielectric function of EA thin film on gold after the excitation by a 3.1 eV pump beam. a) s-polarization and b) p-polarization.

ELI Beamlines authors acknowledge the support of the ELIBIO (No. CZ.02.1.01/0.0/0.0/15-003/0000447) and ADONIS (No. CZ.02.1.01/0.0/0.0/16-019/0000789) projects from the European Regional Development Fund. EB acknowledges the preparation of ellagic acid thin films by physical vapor deposition by the Heliatek GmbH, Dresden.

- [1] Bittrich, E.; Domke, J.; Jehnichen, D.; et al. Morphology of Thin Films of Aromatic Ellagic Acid and its Hydrogen Bonding Interactions. *J. Phys. Chem. C*, 124 (30), 16381 – 16390, (2020)
- [2] Espinoza S.; Richter S., Rebarz M.; et al. Transient dielectric functions of Ge, Si, and InP from femtosecond pump-probe ellipsometry. *Appl. Phys. Lett.* 115, 052105 (2019)
- [3] Bittrich, E.; Domke, J.; Levichkova, M.; et al. Structural Templating of an Organic Solar Cell Absorber by Ellagic Acid To Tune Its Aggregation, Molecular Orientation, and Optical Properties. *ACS Appl. Energy Mater.* 4, 12, 14273 – 14286, (2021)

Investigation of the interaction of formic acid with flat and stepped palladium surfaces

J. Fingerhut, L. Lecroart, D. Borodin, M. Schwarzer, A. Kandratsenka¹,
T. N. Kitsopoulos^{1, 2, 3}, and A. M. Wodtke^{1, 2, 4}

*Institut für Physikalische Chemie, Georg-August-Universität Göttingen, D-37077 Göttingen,
Deutschland*

(corresponding author: J. Fingerhut, e-mail: jfinger1@gwdg.de)

¹ *Department of Dynamics at Surfaces, Max Planck Institute for Multidisciplinary Sciences, D-37077
Göttingen, Germany*

² *Department of Chemistry, University of Crete, GR-71003 Heraklion, Greece*

³ *Institute of Electronic Structure and Laser – FORTH, GR-71003 Heraklion, Greece*

⁴ *International Center for Advanced Studies of Energy Conversion, Georg-August University of
Göttingen, D-37077 Göttingen, Germany*

Understanding heterogeneous catalysis is based on knowing the energetic stability of adsorbed reactants, intermediates, and products as well as the energetic barriers separating them. Formic acid (HCOOH) for example is a potential hydrogen carrier and its decomposition on transition metals such as platinum or palladium is important to derive insights into the development of direct formic acid fuel cells. While the HCOOH chemistry was investigated especially under oxidative conditions^[1], less attention has been paid to oxygen lean conditions which are more representative to industrial applications. The decomposition on the bare metal surface has been mostly covered by theoretical studies^[2], but critical comparison to experimental rates are rare.

Here, we investigate the interaction of formic acid with atomically flat and stepped palladium surfaces by using Velocity-Resolved Kinetics (VRK)^[3]. We obtain accurate rates for formic acid desorption as well as CO₂ formation. Substitution of the C-end hydrogen with deuterium guides us to the key intermediates participating in the decomposition process. Furthermore, we identify these key intermediates and quantify reaction barriers with support of DFT calculations. Our results indicate that step sites increase the conversion of formic acid to CO₂ and H₂.

Furthermore, formic acid decomposition also yields the formation of hyperthermal CO₂. This dynamic component has only been observed for CO oxidation before while we clearly discard

a contribution of this reaction to our results. However, the formation of hyperthermal CO₂ might be intermediate and/or site selective.

Support from the European Research Council (ERC) under the European Union's Horizon 2020 research and innovation program (grant agreement no. [833404]) is gratefully acknowledged.

[1] T. L. Silbaugh, E. M. Karp and C. T. Campbell, *J. Am. Chem. Soc.* 136, 3964 (2014)

[2] J. Scaranto and M. Mavrikakis, *Surf. Sci.* 650, 111 (2016)

[3] J. Neugeboren, D. Borodin, H. W. Hahn, J. Altschäffel, A. Kandratsenka, D. J. Auerbach, C. T. Campbell, D. Schwarzer, D. J. Harding, A. M. Wodtke and T. N. Kitsopoulos, *Nature* 558, 280 (2018)

Nc-AFM and XPS studies of UHV-cleaved and hydrated mica

G. Franceschi, J. Balajka, S. Brandstetter, I. Sokolović, J. Pavelec, M. Schmid, M. Setvín, and U. Diebold

*Institute of Applied Physics, TU Wien, A-1040 Wien, Austria
(presenting author: G. Franceschi, e-mail: franceschi@iap.tuwien.ac.at)*

Muscovite mica is a common layered phyllosilicate with the nominal composition $\text{KAl}_2(\text{Si}_3\text{Al})\text{O}_{10}(\text{OH})_2$. Silica sheets with a honeycomb structure are held together by layers of K^+ ions that maintain charge neutrality when Al^{3+} substitutes Si^{4+} . The material cleaves easily at these layers and yields virtually step-free surfaces. For electrostatic reasons, one expects half of the K^+ ions to remain on each freshly-created surface.

The interaction between the K^+ ions and water has been extensively investigated both experimentally and computationally, focusing on liquid water [1–3]. However, experimental data on the atomic-scale hydration processes have remained elusive.

We present atomically-resolved constant-height nc-AFM and XPS data that shed new light on the properties of UHV-cleaved mica surface and its interaction with water vapor and clean liquid water. The latter experiments are based on a previously-established UHV-compatible method of dosing ultraclean liquid water [4].

The as-cleaved surface (Fig. 1) shows an array of protrusions with short-range order that we assign to the K^+ ions. Water vapor dosed in UHV at 100 K adsorbs molecularly and hydrates these cations. Exposing the sample to clean liquid water induces cation mobility.

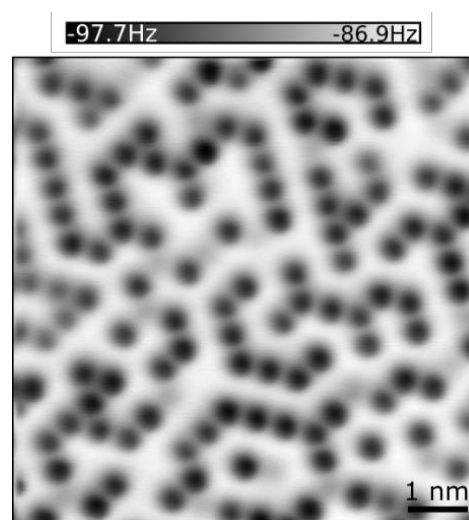


Fig. 1. Constant-height nc-AFM image of the surface of mica after cleavage in UHV.

Support by the European Research Council (ERC) under the European Union's Horizon 2020 research and innovation program (grant agreement No. 883395, Advanced Research Grant 'WatFun') is gratefully acknowledged.

- [1] H. K. Christenson, N. H. Thomson, *Surf. Sci. Reports* 71 367 (2016)
- [2] K. Kobayashi, N. Oyabu, K. Kimura, S. Ido, K. Suzuki, T. Imai, K. Tagami, M. Tsukada, and H. Yamada, *J. Chem. Phys.* 138, 184704 (2013)
- [3] S. Adapa, D. R. Swamy, S. Kancharla, S. Pradhan, and A. Malani, *Langmuir* 34, 14472 (2018)
- [4] J. Balajka, J. Pavelec, M. Komora, M. Schmid, U. Diebold, *Rev. Sci. Instrum.* 89, 083906 (2018)

No telluride formation on Ir(111), Ir(100), and Au(100) - just repelling adatoms

L. Hammer, T. Kißlinger, A. Schewski, A. Raabgrund, and M.A. Schneider

*Festkörperphysik, Friedrich-Alexander Universität Erlangen-Nürnberg, D-91058 Erlangen, Germany
(corresponding author: L. Hammer, e-mail: lutz.hammer@fau.de)*

Tellurium as the heaviest stable member of the chalcogen group (oxygen family) is metallic in its elemental form. Being adsorbed at a transition metal surface, however, it doesn't behave like a metal, which usually forms either islands or surface alloys. Instead, the adsorption behavior of Te is found to be comparable to that of oxygen. At a number of noble metal substrates like Cu(111) [1,2], Ag(111) [3] and Pt(111) [4,5] complex surface telluride phases are found, partly even inducing severe displacive substrate reconstructions [2]. Recently, the formation of a IrTe₂ monolayer was also claimed for Ir(111) upon Te adsorption and thermal reaction [6] and the Au(100) surface was even suspected to stabilize a plane square phase of monolayer tellurene [7]. Thus, we have investigated the development of tellurium phases at the (100) surfaces of Au and Ir as well as on Ir(111) as a function of submonolayer coverage and analyzed the crystallographic structure of all ordered phases by means of quantitative LEED-IV supported by STM and DFT.

On Au(100) we find a sequence of three ordered phases (2×2), c(10×2), and c(12×2) for Te coverages of $\theta_{\text{Te}} = 0.25$ ML, 0.30 ML, and 0.33 ML (cf. left part of Fig.1), respectively, in partial agreement with early reports for electrodeposited Te layers [8]. In contrast to these findings we were not able to produce under UHV conditions phases of higher coverage, in particular no c(2×2). The LEED-IV analyses of the detailed crystallographic structure of these phases proves Te always sitting in fourfold hollow sites, whereby substantial atomic relaxations of substrate Au atoms (of the order of 0.1 Å) are induced. For the c(10×2) phase, where first shorter Te-Te distances of nominally $\sqrt{2} \cdot a_{\text{Au}} = 4.07$ Å appear, we find a strong, presumably substrate-mediated, repulsive interaction, which pushes the Te atoms off-center by as much as 0.22 Å each. The revealed structural parameters as well as the STM appearance are quantitatively reproduced by total energy calculations. DFT also reveal that the binding energy drastically diminishes with the formation the c(10×2) phase, which substantiates the finding of severe Te-Te repulsion. We suspect that in case of a complete c(2×2) phase, where any evasive relaxation is prohibited by symmetry, the differential binding energy falls below the value for Te film formation, so that it can no more develop under our experimental conditions. Finally, there is no hint for any covalent Te-Te interaction in this system, which would be necessary for the predicted tellurene formation.

For Te adsorption on Ir(100) the situation is quite similar. However, the binding energy of Te is by about 2 eV higher compared to Au(100) and thus the Te-Te repulsion, which turns out to

be of nearly the same size, does not play such a crucial role for the development of ordered phases. Two simple phases are found with (2×2) and $c(2\times 2)$ periodicity. The structural analyses reveal similar substrate relaxation pattern, however, with much smaller amplitudes in accordance to the much larger elastic modulus of Ir.

On Ir(111) we find only one commensurate ordered Te phase, which is a $(\sqrt{3}\times\sqrt{3})R30^\circ$ structure (Fig.1, right), where Te atoms assume fcc hollow sites and thus are only threefold coordinated to Ir. Consequently, the binding energy is significantly lower compared to the fourfold coordination at the (100) surface (≈ 0.9 eV w.r.t. the (2×2) phase). Again, the local displacements of substrate atoms are quite small (≈ 0.02 Å). With further Te deposition the structure becomes increasingly compressed but in one dimension only. By that all atoms can follow an "easy path" from fcc via bridge to hcp sites and vice versa. The maximum achievable coverage is around $\theta_{\text{Te}} = 0.4$ ML again limited by the strong Te-Te repulsion ($d_{\text{Te-Te}} = 4.25$ Å). A comparison of STM images proves that it is just this compressed adatom structure, which was formerly misinterpreted to be an IrTe₂ monolayer [6].

We gratefully acknowledge supply of computing resources and support provided by the Erlangen Regional Computing Center (RRZE).

- [1] T. Kießlinger et al., Phys. Rev. B 102, 155422 (2020)
- [2] T. Kießlinger, L. Hammer, and M. A. Schneider, Phys. Rev. B 104, 155426 (2021)
- [3] M. Ünzelmann et al., Phys. Rev. Letters 124, 176401 (2020)
- [4] M. A. Schneider, this conference
- [5] L. Liu, D. Zemlyanov, and Y. P. Chen, 2D Mater. 8, 045033 (2021)
- [6] A. Wang et al., Chin. Phys. B 29, 078102 (2020)
- [7] W. Zhang et al., Phys. Rev. B 98, 115411 (2018)
- [8] N. Ikemiya et al, Surf. Sci. 369, 199 (1996); T.A. Sorensen et al., J. Electroanal. Chem. 467, 270 (1999)

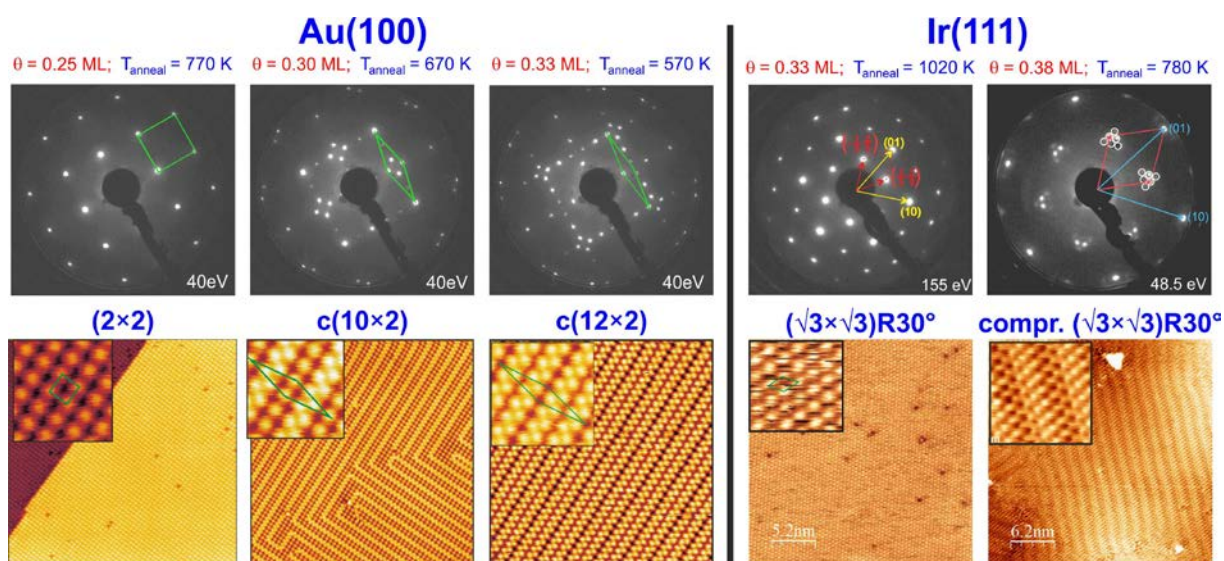


Fig. 1: Sequence of ordered phases observed for Au(10) (left) and Ir(111) (right) as a function of Te coverage. Top Row: LEED patterns, bottom row: STM images.

Surface investigations of zirconia films on Rh(111)

Johanna Hütner, Jan Balajka, Peter Lackner, Jiri Pavelec, Michael Schmid,
and Ulrike Diebold

Institut für Angewandte Physik, Technische Universität Wien, A-1040 Wien, Austria

(corresponding author: J.Hütner, e-mail: huetner@iap.tuwien.ac.at)

Zirconia (ZrO_2) is a material with a wide range of technological applications, spanning from catalysis [1] to biocompatible implants [2]. Doped ZrO_2 can be tuned for different properties such as partially stabilized zirconia for its toughness [3] and yttrium-doped zirconia as a solid-state electrolyte using oxygen vacancy diffusion [4]. Zirconia is a material that we often encounter in our daily lives, which substantiates the need to understand its properties at the atomic level.

Much work to synthesize and analyze crystalline ZrO_2 thin films at the nanoscale has been conducted by Lackner et al. [5-7]. They imaged the atomic structure of zirconia films grown on Rh(111), Pt(111) and created by oxidation of a Pt-Zr alloy $\text{Pt}_3\text{Zr}(0001)$ with STM. Combined with XPS and LEED measurements, the results gave new insights into the behavior of thin ZrO_2 films. ZrO_2 films on a Rh(111) substrate form a tetragonal phase at temperatures up to 730°C [5]. At higher temperatures and an oxygen pressure of 5×10^{-7} mbar, this tetragonal film undergoes a phase transition to the monoclinic phase and fully transforms at 850°C [5]. The tetragonal zirconia film is stabilized by oxygen vacancies, and the transformation to a monoclinic film is mediated by filling these vacancies with oxygen from the oxidized Rh(111) substrate [5-7]. Hence, breaking up the tetragonal film at higher temperatures and dewetting the metal substrate is essential for the transformation to monoclinic ZrO_2 . In order to obtain a monoclinic film at lower temperatures and without forming holes to the substrate, Rh can be deposited onto the ZrO_2 surface, which acts as a catalyst for O_2 dissociation and enables the transformation [6].

In order to study zirconia surface properties, a single crystalline film is needed. However, ZrO_2 has a low vapor pressure even at its high melting point, making it unfeasible to deposit via thermal evaporation. This challenge has been overcome by utilizing a sputter source adapted for the deposition of zirconia under UHV conditions [8, 9]. The sputter source is composed of a Zr target, bombarded by Ar^+ ions generated by electron collisions with Ar gas inside the source. The sputtered Zr is deposited onto a substrate in front of the source, while keeping an oxygen background pressure in the UHV chamber.

ZrO_2 has a large bandgap of 5 to 6 eV [10] which is why STM, as a technique relying on the tunneling current between a surface and a metallic tip, will naturally fail on bulk crystals or thicker films beyond ten monolayers [5]. As a step towards the structural analysis of bulk ZrO_2 , we obtained the first atomically resolved AFM images of ZrO_2 films grown on a Rh(111) substrate with the ZrO_2 sputter source described above. With this, we lay the basis for AFM

measurements of thick bulk-like zirconia films, where the influence of the substrate on the film can be neglected. We will discuss the scanning probe measurements in combination with LEED and XPS.

In addition, we explored the interaction of ZrO_2 films with a realistic environment by exposing the crystalline ZrO_2 films to mbar-range pressures of water vapor in a custom-built high-pressure cell. The exposure to clean water vapor may provide insights into the mechanisms controlling macroscopic properties of zirconia surfaces under ambient conditions.

The authors acknowledge funding from the Austrian Science Fund (FWF, Project SFB 'FOXSI' F45), and the European Research Council (ERC Advanced Reserach Grant 'WatFun', Grant Agreement No. 883395)

- [1] K. Tanabe, *Mater. Chem. Phys.*, 13, 347–364 (1985).
- [2] M. Hisbergues, S. Vendeville and P. Vendeville, *J. Biomed. Mater. Res., Part B*, 88, 519–529 (2009).
- [3] R. C. Garvie, R. H. Hannink and R. T. Pascoe, *Nature* 258, 703–704 (1975).
- [4] S. McIntosh and R. J. Gorte *Chem. Rev.* 104, 10, 4845–4866 (2004).
- [5] P. Lackner, Z. Zou, S. Mayr, J. I. J. Choi, U. Diebold and M. Schmid, *Surf. Sci.* 679, 180-187 (2019).
- [6] P. Lackner, Z. Zou, S. Mayr, U. Diebold and M. Schmid, *Phys. Chem. Chem. Phys.*, 21, 17613-17620 (2019).
- [7] P. Lackner, J. I. J. Choi, U. Diebold and M. Schmid, *J. Mater. Chem. A*, 7, 24837-24846 (2019).
- [8] L. Mayr, N. Köpfle, A. Auer, B. Klötzer and S. Penner, *Rev. Sci. Instrum.* 84, 094103 (2013).
- [9] P. Lackner, J.I.J. Choi, U. Diebold and M. Schmid, *Rev. Sci. Instrum.*, 88, 103904 (2017).
- [10] H. Jiang, R. I. Gomez-Abal, P. Rinke and M. Scheffler, *Phys. Rev. B* 81, 085119 (2010).

Introducing ViPErLEED: The Vienna Package for TensErLEED

Alexander M. Imre, Florian Kraushofer, Florian Doerr, Michael Schmid, Tilman Kießlinger, Ulrike Diebold, Lutz Hammer, Michele Riva

¹*Institute of Applied Physics, Technische Universität Wien, Wien, Austria
(presenting author: Alexander M. Imre, e-mail: imre@iap.tuwien.ac.at)*

²*Institute of Condensed Matter Physics, FAU Erlangen-Nürnberg, Germany*

Low-Energy Electron Diffraction (LEED) is a commonly employed technique in the field of surface science as it allows for quick qualitative assessment of surface structure. A quick check of the surface periodicity often serves as an indicator for successful sample preparation. However, simple LEED analysis overlooks a large amount of additional quantitative information contained in the diffracted electron beams beyond the Bragg condition.

Dynamic multiple scattering of incident electrons with surface layer atoms leads to strongly energy-dependent diffraction beam intensities I . In LEED $I(V)$, these intensities are evaluated as a function of the electron acceleration voltage V . The resultant spectra turn out to be sensitive to surface atom positions and vibrational amplitudes on the picometer scale [1]. Theoretical intensity curves can be calculated for a given trial structure model by performing computationally intensive dynamic scattering calculations and local optimization of structure parameters. Comparison of experimental and theoretical spectra can be reduced to a single number – the R factor – which is a strong indicator of the model's correctness [2].

As such, LEED $I(V)$ can be used to confirm or rule out theoretical structure models, making it a suitable complementary technique to scanning probe microscopy. Yet, in our opinion, the technique has been heavily underutilized and has seen bafflingly little progress in the last decades. That is despite the fact that most surface science laboratories already have LEED setups readily accessible that would need little modification to enable LEED $I(V)$. However, the main obstacle is that software support for LEED $I(V)$ is lacking, and existing solutions require prohibitively complex manual user input that makes getting started with the technique difficult and the comparison of many models tedious.

With the hope to make LEED $I(V)$ accessible to everyone in the surface science community, we introduce the Vienna Package for TensErLEED (ViPErLEED), a new all-in-one software and hardware package that tackles the main shortcomings of existing LEED $I(V)$ solutions. On the hardware side, ViPErLEED includes freely available schematics for electronics, based

on an Arduino, that allows upgrading existing LEED setups without extensive modifications. On the software side, we introduce a spot-tracking tool for automatic $I(V)$ curve extraction and a complete overhaul for the well-established TensErLEED code [3]. This includes additional functionality, comprehensible input and output files, automatic parameter selection based on the input, and significant improvements in performance.

- [1] T. Fauster, L. Hammer, K. Heinz, and M. A. Schneider, *Surface Physics: Fundamentals and Methods*. De Gruyter Oldenbourg, 2020. doi: 10.1515/9783110636697.
- [2] J. B. Pendry, “Reliability factors for LEED calculations,” *J. Phys. C Solid State Phys.*, vol. 13, no. 5, pp. 937–944, Feb. 1980, doi: 10.1088/0022-3719/13/5/024.
- [3] V. Blum and K. Heinz, “Fast LEED intensity calculations for surface crystallography using Tensor LEED,” *Comput. Phys. Commun.*, vol. 134, no. 3, Art. no. 3, Mar. 2001, doi: 10.1016/S0010-4655(00)00209-5.

Stable metal-organic networks on a weakly-interacting substrate: Fe-, Ni-, and Mn-TCNQ on graphene

Zdeněk Jakub, Anna Kurowská, Ondrej Herich, Lenka Černá, Pavel Procházka, Lukáš Kormoš, Azin Shahsavari, Jan Čechal

*CEITEC, Brno University of Technology, Purkyňova 123
61200 Brno, Czech Republic*

(Corresponding author: J. Čechal, e-mail: cechal@fme.vutbr.cz)

Metal-organic frameworks (MOF) are a class of materials commonly featuring long-range ordered arrays of single metal atoms residing in identical local environment, which makes them appealing for applications in catalysis, spintronics, sensing or quantum computing. Detailed atomic-scale views on MOFs can be gained through synthesis and analysis of 2D MOFs supported on surfaces, but to ascertain the intrinsic MOF properties it is necessary to choose a support that does not chemically interact with the MOF. Such systems have been recently reported,⁽¹⁻⁶⁾ but often show limited thermal and chemical stability which makes it difficult to study them using multi-technique approaches.

Here, we present three remarkably stable 2D MOFs supported on an inert graphene/Ir(111) substrate. As the organic linker we utilize a TCNQ molecule (7,7,8,8-tetracyanoquinodimethane), which is a strong electron acceptor and a popular choice for MOF synthesis both on-surface and in solution. We synthesized 2D MOF systems using three different transitional metals (M = Fe, Mn, Ni) and studied them at both atomic-scale and mesoscopic scale using scanning tunneling microscope (STM) and Low-Energy Electron Microscope (LEEM) combined with X-Ray Photoelectron Spectroscopy (XPS). The M-TCNQ preparation protocol is very robust, and we observe only a single structure with a $M_1(\text{TCNQ})_1$ stoichiometry for all the studied MOFs. This structure is present in 15 rotational domains on the graphene substrate, which can be described by three non-equivalent MOF/graphene rotations and mirrors.

Studies of thermal and chemical stability of the M-TCNQ networks reveal dramatic differences between the three systems: The most robust system is Fe-TCNQ, which survives annealing temperatures above 500 °C and even short exposures to ambient environment. In contrast, Ni-TCNQ decomposes already upon heating to 330 °C. The three systems also differ in their decomposition mechanism: While Fe- and Ni-TCNQ decompose into metallic clusters on the surface and TCNQ in the gas phase, Mn-TCNQ transforms into poorly defined 3D metal-organic structures upon annealing above 400 °C.

Overall, we propose the M-TCNQ networks on graphene to be ideal model systems for fundamental studies of single-atom reactivity or charge-transfer induced phenomena.

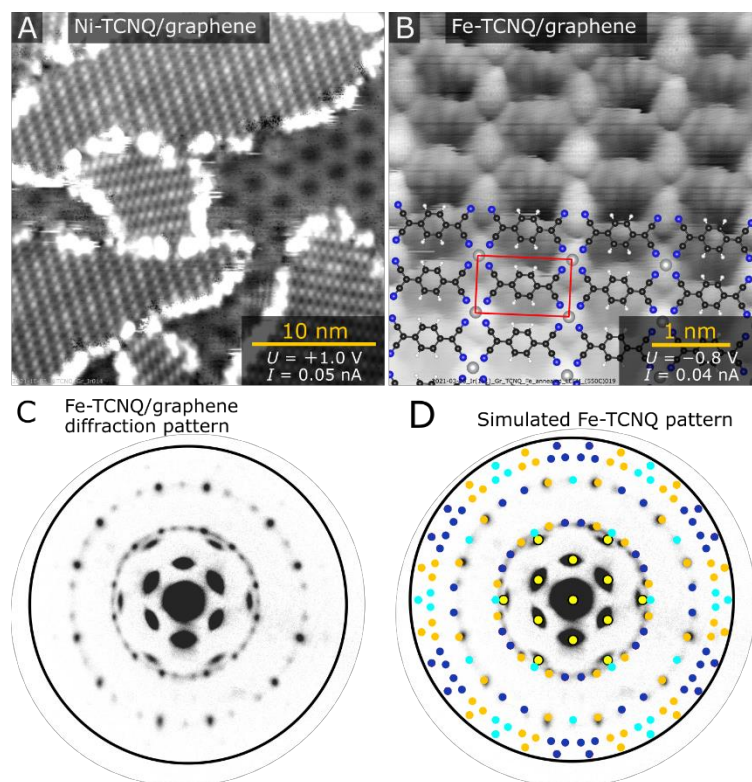


Figure 1: Characterization of M-TCNQ 2D MOFs supported on graphene by scanning tunneling microscopy and low energy electron diffraction. Fifteen rotational domains are observed in both STM and LEED, but these consist of only three non-equivalent graphene/MOF orientations.

This project has received funding from the European Union's Horizon 2020 research and innovation programme under the Marie Skłodowska-Curie grant agreement No. [101027667]. The research was in part supported by the GAČR project (No. 19-01536S). We also acknowledge CzechNanoLab Research Infrastructure supported by MEYS CR (LM2018110).

1. A. Kumar, K. Banerjee, A. S. Foster, P. Liljeroth, Two-Dimensional Band Structure in Honeycomb Metal–Organic Frameworks. *Nano Letters* **18**, 5596-5602 (2018).
2. J. Li *et al.*, Low-Dimensional Metal–Organic Coordination Structures on Graphene. *J. Phys. Chem. C* **123**, 12730-12735 (2019).
3. D. Moreno *et al.*, Dysprosium-directed metallocsupramolecular network on graphene/Ir(111). *Chemical Communications* **57**, 1380-1383 (2021).
4. L. Yan *et al.*, Synthesis and Local Probe Gating of a Monolayer Metal–Organic Framework. *Advanced Functional Materials* **31**, 2100519 (2021).
5. J. I. Urgel *et al.*, Controlling Coordination Reactions and Assembly on a Cu(111) Supported Boron Nitride Monolayer. *J. Am. Chem. Soc.* **137**, 2420-2423 (2015).
6. L. Schüller *et al.*, Deposition Order Controls the First Stages of a Metal–Organic Coordination Network on an Insulator Surface. *J. Phys. Chem. C* **120**, 14730-14735 (2016).

Plantae

Our Unity in Their Own Code

*Adriana Jelínková**Institute of Experimental Botany of the Czech Academy of Sciences, Prague, Czech Republic*

Plants are living organisms with sessile life style. Wikipedia says: Plants are predominantly photosynthetic eukaryotes of the kingdom *Plantae*. From our point of view, animals and plants could hardly have adopted different life strategies since we diverged from an ancient common ancestor. The cells of Kingdom *Plantae* are commonly confined within a rigid cell wall made of cellulose. There are some cases, where the cell wall is compromising its role, due to the plant cell specialization e.g. pollen tube growth, egg ovule opening and differentiation of the vasculature. Vasculature is a circulatory system of vascular plants consisting of Xylem and Phloem. Phloem in particular conducts assimilates and signals from photosynthetic parts of the plant body to the root.

For Kingdom *Animalia* is crucial nervous system. The electrical signal from one cell to the other (from an axon button to its effector) has to pass synaptic cleft. One of the two cells secrete neurotransmitters into the cleft. These chemical messengers diffuse through the cleft and act on the receptors present in the other cell. In some cases, the two cells are connected via gap junctions. The cytoplasm of these cells is connected in such a way that ions can freely diffuse among the cells. The action potential generated in one cell is transmitted to the next cell by the flow of ions.

The scientific controversy over whether or not plants have a nervous system is a long-term debate and is the crucial point of our perception of plants. Based on my recent results, I would like to bring up here a case where we are not all that different. I will show you *in vivo* the passage of actin from one plant cell to the other, “actin hopping “ in my terms, which has not been observed so far.

The actin cytoskeleton plays an essential role in several biological processes, including cell division, cell expansion, organelle movement, vesicle trafficking, and the establishment of polar cell growth [1]. Actin dynamics is crucial for the mammalian cells' ability to deform their membrane. The importance of F-actin during synapse formation has been shown quite recently [2]. It has been proposed that actin has a molecular scaffolding role in presynaptic function [3].

I will try to demonstrate the similarities of the life strategies between the two kingdoms on the example of actin dynamics at the hub of protophloem differentiation terminus. Protophloem is the primary phloem, it is the beginning in developmental way and end in the morphological [4]. Passage of F-actin from one cell (differentiated protophloem cell) to the other (companion cell) in lateral direction might be a signal for the termination of sieve cell element differentiation and transposing the over control of the companion cell which supports the future conductive wiring energetically and informationally. There are many questions that remains open. What happens with the cell wall between the cells? Is really F-actin passing from one cell to the other or is it just a signal transfer between the cells like in synapses at the interface of two plasma membranes. Process that would include rapid actin (de)polymerization. Or transient pore unit forms and actin has a propulsive role to transfer e.g. transcriptional factors and signal molecules as in gap junctions. Moreover, I observed that protophloem is literally loaded with Ca^{2+} (followed by R-GECO Ca^{2+} indicator) until the last undifferentiated cell. Differentiation of the protophloem terminates with Ca^{2+} "hopping"/trespassing of the calcium signal from cell to cell in the same fashion actin does.

At the end I would like to open a discussion on the theme: "Are plants really so rigid? Or are they "just slower" with their own time perception. Should we revise our point of view?"

Support by Czech Science Foundation (project no. 21-08021L). Lead Agency project between SNSF (Swiss National Science Foundation) and CSF (Czech Science Foundation) is gratefully acknowledged.

[1] A. Paez-Garcia, J.A. Sparks, L. de Bang, E.B. Blancaflor, *Plant Cell Monographs*, 23. Springer (2018)

[2] W. Zhang, D.L. Benson, *J. Neurosci. Res.*, 69, 427-436 (2002)

[3] S. Sankaranarayanan, P. Atluri, T. Ryan, *Nat Neurosci* 6, 127–135 (2003)

[4] H. Bauby, F. Divol, E. Truernit, O. Grandjean, J.C. Palauqui, *Plant and Cell Phys.*, 48, 97–109 (2007)

Characterization and comparison of model and industrial steel samples to get insight about corrosion and passivation processes.

Lukas Kalchgruber^{1*}, Michael Hahn¹, Jiri Pavelec² and Markus Valtiner¹

¹Applied Interface Physics, Institute of Applied Physics, Vienna University of Technology, Vienna, Austria

²Surface Physics, Institute of Applied Physics, Vienna University of Technology, Vienna, Austria

*E-Mail address: kalchgruber@iap.tuwien.ac.at

Steel has many different applications in industry. In 2020, a total of 1877.5 Mt of crude steel was produced [1]. Due to corrosion, much of this important resource is lost. Thus, it is necessary to gain a fundamental knowledge of corrosion and passivation processes of steel samples. To achieve that, various methods may be applied; the ones utilized for this project include EC (= **E**lectro**c**hemistry), ICP-MS (= **I**nductively **c**oupled **p**lasma **m**ass **s**pectrometry), XPS (= **X**-ray **p**hotoelectron **s**pectroscopy), SEM (= **S**canning **e**lectron **m**icroscopy), SFA (= **S**urface **f**orce **a**pparatus) and confocal microscopy. Additionally, different samples with a known composition are needed. These include industrial samples and model samples, which have a defined amount of iron, chromium, nickel, molybdenum and manganese.

To gain insight about the passivation and corrosion processes, three different approaches were taken. Moreover, a new cell design will be suggested to increase the effectiveness of the conducted research.

The first approach is utilizing the SEM to analyze the oxide layers on the steel surface which were generated thermally or via a plasma. Firstly, a part was cut by using FIB (= **F**ocused **I**on **B**eam) and secondly, the samples were analyzed via SEM in the channeling contrast mode. The obtained results demonstrated a good comparability to literature values [2]. The results for the thermally treated samples showed an advantageous distribution of the oxide layer over the whole surface when applying a temperature of about 300°C for 30 minutes. The results of the plasma treated samples suggested that the energy input of the plasma has nearly no impact on the oxide layer distribution. To get further information about the oxide layer, the adhesive interaction of a polymer with the surface of differently treated steel samples was analyzed by utilizing the SFA. The adhesive pressure that was calculated could be directly compared to the ratio of Oxide vs Hydroxide on the surface by measuring with XPS. The trends of this experiment indicated that thermally treated samples have a lower amount of hydroxide on the surface and show lower adhesive pressures (polymer: SEBS). In contrast to that, the samples treated with a plasma showed higher hydroxide amounts and higher adhesive pressures.

The second approach involves a coupling of ICP-MS with an electrochemical flow cell. With this powerful tool, it is possible to gain an understanding of corrosion and passivation processes on the surface. Within this setup, the dissolved material can then be transported directly into the ICP-MS, where the ratio of dissolved elements can be analyzed [3]. After this, the corrosion and passivation sections within the plot can be fitted with a combination of a linear and exponential function. The working theory is that the first exponential part shows the kinetic reaction of the first order, which relates to a concentration dependent step. The linear part of the fit implies that a reaction of order zero takes place. A concentration independent process could be the transport of species from underneath the oxide layer to the surface along the defects of the oxide layer. Over time, the defects on the surface heal, which gives the species less pathways to dissolve through. Therefore, less dissolution over time is monitored in the ICP-MS. One attempt to prove this working theory is performing impedance spectroscopy.

One further approach to retrieve information about the ability of the oxide layer to re-passivate is building a scratching cell. For this, the currently used EC flow cell was adapted in a way that makes it possible to scratch the surface off the steel sample in situ. After scratching the surface, the dissolution first increases, but then decreases over time. This connection can also be fitted with a combination of an exponential and linear function. In this way, the “half-live time” can be calculated, which gives insight on the re-passivation speed of different samples after mechanically damaging the surface.

For the second and third approach, an EC flow cell was used. This flow cell has some major drawbacks, such as the following:

- Poor distribution of the electrolyte current density
- Increased crevice corrosion due to the O-Ring
- Transport of species to the WE
- Peak broadening due to electrolyte transfer

To increase the effectiveness of this coupling, a new cell is designed. The idea for the new cell is based on the Avesta cell, which was designed to study pitting corrosion instead of crevice corrosion. In this setup, a slow water stream is directed from the outside to the crevice (formed between O-ring and WE) via filter paper to remove the material stagnating in the crevice. [4] The adaption (to increase the effectiveness) was to remove the filter paper and instead use sapphire as material which is hard enough to form a well-defined crevice by press fitting. Furthermore, the flow profile and the performance of the electrochemical process were improved. To evaluate these adaptations of the Avesta cell, COMSOL Multiphysics was used.

This project is supported and funded by the BBG (= **B**erndorf **B**and **G**roup) and FFG (= Österreichische **F**orschungsförderung **G**mbH).

[1] https://en.wikipedia.org/wiki/List_of_steel_producers Retrieved 14.01.2021.

[2] C. Degueldre, D. Buckley, J. Dran, and E. Schenker, “Study of the oxide layer formed on stainless steel exposed to boiling water reactor conditions by ion beam techniques, ”Journal of Nuclear Materials, vol. 1252, pp. 22 – 27, **1998**.

[3] D. Dworschak, C. Brunnhofer, and M. Valtiner, “Complementary electrochemical icp-ms flow cell and in-situ afm study of the anodic desorption of molecular adhesion promoters, ”Preprint submitted to Applied Surface Science, **2021**

[4] H. Andersen, C.-O. Olsson, and L. Wegrelius, “Critical pitting temperatures in sodium chloride and ferric chloride solutions - determined using the 'avestacell', ”Material Science Forum, vol. 289-292, pp. 925 – 932, **1998**

Design and Testing of a Home-Built UHV Suitcase

L. Lezuo, L. Dockalová¹, J. Pavelec, G. Parkinson and U. Diebold

*Institute of Applied Physics, TU Wien, Wiedner Hauptstrasse 8-10/134, Vienna, Austria
(corresponding author: J. Pavelec, e-mail: pavelec@iap.tuwien.ac.at)*

¹*Institute of Physical Engineering, Brno University of Technology*

Due to their extreme sensitivity to adsorbate molecules, most experiments on surfaces have to be carried out in ultrahigh vacuum (UHV). Several different techniques and experiments are needed to explain and understand the phenomena happening on the atomic scale. Although the instrumentation of most vacuum chambers in our surface physics group allows exciting results, occasionally, a sample has to be transferred from one chamber to another. In these instances, a vacuum suitcase like the one presented here is needed to ensure UHV conditions during the transfer process and avoid contamination by air preserving the sample surface.

The UHV suitcase consists of three chambers (see Figure 1) divided by gate valves and various pumps to reach the needed vacuum in a short time and reduce the contamination of the sample surface further. The storage stage (a) contains the sample during a transfer, is pumped by a NEG/ion-pump combination (g) and is located at the back of the system. The transfer stage (b) is pumped by a turbo molecular pump (d), a cryopump (LN₂ or LHe temperature) (e) and a NEG-pump (f). The cryopump consists of two aluminium parts in thermal contact with the cryostat containing the liquid gas. They are constructed in such a way that the sample is in direct line-of-sight with only the cold surface during the transfer process to ensure the cleanliness of the transfer process further. Possible desorbing molecules get trapped on the cold surface ($T \approx 105$ K). Finally, the venting stage (c), which is vented during a transfer process, is constrained to the smallest possible volume to reduce the inner surface of the system and hence decrease the possible achievable pressure.

The design of the system and a first test with transferred samples between a UHV-based PLD growth chamber and a q+ based LT STM/AFM chamber will be discussed.

Support by the European Research Council (ERC) under the European Union's Horizon 2020 research and innovation program (grant agreement No. 883395, Advanced Research Grant 'WatFun') is gratefully acknowledged.

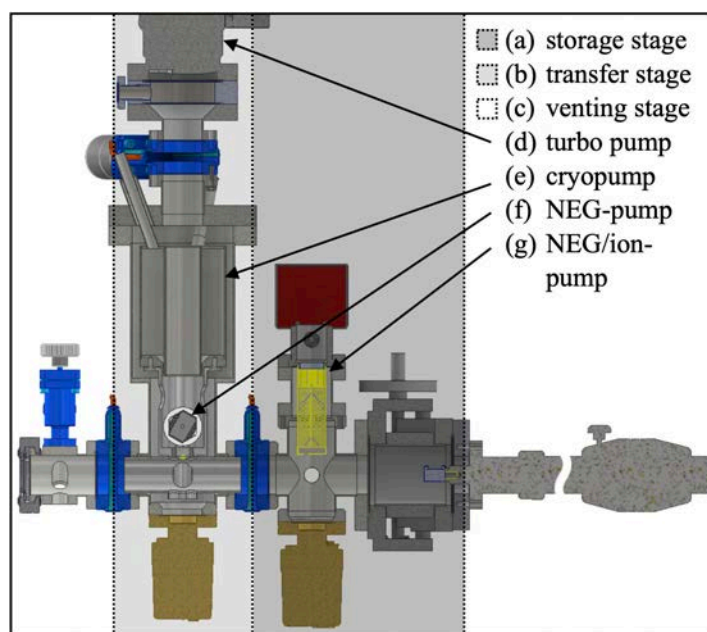


Figure 1: Corss section of the Vacuum suitcase consisting of the storage stage (a), the transfer stage (b) and the venting stage (c). The system is pumped by a scroll pump (not shown), a turbo pump (d), a cryopump (e), a NEG-pump (f) and a NEG/ion-pump (g).

Surface electromigration of 2D confined islands

S. Curiotto, F. Cheynis, P. Müller, F. Leroy

Aix Marseille Univ., CNRS, CINAM, Campus de Luminy, Marseille France

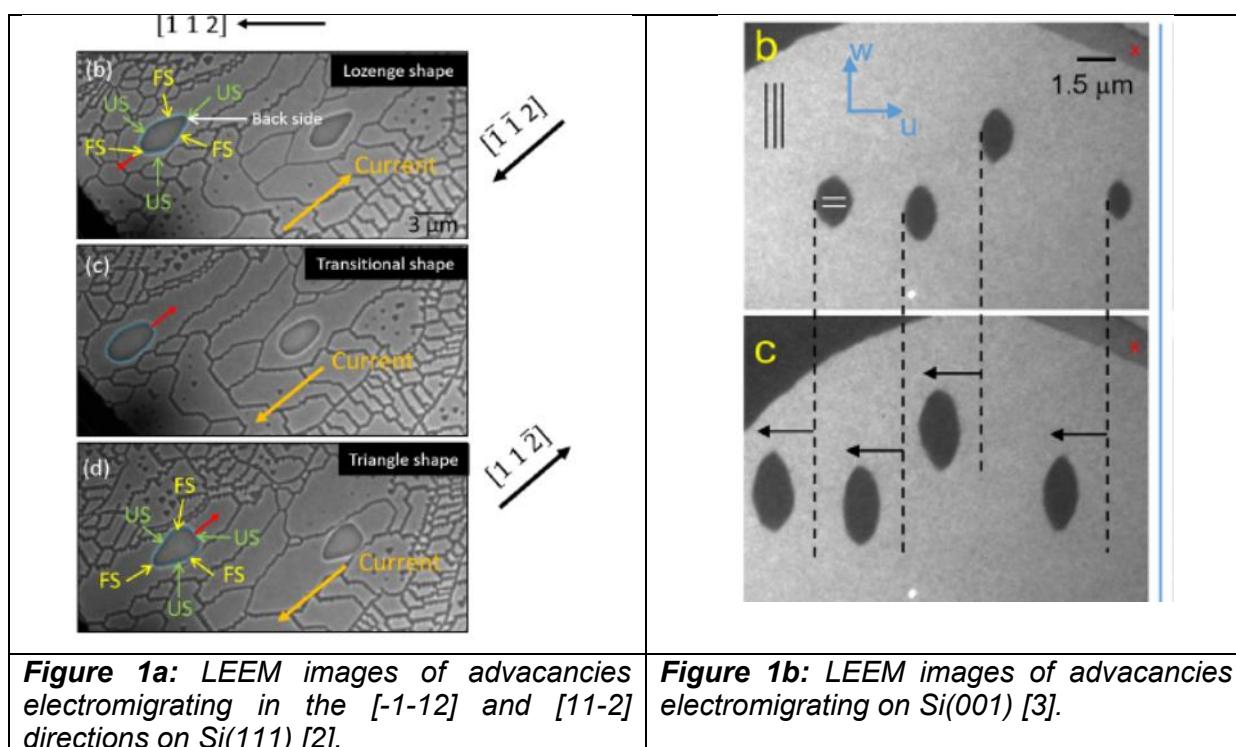
(corresponding author: P. Müller, e-mail: pierre.muller@univ-amu.fr)

In this work we investigate the electromigration of nanoobjects as a result of atomic diffusion biased by the application of an electric field [1-5].

More precisely we use Low Energy Electron Microscopy to investigate in operando (in presence of an electric field) the migration of Si(111)-1×1 negative islands (advacancies) confined on Si(111)-7×7 terraces and the migration of Si(001) negative and positive (ad-islands) confined on Si(001)-1×2 terraces.

The main results are the following:

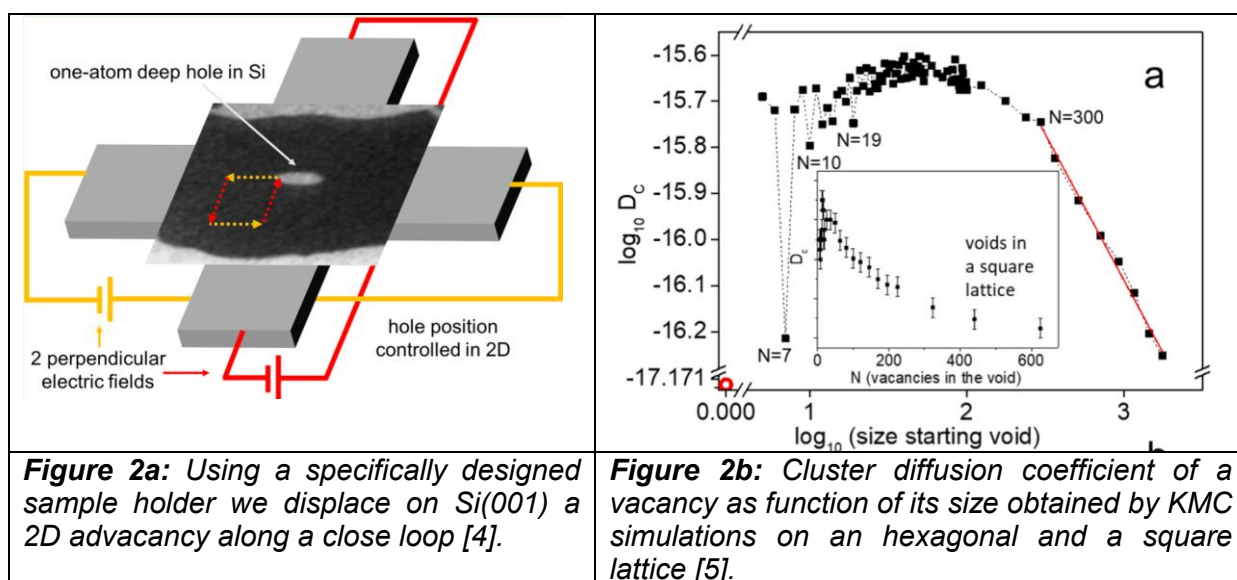
1/ Si(111) advacancies confined on Si(111)-7×7 terraces move opposite to the current direction, with velocity increasing with the radius [2]. The effective charge of Si adatoms is found to be 2.8 ± 0.5 and the kinetic length of attachment-detachment about 500 nm. Moreover, the analysis of the island's shape reveals that the electric current significantly biases the kinetic rate of mass transfers at step edges (Figure 1a)



2/ The direction of motion of Si(001) advacancies depends on the diffusion anisotropy [3]. Thus it does not necessarily coincide with the electric field direction. A simple analytical model explains most of the observations (Figure 1b).

3/ We show that the displacement of Si(001) advacancies can be controlled by means of two perpendicular electric fields [4]. Such a proof of concept opens the way to the manipulation of 2D objects on surfaces (Figure 2a).

4/ Complementary Kinetic Monte Carlo simulations show that the diffusion coefficient of small clusters strongly depends on their size [5]. In particular, the diffusion coefficient of small voids on an hexagonal lattice increases with the cluster size, reaches a plateau and then decreases (Figure 2b).



- [1] F. Leroy, A. El Barra, F. Cheynis, P. Müller, S. Curiotto, Phys. Rev. Lett. 123, 176101 (2019).
- [2] S. Curiotto, P. Müller, A.El-Barra, F. Cheynis, O. Pierre-Louis, Appl. Surf. Sci. 469, 463 (2019).
- [3] F. Leroy, A. El Barra, F. Cheynis, P. Müller, S. Curiotto, Phys. Rev. B 102,235412 (2020).
- [4] S. Curiotto, F. Cheynis, P. Müller, F. Leroy, ACS Appl. Mat. 3, 1118 (2020).
- [5] S. Curiotto, F. Cheynis, P. Müller, F. Leroy, Appl. Surf. Sci. . 149454, (2020)

Combined spectro-electrochemical methods to investigate electrochemical corrosion in real-time

M. Olgiati^{1,2}, M. Valtiner^{1,2}

*Institut für Allgemeine Physik, Technische Universität Wien, A-1040 Wien, Austria
(corresponding author: M. Olgiati, e-mail: olgiati@iap.tuwien.ac.at)*

¹ *Vienna University of Technology, Institute of Applied Physics, Wiedner Hauptstrasse 8-10, A-1040, Vienna, Austria*

² *Centre of Electrochemical Surface Technology CEST, Viktor-Kaplan-Straße 2, 2700 Wiener Neustadt, Austria.*

Many engineering alloys, such as the aerospace grade aluminium alloys 2024 and 7075, are vulnerable to corrosive degradation, that is both i) localised and ii) time-dependent.

The local nature of corrosion is most of the time induced by the intrinsic features of the microstructure (e.g. intermetallic second phases), which may determine the spatial location of the corrosive attack [1]. As for the time-dependency, it is known that corrosion-induced microstructural changes may activate different types of corrosion (e.g. dealloying, meta-stable pitting, intergranular attack, etc.) at different exposure/immersion times and with different propagation rates [2].

For these reasons, characterization and, consequently, understanding the degradation mechanism of these alloys is not only complex, but must also rely on in-situ and highly spatio-temporally resolved techniques [3] [4].

In this work, we developed an in-situ spectro-electrochemical scanning flow cell to study corrosive degradation with non-destructive techniques. Thanks to our set-up we were able to extract online information on the elemental dissolution at different immersion times via inductively coupled plasma mass spectroscopy (ICP-MS) and relate them to the optical changes detected on in-situ optical micrographs as well as to the characteristic transients appearing during electrochemical noise measurements.

Support by the Österreichische Forschungsförderungsgesellschaft (FFG) is gratefully acknowledged.

- [1] A. Boag, A. E. Hughes, A. Glenn, T. Muster and D. McCulloch, *Corrosion Science* 53(1), 17-26 (2011)
- [2] M. Olgiati, P. J. Denissen and S. J. Garcia, *Corrosion Science* 192, 109836 (2021)
- [3] A. Kosari, F. Tichelaar, P. Visser, H. Zandbergen, H. Terryn and J. M. C. Mol, *Corrosion Science* 177, 108947 (2020)
- [4] A. Kosari, H. Zandbergen, F. Tichelaar, P. Visser, P. Taheri, H. Terryn and J. M. C. Mol, *Corrosion Science* 177, 108912 (2020)

Design of apparatus for surface tension measurement of pure water in vacuum.

J. Pavelec, P. Ryan, J. Balajka, U. Diebold

*Institute of Applied Physics, Vienna University of Technology, A-1040 Wien, Austria
(corresponding author: J. Pavelec, e-mail: pavelec@iap.tuwien.ac.at)*

Very little is known about the surface tension of pure liquids in contact with their pure gaseous phases, i.e., without the presence of other gases or spurious contaminants. This is surprising given that contaminants are known to greatly affect surface tension values [1].

Recently, we have developed a method to dose liquid water onto pristine surfaces in UHV using a small cryostat [2,3]. We combine this approach with the pendant drop method [4] to measure the surface tension of ultra-clean liquids in contact with their pure gaseous phases. The upgraded version of the small cryostat replaces the syringe typically used in the pendant-drop method. The ultra-clean liquid is condensed onto a small cryostat placed in a vacuum chamber. A pendant drop is formed, photographed, and analyzed, allowing the surface tension of the liquid to be directly determined.

The value of surface tension of water/water vapour compared to water/air may differ only a little (0.1%). This requires many design considerations for the pendant drop apparatus to achieve the required precision. The main factors affecting measurement are temperature stability, absolute temperature control of the drop, optical aberrations and water purity.

We have assessed these factors in the design of the apparatus shown in Figure 1. Temperature stability is provided by an improved version of LN₂ coldfinger [2], where a calibrated diode measures the temperature. The same diode type is used to control the temperature of a water bath, which is in equilibrium with the drop. Additionally, the vapour pressure is measured by a capacitive gauge. A telecentric lens, uniform LED illumination and CMOS camera are used to acquire high-quality images of the drop. Purity is achieved by using only selected materials in the chamber: 316LN stainless steel, Viton and sapphire. The apparatus is connected to a UHV setup equipped with XPS which allows measurement of the drop purity. This is achieved by evaporating many drops onto a gold foil pre-cleaned in UHV. Then the gold foil is transferred to the UHV setup, and the water residue composition is characterized by XPS.

The design of the apparatus is discussed and preliminary measurements of ultra-clean water are presented.

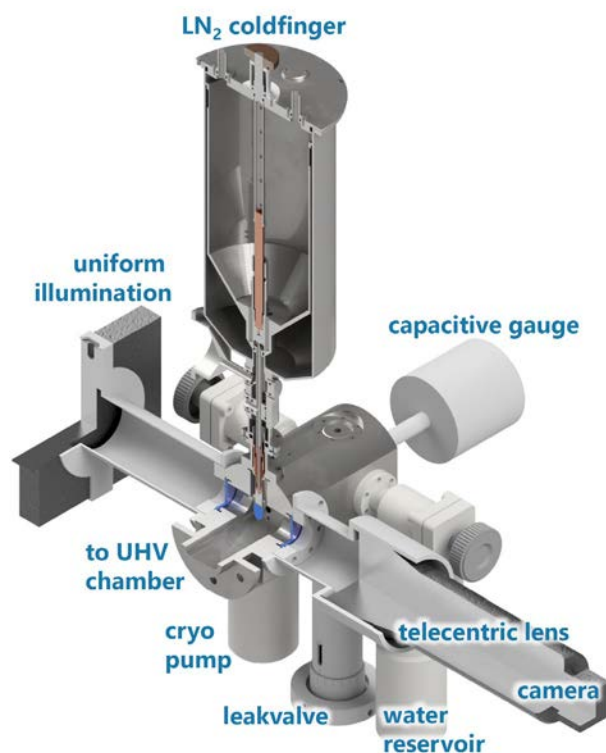


Figure 1: Apparatus for surface tension measurement of pure liquids in contact with their pure gaseous phases.

Support by the European Research Council, Advanced Research Grant ‘WatFun’ (project No. 883395) is gratefully acknowledged.

[1] Y. Uematsu, D.J. Bonthuis, R.R. Netz, "Impurity effects at hydrophobic surfaces", *Current Opinion in Electrochemistry*, Vol. 13, Pages 166-173, (2019)

[2] J. Balajka, J. Pavelec, M. Komora, M. Schmid, and U. Diebold, "Apparatus for dosing liquid water in ultrahigh vacuum.", *Review of Scientific Instruments* 89(8), 083906, (2018)

[3] J. Balajka, M.A. Hines, W.J.I. DeBenedetti, M. Komora, J. Pavelec, M. Schmid, U. Diebold, "High-affinity adsorption leads to molecularly ordered interfaces on TiO₂ in air and solution.", *Science*, 361, 786-789, (2018)

[4] J.D. Berry, M.J. Neeson, R.R. Dagastine, D.Y.C. Chan, R.F. Tabor, "Measurement of surface and interfacial tension using pendant drop tensiometry.", *Coll. Interface Sci.* 454, 226, (2015)

Mesoscopic structures in ultrathin silica films

Kristen M. Burson,¹ Hyun Jin Yang,² Daniel S. Wall,¹ Thomas Marsh,¹ Zechao Yang,² David Kuhness,² Matthias Brinker,² Leonard Gura,² Markus Heyde,² Wolf-Dieter Schneider,² and Hans-Joachim Freund²

¹Hamilton College, 198 College Hill Road, Clinton, NY, 13323 USA

²Fritz-Haber-Institut der Max-Planck-Gesellschaft, Faradayweg 4-6, 14195 Berlin, Germany,

(corresponding author W.-D. Schneider, e-mail: wolf-dieter.schneider@epfl.ch)

Silica films can be prepared in both crystalline and vitreous forms as well as of mixtures between them. In the past, the atomic-scale structure of this film system has been in the center of interest. [1,2] However, at a larger scale, mesoscale structures like holes and substrate steps can play an important role for confined space reactions [3-6] and other applications of silica films. In the present investigation we report on mesoscale structures in silica films grown on Ru(0001) in ultra-high vacuum, and probed with scanning tunneling microscopy (STM). We find that silica films can exhibit coexisting phases of monolayer [2], zigzag [7], and bilayer [2,8] structures. These coexisting phases were observed to be influenced by holes in the film structure and also by atomic-scale substrate steps [9]. Specifically, film regions bordering holes in silica bilayer films exhibit vitreous character [10–13], even in regions with predominant crystalline film structure.

Silica films were prepared on a Ru(0001) substrate in ultrahigh vacuum. Ru(0001) surfaces were cleaned with cycles of Ar⁺ sputtering and annealing in UHV at 1450 K. A 3O-(2x2)-precover on Ru(0001) was established by annealing at 1180K temperature in 10⁻⁶ mbar O₂ for 10 minutes. Silicon was deposited from a rod via an e-beam evaporator in 2 x 10⁻⁷ mbar O₂ and the sample was subsequently annealed to 1180K in 2 x 10⁻⁶ mbar O₂ for 20 minutes. Finally, samples were cooled to below 500 K in an oxygen environment for 20-30 minutes.

The present characterization of mesoscale structures in Ru-supported ultrathin silica films provides a scale-up of the former atomic-scale investigations with implications for catalysis and chemistry in confined space. Specifically, the transition from the amorphous to the crystalline phase near film holes is an exciting observation which may be expected to have implications for structural control of materials.

This project has received funding from the European Research Council (ERC) under the European Unions Horizon 2020 Research and Innovation Program (Grant Agreement No. 669179).

- [1] L. Lichtenstein, C. Buechner, B. Yang, S. Shaikhutdinov, M. Heyde, M. Sierka, R. Wlodarczyk, J. Sauer, H.-J. Freund, *Angew. Chem.Int. Ed.* 51, 404 (2012)
- [2] C. Büchner, M. Heyde, *Progress in Surf. Sci.* 92, 341 (2017)
- [3] F. Goettmann, C. Sanchez, *J. Mater. Chem.* 17, 24 (2006)
- [4] M. J. Prieto, H. W. Klemm, F. Xiong, D. M. Gottlob, D. Menzel, T. Schmidt, H.-J. Freund, *Angew. Chem. Int. Ed.* 57, 8749 (2018)
- [5] Q. Fu, X. Bao, *Chem. Soc. Rev.* 46, 1842 (2017)
- [6] M. J. Prieto, T. Mullan, M. Schlutow, D. M. Gottlob, L. C. Tănase, D. Menzel, J. Sauer, D. Usvyat, T. Schmidt, H.-J. Freund, *J. Am. Chem. Soc.* 143, 8780 (2021)
- [7] D. Kuhness, H. J. Yang, H. W. Klemm, M. Prieto, G. Peschel, A. Fuhrich, D. Menzel, T. Schmidt, X. Yu, S. Shaikhutdinov, et al. , *J. Am. Chem. Soc.* 140, 6164 (2018)
- [8] K. M. Burson, C. Büchner, M. Heyde, H.-J. Freund, *J. Phys.: Condens. Matter* 29, 035002 (2017)
- [9] L. Gura, S. Tosoni, A. L. Lewandowski, P. Marschalik, Z. Yang, W.-D. Schneider, M. Heyde, G. Pacchioni, H.-J. Freund, *Phys. Rev. Materials* 5, L071001 (2021)
- [10] H. W. Zachariasen, *J. Am. Chem. Soc.* 54, 3841 (1932)
- [11] L. Lichtenstein, M. Heyde, H.-J. Freund, *Phys. Rev. Lett.* 109, 106109 (2012)
- [12] A. Malashevich, S. Ismail-Beigi, E. J. Altman, *J. Phys. Chem. C* 120, 26770 (2016)
- [13] E. I. Altman, J. Götzen, N. Samudrala, U. D. Schwarz, *J. Phys. Chem. C* 117, 26144 (2013)

Towards Elementary Rate Constants of Water Formation from the Reaction of Hydrogen and Oxygen on Palladium

M. Schwarzer, N. Hertl¹, D. Borodin, J. Fingerhut, T. N. Kitsopoulos^{1,2,3},
and A. M. Wodtke^{1,4}

*Institute for Physical Chemistry, Georg-August University of Goettingen, Tammannstraße 6, 37077
Goettingen, Germany*

(corresponding author: M. Schwarzer, e-mail: michael.schwarzer1@stud.uni-goettingen.de)

¹ *Department of Dynamics at Surfaces, Max Planck Institute for Biophysical Chemistry, Am Fassberg
11, 37077 Goettingen, Germany*

² *Department of Chemistry, University of Crete, Heraklion, Greece*

³ *Institute of Electronic Structure and Laser – FORTH, Heraklion, Greece*

⁴ *International Center for Advanced Studies of Energy Conversion, Georg-August University of
Goettingen, Tammannstraße 6, 37077 Goettingen, Germany*

Even though the interaction of hydrogen and oxygen adsorbed on single crystal palladium surfaces has been studied in great detail,^[1] there is still uncertainty about the elementary chemical processes which govern the catalytic action. The mechanism of water formation is studied under ultra-high vacuum conditions by either dosing the oxygen atom covered surface with a temporally narrow molecular pulse of H₂ (30 μs) or by dosing the hydrogen atom covered surface with a pulse of O₂. The transient kinetics of water formation is obtained by applying the velocity resolved kinetics^[2] method, which allows for direct measurement of the reactive flux. Both experiments lead to fundamentally different kinetic behavior. Using the tools of rigorous kinetic modeling and advanced application of transition state theory allows for extraction of elementary energetic parameters. These can be used directly for testing density functional theory calculations.

Support from BENCH graduate school, funded by the DFG (389479699/GRK2455) and from the European Research Council (ERC) under the European Union's Horizon 2020 research and innovation programme (grant agreement no. [833404]) is gratefully acknowledged.

[1] T. Engel, H. Kuipers, Surf. Sci. 90, 181 (1979)

[2] J. Neugeboren, D. Borodin, H. W. Hahn, J. Altschäffel, A. Kandratsenka, D. J. Auerbach, C. T. Campbell, D. Schwarzer, D. J. Harding, A. M. Wodtke & T. N. Kitsopoulos, Nature 558, 280 (2018)

Single-layer graphene on epitaxial FeRh thin films

V. Uhlír^{1,2}, F. Pressacco³, J. A. Arregi¹, P. Procházka^{1,2}, S. Průša^{1,2},
M. Potoček^{1,2}, T. Šíkola^{1,2}, J. Čechal^{1,2}, A. Bendounan⁴, F. Sirotti^{4,5}

¹ CEITEC BUT, Brno University of Technology, 612 00 Brno, Czech Republic
(corresponding author: T. Šíkola, e-mail: sikola@fme.vutbr.cz)

² Institute of Physical Engineering, Brno University of Technology, 61669 Brno, Czech Republic

³ Center for Free Electron Laser Science, University of Hamburg, 22761 Hamburg, Germany

⁴ Synchrotron SOLEIL, F-91192 Gif-sur-Yvette Cedex, France

⁵ Physique de la Matière Condensée, CNRS and École Polytechnique, IP Paris, F-91128 Palaiseau,
France

Graphene is a 2D material that displays excellent electronic transport properties with prospective applications in many fields. Inducing and controlling magnetism in the graphene layer, for instance by proximity of magnetic materials, may enable its utilization in spintronic devices.

This poster presents fabrication and detailed characterization of single-layer graphene formed on the surface of epitaxial FeRh thin films. The work was done at the TEMPO beamline at the SOLEIL synchrotron radiation facility and at the CEITEC Nano research infrastructure using a complex UHV apparatus (see Fig. 1). Its results are presented in detail in [1]. FeRh is a highly tunable material [2, 3] and the magnetic state of its surface can be controlled by temperature, magnetic field or strain due to interconnected order parameters. Characterization of graphene layers by X-ray Photoemission and X-ray Absorption Spectroscopy, Low-Energy Ion Scattering, Scanning Tunneling Microscopy, and Low-Energy Electron Microscopy shows that graphene is single layered, polycrystalline and covers more than 97% of the substrate. Graphene displays several preferential orientations on the FeRh(0 0 1) surface with unit vectors of graphene rotated by 30°, 15°, 11°, and 19° with respect to FeRh substrate unit vectors. In addition, the graphene layer is capable to protect the films from oxidation when exposed to air for several months. Therefore, it can be also used as a protective layer during fabrication of magnetic elements or as an atomically thin spacer, which enables incorporation of switchable magnetic layers within stacks of 2D materials in advanced devices.

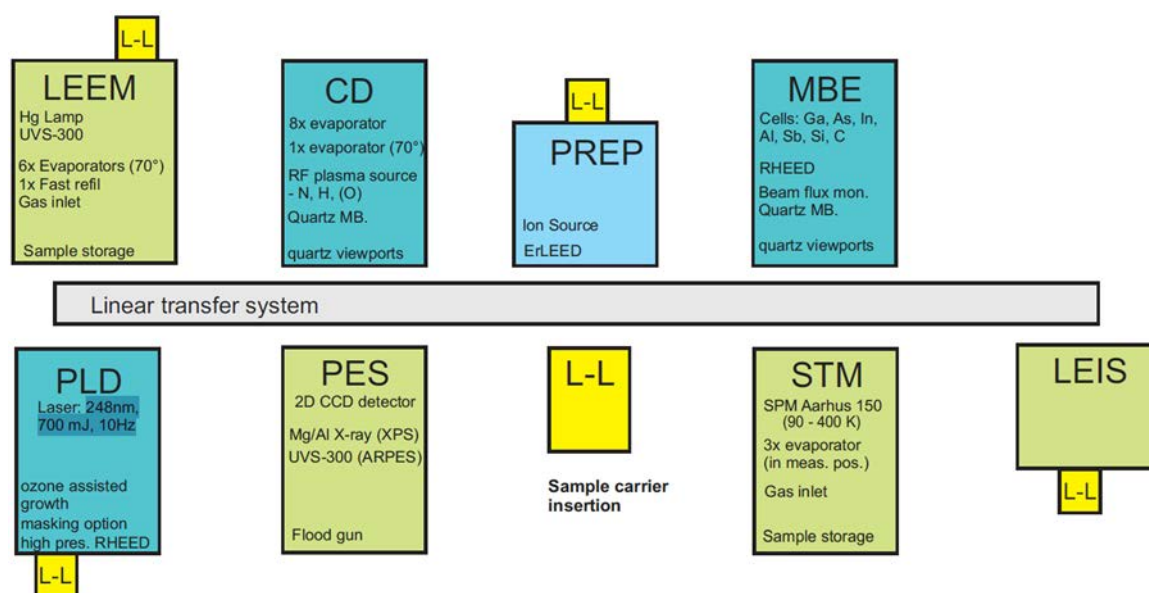


Fig. 1: Schematic of the complex UHV apparatus at CEITEC Nano Research Infrastructure

Access to the CEITEC Nano Research Infrastructure was supported by the Ministry of Education, Youth and Sports (MEYS) of the Czech Republic under the projects CEITEC 2020 (LQ1601) and CzechNanoLab (LM2018110). M.P. and T.S. acknowledge the support from the H2020 Twinning program (project SINNCE, 810626), V. U. acknowledges funding from the EU-H2020 research and innovation program under grant agreement No 654360 having benefitted from the access provided by CNRS to the SOLEIL Synchrotron, within the framework of the “NFFA-Europe Transnational Access Activity”.

- [1] V. Uhlíř et al., *Applied Surface Science* 514 (2020) 145923.
- [2] S. Maat, J.-U. Thiele, E.E. Fullerton, FeRh films, *Phys. Rev. B* 72 (2005) 214432, <https://doi.org/10.1103/physrevb.72.214432>.
- [3] R. Barua, F. Jiménez-Villacorta, L.H. Lewis, *Appl. Phys. Lett.* 103 (2013) 102407, <https://doi.org/10.1063/1.4820583>.

Image-potential states in graphene

V. M. Silkin^{1,2,3}, E. Kogan⁴, and G. Gumbs⁵

¹*Donostia International Physics Center, Donostia/San Sebastian, Spain
(corresponding author: V. M. Silkin, e-mail: waxslavas@ehu.es)*

²*Departamento de Física de Materiales, Facultad de Ciencias Químicas, Universidad del País Vasco/Euskal Herriko Unibertsitatea, Donostia/San Sebastián, Spain*

³*IKERBASQUE, Basque Foundation for Science, Bilbao, Spain*

⁴*Department of Physics, Jack and Pearl Resnik Institute, Bar-Ilan University, Ramat-Gan 52900, Israel*

⁵*Department of Physics and Astronomy, Hunter College of the City University of New York, New York, USA*

A double Rydberg series of even and odd image-potential states has been predicted to exist in a free-standing graphene sheet [1]. Such states in graphene deposited on various substrates have been investigated by two-photon photoemission and scanning tunnelling spectroscopy [2-18]. Moreover, in several works different forms for describing the electron potential in free-standing and supported graphene were proposed [2,4,19-21] by assuming that an image plane position, z_{im} , coincides with the carbon atom plane position. Recently it was demonstrated that indeed, z_{im} is located at about 1 Å away. Considering this value of z_{im} for construction of the one-electron potential, it was found that the energies for image-potential states can change significantly [22].

In the present work we analyze this problem in more detail and consider various approaches for the construction of the one-electron potential in graphene. Based on the resulting hybrid potentials, we determine in which limits the binding energies of the image-potential states in graphene can vary.

Support by the Fonds zur Förderung der Wissenschaftlichen Forschung (projects S6204 and S6201), Royal Society (London), British Council (Vienna) and the European Union (ER-BCHRX-CT94-0571 and HCM \square k) is gratefully acknowledged.

[1] V. M. Silkin et al., Phys. Rev. B 80, 121408(R) (2009)

[2] S. Bose et al., New J. Phys. 12, 023028 (2010)

[3] A. Sandin et al., Appl. Phys. Lett. 97, 113104 (2010)

- [4] B. Borca et al., Phys. Rev. Lett. 105, 036804 (2010)
- [5] H. G. Zhang et al., J. Phys. Condens. Matter 22, 302001 (2010)
- [6] D. Niesner et al., Phys. Rev. B 85, 081402(R) (2012).
- [7] N. Armbrust, J. Gdde, P. Jakob, and U. Hfer, Phys. Rev. Lett. 108, 056801 (2012)
- [8] F. Craes et al., Phys. Rev. Lett. 111, 056804 (2013)
- [9] D. Nobis, M. Potenz, D. Niesner, and Th. Fauster, Phys. Rev. B 88, 195435 (2013)
- [10] F. Craes et al., Phys. Rev. Lett. 111, 056804 (2013)
- [11] K. Takahashi et al., Phys. Rev. B 89, 155303 (2014)
- [12] D. Niesner and Th. Fauster, J. Phys. Condens. Matter 26, 393001 (2014)
- [13] D. Gugel et al., 2D Mater. 2, 045001 (2015)
- [14] S. Achilli et al., New J. Phys. 20, 103039 (2018)
- [15] Y. Lin et al., Phys. Rev. B 97, 165413 (2018)
- [16] L. Fan, S. K. Lee, P. Y. Chen, and W. Li, J. Phys. Chem. Lett. 9, 1485 (2018)
- [17] S. Tognolini et al., Surf. Sci. 679, 11 (2019)
- [18] G. Ambrosio et al., Surf. Sci. 703, 121722 (2021)
- [19] P. L. De Andres et al., New J. Phys. 16, 023012 (2014)
- [20] N. Ambrust, J. Gdde, and U. Hfer, New J. Phys. 17, 103043 (2015)
- [21] I. Hamada, Y. Hamamoto, and Y. Morikawa, J. Chem. Phys. 147, 044708 (2017)
- [22] V. M. Silkin, E. Kogan, and G. Gumbs, Nanomaterials 11, 1561 (2021)

Charge Accumulation and Reactions Dynamics on Copper Electrodes Surfaces study by Electrochemical and Optical Polarization Techniques

Saul Vazquez-Miranda^{1,3}, Raul E. Balderas Navarro², Shirly Espinoza³, Jakob Andreasson³, Kurt Hingerl¹ and Christoph Cobet^{1,4}

¹*Center for Surface- and Nanoanalytics (ZONA), Johannes Kepler Universität, A4040 Linz, Austria*

²*Instituto de Investigación en Comunicación Óptica, Universidad Autónoma de San Luis Potosí, 78000, Mexico*

³*ELI Beamlines/Fyzikální ústav AV ČR, v.v.i., Za Radnicí 835, 25241 Dolní Břežany, Czech Republic*

⁴*Linz School of Education and Center for Surface- and Nanoanalytics (ZONA), Johannes Kepler Universität, A-4040 Linz, Austria*

(Corresponding author: Saul Vazquez-Miranda, e-mail: saul.miranda@eli-beams.eu and Christoph Cobet, e-mail: christoph.cobet@jku.at)

The assessment of surface chemistry occurring during electrocatalysis is key to understanding the detailed reaction mechanism. In this contribution we describe the use of both, electrochemical (EC) and optical polarization methods, to investigate the charge accumulation and reactions kinetics in Cu surfaces of single crystals interacting with a supra pure HCl solution with a concentration of 10 mM.

The experiments of the adsorption/desorption of Cl⁻ ions was carried out using cyclic voltammetry prompted by EC-scanning tunneling microscopy (EC-STM) observations [1,2], for which the integrated charge and ion exchange rate are measured in an electrical potential window, avoiding the hydrogen evolution reaction (HER) and copper dissolution (Cu²⁺) to prevent damage of the Cu surface.

Electrochemical impedance spectroscopy (EIS) measurements for the (111) and (110) faces of Cu were used to obtain capacitance and resistance parameters. Equivalent electric circuit modeling suggests a value for the potential at which the adsorption of Cl⁻ ions starts. As the operating frequency increases, the alternating electric field changes direction with different rates for polar and nonpolar molecule ions, besides exhibiting relaxation times. As a matter of fact, large nonpolar molecules have relaxation times in the order of seconds, whereas smaller and more polar ionic species relax in the KHz-MHz frequency range and show millisecond to microsecond relaxation times [3].

In addition, with the information obtained from EIS, we estimate the potential for which the adsorption takes place, and is correlated using chronoamperometry (CA) with a scanning resolution of 100 μ s. Spectroscopy Ellipsometry (SE) for the in operando characterization allows

probing the solid/liquid interface directly while applying an external potential during CA.

By using the experimental data obtained from the electrochemical and Ellipsometry techniques, previously assessed by EC-STM, we can determine a well-defined electrical potential value where possible adsorption occurs. Our results demonstrate the versatility of the combination of SE with CA to study fine details in electrochemistry environments.

Finally, from the necessity of ultrafast optical measurements to unveil many important processes that are not time-resolved with our commercial ellipsometers, such as solvent reorganization, electron tunneling, and isomerization[4], led us to resort to a set-up at ELI Beam Lines in Czech Republic to elucidate these processes on different surfaces.

ELI Beamlines authors acknowledge the support of the ELIBIO (No. CZ.02.1.01/0.0/0.0/15-003/0000447) and ADONIS (No. CZ.02.1.01/0.0/0.0/16-019/0000789) projects from the European Regional Development Fund.

[1] P. Broekmann, M. Wilms, M. Kruff, C. Stuhlmann, K. Wandelt, In-situ STM investigation of specific anion adsorption on Cu (111), *Journal of Electroanalytical Chemistry*, **467** (1-2), (307-324) (1999).

[2] Gholamreza Barati, Vladyslav Solokha, Klaus Wandelt, Kurt Hingerl, and Christoph Cobet, Chloride-Induced Morphology of the Cu(110) Surface in Dilute HCl *Langmuir*, **30** (48), (14486-14493) (2014).

[3] Lvovich, Vadim F, *Impedance spectroscopy: applications to electrochemical and dielectric phenomena*, John Wiley & Sons. (2012).

[4] Zwaschka, Gregor, François Lapointe, R. Kramer Campen, and Yujin Tong. "Characterization of ultrafast processes at metal/solution interfaces: Towards femtoelectrochemistry." *Current Opinion in Electrochemistry* 29 (2021).

Ion charge exchange spectroscopy with 2D materials

R.A. Wilhelm, A. Niggas, M. Werl, and F. Aumayr

Institut für Angewandte Physik, TU Wien, A-1040 Wien, Austria

(corresponding author: R.A. Wilhelm, e-mail: wilhelm@iap.tuwien.ac.at)

The scattering of ions on surfaces not only leads to momentum transfer and electronic excitations driven by the ion's stopping, but also to charge exchange with the material [1]. For slow ions in high charge states, the latter leads to an energy transfer to the target's electronic system in the range of several keV per ion. Consequently, single-ion-induced material modifications on the nanoscale can occur on surfaces susceptible to electronic sputtering [2]. While the semi-metallic 2D material graphene does not show signs of permanent perforation [3], the transition metal dichalcogenide MoS₂ can be well perforated [4]. Interestingly, the combination of both materials in a van-der-Waals heterostructure also shows perforation only in the MoS₂ layer and not in the graphene when the former faces the incoming ion beam. By changing the sample orientation perforation can be avoided entirely, since the graphene takes up most of the ion's potential energy upon neutralization and protects the MoS₂ underneath, see Fig. 1 [5].

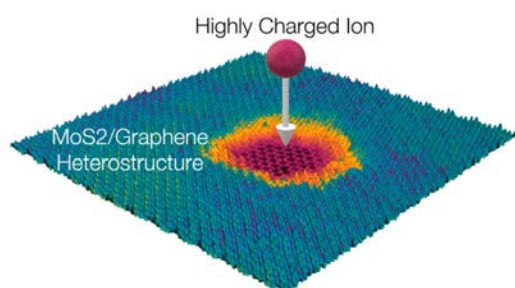


Figure 1: Scanning TEM image of a MoS₂/graphene heterostructure with an ion-induced hole in the MoS₂ layer, but not in the material below [5].

The monolayer-specific deposition of the potential energy points towards an ultrafast charge exchange process which is currently not well understood. We already showed that slow ions capture electrons from the material and neutralize on a timescale of femtoseconds [3,6]. With the help of freestanding 2D materials and van-der-Waals heterostructures thereof, we can limit the interaction time of the ion with a solid target to the same order of magnitude. As a result, we can determine the charge exchange in the non-equilibrium regime, i.e., before the ion has fully accommodated to an equilibrium charge state distribution.

Here we show that velocity- and layer-number-dependent charge exchange of slow highly charged ions in graphene reveals an universal scaling of the neutralization efficiency inside carbon-based materials [7]. Further, angle-dependent measurements show, that about 3 scattering events along the ion trajectory are enough to randomize any impact parameter dependence of charge exchange [8].

With the method of charge state sensitive detection of scattered highly charged ions we can virtually look inside a solid and follow the neutralization in a quasi-time-resolved manner. Even more so, we can clearly determine the point where the single-scattering regime changes towards a multiple-collision regime. These fundamental results pave the way to apply ion charge exchange spectroscopy to use cases of material structure determination where other methods fail. For example, short-range ordered molecular nanosheets [9] consist mostly of light carbon atoms and are strongly radiation sensitive. As a consequence, electron- and x-ray-based imaging and scattering techniques are not able to reveal the atomistic structure of these materials, whereas the structure determines the function we want to know and tune. With the help of our ion-based method we can use very small fluences in order to extract information on the sub-nm scale atomic ordering of the material. In order to do so we apply a model for angle-dependent charge exchange [10] to possible materials structures [11] and compare the results to our measurements.

Support by the Austrian Science Fund FWF (projects Y1174-N36 and I4914-N) and TU Wien's innovative projects program is gratefully acknowledged.

- [1] Arnau, A. *et al.*, Surf. Sci. Rep. **27**, 113-239 (1997).
- [2] Wilhelm, R.A.; El-Said, A.S.; Krok, F.; Heller, R.; Gruber, E.; Aumayr, F.; Facsko, S., Prog. Surf. Sci. **90**, 377-395 (2015).
- [3] Gruber, E. *et al.*, Nat. Commun. **7**, 13948 (2016)
- [4] Kozubek, R. *et al.*, J. Phys. Chem. Lett. **10**, 904-910 (2019)
- [5] Schwestka, J.; Inani, H.; Tripathi, M.; Niggas, A.; McEvoy, N.; Libisch, F.; Aumayr, F.; Kotakoski, J.; Wilhelm, R.A., ACS Nano **14**, 10536-10543 (2020)
- [6] Wilhelm, R.A.; Gruber, E.; Ritter, R.; Heller, R.; Facsko, S.; Aumayr, F., Phys. Rev. Lett. **112**, 153201 (2014)
- [7] Niggas, A. *et al.*, Commun. Phys. **4**, 180 (2021)
- [8] Creutzburg, S.; Niggas, A.; Weichselbaum, D.; Grande, P.L.; Aumayr, F.; Wilhelm, R.A., Phys. Rev. A, **104**, 042806 (2021)
- [9] Feng, X.; Schlüter, A.D., Angew. Chem. **130**, 13942-13959 (2018)
- [10] Wilhelm, R.A.; Grande, P.L., Commun. Phys. **2**, 89 (2019)
- [11] Ehrens, J.; Gayk, F.; Vorndamme, P.; Heitmann, T.; Biere, N.; Anselmetti, D.; Zhang, X.; Gölzhäuser, A.; Schnack, J., Phys. Rev. B **103**, 115416 (2021)

Multiple-pump system for combinatorial thin-film deposition by ultrasonic spray pyrolysis

M. Wolf^{1,2}, G.K.H. Madsen², T. Dimopoulos¹

¹*AIT Austrian Institute of Technology,
Center for Energy, Energy Conversion and Hydrogen, 1210 Wien, Austria
(corresponding author: M. Wolf, e-mail: maximilian.wolf@ait.ac.at)*

²*Institut für Materialchemie, Technische Universität Wien, 1060 Wien, Austria*

Ultrasonic spray pyrolysis (USP) is a well-suited deposition method for combinatorial thin-film material libraries, as it allows for easy and precise control of the spraying position. Combined with a gradual composition change of the precursor solution and variation of overlapping spray patterns, one can achieve spatially varying deposits with high two-dimensional precision.

In this work, we show how to upgrade a commercial USP tool with an inexpensive, custom-built pump system for combinatorial deposition purposes. To this respect, we demonstrate and validate the realized equipment by coating glass substrates with a two-dimensional composition gradient of copper-gallium-iron oxides, materials that find application in energy conversion, including solar photovoltaics and photo-electrochemical water splitting [1-4]. A simple method for automatized material analysis approaches using limited software resources and tools is also shown, through expanding the capabilities of a scanning electron microscopy and energy dispersive spectroscopy (SEM/EDS) instrument.

The pump system was designed to operate using three or two of the four available pumps simultaneously, separating a metal precursor line, consisting of 2 precursor pumps and 1 solvent pump, from a nanoparticle line, consisting of 1 particle pump and 1 solvent pump. This configuration enables a large set of different deposition procedures, like thickness and composition gradients, alternating layers, or even complete device fabrication.

As far as technical aspects are concerned, each pump is composed of a NEMA 14 stepper motor which drives a threaded nut on a turning spindle and a sled that is connected to the nut and pushes or pulls the piston of a 50 ml glass barrel syringe. The major part of the structural components were produced by rapid prototyping techniques. A single-board computer is used for controlling the pump system and providing a graphical user interface (GUI) based on a Django-React-stack [5, 6]. The communication with the USP tool is established over serial I/O modules.

Thin-film deposition by USP is not trivial and depends on many parameters which need to undergo optimization processes [7, 8]. Therefore, we relied on established recipes for Cu₂O

[9] and Ga₂O₃ [10], as well as a modification of the latter one where we replaced the gallium acetylacetonate precursor with iron(III) acetylacetonate. Alternating concentration gradients of copper-gallium and copper-iron solutions were sprayed in line patterns perpendicular to each other to yield a two-dimensional gradient of the three elements.

Elemental quantification took place by automatized SEM/EDS for which a special sample holder was built, again by employing rapid prototyping techniques. It holds an array of 3 x 3 glass substrates (25mm x 25mm) which constitutes the entire sprayed area. 225 equally spaced measurements were carried out with the only user interaction being the preparation and setup of the routine. The instruments, running on different computers, were coupled using a webserver-based communication and user interaction was supplied by a GUI, based on IPython [11]. Since neither of the instrument software packages provided an application programming interface (API), Python [12] modules for image recognition and input control were used to operate the instrument GUIs directly. This versatile automatization method is highly recommended for similar situations since software upgrades either are pricey or do not include the required functionalities.

The analysis confirmed the intended element concentration distribution of the metal oxides over the sample area, validating the implemented combinatorial deposition approach.

- [1] T. Jafari, E. Moharreri, A. S. Amin, R. Miao, W. Song and S. L. Suib, *Molecules* 21(7) (2016)
- [2] M. Lee, D. Kim, Y. T. Yoon and Y. I. Kim, *Bulletin of the Korean Chemical Society* 35(11), 3261 (2014)
- [3] Q.-L. Liu, Z.-Y. Zhao, R.-D. Zhao and J.-H. Yi, *Journal of Alloys and Compounds* 819, 153032 (2020)
- [4] D. Ursu, M. Miclău, R. Banica and N. Vazilescu, *Materials Letters* 143, 91 (2015)
- [5] Django (3.2.3), Django Software Foundation (2021)
- [6] React (17.0.2), Meta Platforms Inc. (2021)
- [7] D. Perednis and L. J. Gauckler, *Journal of electroceramics* 14(2), 103 (2005)
- [8] S. Rahemi Ardekani, A. Sabour Rouh Aghdam, M. Nazari, A. Bayat, E. Yazdani and E. Saievar-Iranizad, *Journal of Analytical and Applied Pyrolysis* 141, 104631 (2019)
- [9] N. Plankensteiner, W. Kautek and T. Dimopoulos, *ChemNanoMat* 6(4), 663 (2020)
- [10] N. Winkler, R. A. Wibowo, W. Kautek, G. Ligorio, E. J. W. List-Kratochvil and T. Dimopoulos, *Journal of Materials Chemistry C* 7(1), 69 (2019)
- [11] F. Pérez and B. E. Granger, *Computing in Science and Engineering* 9(3), 21 (2007)
- [12] G. Van Rossum and F. L. Drake, *Python 3 Reference Manual*, CreateSpace (2009)

Thursday

Epitaxial Graphene Nanoribbons: One-dimensional confinement and pn-junction array

U. Starke, H. Karakachian, P. Rosenzweig, B. Matta, T.T.N. Nguyen¹, J. Aprozanz^{1,2},
A.A. Zakharov³, R. Yakimova⁴, T. Balasubramanian³, Z. Mamiyev¹,
S.R. Power⁵, C. Tegenkamp^{1,2}, and C.M. Polley³

Max-Planck-Institut für Festkörperforschung, D-70569 Stuttgart, Germany

(corresponding author: U.Starke, e-mail: u.starke@fkf.mpg.de)

¹Institut für Physik, Technische Universität Chemnitz, 09126, Chemnitz, Germany

²Institut für Festkörperphysik, Leibniz Universität Hannover, 030167 Hannover, Germany

³MAX IV Laboratory, Lund University, 22484 Lund, Sweden

⁴IFM, Linköping University, 58183 Linköping, Sweden

⁵School of Physics, Trinity College Dublin, Dublin 2, Ireland

Wafer scale epitaxial graphene grown on Silicon Carbide (SiC) is regarded as a suitable candidate for carbon based electronics. In recent years, our group has demonstrated many possibilities to tune the electronic properties of this two-dimensional (2D) material by controlled doping schemes or intercalation between SiC substrate and the graphene layer. However, for application in logical electronics, the necessity to define an off state is a key ingredient, which – due to the absence of an electronic bandgap – is so far impossible in conventional pristine graphene layers. Spatial constriction of the material can provide a way to circumvent this problem. Indeed, arm-chair graphene nanoribbons (AGNRs) were theoretically predicted to display a bandgap. However, lithographical patterning of the graphene creates irregular edges. The self-assembly of molecular precursors is restricted to metallic substrates which introduce an electrical short-circuit. Here, we grow high-quality AGNRs on the sidewalls of 6H-SiC mesa structures, a semi-insulating substrate (see Fig. 1a,b). Angle-resolved photoelectron spectroscopy (ARPES) and scanning tunneling spectroscopy measurements reveal the development of a width-

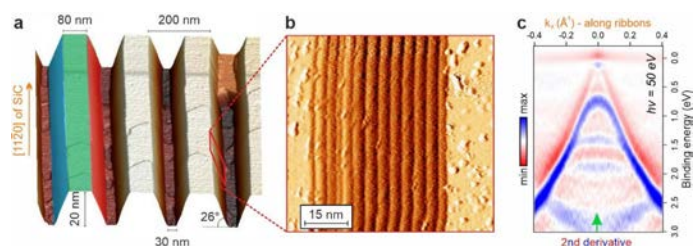


Figure 1: **a)** Perspective AFM view of the mesa structures with a periodicity of 200 nm. The trench depth is 20 nm and the facet inclination is around 26°. **b)** First derivative of a STM topography image taken on a single facet displaying the “ladder structure” **c)** High-resolution ARPES energy-momentum cut taken along the ribbons using a photon energy of 50 eV and its second derivative plot along the energy axis.

dependent semiconducting gap driven by quantum confinement effects. Furthermore, ARPES demonstrates an ideal one-dimensional (1D) electronic behavior that for the first time is realized in a graphene-based environment, consisting of well-resolved subbands (Fig. 1c), dispersing and non-dispersing along and across the ribbons, respectively [1]. Our experimental findings, coupled with tight-binding calculations, set the grounds for a deeper exploration of quantum confinement phenomena and may open intriguing avenues for new low-power electronics.

On the facets, the nano-sized AGNRs are defined by a periodic ladder of nano-buffer stripes and free-standing ribbons as demonstrated by low-energy electron diffraction (LEED), spot-profile analysis (SPA)-LEED and scanning tunneling microscopy (STM), cf. Fig. 1b. By hydrogen intercalation the buffer stripes become decoupled, so that the series of 1D confined nanoribbons is transformed into a single 2D graphene sheet rolling over the 6H-SiC mesa structures. Simultaneously, the buffer layer sheets on the mesas and trenches are also decoupled and turn into the well-known quasi-free standing monolayer graphene (QFMLG). The different constituents of the graphene-SiC interface are identified using X-ray photoelectron spectroscopy (XPS). Due to the different surface terminations of the basal and vicinal SiC planes constituting the mesa structures, different types of charge carriers are locally induced into the graphene layer. By ARPES, we can selectively measure the electronic band structure of the two graphene regions, finding two symmetrically doped phases with p-type being located on the basal planes and n-type on the facets, cf. Fig. 2. Our results demonstrate that through a careful structuring of the substrate, combined with H-intercalation, an array of graphene pn-junctions could be engineered at the nanoscale [2]. Such graphene pn-junctions represent potential building-blocks for a broad spectrum of future technologies, ranging from electronic lenses analogous to metamaterials in optics, to high-performance photodetectors important for a variety of optoelectronic applications.

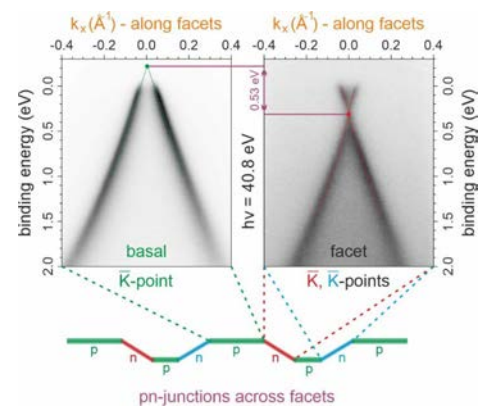


Figure 2: ARPES energy-momentum cuts acquired at the K-points of basal and facet QFMLGs, respectively, as indicated in the schematic side-view of the mesa structure.

This work was supported by the Deutsche Forschungsgemeinschaft (DFG) via Sta315/9-1, Te386/12-1 and Te386/13-1. We would like to thank Ulrike Waizmann and Thomas Reindl for performing the e-beam lithography and reactive ion etching at the Nanostructuring lab of MPI-FKF. We acknowledge the MAX IV and HZB/Bessy laboratories for the allocation of synchrotron radiation beamtime and the support by their beamline staff. S.R.P. acknowledges funding from the Irish Research Council under the Laureate awards programme.

- [1] H. Karakachian, T.T. Nhung Nyuyen, J. Aprojanz, A.A. Zakharov, R. Yakimova, P. Rosenzweig, C.M. Polley, T. Balasubramanian, C. Tegenkamp, S.R. Power, U. Starke, *Nat. Commun.* **11**, 6380 (2020). *One-dimensional confinement and width-dependent bandgap formation in epitaxial graphene nanoribbons.*
- [2] H. Karakachian, P. Rosenzweig, T.T. Nhung Nyuyen, B. Matta, A.A. Zakharov, R. Yakimova, T. Balasubramanian, Z. Mamiyev, C. Tegenkamp, C.M. Polley, and U. Starke, *Advanced Functional Materials*, in press. *Periodic Nanoarray of graphene pn-junctions on silicon carbide obtained by hydrogen intercalation.*

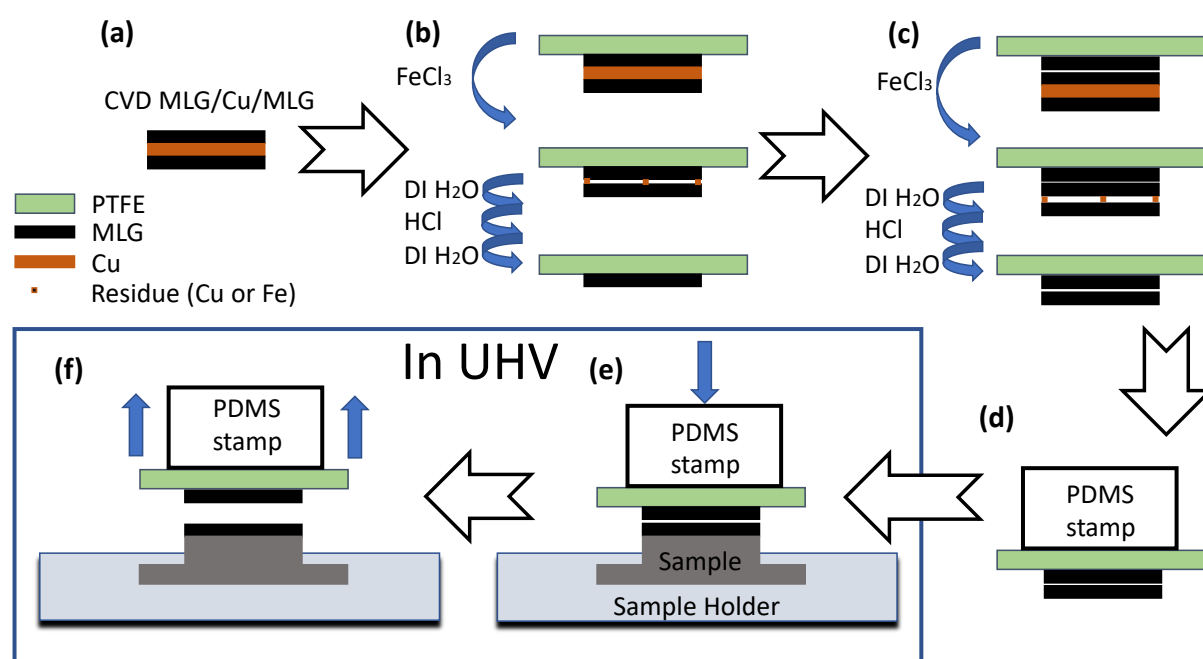
Transfer of Graphene under Ultra-High-Vacuum

D. Merk, S. Rusponi, and H. Brune

Institute of Physics, EPFL, CH-1015 Lausanne, Switzerland

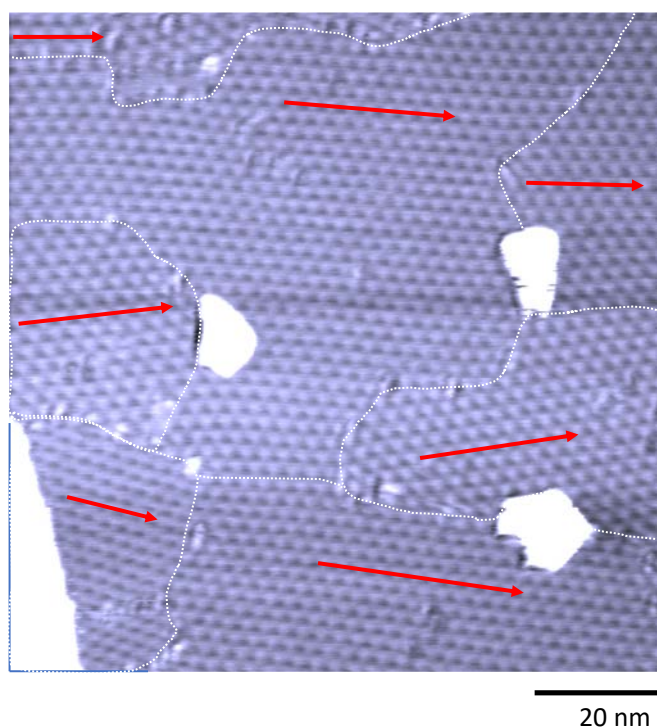
(harald.brune@epfl.ch)

Current graphene transfer techniques most often require drop-coating of a supporting layer on top of graphene and immersion in an etching solution to remove the growth substrate, followed by removal of the supporting layer in another solution post-transfer, making them incompatible with ultra-high vacuum (UHV). We present a novel technique for graphene transfer fully compatible with UHV, based on the chemical etching of a Cu growth substrate, using teflon (PTFE) as a supporting layer combined with a wafer-bonding approach. We demonstrate successful transfer to both Ir(111) and Cu(100) crystals. The Figure below shows a schematic of our transfer procedure.



Schematic of the transfer procedure. (a) CVD grown monolayer graphene (MLG) on both sides of a polycrystalline Cu film. (b) MLG on Cu covered with PTFE tape as support layer. Etching of Cu in FeCl_3 solution and rinsing in de-ionized (DI) water followed by etching in HCl and rinsing in DI water removes the bottom layer of graphene and etching residue and leaves a MLG on PTFE. (c) Same procedure as (b) but using PTFE/MLG as support layer. Etching and subsequent rinsing in DI water leaves a BLG on PTFE. (d) Attach PTFE/BLG onto PDMS stamp and insert into UHV chamber. (e) Press on clean target sample in UHV. (f) Lift off PDMS/PTFE/MLG leaving behind MLG on target.

Auger electron spectroscopy after transfer shows that $90 \pm 10 \%$ of a monolayer is transferred. We perform Raman spectroscopy throughout the transfer steps shown in the above Figure in order to monitor the graphene quality. After transfer, the Raman spectra of graphene on Cu(100) show a very low defect density. On Ir(111), the substrate background was too high to quantify the graphene quality with Raman spectra. STM measurements of graphene transferred onto Ir(111) and annealed to 1270 K show the moiré pattern characteristic of CVD grown graphene on that substrate and domain sizes that are comparable to CVD growth, see Figure below. The annealing temperature required after transfer, and the residues visible in the STM image are items where our method can further be improved. Once perfect graphene, or other 2D materials, can be transferred in UHV without or with only mild annealing, we can build clean heterostructures and metamaterials with original physical properties.



STM image of UHV transferred graphene on Ir(111) after annealing to 1270 K ($1000 \text{ \AA} \times 1000 \text{ \AA}$, $V_t = 0.3 \text{ V}$, $I_t = 10 \text{ nA}$, $T = 300 \text{ K}$).

Support from the Swiss National Science Foundation (200020_176932) is gratefully acknowledged.

Boron Substitution in Graphene Nanoribbons: One-dimensional Spin Chains with Tuneable Interactions

N Friedrich¹, P Brandimarte², J Li¹, S Saito³, S Yamaguchi⁴, I Pozo⁵, D Peña⁵, T Frederiksen^{2,6}, A García-Lekue^{2,6}, JI Pascual^{1,6} and D Sánchez-Portal^{1,7}

¹ *CIC nanoGUNE BRTA, 20018 Donostia-San Sebastián, Spain*

² *Donostia International Physics Center (DIPC), 20018 Donostia-San Sebastián, Spain*

³ *Graduate School of Science, Kyoto University, Kyoto 606-8502, Japan*

⁴ *Graduate School of Science, Nagoya University, Nagoya 464-8602, Japan*

⁵ *Centro de Investigación en Química Biológica e Materiais Moleculares (CiQUS) and Dep. de Química Orgánica, Universidade de Santiago de Compostela, 15782 Santiago de Compostela, Spain*

⁶ *Ikerbasque, Basque Foundation for Science, 48013 Bilbao, Spain*

⁷ *Centro de Física de Materiales CSIC-UPV/EHU, 20018 Donostia-San Sebastián, Spain*
(corresponding author: D. Sánchez-Portal, e-mail: daniel.sanchez@ehu.eus)

Graphene nanoribbons (GNRs), low-dimensional platforms for carbon-based electronics, show the promising perspective to also incorporate spin polarization in their conjugated electron system. However, these magnetic moments are usually localized around zigzag edges, difficult to fabricate and very reactive. This combined theoretical and experimental study demonstrates that magnetism can also be induced away from physical edges through atomically precise engineering of topological defects in its interior. A pair of substitutional boron atoms inserted in the carbon backbone of the 7-armchairGNR breaks the conjugation of its topological bands and builds two spin-polarized boundary states around them. Therefore, a spin moment of 2 Bohr magnetons localizes around each pair of B atoms in the structure (see Figure 1).

First indications of the presence of magnetism were given by the appearance of characteristic Kondo peaks in electrical transport experiments performed at nanoGUNE. Transport was measured through boron-substituted GNRs suspended between the tip and the sample of a scanning tunneling microscope (STM). These observations were rationalized in terms of the theory and first-principles simulations performed at CFM and DIPC, which predicted for each isolated boron pair a $S=1$ spin state as well as a strong dependence on the spacing between pairs. The interaction between two of such topological defects was further explored, outlining

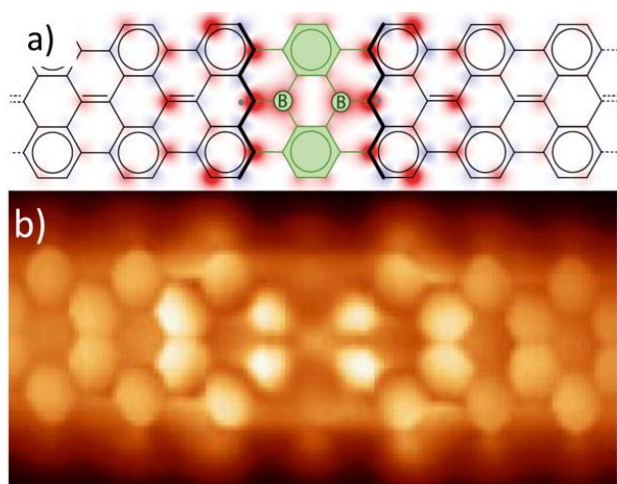


Figure 1: a) Structure of the 2B-7AGNR defect together with the computed spin density map. b) Constant height STM scan ($V=2$ mV) using a CO-functionalized tip of a 2B-7AGNR defect.

a route to engineer topological spin chains, with the promising tunability of their magnetism by modifying their spacing [1].

Therefore, the present results demonstrate a route to embed spin chains in graphene nanoribbons, turning them into basic elements of spintronic devices. We are currently examining the effect of B substitution for other GNRs.

We gratefully acknowledge financial support from Spanish Agencia Estatal de Investigación (AEI)(MAT2016-78293, PID2019-107338RB, FIS2017-83780-P, and the Maria de Maeztu Units of Excellence Programme MDM-2016-0618), from the European Union (EU) through Horizon 2020 (FET-Open project SPRING Grant. No. 863098), the Basque Departamento de Educación through the PhD fellowship No. PRE_2019_2_0218 (S.S.), the Xunta de Galicia (Centro de Investigación de Galicia accreditation 2019–2022, ED431G 2019/03), the University of the Basque Country (Grant IT1246-19), and the European Regional Development Fund (ERDF). I. P. also thanks Xunta de Galicia and European Union (European Social Fund, ESF) for the award of a predoctoral fellowship. N. F. and P. B. contributed equally to this work.

[1] N Friedrich, P Brandimarte, J Li, S Saito, S Yamaguchi, I Pozo, D Peña, T Frederiksen, A García-Lekue, D Sánchez-Portal and JI Pascual, *Physical Review Letters* 125, 146801 (2020)

Dimensionality effects in the nonlinear optical properties of TMD nanotubes

J. Krishna¹, and J. Ibañez-Azpiroz^{1,2}

(corresponding author: J. Ibañez-Azpiroz, e-mail: julen.ibanez@ehu.eus)

¹ Centro de Física de Materiales, Universidad del País Vasco (UPV/EHU), 20018 San Sebastián, Spain

² Ikerbasque Foundation, 48013 Bilbao, Spain

Quick and efficient conversion of light into electricity is key for future clean-energy technologies. Recently a focus of renewed attention, the bulk photovoltaic effect is a nonlinear absorption process that converts light into electrical current intrinsically, i.e. without the need of any pn-junction for driving the photoexcited electrons. The bulk photovoltaic effect can surpass the standard Shockley-Queisser limit for the solar-cell efficiency [1, 2], opening the way for devices exceeding current capabilities. Furthermore, the photovoltage attained in this process is not limited by the band gap of the material, giving rise to large measured values [3, 4].

In the last years, the study of the bulk photovoltaic effect, and in particular the shift-current contribution, has witnessed a huge progress. While traditionally this effect has been mostly studied in bulk ferroelectrics such as BaTiO₃ [5], recent theoretical works have emphasized that the shift current undergoes a significant enhancement in 2D systems such as single-layer monochalcogenides [6, 7]. Current efforts include searching for suitable crystal structures with 2D-like properties, in the hope that they may yield an efficient harvesting of light.

In this context, *nanotubes*, which consist of a stack of rolled monolayers, offer an ideal bridge between a purely 2D system and a bulk crystal structure. Interestingly, a recent experiment on transition metal-dichalcogenides nanotubes measured a short-circuit current that is several orders of magnitude larger as compared to the monolayer value [8]. This remarkable enhancement may find its origin on the shift-current contribution, which is allowed by the lack of inversion symmetry of the material.

In this contribution we will analyze the dc current generated in MoS₂ nanotubes upon light absorption. Our analysis is based on *ab-initio* density functional theory calculations that make use of the Wannier interpolation technique for handling the transition matrix elements [9, 10]. Among other features, we will study the relation between internal structure, radius and the photoconductivity of a single-wall nanotube, and how it compares with the results calculated

in a flat monolayer. Based on these results, we will then estimate the total dc photoconductivity of a multi-wall nanotube typically employed in experiment. Finally, we will discuss our results and the role of the bulk photovoltaic effect in the context of the measurements reported in Ref. [8], and how the absorption could be enhanced in future studies.

Funding provided by the European Union's Horizon 2020 research and innovation programme under the European Research Council (ERC) grant agreement No 946629.

- [1] B. I. Sturman and V. M. Fridkin, (Gordon and Breach, Philadelphia, (1992)
- [2] V. M. Fridkin, *Crystallogr. Rep.* 46, 654 (2001)
- [3] J. E. Spanier, V. M. Fridkin, A. M. Rappe, A. R. Akbashev, A. Polemi, Y. Qi, Z. Gu, S. M. Young, C. J. Hawley, D. Imbrenda, G. Xiao, A. L. Bennett-Jackson, and C. L. Johnson, *Nature Photonics*, 10, 9, 611–616, (2016)
- [4] J. Ma, Q. Gu, Y. Liu, J. Lai, P. Yu, X. Zhuo, Z. Liu, J.-H. Chen, J. Feng, and D. Sun, *Nature Materials*, 18, 5, 476–481 (2019)
- [5] W. T. H. Koch, R. Munser, W. Ruppel, P. Würfel, *Ferroelectrics*, 305-307 (1975)
- [6] A. M. Cook, B. M. Fregoso, F. de Juan, S. Coh, and J. E. Moore, *Nat. Commun.* 8, 14176 (2017)
- [7] T. Rangel, B. M. Fregoso, B. S. Mendoza, T. Morimoto, J. E. Moore, and J. B. Neaton, *Phys. Rev. Lett.* 119, 067402 (2017)
- [8] Y. J. Zhang, T. Ideue, M. Onga, F. Qin, R. Suzuki, A. Zak, R. Tenne, J. H. Smet, and Y. Iwasa, *Nature*, 570, 7761, 349 (2019)
- [9] G. Pizzi, V. Vitale, R. Arita, S. Blügel, F. Freimuth, G. Géranton, M. Gibertini, D. Gresch, C. Johnson, T. Koretsune, J. Ibañez-Azpiroz, H. Lee *et al.*, *Journal of Physics: Condensed Matter* (2019)
- [10] J. Ibañez-Azpiroz, S. S. Tsirkin and I. Souza, *Phys. Rev. B* 97, 245143 (2018)

Growth of supported boron-based monolayers: h-BN and borophene on Pt(110)

F. Mittendorfer, M. Thaler¹, D. Steiner¹, A. Menzel¹, E. Bertel¹

*Institut of Applied Physics and Center for Computational Materials Science, Vienna University of
Technology, A-1040 Vienna, Austria*

(corresponding author: F. Mittendorfer, e-mail: Florian.Mittendorfer@tuwien.ac.at)

¹ *Institute of Physical Chemistry, University of Innsbruck, 6020 Innsbruck, Austria*

In the last decade the investigation of stackable, two-dimensional (2D) materials has become a major research area in the field of surface science. One of the most prominent examples, hexagonal boron nitride (h-BN), has a large bandgap and can thus be used as a dielectric support, e.g. for graphene-based nanomaterials. In addition, the high chemical inertness allows it to serve as a protective layer or a template for cluster growth. For obtaining a high-quality film for these applications understanding and controlling the growth of the h-BN layer is of central interest.

In the first part of this presentation, I will discuss our recent results [1, 2] of a combined theoretical and experimental study of the growth of h-BN on Pt(110) using density functional theory (DFT), scanning tunneling microscopy (STM) and angle-resolved photoemission (ARPES). The experimental observations clearly indicate that the growth temperature plays a key role when using a borazine precursor: while growth at a lower temperature leads to the formation of small terraces with a high density of defects and domain boundaries, the quality of the h-BN film is strongly enhanced at growth temperatures above ~1100K leading to a single-domain film on a (1x5) or (1x6) missing-row reconstructed Pt(110) surface (Fig.1). Our results indicated that the difference is related to the high mobility of the surface Pt atoms during the growth conditions, comparable to h-BN growth on liquid gold.

The comparison of the calculated bandstructure and the APRES measurements [2] offers further insights: while the h-BN film interacts with the substrate mainly via a weak van-der-Waals like binding, and hence shows a dispersion of the π and σ bands similar to the freestanding monolayer, we find a pronounced hybridization at the N atoms located in the channels of the Moire structure close to the substrate Pt surface atoms.

In the final part of the presentation, I will discuss recent results on the interaction of an atomically thin layer of boron, borophene, on Pt(110). In contrast to the hexagonal BN mesh, borophene can exhibit a large number of allotrops which are close in energy. The calculations suggest that the local matching at the interface plays a key role for the stabilization of the film.

Support by the Fonds zur Förderung der Wissenschaftlichen Forschung is gratefully acknowledged.

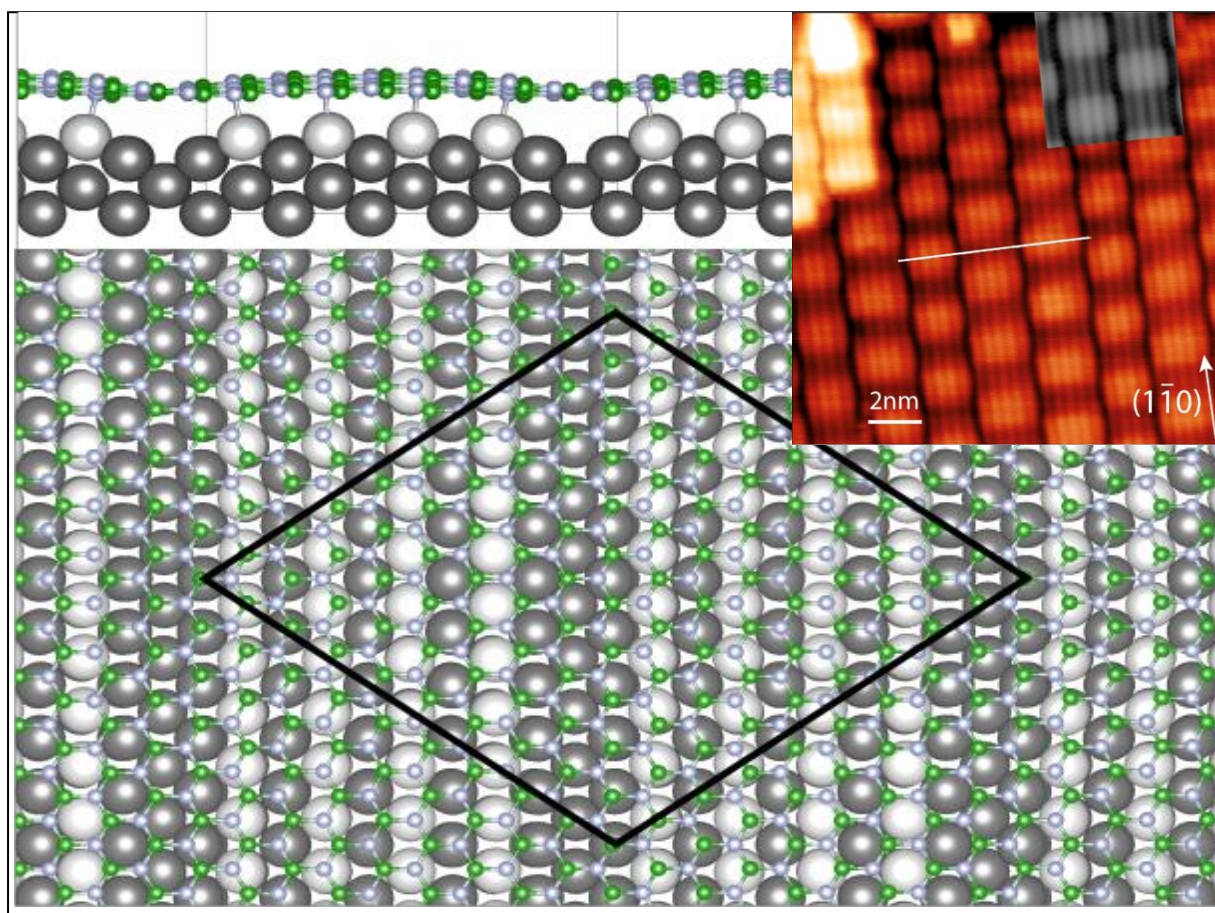


Fig.1) Side- and top view of a c(10x10) h-BN film (small balls: B green, N white) on a (1x5) missing row Pt(110) surface . Insert: Experimental (red) and simulated (gray) STM Moire structure.

- [1] D. Steiner, F. Mittendorfer and E. Bertel, ACS Nano **13**, 7083 (2019)
- [2] M. Thaler, D. Steiner, A. Menzel, F. Mittendorfer and E. Bertel, Phys. Rev. Research **2**, 043156 (2020)

Energy distribution of electrons emitted from atomically thin materials due to highly charged ion impact

A. Niggas, D. Weichselbaum, F. Aumayr, and R.A. Wilhelm

*Institute of Applied Physics, TU Wien, 1040 Vienna, Austria
(corresponding author: A. Niggas, e-mail: niggas@iap.tuwien.ac.at)*

Electron emission induced by slow highly charged ions from bulk materials has been studied extensively in the past [1, 2]. Typically, the measured total electron emission is a composite of primary electrons emitted from the ion-surface interaction and secondary electrons, e.g., from multiplication processes inside the target. The latter is suppressed in 2D materials, and thus using these surface-only materials allows us to study primary electron emission itself [3].

In our experiment, we developed a coincidence spectrometer [4]: we detect correlated pairs of ions after transmission through the target (charge state, scattering angle, energy loss) and emitted electrons (yield, energy) and store the data in a list mode file, i.e., posteriori filtering for certain parameters is possible. The ion energy loss and the ion charge state give access to the information on whether the ion was transmitted through the support structure or solely through the pre-cleaned 2D sample [5].

Here we show coincidence measurements of slow xenon ions in charge states up to $q=20$ transmitted through bilayer graphene samples and compare them to non-coincident measurements with highly oriented pyrolytic graphite (HOPG) samples. Exemplary spectra for both samples are shown in Figure 1.

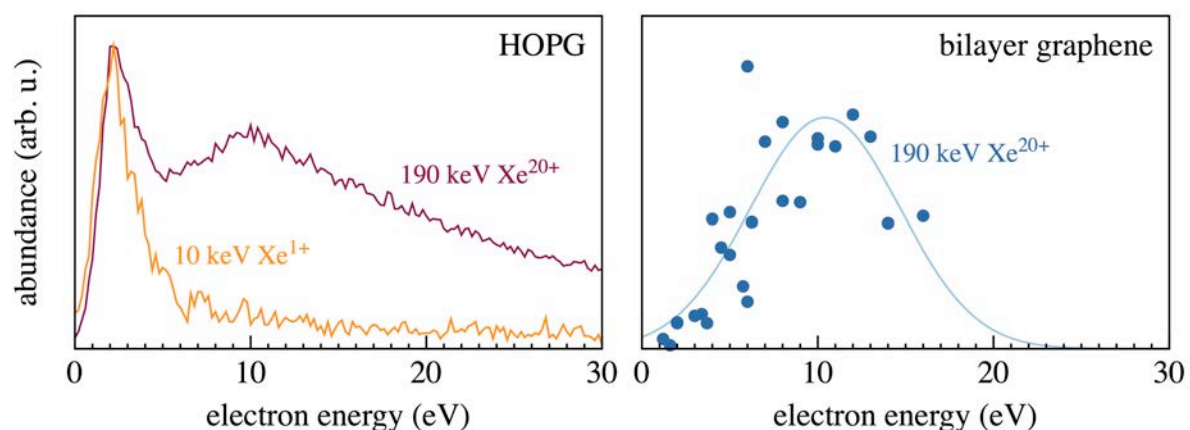


Figure 1 – Electron energy spectra induced by 10 keV Xe¹⁺ and 190 keV Xe²⁰⁺ impact on HOPG (left) and by 190 keV Xe²⁰⁺ impact on bilayer graphene (right).

By comparing charge-state-dependent and kinetic energy-dependent electron energy spectra, we can distinguish kinetic and potential emission processes for HOPG: In Figure 1 (left) we see only a low-energy distribution at electron energies <5 eV for Xe^{1+} (only kinetic electron emission), while we find an additional potential electron emission distribution at ~ 10 eV for Xe^{20+} . Consistent with our setup geometry with the electron detector mounted at 90° with respect to the ion beam, kinetically emitted primary electrons cannot reach the electron detector. Therefore, we only find the potential energy contribution for bilayer graphene (cf. Figure 1 (right)).

Support by the Austrian Science Fund (FWF; projects Y 1174-N36 and I 4914-N) as well as TU Wien's Innovative Projects program is gratefully acknowledged.

- [1] F. Aumayr, H. Kurz, D. Schneider, M.A. Briere, J.W. McDonald, C.E. Cunningham, and H.P. Winter, *Physical Review Letters* 71, 1943 (1993)
- [2] M. Vana, F. Aumayr, C. Lemell, and H.P. Winter, *International Journal of Mass Spectrometry and Ion Processes* 149-150, 45 (1995)
- [3] J. Schwestka, A. Niggas, S. Creutzburg, R. Kozubek, R. Heller, M. Schleberger, R. Wilhelm, and F. Aumayr, *Journal of Physical Chemistry Letters* 10, 4805 (2019)
- [4] J. Schwestka, D. Melinc, R. Heller, A. Niggas, L. Leonhartsberger, H. Winter, S. Facsko, F. Aumayr, and R. Wilhelm, *Review of Scientific Instruments* 89, 085101 (2018)
- [5] A. Niggas, J. Schwestka, S. Creutzburg, T. Gupta, D. Eder, B.C. Bayer, F. Aumayr, and R.A., *Journal of Chemical Physics* 153, 014702 (2020)

Reduced graphene oxide: From industrialisable production to de-icing application

Markus Ostermann¹, Pierluigi Bilotto¹, Peter Lieberzeit², and Jürgen Schodl¹

¹ *CEST GmbH, Centre for Electrochemical Surface Technology, A-2700, Wiener Neustadt, Austria*

² *Institute of Physical Chemistry, University of Vienna, A-1090, Vienna, Austria*

markus.ostermann@cest.at

Graphene and its derivatives show unique characteristics like high electrical conductivity, low density and high surface area making them a reasonable option for various applications, *i.e.* de-icing, water impermeability and corrosion protection. [1, 2] However, a cost efficient and environmentally friendly industrial production of graphene-based materials is not established yet.

In the last decade, the scientific community put a lot of effort in producing graphene derivatives, whereby fabrication via the exfoliation of graphite are commonly used for large scale-production. [3] This method leads to graphene oxide (GO) due to the simultaneous oxidation of the aromatic backbone during the process. Further reduction of the oxidic groups via different reducing agents or thermal decomposition produces reduced graphene oxide (rGO), which expresses a significant conductivity. [4] This final product can be coated on surfaces to enhance their properties, as reported by Bondavalli et al. on the application of spray-coating of nanomaterials for electrical application. [5]

In our work, we aim to transfer the incredible nanoscale-properties of graphene to the scale of industrial applications. First, we utilize electrochemical exfoliation on graphite to produce graphene oxide in a straightforward and up-scalable way. The process involves a swelling with diluted NaOH, an exfoliation with diluted H₂SO₄ and a post-treatment step keeping the overall environmental impact low. The reduction of graphene oxide is executed in an environmental-caring approach by using ascorbic acid over more harmful chemicals. [4] Second, by applying the rGO-powder via spray-coating on different test panels, we investigate the conductivity of the layers. Finally, we utilize these conductive materials to test De-Icing properties by means of Joule's heating (see Figure 1).

Specifically, by applying increasing amounts of rGO, the resistance of the layer is adjustable to suit de-icing applications. For powder layers of thickness about $5\ \mu\text{m}$, we find sheet resistances down to about $150\ \Omega/\text{sq}$. This corresponds to about $2\ \text{mg}$ rGO per cm^2 . Then, we apply a potential to the test panel to achieve electrical heating monitored by thermal imaging. Reproducibility of the layer, multiple heating cycles and various conditions are investigated to fully characterise the functionality and show the reliability of the rGO-based heating layer. We employ SEM/EDX, AFM and Raman spectroscopy to additionally characterise the system.

To conclude, the implementation of graphene oxide related species into next generation coating systems paves the way for novel green technological advances as weight-saving, *i.e.* reduction of fuel consumption in aeronautical vehicles. Moreover, via a multilayering strategy we intent to bring together the individual properties we have observed in graphene based materials, to develop coatings expressing multifunctionalities, such as De-icing, lightning strike protection, fire inhibition and water uptake.

The authors acknowledge support by the European Union Horizon 2020 Clean Sky Programme (Grant No. 886376). The authors acknowledge the Gesellschaft für Forschungsförderung Niederösterreich m.b.H. for financial support through its FTI PhD Funding Programme (SC19-018).

- (1) Raji, A.-R. O.; Varadhachary, T.; Nan, K.; Wang, T.; Lin, J.; Ji, Y.; Genorio, B.; Zhu, Y.; Kittrell, C.; Tour, J. M. *ACS Applied Materials & Interfaces* **2016**, *8*, PMID: 26780972, 3551–3556.
- (2) Chauhan, D. S.; Quraishi, M.; Ansari, K.; Saleh, T. A. *Progress in Organic Coatings* **2020**, *147*, 105741.
- (3) Whitener, K. E.; Sheehan, P. E. *Diamond and Related Materials* **2014**, *46*, 25–34.
- (4) De Silva, K.; Huang, H.-H.; Joshi, R.; Yoshimura, M. *Carbon* **2017**, *119*, 190–199.
- (5) Bondavalli, P.; Pribat, D.; Legagneux, P.; Martin, M.-B.; Hamidouche, L.; Qassym, L.; Feugnet, G.; Trompeta, A.-F.; Charitidis, C. A. *Journal of Physics: Materials* **2019**, *2*, 032002.

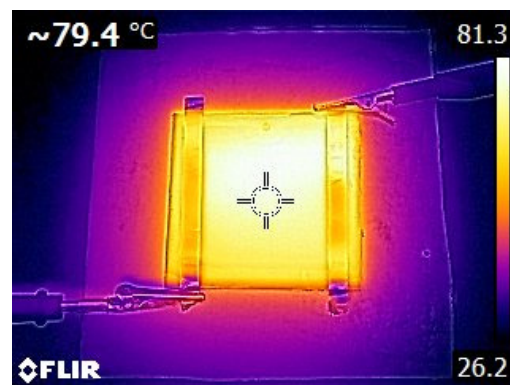


Figure 1: Heating test panel of rGO based coating for De-icing applications.

A novel membrane-on-a-chip setup demonstrates in-plane conductivity of Q-lipid membranes

Ulrich Ramach, Jakob Andersson¹, Markus Valtiner

Institut für Allgemeine Physik, Technische Universität Wien, A-1040 Wien, Austria
(corresponding author: U.Ramach, e-mail: ramach@iap.tuwien.ac.at)

¹ Biosensor Technologies, 3430 Tulln, Austria

Quinone motives in molecules of higher life forms are an abundant molecular electron, redox and proton shuttle, serving very diverse purposes. [1] For instance, water soluble ortho-quinones such as adrenaline are important neurotransmitters while para-quinones act as amphiphilic "membrane-active" redox-shuttles and co-enzymes. For instance, ortho-quinone containing K-vitamins control blood coagulation and support enzymatic activities. [2,3] The thylakoid membrane, which hosts the photosynthetic redox-chain, contains plastoquinone (PC) for delivering electrons from photosystem II to plastocyanin, and for building up a proton gradient across a cell membrane.[4,5]

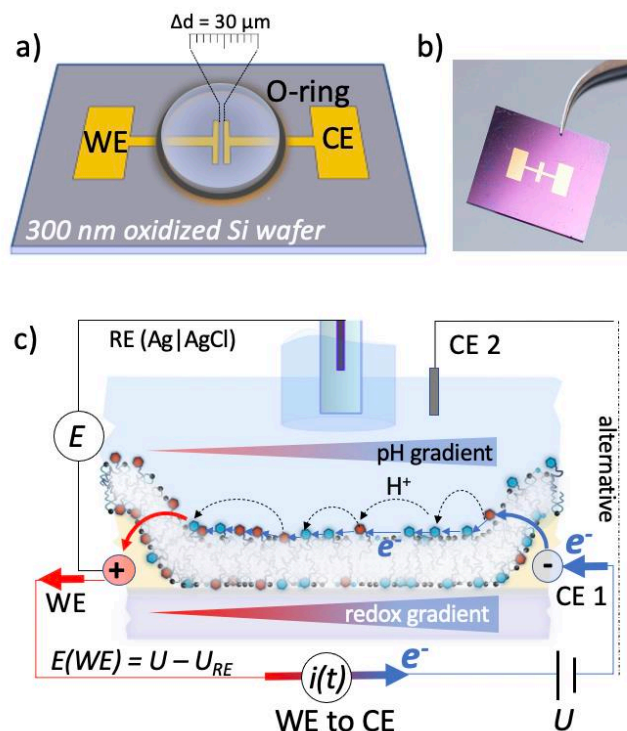


FIGURE 2 a) Schematic of the chip used. b) Photograph of the chip. c) Schematic of the experimental setup, showing the working (WE), counter (CE1 or CE2) and the reference electrode, as well as the deposited lipid bilayer

Protein mobility and diffusion of redox lipids is believed to be the *in-plane* charge transfer mechanism along such cell membranes. Using a *membrane-on-a-chip* setup (Figure 2), we show that redox-active model membranes can conduct and sustain surprisingly high (mA) *in-plane* at distances of 25 μm . We further demonstrate the same level of conductivity for free-standing monolayers at the air water interface at varying surface pressure, and once the distance between redox centers is below 1 nm. Our data suggest that charge transfer within cell walls hosting electron-transfer-chains is sustained by an effective coupling of redox-lipids by a simultaneous electron and proton *in-plane* hopping, similar to conductive polymers. This completely alters our understanding of

the role of lipid membranes with wide-range implications suggesting, e.g. that conducting membranes may be the precursor for evolving complex redox-machineries of life, and electrochemical membrane deterioration may play an important role in mitochondrial ageing. Further, these self-assembling organic 2D-conductors offer technologically exploitable features allowing for designing self-assembling and adaptive bio-electronics.

The authors acknowledge the European Research Council (ERC-StG 663677).

- [1] Waite JH. The DOPA Ephemera: A Recurrent Motif in Invertebrates. *Biol. Bull.* 2016. doi: 10.2307/1542421
- [2] DiNicolantonio JJ, Bhutani J, O’Keefe JH. The health benefits of vitamin K. *Open Heart* 2015; 2(1). doi: 10.1136/openhrt-2015-000300
- [3] Shearer MJ, Newman P. Metabolism and cell biology of vitamin K. *Thromb. Haemost.* 2008; 100(4): 530–547.
- [4] Junge W. Oxygenic photosynthesis: history, status and perspective. *Q. Rev. Biophys.* 2019; 52. doi: 10.1017/S0033583518000112
- [5] Zhao LS, Huokko T, Wilson S, et al. Structural variability, coordination and adaptation of a native photosynthetic machinery. *Nat. Plants* 2020; 6(7): 869–882. doi: 10.1038/s41477-020-0694-3

Competition at crowded interfaces

Pierluigi Bilotto¹, Alexander M. Imre², Dominik Dworschak³, Laura L.E. Mears², and Markus Valtiner^{1,2}

¹Centre for Electrochemical Surface Technology, Wiener Neustadt, Austria

²Institute of Applied Physics, Vienna University of Technology, 1040, Vienna, Austria

³Helmholtz-Institut Erlangen-Nürnberg für Erneuerbare Energien, Germany

pierluigi.bilotto@cest.at

Generating a detailed molecular understanding of complex, simultaneous interactions at reactive and/or dynamic solid|fluid interfaces is a challenge across disciplines, and has intrigued researchers for decades.[1, 2] Whether it is, for example, in medical adhesives, friction of articular cartilage,[3] or the adhesion of organisms in seawater,[2] complex macroscopic properties at crowded biologic solid|liquid interfaces are mediated by large numbers of individual nanoscale interactions;[4] namely similar or dissimilar molecule/molecule and molecule/surface interactions, surface-dipole interactions[5] or the competing interactions with cations and water.[6]

Exactly this complex competition and molecular structuring at interfaces are central to a multitude of interfacial phenomena, such as membrane transport,[7] membrane conductance, [8, 9] cellular adhesion [10] and adhesion regulation in the marine environment. [11]

In our previous work, we characterised a lipid-based model system (LMS) in terms of its stability and bending properties. [12] Here, we further modify its outer face with amine-terminating polymers (varied in density during the experiments) to investigate the specific electrostatic interaction between the amine and a negatively charged mica surface. We utilised a surface forces apparatus (SFA) and an atomic force microscope (AFM) to appreciate the force-distance interaction profile and the sample topography. Moreover, we examine how interaction forces are affected

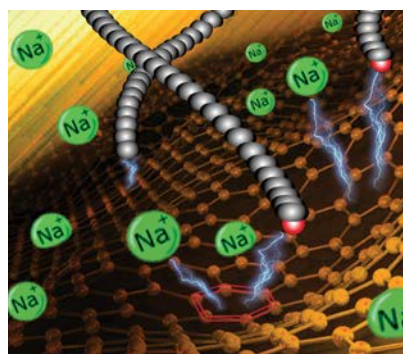


Figure 1: Graphic representation of a crowded interface. In the centre, the competition for a mica binding site between polymers presenting amine at their termination and sodium cations.

by the electrolyte concentration.[13] In details, at the mica interface, we observe that cations and polymers begin a nanoscopic competition for the available binding site. We support this observation with experimental data showing the correlation between electrolyte concentration and the measured work of adhesion for LMS on mica. Specifically, we observe a loss in adhesion of 90% when the electrolyte concentration is increased to 1M. Visualisation of super resolved ionic layers onto the mica lattice further confirms the cations presence increasing with concentration. Finally, based on a kinetic model using two competing Langmuir adsorption isotherms we can estimate ion/surface interaction energies from the experimentally recorded interaction force measurements, demonstrating a path for a comprehensive combined experimental and modelling approach.[13]

The authors acknowledge support by the European Research Council (ERC-StG Grant No. 677663). The authors acknowledge the TU Wien Bibliothek for financial support through its Open Access Funding Program.

- (1) Israelachvili, J.; Wennerström, H. *Nature* **1996**, *379*, 219–225.
- (2) Stock, P.; Monroe, J. I.; Utzig, T.; Smith, D. J.; Shell, M. S.; Valtiner, M. *ACS Nano* **2017**, *11*, 2586–2597.
- (3) Shoaib, T.; Yuh, C.; Wimmer, M. A.; Schmid, T. M.; Espinosa-Marzal, R. M. *Biomater. Sci.* **2020**, *8*, 3944–3955.
- (4) Cai, L.; Sun, Q.; Bao, M.; Ma, H.; Yuan, C.; Xu, W. *ACS Nano* **2017**, *11*, PMID: 28383885, 3727–3732.
- (5) Kristiansen, K.; Stock, P.; Baimpos, T.; Raman, S.; Harada, J. K.; Israelachvili, J. N.; Valtiner, M. *ACS Nano* **2014**, *8*, 10870–10877.
- (6) Alvarez-Garcia, D.; Barril, X. *Journal of Medicinal Chemistry* **2014**, *57*, PMID: 25275946, 8530–8539.
- (7) Gage, P. W.; Quastel, D. M. J. *The Journal of Physiology* **1966**, *185*, 95–123.
- (8) Stieve, H.; Bruns, M. *Zeitschrift für Naturforschung C* **1978**, *33*, 574–579.
- (9) Stieve, H.; Pflaum, M.; Klomfaß, J.; Gaube, H. *Zeitschrift für Naturforschung C* **1985**, *40*, 278–291.
- (10) Ohgaki, M.; Kizuki, T.; Katsura, M.; Yamashita, K. *Journal of Biomedical Materials Research* **2001**, *57*, 366–373.
- (11) He, X.; Wang, J.; Abdoli, L.; Li, H. *Colloids and Surfaces B: Biointerfaces* **2016**, *146*, 289–295.
- (12) Bilotto, P.; Lengauer, M.; Andersson, J.; Ramach, U.; Mears, L. L.; Valtiner, M. *Langmuir* **2019**, *35*, 15552–15563.
- (13) Bilotto, P.; Imre, A. M.; Dworschak, D.; Mears, L. L. E.; Valtiner, M. *ACS Physical Chemistry Au* **2021**, *0*, null.

Getting control over magnesium corrosion

T. Würger^{1,2}, C. Feiler², and R. Meißner^{1,2}

¹ *Institut für Kunststoffe und Verbundwerkstoffe, Technische Universität Hamburg, D-21073
Hamburg, Germany*

(corresponding author: R. Meißner, e-mail: robert.meissner@tuhh.de)

² *Institut für Oberflächenforschung, Helmholtz-Zentrum Hereon, D-21494 Geesthacht, Germany*

Magnesium (Mg) is among the most abundant elements on our planet and exhibits high potential to revolutionize light metal engineering in a large number of application fields. Treated magnesium-based alloys, for example, are promising candidates to satisfy a variety of current demands in the automotive industry, either as structural elements or in battery applications and thus contributing to the battle against the ongoing climate change. Furthermore, its biocompatibility enables Mg as biodegradable medical implant material [1]. However, as it is susceptible to corrosion, various target applications require domain-specific tailoring of the degradation behavior of Mg. For instance, medical applications where Mg is used in stents or temporary biodegradable bone implants require a degradation rate tailored to a patient-specific injury to support recovery.

An essential prerequisite for the control and prevention of the degradation process is hence a deeper understanding of the underlying degradation mechanisms. Prior investigations of the formation of gaseous hydrogen during the corrosion of magnesium indicated that the predominant mechanism for this process follows the Volmer–Heyrovský rather than the previously assumed Volmer–Tafel pathway. However, the energetic and electronic states of both reaction paths as well as the charge state of dissolved magnesium have not been fully unraveled yet. By using density functional theory calculations (DFT), we show how the major reaction pathways of pure Mg degradation involving the dissolution of Mg and the evolution of hydrogen can be identified [2] to gain a comprehensive understanding of the major corrosion mechanisms responsible for the degradation of magnesium.

Subsequent to these findings, benign strategies to modulate degradation are consequently required. There are several approaches to protect magnesium from corrosion, including alloying and surface coatings. Apart from that, small organic molecules, which form complexes with ions (e.g., iron) that promote the corrosion process, have shown great potential to control the dissolution properties of pure Mg materials and its alloys [3]. This approach particularly facilitates tailored degradation rates of resolvable medical implants (e.g., stents) or adjustment of properties of the anode material in magnesium-air batteries to achieve high utilization efficiencies while maintaining a high discharge potential. The vast chemical space of potentially useful compounds can be explored by machine learning-based

quantitative structure-property relationship (QSPR) models, accelerating the discovery of degradation modulators. In a comprehensive experimental study employing hydrogen evolution experiments, Lamaka et al. measured the corrosion inhibition performance of over 150 organic compounds for nine distinct Mg-based materials [4], thus providing a suitable training set. We demonstrate how unsupervised clustering of potential Mg dissolution modulators based on structural similarities [5] and sketch-maps [6] can quantitatively predict their experimental performance when combined with a kernel ridge regression (KRR) model [7]. The prediction accuracy of the KRR model is benchmarked against an artificial neural network (ANN) model that was trained on a combination of atomistic and structural molecular descriptors [8]. These synergistic computational approaches significantly improve the model interpretation and predictive power of the underlying machine learning models [9], thus paving the way for the discovery or rational design of tailored Mg dissolution agents.

Support by the Deutsche Forschungsgemeinschaft (projects 390794421 and 192346071) is gratefully acknowledged.

- [1] B. Zeller-Plumhoff, M. Gile, M. Priebe, H. Slominska, B. Boll, B. Wiese, T. Würger, R. Willumeit-Römer and R. H. Meißner, *Corros. Sci.* 182, 109272 (2021)
- [2] T. Würger, C. Feiler, G. B. Vonbun-Feldbauer, M. L. Zheludkevich and R. H. Meißner, *Sci. Rep.* 10, 15006 (2020)
- [3] L. Fockaert, T. Würger, R. Unbehau, B. Boelen, R. H. Meißner, S. V. Lamaka, M. L. Zheludkevich, H. Terryn, *J. M. C. Mol, Electrochim. Acta* 345, 136166 (2020)
- [4] S.V. Lamaka, B. Vaghefinazari, Di Mei, R.P. Petruskas, D. Höche and M.L. Zheludkevich, *Corros. Sci.* 128, 224 (2017)
- [5] T. Würger, C. Feiler, F. Musil, G. B. V. Feldbauer, D. Höche, S. V. Lamaka, M. L. Zheludkevich and R. H. Meißner, *Front. Mater.* 6, 53 (2019)
- [6] M. Ceriotti, G. A. Tribello and M. Parrinello, *PNAS* 108, 13023 (2011)
- [7] T. Würger, D. Mei, B. Vaghefinazari, D. A. Winkler, S. V. Lamaka, M. L. Zheludkevich, R. H. Meißner and C. Feiler, *npj Mater. Degrad.* 5, 2 (2021)
- [8] C. Feiler, D. Mei, B. Vaghefinazari, T. Würger, R. H. Meißner, B. J. C. Luthringer-Feyerabend, D. A. Winkler, M. L. Zheludkevich and S. V. Lamaka, *Corros. Sci.* 163, 108245 (2020)
- [9] E. J. Schiessler, T. Würger, S. V. Lamaka, R. H. Meißner, C. J. Cyron, M. L. Zheludkevich, C. Feiler and R. C. Aydin, *npj Comput. Mater.* 7, 193 (2021)

Order and disorder in Li-ion batteries: a Surface-Science perspective

H.E. Hoster, D. Kramer¹, E.P.M. Leiva², M. P. Mercer³

*Lehrstuhl Energietechnik, Universität Duisburg-Essen, 47048 Duisburg, Germany
(corresponding author: H.E. Hoster, e-mail: harry.hoster@uni-due.de)*

¹ *Faculty of Mechanical Engineering, Helmut-Schmidt University, Holstenhofweg 85, 22043 Hamburg, Germany*

² *Departamento de Química Teórica y Computacional, Facultad de Ciencias Químicas, Universidad Nacional de Córdoba, INFIQC, Córdoba, Argentina*

³ *Energy Lancaster, Department of Chemistry, Lancaster University, LA1 4YB, United Kingdom*

Like adsorbate layers known in Surface Science, Li-ions in rechargeable batteries assume ordered and disordered distribution phases in their host electrodes. Thermodynamically, they are in a grand-canonical equilibrium with Li-ions in the electrolyte and with Li hosted in the counter electrode [1,2]. The electrochemical potential of an electrode steers its Li contents and phases in the same way as the vapour pressure steers adsorbate layers in Surface Science.

We will explain the unique markers in voltage profiles as created by Li-distribution phases during battery charge/discharge. Their meaning goes beyond scientific curiosity: such markers are used in battery management systems; changes in marker patterns over time provide non-destructive insights into battery degradation mechanisms.

Partial molar enthalpy and entropy are experimentally disentangled by recording voltage responses on temperature modulations [3-5]. This provides a thermodynamic understanding of marker patterns in voltage profiles and a basis for atomistic models and their validation.

Lattice gas modelling tools transferred from Surface-Science [6,7] to the world of batteries created a framework to interpret, model, and understand the phase behaviour of lithiated electrodes [1,2,4,5].

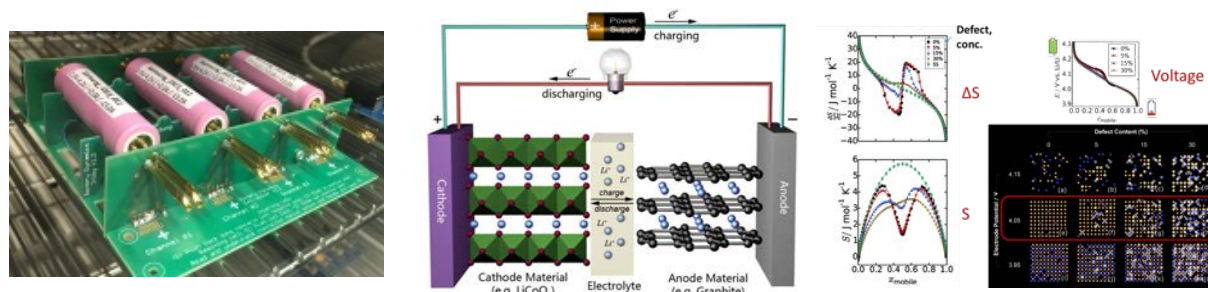


Figure: Illustration of voltage profiles and underlying lattice superstructures in Lithium-Ion Batteries. The related phases are relevant for non-destructive diagnostics and safety monitoring of commercial cells and their understanding is crucial for the development of new battery materials. On the right, we illustrate how increasing densities of point defects [2] reduce the amplitudes of entropy profiles [3] related to order-disorder transitions.

We thank the Faraday Institution (<https://faraday.ac.uk/>; EP/S003053/1), Grant No. FIRG003, for funding.

- [1] L. Morgan, M. Mercer et al., *Progress in Energy* (2022), *in press*.
- [2] M.P. Mercer, S. Finnigan, D. Kramer, D. Richards, H.E. Hoster, *Electrochim. Acta* 241, 141 (2017)
- [3] P.J. Osswald, M. del Rosario, J. Garche, A. Jossen, H.E. Hoster, *Electrochim. Acta* 177, 270 (2015)
- [4] M.P. Mercer, M Otero et al., *Electrochim. Acta* 324, 134774 (2019)
- [5] S. Schlueter, R. Genieser, D. Richards, H.E. Hoster, M.P. Mercer, *Phys. Chem. Chem. Phys.* 20, 21417 (2018)
- [6] A. Breittruck, H.E. Hoster, R.J. Behm, *J. Phys. Chem. C* 113, 21265 (2009)
- [7] A. Bergbreiter, H.E. Hoster, S. Sakong, A. Groß, R.J. Behm, *Phys. Chem. Chem. Phys.* 9, 5127 (2007)



HiPACE 80 Neo

The hybrid bearing vacuum pump with patented Laser Balancing™ technology

- Best combination of size and performance due to intelligent rotor temperature measurement
- Lowest vibration level in the market due to Laser Balancing™ technology
- High compression ratio for light gases
- Oil lubrication with synthetic filtering media to maximize bearing lifetime

Are you looking for a perfect vacuum solution? Please contact us:
Pfeiffer Vacuum GmbH · Germany · T +49 6441 802-0 · www.pfeiffer-vacuum.com

Friday

Nature of Interfacial Dzyaloshinskii-Moriya Interactions in Graphene/Co/Pt(111) Multilayer Heterostructures

M. Blanco-Rey,^{1,2} G. Bihlmayer,³ A. Arnau,^{4, 1, 2} and J.I. Cerdá⁵

(corresponding author: A. Arnau, e-mail: andres.arnau@ehu.es)

¹ Departamento de Polímeros y Materiales Avanzados: Física, Química y Tecnología, Facultad de Química UPV/EHU, Apartado 1072, 20080 Donostia-San Sebastián, Spain

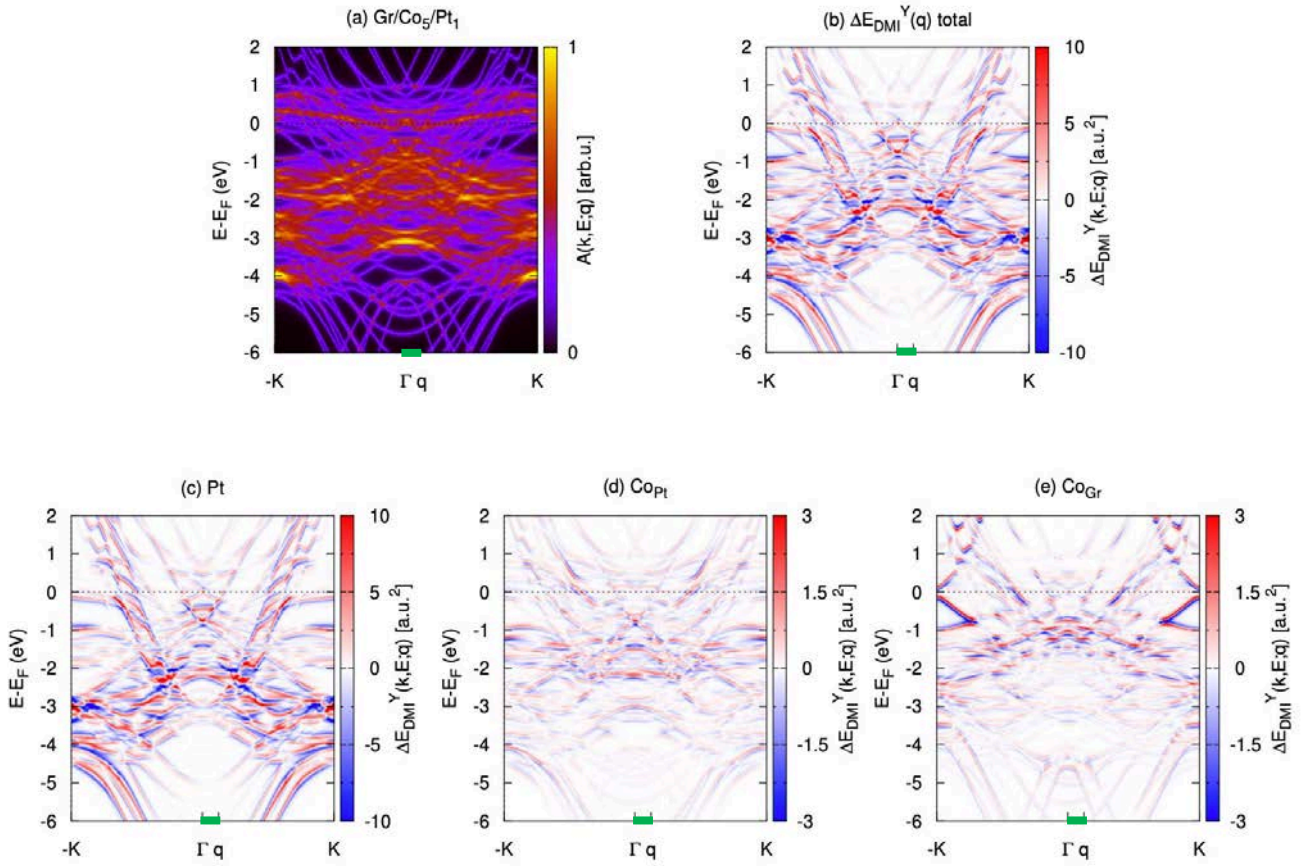
² Donostia International Physics Center, Paseo Manuel de Lardizábal 4, 20018 Donostia-San Sebastián, Spain

³ Peter Grünberg Institut and Institute for Advanced Simulation, Forschungszentrum Jülich and JARA, 52425 Jülich, Germany

⁴ Centro de Física de Materiales CFM/MPC (CSIC-UPV/EHU), Paseo Manuel de Lardizábal 5, 20018 Donostia-San Sebastián, Spain

⁵ Instituto de Ciencia de Materiales de Madrid, CSIC, Cantoblanco, 28049 Madrid, Spain

DFT calculations utilizing the generalized Bloch theorem show that interfacial Dzyaloshinskii-Moriya interactions (DMI) at both interfaces of Graphene/Co_n/Pt(111) multilayer heterostructures are decoupled for $n > 3$. Unlike the property of magnetocrystalline anisotropy, DMI in this system is not strongly affected by stacking defects in the Co layer. The effect of Graphene (Gr) is to invert the chirality of the vacuum/Co interfacial DMI, overall reducing the DMI of the heterostructure, which is nevertheless dominated by the strong spin-orbit coupling (SOC) of Pt. A spectral analysis in reciprocal space shows that DMI at both the Gr/Co and Co/Pt interfaces has the same nature, namely SOC-split hybrid bands of d-orbital character. Our analysis proves that a DMI model based on a single band, such as the Rashba DMI model, is insufficient to describe the behavior of this family of Gr-capped 3d/5d metal heterostructures.



k-resolved spectral DMI energy for Gr/Co₅/Pt₁.

(a) Spectral density of the Gr/Co₅/Pt₁ system calculated without SOC for the q-vector $\mathbf{q} = 2\pi/a(1/24, 1/24, 0)$ ($q=0.125|\Gamma K|$), indicated with a green arrow. The lateral splitting introduced by the spiral in the bands is observed.

(b) Density of energy $\Delta E_{DMI}^Y(\mathbf{q})$. The actual DMI energy is the integral over occupied states, which involves many cancellations of positive and negative contributions.

(c-e) The contributions of the indicated interfacial atoms to the density of panel (b). The more intense DMI contributions in panels (c,d) map the broad bands mainly originated from Pt(d) and Co(d) orbitals, centred at $E_F - 3.5$ and $E_F - 1.5$ eV, respectively. The Co_{Gr} interfacial states show high intensity at the Co-C hybrid conical bands. Nevertheless, as in the other panels, cancellations of DMI energies of opposite sign attenuate the contribution of this band structure feature to the total DMI energy.

$$\Delta E_{DMI}^Y(n_e; \mathbf{q}) = \sum_{nk} \epsilon_{nk}^{Y+}(\mathbf{q}) f\left(\epsilon_{nk}^{Y+}(\mathbf{q}) - \epsilon_F^{Y+}(n_e; \mathbf{q})\right) - \epsilon_{nk}^{Y-}(\mathbf{q}) f\left(\epsilon_{nk}^{Y-}(\mathbf{q}) - \epsilon_F^{Y-}(n_e; \mathbf{q})\right)$$

An intercalated Cu_{2-x}O thin film confined underneath hexagonal boron nitride on top of Cu(111)

Z. Novotny^{1,2}, J.T. Diulus^{1,2}, N. Comini^{1,2}, J. Beckord¹, M. Muntwiler², M. Hengsberger¹, and J. Osterwalder¹

¹ Physics Institute, University of Zürich, Irchel Campus; 8057 Zürich, Switzerland
(corresponding author: J. Osterwalder, e-mail: osterwal@physik.uzh.ch)

² Swiss Light Source, Paul Scherrer Institute; 5232 Villigen PSI, Switzerland

Cuprous oxide (Cu_2O) is a promising photocathode material for the hydrogen evolution reaction (HER) due to its bandgap in the visible spectrum, relative abundance, and low cost [1]. However, Cu_2O is unstable in aqueous solutions. To increase the corrosion resistance of Cu_2O cathodes under photoelectrochemical cell conditions, a chemically stable capping layer, such as hexagonal boron nitride (h-BN), can be deposited on the Cu_2O surface. While the growth of h-BN on top of metal oxides is difficult, an alternative approach is to oxidize a Cu substrate underneath an h-BN monolayer *via* O_2 intercalation [2]. Due to weak interactions between h-BN and Cu(111) [3], the Cu(111) substrate can be oxidized, forming a thin oxide film while the h-BN remains intact. Catalytic activity may also be enhanced due to the nano-confinement effect as confined reactions can occur underneath the h-BN layer [4].

Growth of h-BN on Cu(111) was achieved through chemical vapor deposition by borazine exposure in the ultra-high vacuum preparation chamber of the Solid Liquid Interface Chamber endstation, attached to the In Situ Spectroscopy beamline at the Swiss Light Source (SLS) [5]. Initially, the surface structure and the chemical composition of the bare Cu(111) substrate and the as-grown h-BN/Cu(111) heterostructure were characterized using Auger electron spectroscopy and low-energy electron diffraction (LEED). Once the h-BN/Cu(111) sample was prepared, X-ray photoelectron spectroscopy (XPS) was used to characterize the coverage and uniformity of h BN on the surface. Oxidation of the Cu(111) underneath the h-BN cover *via* O_2 intercalation was executed by exposure to near-ambient partial pressures of O_2 (0.001 to 1 mbar) at temperatures ranging from room temperature up to 200 °C. Ambient pressure XPS (AP-XPS) and X-ray absorption spectroscopy (XAS) were utilized at each temperature and pressure to determine the oxidation state of Cu throughout the experiment and develop a recipe for preparing the h-BN/ Cu_{2-x}O /Cu(111) heterostructure.

Further characterization of h-BN/ Cu_{2-x}O /Cu(111) was obtained at the PEARL beamline at the SLS [6]. Scanning tunneling microscopy (STM) provided atomic-resolution imaging of the sample held at 78 K, displaying a surface resembling the “29”- Cu_2O superstructure [7], further verified with LEED. Through STM, we additionally determined that the oxidation of the Cu(111) substrate occurs *via* oxygen intercalation at the h-BN grain boundaries. X-ray photoelectron diffraction (XPD) provided additional structural information, combined with

simulated photoelectron diffraction with the Electron Diffraction in Atomic Clusters (EDAC), to fully model the entire h BN/Cu_{2-x}O/Cu(111) heterostructure.

This work was supported by the Swiss National Science Foundation and the European Union's Horizon 2020 program.

- [1] A. Paracchino. *et al.*, Nat. Mater. 10 456–61 (2011)
- [2] C. Ma. *et al.*, Phys. Rev. B 94 064106 (2016)
- [3] S. Joshi *et al.*, Nano Lett. 12 5821–8 (2012)
- [4] Q. Fu *et al.*, Chem. Soc. Rev. 46 1842–74 (2017)
- [5] Z. Novotny *et al.*, Rev. Sci. Instrum. 91 023103 (2020)
- [6] M. Muntwiler *et al.*, J. Synchrotron Radiat. 24 354–66 (2017)
- [7] A. Therrien *et al.*, J. Phys. Chem. C 120 10879–86 (2016)

How stable are 2-D oxide lattices against doping?

¹Malihe Mohammadi, ²Fabio R. Negreiros, ¹Svetlozar Surnev, ¹**Falko P. Netzer**

¹*Surface and Interface Physics, Institute of Physics, Karl-Franzens University Graz, Austria*

²*INFIQC, CONICET, Universidad Nacional de Córdoba, Argentina*

The doping of oxide materials with foreign atoms is a viable approach to achieve a precise control of their electronic, optical, magnetic, and chemical behavior via electron band structure engineering. Tungsten trioxide, WO_3 , is a key material in several important applications, including electrochromic devices, rechargeable batteries, and photo-electrochemical water splitting. Most of these applications are not intrinsic to the pure WO_3 compound but originate from its ability to incorporate small dopant ions (e.g. H^+ , Li^+ , Na^+). The doping of tungsten trioxide with alkali metals is of particular interest, leading to the so-called alkali bronzes. The sodium bronzes (Na_xWO_3 , $x = 0 - 1$), the most important compounds, are non-stoichiometric systems, in which the Na atoms are incorporated into the A sites of a perovskite structure; they display a dramatic variation of optoelectronic properties with composition. The Na bronzes are of fundamental interest (e.g. they feature a metal-semiconductor transition, at $x \sim 0.25$), as well as of technological relevance (they support “green energy devices”, e.g. electrochromism in “smart windows” technology). In view of the ongoing trend towards the reduction of size and dimensionality of active elements in advanced nanotechnologies, two-dimensional (2-D) oxide layers become increasingly important [1]. Here we report the investigation of the interaction of Na atoms with a 2-D WO_3 layer supported on a Pd(100) surface and address the charge transfer and the stability of the oxide layer against the dopants.

The 2-D WO_3 on Pd(100) model system has been characterized previously at the atomic level both experimentally and theoretically [2]. WO_3 on Pd(100) forms a commensurate monolayer with a local $c(2 \times 2)$ structure, exhibiting an ordered anti-phase domain lattice as a result of interfacial strain relief. DFT calculations have identified the $c(2 \times 2)$ layer as a $\text{WO}_2 + \text{O}$ bilayer, as generated by cutting a slice perpendicular to the [100] direction of the cubic WO_3 bulk structure. The Na atoms in the present experiments have been deposited onto the 2D WO_3 layer from SAES getter sources and the modifications of geometry and electronic structure have been followed in a surface science approach with LEED, STM, UPS, XPS and work function measurements [3].

We find two specific interaction regimes in terms of the Na concentration dependence: a low coverage regime up to 0.25 ML, which we describe in terms of **doping** interactions, and a **reaction** regime, where at higher Na coverages the 2-D WO_3 lattice becomes unstable and is destroyed and several ordered 2D Na_xWO_3 bronze-type phases with different structures are formed upon thermal activation. In the doping regime, the Na adsorption sites and charge transfer processes to the oxide have been specified by STM and DFT simulations. The Na atoms decorate initially the oxide domain boundaries, and subsequently adsorb in a (2×2) superstructure filling the regular fourfold hollow sites between the terminal O atoms

within the oxide domains. The Na adatoms are almost completely ionic, however the transferred charge resides mostly on the nearest-neighbor oxygen atoms rather than on the W atoms (as expected from the 3-D case). In the reaction regime, the most prominent and energetically stable phase is a hexagonal 2-D Na bronze-like structure, whose atomic details have been revealed in the DFT analysis. The comparison of the Na interactions with the 2-D oxide system and the behavior of the 3-D Na bronzes suggests that the cubic 2-D oxide phase is less stable against doping, as a result of a poorer electrostatic screening capability, than the 3-D case. However, the flexibility of the 2-D oxide lattice enables the facile formation of a stable hexagonal 2-D bronze polymorph.

[1] S. Surnev and F.P. Netzer, "Tungsten- and Molybdenum-oxide nanostructures: Two-dimensional layers and nanoclusters", *Topical Review*, J. Phys. Condens. Matter, 2022

[2] N. Doudin et al., J. Phys. Chem. C120, 28682 (2016)

[3] M. Mohammadi, F. R. Negreiros, T. Radlinger, P. Edelmayer, F. P. Netzer, S. Surnev, submitted

Comparison of single Rh and Ir adatoms on α - $\text{Fe}_2\text{O}_3(1\bar{1}02)$ – stabilization with and without water

L. Haager, F. Kraushofer, M. Eder¹, A. Rafsanjani-Abbasi, G. Franceschi, M. Riva, M. Meier²,
M. Schmid, U. Diebold, and G. S. Parkinson

Institut für Allgemeine Physik, Technische Universität Wien, A-1040 Wien, Austria

(corresponding author: L. Haager, e-mail: haager@iap.tuwien.ac.at)

¹*Chair of Physical Chemistry, TU München, Germany*

²*University of Vienna, Vienna, Austria*

So-called “single-atom” catalysis offers an opportunity to reduce the amount of catalyst material required for traditional heterogeneous catalysis, and to “heterogenize” reactions presently requiring homogeneous catalysis; this would eliminate the problem of separating catalyst and product.

In single atom catalysis, simplified models are often proposed, in which the single metal atoms are in a cationic site and bound to surface oxygen of the support. In a more realistic model, hydroxylation should be considered, but this additional complexity is usually left out.

Using STM, nc-AFM, and XPS, we compare the stability of Rh and Ir adatoms on α - $\text{Fe}_2\text{O}_3(1\bar{1}02)$, both after deposition in UHV and in a background of 2×10^{-8} mbar water. We show that the Rh adatoms sinter in UHV but are stabilized by water up to 150 °C through coordination to 2-3 OH ligands [1]. In contrast, Ir adatoms are already stable when deposited in UHV at room temperature.

1. Kraushofer, F., et al., *Single Rh Adatoms Stabilized on α - $\text{Fe}_2\text{O}_3(1\bar{1}02)$ by Coadsorbed Water*. ACS Energy Letters, 2021. 7: p. 375-380.

Polaronic Diffusion in Doped Hematite – experiment vs. Kinetic Monte Carlo simulations

P. Kocán¹, V. Gabriel¹, J. Redondo¹, D. Wrana¹, G. Francheschi², E. Rheinfrank², I. Sokolovic², G. S. Parkinson², U. Diebold², M. Riva² and M. Setvín^{1,2}

*¹Department of Surface and Plasma Science, Faculty of Mathematics and Physics
Charles University, Prague, Czech Republic*

²Institute of Applied Physics, TU Wien, Austria

(corresponding author: P. Kocán, e-mail: pavel.kocan@mff.cuni.cz)

Polarons are quasiparticles formed by the stabilization of electrons or holes in potential wells created by the distortion of the surrounding lattice of a polarizable material [1]. These quasiparticles are responsible for the electrical conductivity [2] of dielectrics, which is crucial for chemical activity of photo- or electrocatalysis [3]. Hematite (α -Fe₂O₃) as a material with high theoretical solar-to-hydrogen conversion efficiency is especially important for the development of a sustainable clean-energy economy [4]. Here we focus on the fundamentals of polaronic conductivity, which is a key factor in the photoelectrochemical water splitting reaction [5] on this material.

Mobility of polarons in hematite can be easily modified by doping. Ti dopants substitute Fe³⁺ by Ti⁴⁺, donating free electrons and increasing electron conductivity [6]. Oppositely, Ni²⁺ dopants introduce trap states for electrons and increase the hole-polaron concentration.

Previously we presented how electrons and holes can be injected into the hematite (1-102) surface [7]. Both injection and mapping are realized by means of the Q-Plus sensor. The charges localized as small polarons are immobile at low temperatures (at 4.7 K for electrons). Hopping of the polarons can be activated by increasing the temperature, as evidenced by means of local contact potential difference (LCPD) mapping. We used single-crystalline films grown on bulk hematite crystals [8], which provide well-defined doping levels and high-quality surfaces.

Here we will present experimental data with differently doped hematite samples to show how the doping influences the mobility of electron polarons (Ti-doping) and hole polarons (Ni-doping). To gain insights on the kinetics of the injected cloud of polarons we have developed several kinetic Monte Carlo (KMC) models. Initially we simulate the effect of the dopants by decreasing of hopping barriers uniformly in the whole sample. The model is kept as simple as possible in order to minimize the number of free parameters, while implementing electrostatic interactions between all injected charges. Even though an excellent agreement with the LCPD data is obtained, the mechanism how the dopants influence the hopping is not clear. In the presentation we will introduce and discuss further more realistic models in order to support or exclude the possible mechanisms.

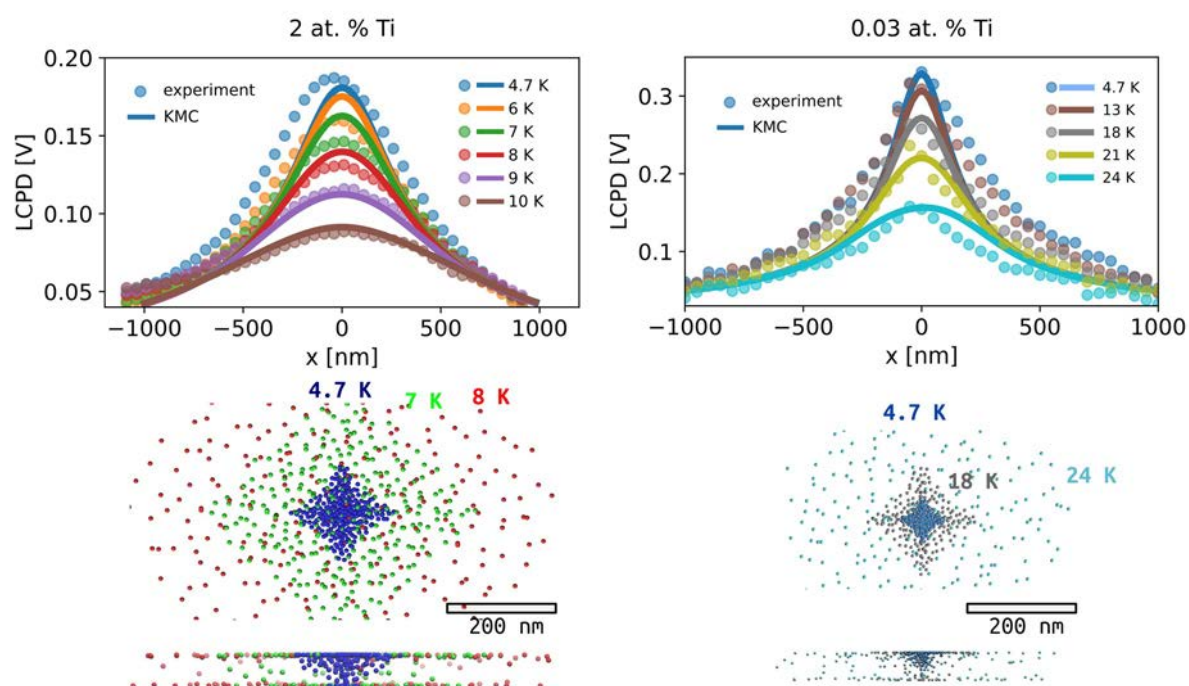


Figure. top: Comparison of experimental and simulated LCPDs at increasing temperatures for highly (left) and low (right) Ti-doped hematite samples. Bottom: Spreading of injected clouds of polarons simulated by KMC. Different colors correspond to the indicated temperatures to which the system was shortly heated.

This work was supported by the Czech Science Foundation (GACR 20-21727X) and by GAUK/Primus/20/SCI/009.

- [1] C. Franchini, M. Reticioli, M. Setvin, U. Diebold, Nat. Rev. Mater. 0123456789 (2021).
- [2] K. M. Rosso, D. M. A. Smith, M. Dupuis, J. Chem. Phys. 118, 6455–6466 (2003).
- [3] C. Lohaus, A. Klein, W. Jaegermann, Nat. Commun. 9, 1–7 (2018).
- [4] A. G. Tamirat, J. Rick, A. A. Dubale, W. N. Su, B. J. Hwang, Nanoscale Horizons. 1, 243–267 (2016).
- [5] Li, C., Luo, Z., Wang, T. & Gong, J., Adv. Mater. 30, (2018).
- [6] Kronawitter, C. X. et al., Energy Environ. Sci. 7, 3100–3121 (2014).
- [7] J. Redondo et al., Polarons frozen in a crystal lattice observed by nc-AFM, Symposium on Surface Science 2020, St. Christoph am Arlberg, Austria
- [8] Franceschi, G. et al., Chem. Mater. 32, 3753–3764 (2020)

The link between surface diffusion and surface reconstructions on oxides

Giada Franceschi, Michael Schmid, Ulrike Diebold, and Michele Riva

*Institute of Applied Physics, TU Wien, A-1040 Wien, Austria
(corresponding author: M. Riva, e-mail: riva@iap.tuwien.ac.at)*

Surface diffusion on metal oxides is key in many areas of materials technology, yet it has been scarcely explored at the atomic scale. The work presented in this contribution [1] provides phenomenological insights from scanning tunneling microscopy on the link between surface diffusion, surface atomic structure, and oxygen chemical potential based on three model oxide surfaces: $\text{Fe}_2\text{O}_3(1-102)$, $\text{La}_{1-x}\text{Sr}_x\text{MnO}_3(110)$ and $\text{In}_2\text{O}_3(111)$. Despite the difference in their surface atomic details, the chosen case studies show overall consistent diffusion behavior: When the preparation conditions promote the formation of a different reconstruction, the surface morphology becomes remarkably flatter. It is argued that the main factor behind the flattening is of thermodynamic nature. When the preparation conditions change, the system switches between reconstructions to minimize its surface free energy. The different composition of the reconstructions creates a strong driving force to displace material across the surface, in turn promoting surface flattening.

- [1] G. Franceschi, M. Schmid, U. Diebold and M. Riva “Surface reconstructions drive surface diffusivity and determine the flatness of oxide surfaces”, submitted (2021).

Stability investigations of sputtered molybdenum oxide thin films in the presence of water

S. Goetz^{1,2}, R. A. Wibowo¹, E. Franzke³, C. Linke³, J. Winkler³,
M. Valtiner², and T. Dimopoulos¹

¹ AIT Austrian Institute of Technology, Center for Energy, 1210 Wien, Austria
(corresponding author: S. Goetz, e-mail: selina.goetz@ait.ac.at)

² Institut für Angewandte Physik, Technische Universität Wien, 1040 Wien, Austria

³ Plansee SE, 6600 Reutte, Austria

Molybdenum oxides comprise a large family of materials with a broad range of adaptable and functional properties, specifically interesting for the application in (opto-)electronic devices, catalysis and sensors. Due to the existence of different stoichiometries and crystal structures they have different electronic and optical characteristics, ranging from semi-metallic MoO₂ (with oxidation state +4) to transparent and, insulating MoO₃ (+6) [1]. In MoO₃, the valence band edge is governed by O p-orbitals and the empty Mo d-orbitals form the conduction band minimum, resulting in a wide band gap of ~3 eV and a high work function up to 6.9 eV, which makes MoO₃ especially interesting for implementation as charge transport layers in organic solar cells and LEDs [2,3]. As oxygen is removed from the system, the Mo d-orbitals become occupied, leading to a smaller band gap and, ultimately, to semi-metallic behaviour in MoO₂ [4].

However, essential electronic properties, like the work function, can also be altered by other surface modifications, such as adsorption of water by exposure to ambient conditions [5]. While on ideal, stoichiometric and oxygen-terminated MoO₃ surfaces water adsorption and hydroxylation is weak, the introduction of defects, such as oxygen vacancies, significantly increases the reactivity with water [6]. A similar trend has also been observed for MoO₃ thin films by Sian and Reddy [7], where structural disorder causes increased surface reactions with humidity. They reported the highest amount of hydrolysed bonds in amorphous, nearly stoichiometric MoO₃ films using infrared spectroscopy.

Moreover, it has been observed that exposure to liquid water leads to a fast and complete disintegration of amorphous MoO₃ thin films, which makes further processing with water-based solutions impossible [8].

Using inductively coupled plasma mass spectrometry (ICP-MS) measurements with a downstream flow-cell setup, the dissolution behaviour of sputtered thin films in water is investigated in more detail. To this end, a specially designed, sub-oxidic sputtering target is used to deposit compact thin films of MoO_x. Depending on the oxygen content during the

sputtering process, the resulting layers are either transparent and nearly stoichiometric or show high optical absorption and increased electrical conductivity (when sputtered in pure Ar atmosphere). While 50 nm of oxygen-rich MoO₃ are completely dissolved within ~3 minutes, the dissolution rate of highly reduced films is significantly diminished [8]. The lack of oxygen introduces more metallic Mo-Mo bonds, leading to less hydrolysis and thus, to more stable films. However, the increased stability comes with high optical absorption, which makes the reduced film unfavourable for many applications that require high transparency.

Therefore, another approach is investigated to increase the water stability of molybdenum oxide, while maintaining the desired electronic and optical properties and that is by alloying with another refractory metal oxide. To this end, titanium oxide is introduced to form a mixed molybdenum-titanium oxide (MTO) compound material. Compact thin films are sputtered from a sub-oxidic MTO target, which allows fast deposition in direct current (DC) magnetron mode, achieving high sputtering rates that are relevant for industrial applications. The sputtered MTO layers are investigated using ICP-MS as well as infrared spectroscopy and show significantly increased stability in humidity and liquid water as compared to MoO₃. Even the oxygen-rich, transparent MTO layers can withstand processing with aqueous solutions and are found to be 20 times more stable in water than MoO₃ due to a partial passivation by the incorporated TiO₂. Nonetheless, the optical and electronic properties of the MTO layers, having an indirect optical band gap of 3.2 eV and a work function of ~5 eV, were found very similar to MoO₃.

- [1] I. de Castro, R. Datta, J. Ou, A. Castellanos-Gomez, S. Sriram, T. Daeneke and K. Kalantar-Zadeh, *Adv. Mat.* **29**, (2017)
- [2] A. L. F. Cauduro, R. dos Reis, G. Chen, A. K. Schmid, C. Méthivier, HG. Rubahn, L. Bossard-Giannesini, H. Cruguel, N. Witkowski and M. Madsen, *ACS Appl. Mater. Interfaces*, **9**, 8, (2017)
- [3] M. Greiner, M. Helander, WM. Tang, ZB. Wang, J. Qui and ZH. Lu, *Nature Mater* **11**, 76–81 (2012)
- [4] M. Vasilopoulou, A. M. Douvas, D. G. Georgiadou, L. C. Palilis, S. Kennou, L. Sygellou, A. Soultati, I. Kostis, G. Papadimitropoulos, D. Davazoglou, and P. Argitis, *J. Am. Chem. Soc.*, **134**, 39, (2012)
- [5] K. T. Butler, R. Crespo-Otero, J. Buckeridge, D. O. Scanlon, E. Bovill, D. Lidzey and A. Walsh, *Appl. Phys. Lett.* **107**, 231605 (2015)
- [6] A. R. Head, C. Gattinoni, L. Trotochaud, Y. Yu, O. Karşlıoğlu, S. Pletincx, B. Eichhorn and H. Bluhm, *J. Phys. Chem. C*, **123**, 27, (2019)
- [7] T. S. Sian and G. B. Reddy, *Chem. Phys. Lett.* **418**, (2006)
- [8] S. Goetz, R. A. Wibowo, M. Bauch, N. Bansal, G. Ligorio, E. List-Kratochvil, C. Linke, E. Franzke, J. Winkler, M. Valtiner and T. Dimopoulos, *J. Mater. Sci.* **56**, (2021)

Tuning the surface properties of thin films via disorder

A. Troglia¹, S. van Vliet¹, and R. Bliem^{1,2}

¹*Advanced Research Center for Nanolithography, Science Park 106, 1098 XG Amsterdam, The Netherlands (corresponding author: R. Bliem, e-mail: r.bliem@arcnl.nl)*

²*Institute of Physics, University of Amsterdam, Science Park 904, 1098XH Amsterdam, The Netherlands*

Crystalline order is typically considered a prerequisite for an ideal material. Disorder is thus commonly perceived as detrimental, even though it is a key advantage in important classes of materials. Structural disorder in amorphous alloys, for example, benefits various macroscopic properties, such as hardness or corrosion resistance, leading to an excellent performance as coatings, barrier layers, catalysts, or in advanced electronics [1,2]. So rather than distracting and detracting from perfection, structural disorder can serve as an ideal design parameter for new corrosion-resistant, hard, and selectively reactive alloys.

Typically, crystallinity and amorphicity in alloys are connected to specific stoichiometries, making the effects of structure and composition difficult to disentangle. In the present work we make use of pulsed laser deposition (PLD) to prepare crystalline and amorphous alloy layers of identical composition by growing thin films under two very different types of conditions, close to and far from equilibrium. We study the structural, mechanical, and electronic properties as well as the surface chemistry of polycrystalline and amorphous films for two selected alloys: CuZr and HfMoNbTiZr. CuZr is a model system for metallic glasses with composition-dependent glass-forming ability [3,4], whereas the high-entropy alloy (HEA) HfMoNbTiZr has exclusively been observed in its crystalline form [5].

In contrast to literature results, HfMoNbTiZr films grown with PLD at room temperature show no sign of crystallinity in grazing-incidence X-ray diffraction (GI-XRD). Even an increase of the deposition temperature to 800°C is insufficient to induce crystallization, which starts at 900°C. The liquid-like diffraction features of the amorphous films shift to higher diffraction angles (smaller average atomic distances) and decrease in width with increasing deposition temperature. This indicates that a lower-energy glassy structure is formed for high-temperature growth. It further suggests that the packing density in amorphous HEA thin films is tuneable, which could be of interest for their applications as energy storage medium [6]. The remarkable thermal stability of the amorphous phase and its facile formation highlight the potential of complex alloys for high-temperature applications requiring structural stability.

For CuZr, on the other hand, smaller variations in temperature are sufficient to induce crystallization. Room-temperature PLD leads to amorphous layers according to GI-XRD, while films of the same composition are polycrystalline when deposited at 500°C. Raman spectroscopy measurements show no discernible features for the amorphous layers while

broad but distinct modes are observed for polycrystalline films. The effect of disorder on the surface chemical properties of CuZr was measured using X-ray photoelectron spectroscopy (XPS) by comparing as-grown and air-exposed CuZr films. The XPS results show a remarkable preference in the surface oxidation of the Cu species. Cu is fully metallic for the amorphous film whereas both oxide and hydroxide components are observed for the crystalline layer.

Our results demonstrate that the level of structural disorder in thin alloy films can be tuned from polycrystalline to fully amorphous using PLD. This structural disorder significantly influences the surface reactivity and oxidation resistance of the model compound CuZr.

This work has been carried out at the Advanced Research Center for Nanolithography, a public-private partnership of the University of Amsterdam, the Vrije Universiteit Amsterdam, the Dutch Research Council (NWO) and the semiconductor equipment manufacturer ASML.

- [1] A. Inoue, A. Takeuchi. Stabilization of metallic supercooled liquids and bulk amorphous alloys. *Acta Mater.* 59, 2243 (2011).
- [2] W. Diyatmika, J. P. Chu, B. T. Kacha, C. Yu, C. Lee. Thin film metallic glasses in optoelectronic, magnetic, and electronic applications: A recent update. *Current Opinion in Solid State and Materials Science*, 19, 95 (2015).
- [3] Z. Altounian, T. Guo-hua, and J. O. Strom-Olsen. Crystallization characteristics of Cu-Zr metallic glasses from Cu₇₀Zr₃₀ to Cu₂₅Zr₇₅. *J. Appl. Phys.* 53 4755 (1982).
- [4] D. Wang, Y. Li, B.B. Sun, M.L. Sui, K. Lu, E. Ma. Bulk metallic glass formation in the binary Cu–Zr system. *Appl. Phys. Lett.* 84, 4029 (2004).
- [5] N.N. Guo, L. Wang, L.S. Luo, X.Z. Li, Y.Q. Su, J.J. Guo, H.Z. Fu. Microstructure and mechanical properties of refractory MoNbHfZrTi high-entropy alloy. *Materials & Design* 81, 87 (2015).
- [6] H. Shen, J. Zhang, J. Hu, J. Zhang, Y. Mao, H. Xiao, X. Zhou, X. Zu. A Novel TiZrHfMoNb High-Entropy Alloy for Solar Thermal Energy Storage. *Nanomaterials* 9, 248 (2019).

Prominence of Terahertz Acoustic Surface Plasmon excitation in Gas-Surface interaction with Metals

G. Bracco^{1,2#}, L. Vattuone^{1,2#}, M. Smerieri², G. Carraro^{1,2}, L. Savio², G. Paolini¹, G. Benedek^{3,4}, P. M. Echenique⁴, M. Rocca^{1,2*}

#contributed equally to the work

¹ *Dipartimento di Fisica, Università di Genova; Via Dodecaneso 33, 16146 Genova, Italy*
Corresponding author M.Rocca; Rocca@fisica.unige.it

² *IMEM-CNR Unità di Genova; Via Dodecaneso 33, 16146 Genova, Italy*

³ *Dipartimento di Scienza dei Materiali, Università di Milano Bicocca; Via R. Cozzi 55, 20125 Milano, Italy*

⁴ *DIPC, Paseo Manuel de Lardizabal 4, Donostia 20018, Spain*

Understanding the dynamics of gas-surface interaction has been at the focus of research for the last decades. One reason for this interest is the modelling of the energy transfer to solid surfaces which dictates the drag force on aerospace shuttles. For telecommunication satellites orbiting the Earth typically below 600 km, this process represents the main source of orbital perturbation [1-3]. Another main application is heterogeneous catalysis, since the rate of the processes is often limited by the energy accommodation of the gas phase reactants [4]. In both cases, the interaction of gases up to mild hyperthermal kinetic energies (0.1 to 1 eV) with metal surfaces is of pivotal importance.

The classical understanding of gas-surface dynamics based on direct collisions with the surface atoms is that the excess kinetic energy of the colliding particles is transferred to the vibrational degrees of freedom of the target [5,6]. This process was demonstrated to dominate, e.g., for H₂ dissociation on Cu(111) [7] and Ru(0001) [8], methane on Ni(100) [9], and water on Ni(111) [10]. Energy transfer to the electronic degrees of freedom (electron hole (*e-h*) pair excitations) was observed only for much higher energies: impact energies of several eV for H [11] and HCl [12] scattering off Au(111), and high vibrational excitation for NO dissociation on Au(111) [13]. In all these cases, as well as in the interpretation of friction phenomena,¹⁶ only *e-h* pair generation was considered.

Here we show that this picture does not hold for metal surfaces supporting acoustic surface plasmons [14-16]. Such loss, dressed with a vibronic structure, is shown to make up a prominent energy transfer route down to the terahertz region for Ne atoms scattering off Cu(111) and is expected to dominate for most metals [17]. This mechanism determines, e.g., the drag force acting on telecommunication satellites which are typically gold plated to reduce

overheating by sunshine. The electronic excitations can be unambiguously discerned from the vibrational ones under mild hyperthermal impact conditions.

- [1] Sundén, B.; Fu J. *Heat Transfer in Aerospace Applications*. Elsevier: **2017**.
- [2] Josyula, E.; Burt, J. Review of Rarefied Gas Effects in Hypersonic Applications. Y TIC Document RTO-EN-AVT-194, **2011**, pp. 40.
- [3] Livadiotti, S.; Crisp, N.H.; Roberts, P.C.E.; Worrall, S.D.; Oiko, V.T.A.; Edmondson, S.; Haigh, S.J.; Huyton, C.; Smith, K.L.; Sinpetru, L.A.; *et al.* A review of gas-surface interaction models for orbital aerodynamics applications. *Progress in Aerospace Sciences* **2020**, *119*, 100675.
- [4] Wodtke, A.M. Electronically non-adiabatic influences in surface chemistry and dynamics. *Chem. Soc. Rev.* **2016**, *45*, 3641-3657.
- [5] Alducin, M.; Diez Muino, R.; Inaki Juaristi, J. Nonadiabatic Effects in Gas-Surface Dynamics. In *Handbook of Surface Science*; Rocca, M.; Rahman, T.S.; Vattuone, L. Eds; Springer: **2020**; Chap. 28, pp 937- 973.
- [6] Auerbach, D.J.; Tully, J.C.; Wodtke, A.M. Chemical dynamics from the gas-phase to surfaces. *Nat. Sci.* **2021**, *1*:e10005. <https://doi.org/10.1002/ntls.10005>
- [7] Diaz, C.; Pijper, E.; Olsen, R.A.; Busnengo, H.F.; Auerbach, D.J.; Kroes, G.J. Chemically Accurate Simulation of a Prototypical Surface Reaction: H₂ Dissociation on Cu(111). *Science* **2009**, *326*, 832-834.
- [8] Nieto, P.; Pijper, E.; Barredo, D.; Laurent, G.; Olsen, R.A.; Baerends, E.J.; Kroes, G.J.; Farias, D. Reactive and Nonreactive Scattering of H₂ from a Metal Surface is Electronically Adiabatic. *Science* **2006**, *312*, 86.
- [9] Yoder, B.L.; Bisson, R.; Beck, R.D. Steric Effects in the Chemisorption of Vibrationally Excited Methane on Ni(100). *Science* **2010**, *329*, 553.
- [10] Hundt, P.M.; Jiang, B.; Van Reijzen, M.E.; Guo, H.; Beck, R.D. Vibrationally Promoted Dissociation of Water on Ni(111). *Science* **2014**, *344*, 504.
- [11] Bünermann, O. *et al.*, Electron-hole pair excitation determines the mechanism of hydrogen atom adsorption. *Science* **2015**, *350*, 1346.
- [12] Ran, Q.; Matsiev, D.; Auerbach, D.J.; Wodtke, A.M. Observation of a Change of Vibrational Excitation Mechanism with Surface Temperature: HCl Collisions with Au(111). *Phys. Rev. Lett.* **2007** *98*, 237601.
- [13] Nahler, N.H.; White, J.D.; LaRue, J.; Auerbach, D.J.; Wodtke, A.M. Inverse Velocity Dependence of Vibrationally Promoted Electron Emission from a Metal Surface. *Science* **2008**, *321*, 1191.
- [14] Diaconescu, B. *et al.*, Low-energy acoustic plasmons at metal surfaces. *Nature* **2007**, *448*, 57.
- [15] Pohl, K. *et al.*, M. Acoustic surface plasmon on Cu(111). *Europhys. Lett.* **2010**, *90*, 57006.
- [16] Pischel, J.; Welsch, E.; Skibbe, O.; Pucci, A. Acoustic Surface Plasmon on Cu(111) as an Excitation in the Mid-Infrared Range. *J. Phys. Chem. C* **2013**, *117*, 26964-26968.
- [17] G. Bracco *et al.*, Prominence of acoustic surface plasmons in hyperthermal gas energy transfer to metal surfaces, *J. Phys. Chem. Lett.* **12**, 9894-9898 (2021).

Obituary: Stefan Müller

Sadly Stefan Müller has passed away on January 10, 2022. Since 2010 he had been a professor for atomistic modeling of materials at the TU Hamburg (TUHH). Being strongly involved in surface science and as a regular participant of the Symposium on Surface Science (3S) he had many close colleagues in this scientific community. Talking to his friends, many vividly remember his enthusiasm in general and particularly for science as well as his joyful and lively character.

Stefan Müller was born on October 18, 1966 in Nürnberg. He studied physics at the University Erlangen-Nürnberg from 1987 to 1992. His diploma thesis was supervised by Prof. Klaus Heinz at the Institute of Condensed Matter Physics, who also became his PhD adviser. From 1992 to 1996 Stefan did his PhD on the structure determination of metal films using low-energy electron diffraction (LEED). During this time he spent several months in the group of Prof. Miranda (Universidad Autónoma, Madrid, Spain). After obtaining his PhD with distinction in 1996 he continued to work in Prof. Heinz's group for further two years and then joined Dr. Alex Zunger at the National Renewable Energy Laboratory in Golden, USA, as a postdoctoral fellow for 2 years. There he changed the focus of his research to the computational modeling of metal alloys using *ab initio* methods and then returned to the group of Prof. Heinz until 2007. He completed his habilitation on atomic order phenomena in metal alloys in 2002. In 2003, Stefan was a Visiting Professor at the University of Vienna, Austria. Between 2007 and 2010 he served as an Interim Professor at the Institute of Theoretical Physics at the University of Erlangen-Nürnberg. In 2010, Stefan joined the TU Hamburg (TUHH) as professor for “*Ab-initio* statistical thermodynamics and molecular dynamics” at the Institute of Advanced Ceramics. He held this position until the end of his life.



Driven by his curiosity Stefan always wanted to understand the underlying principles of interesting phenomena. In particular for material systems he aimed to predict properties of micro- and macroscopic materials on a quantum mechanical basis. To this end, he applied electronic-structure methods like density functional theory and approaches from statistical physics such as cluster expansion. This effort culminated in the development of the software package UNCLE (Universal Cluster Expansion) together with Prof. Gus Hart (Brigham Young University, USA). Applying those methods he made numerous significant contributions mainly in the fields of alloy physics and surface science including the first ever Nature paper for the TUHH. In teaching he sparked the interest for solid-state physics and atomistic modeling in many students and he supervised numerous theses. Students and colleagues remember well his lively and excellent lectures and scientific talks.

In 2015 Stefan suffered life-threatening health problems. After extended treatment and therapy he was able to return to work; however, he continued to be physically handicapped and strongly limited in his ambitions. Continuing health issues forced him to recurring extended sick leaves and made the last few years very difficult for him.

Besides science Stefan was a multi-talented person and excited about many other aspects of life. He loved music. While studying physics and being a young scientist, he obtained a opera singer training as a tenor for more than ten years. After his PhD, he was performing the male lead role (“Seymour”) in the musical “Little Shop of Horrors” in Nürnberg for about half a year. Many regulars of the 3S remember well Stefan’s mid-night “birthday song” for Edmund Taglauer. Stefan was also passionate for soccer and he strongly supported the team of the 1.FC Nürnberg (aka der Club). He always enjoyed social gatherings of all kinds and was able to entertain large groups effortlessly.

For most of his life Stefan was able to combine and enjoy his passions for science, music, sports, and many other aspects of life. He never lost his natural positive attitude. Stefan will be remembered and missed.

Gregor Vonbun-Feldbauer

Post deadline contributions

Exploring Percolation in Nanocluster Assemblies for Neuromorphic Computing

M. Baljzović, Y. Niu, J. McCormack, T. Slater¹, R. E. Palmer and R. J. Cobley

*Faculty of Science and Engineering, Swansea University, Swansea, United Kingdom
(corresponding author: M. Baljzović, e-mail: milos.baljzovic@swansea.ac.uk)*

¹ *Electron Physical Science Imaging Centre, Diamond Light Source Ltd., Oxfordshire, OX11 0DE, United Kingdom*

Scaling down the size of silicon-based devices like transistors in order to improve cost and performance has enabled some of the greatest achievements of humankind. However, in order to circumvent limits posed by reaching dimensions where quantum size effects emerge, novel materials and approaches are required.

Brain-inspired computation, named neuromorphic computing, has the potential to overcome the limitations of conventional silicon technology, offering a new generation of faster, low-power computing.^[1,2] While percolating networks of atomic clusters display fascinating physics such as complex dynamics and voltage switching behaviour like those found in a brain, understanding the origins of these effects is lacking.^[3-6] In the context of growing interest in percolating nanocluster networks, no-one yet has demonstrated both the ability to controllably fabricate nanocluster metal networks and the experimental capability to directly study the electrical behaviour of single metallic 'synapses' for unravelling how the first pathways form or change with applied stimulus.

Our first results show that Atomic Force Microscopy (AFM), Scanning Transmission Electron Microscopy (STEM) and multi-probe Scanning Tunneling Microscopy (STM) can be combined in an effort to systematically and controllably investigate electrical, structural and chemical behaviour of both single metal cluster 'synapses' and networks thereof. Planned follow up experiments are expected to provide a deeper understanding of how and why these networks form, pushing forward research in artificial intelligence, nanomaterials, electronic devices, sensing and energy conversion as well as in neuromorphic computing. The similarity of the emergent complex percolating nanocluster network behaviour to the brain suggests that these electronic systems may even allow a deeper understanding of the fundamental nature of intelligence and cognition.

Support by the Leverhulme Trust, project "Single synapse measurements in neuromorphic percolating nanoparticle networks" is gratefully acknowledged.

[1] I. Boybat, M. Le Gallo, S. R. Nandakumar, T. Moraitis, T. Parnell, T. Tuma, B. Rajendran, Y. Leblebici, A. Sebastian, E. Eleftheriou, *Nat Commun* **2018**, *9*, 2514.

- [2] Y. van de Burgt, A. Melianas, S. T. Keene, G. Malliaras, A. Salleo, *Nat Electron* **2018**, *1*, 386–397.
- [3] S. Fostner, S. A. Brown, *Phys. Rev. E* **2015**, *92*, 052134.
- [4] D. R. Chialvo, *Nature Phys* **2010**, *6*, 744–750.
- [5] M. Mirigliano, F. Borghi, A. Podestà, A. Antidormi, L. Colombo, P. Milani, *Nanoscale Advances* **2019**, *1*, 3119–3130.
- [6] H. O. Sillin, R. Aguilera, H.-H. Shieh, A. V. Avizienis, M. Aono, A. Z. Stieg, J. K. Gimzewski, *Nanotechnology* **2013**, *24*, 384004.

Author Index

Abbondanza G.	61	Carraro G.	193
Abuin M.	27	Carvajal J.M.	99
Albertin S.	53	Cebat A.	47
Amann P.	67	Čechal J.	121, 139
Ammon M.	37	Cerdá J.I.	177
Andreasson J.	71, 105, 109, 143, 165	Černá L.	121
Aprojanz J.	151	Cheng H.-W.	73
Arnau A.	177	Cheynis F.	129
Arregi J.A.	139	Cobet C.	143
Auer A.	87	Cobley R.J.	201
Aumayr F.	81, 101, 103, 145, 161	Comini N.	179
Auras S.V.	49	Coraux J.	79
Avarvari N.	47	Cortizo-Lacalle D.	41
Bábor P.	51	Cserveny B.	101
Balajka J.	97, 113, 117, 133	Cupak C.	81, 101, 103
Balasubramanian T.	151	Curiotto S.	129
Balderas Navarro R.E.	143	David P.	79
Baljozović M.	47, 201	de C. Ferreira R.C.	43
Banerjee S.	45	de la Torre B.	63
Barth J.V.	41	Delatowski F.-F.	105
Beckord J.	179	Deng X.	53
Bendounan A.	139	Devarajulu M.	37
Benedek G.	193	Diebold U.	97, 107, 113, 117, 119, 127, 133, 183, 185, 187
Bereczuk A.	29	Dil H.	75
Berger J.	99	Dimopoulos T.	147, 189
Berghaus T.	65	Diulus J.T.	179
Bertel E.	159	Dockalová L.	127
Berwanger J.	29	Doerr F.	119
Biber H.	81, 101, 103	Doležal J.	43
Bihlmayer G.	177	Dworschak D.	167
Bilotto P.-L.	73, 163, 167	Dziadkowiec J.	73
Bittrich E.	109	Echenique P.M.	193
Blanco-Rey M.	177	Eder M.	183
Bliem R.	191	Edström H.	53
Bone T.	35	Eriksson S.	67
Borodin D.	55, 111, 137	Ernst K.-H.	47
Böttcher S.	69	Espinoza S.	71, 105, 109, 143
Bracco G.	193	Feiler C.	169
Brandimarte P.	155	Fellinger M.	103
Brandstetter S.	113	Fingerhut J.	55, 111, 137
Brinker M.	135	Fleig J.	91
Brötzner J.	81, 101	Franceschi G.	97, 113, 183, 185, 187
Brune H.	153	Franzke E.	189
Burson K.M.	135	Frederiksen T.	155
Campana A.	99	Frese N.	31
Canola S.	43	Freund H.-J.	135
Cao Y.-J.	39	Friedrich N.	155
Carnis J.	27		

Gabriel V.	185	Kampen T.	69
Gallardo A.	63	Kandratsenka A.	111
Galli A.	81, 101	Karakachian H.	151
García-Lekue A.	155	Kasai J.	65
Garcia-Martinez F.	49	Keller T.F.	27, 91
Geaymond O.	79	Kern C.	35
Geile S.	53	Khakurel K.	105
Gelisio L.	27	Kim Y.Y.	27
Gericke S.	61	Kißlinger T.	77, 115, 119
Giessibl F.J.	29	Kitsopoulos T.N.	55, 111, 137
Gmitra M.	75	Knecht P.	41
Goetz S.	189	Kocán P.	185
Gözlhäuser A.	31	Kogan E.	141
Goncalves T.J.	27	Kolíbal M.	51
Gonzalez-Arrabal R.	103	Koller G.	35
Guisset V.	79	König M.	31
Gumbs G.	141	Kormoš L.	121
Gura L.	135	Koyama T.	65
Gurrath M.	37	Kramer D.	171
Gustafson J.	53	Kraushofer F.	119, 183
Gutschmidt S.	53	Krempasky J.	75
Haager L.	183	Krishna J.	157
Hagman B.	53	Kuhness D.	135
Hahn M.	125	Kunze-Liebhäuser J.	87
Hammer L.	77, 115, 119	Kurowská A.	121
Hapala P.	43	Lackner P.	117
Hegedüs Z.	53	Larsson A.	61
Hejral U.	53	Lecroart L.	111
Hengsberger M.	179	Lee J.	73
Herich O.	121	Leiva E.P.M.	171
Herrfurth O.	71	Leroy F.	129
Hertl N.	55, 137	Lezuo L.	127
Heyde M.	135	Li J.	155
Hingerl K.	143	Libuda J.	89
Hoster H.E.	171	Lieberzeit P.	163
Hrůza D.	51	Lienert U.	53
Huettig A.	41	Linke C.	189
Hütner J.	117	Liu Y.	37
Ibañez-Azpiroz J.	157	Lopez-Cazalilla A.	103
Imre A.M.	73, 119, 167	Lundgren E.	53, 61
Irziqat B.	47	Lundwall M.	67
Iwaya K.	65	Lungerich D.	37
Jacobse L.	53, 91	M. Silkin V.	141
Jäggi N.	81, 101	Madsen G.K.H.	147
Jakub Z.	121	Mähl S.	69
Janák M.	51	Maier S.	37
Jaroš A.	51	Mallada B.	63
Jelinek P.	63, 99	Mamiyev Z.	151
Jelínková A.	123	Marsh T.	135
Jux N.	37	Martin K.	47
Kalchgruber L.	125	Martinelli L.	79

Matej A.	99	Potoček M.	139
Mateo-Alonso A.	41	Power S.R.	151
Matta B.	151	Pozo I.	155
Mayr-Schmölzer W.	45	Průša S.	139
McCormack J.	201	Presel F.	35
Mears L.L.E.	167	Pressacco F.	139
Meißner R.	169	Procházka P.	121, 139
Menzel A.	159	Puschnig P.	35
Mercer M.P.	171	Raabgrund A.	77, 115
Merino P.	43	Rafsanjani-Abbasi A.	183
Merk D.	153	Ramach U.	165
Meyer B.	37, 107	Rämisch L.	61
Meyer M.	69	Ramsey M.	35
Mieres-Perez J.	39	Ran W.	41
Mildner D.	99	Rappich J.	105
Minar J.	75	Rebarz M.	71, 105, 109
Mittendorfer F.	159	Redl A.	103
Mohammadi M.	181	Redondo J.	185
Mora-Fuentes J.P.	41	Reichert J.	41
Morgenstern K.	39	Renaud G.	79
Moser T.	87	Reuter K.	85
Müller P.	129	Rheinfrank E.	185
Müller S.	45	Richter K.	29
Müller T.	53	Richter S.	71
Mundigl N.	29	Riva M.	97, 119, 183, 185, 187
Muntwiler M.	179	Rocca M.	193
Negreiros F.R.	181	Romero F.	99
Nenning A.	81, 101	Rosenzweig P.	151
Netzer F.P.	181	Rowen J.F.	39
Nguyen T.T.N.	151	Runge H.	27
Niggas A.	145, 161	Rusponi S.	153
Nitz F.	55	Ryan P.	133
Niu Y.	201	Saito S.	155
Novotny Z.	179	Sanchez A.G.	99
Olgati M.	131	Sanchez-Garcia E.	39
Ortega J.E.	49	Sánchez-Portal D.	155
Ostermann M.	163	Sander T.	37
Osterwalder J.	179	Sander W.	39
P. Solé A.	99	Savio L.	193
Palmer R.E.	201	Schaefer A.	53
Palmgren P.	67	Schaff O.	69
Paolini G.	193	Schewski A.	77, 115
Papageorgiou A.C.	41	Schiller F.	49
Parkinson G.S.	127, 183, 185	Schlichting H.	41
Parschau M.	47	Schmerer P.	31
Pascual J.I.	155	Schmid M.	67, 97, 107, 113, 117, 119, 183, 187
Pavelec J.	97, 113, 117, 125, 127, 133	Schneider M.A.	77, 115
Peña D.	155	Schneider W.-D.	135
Pfaff S.	61	Schodl J.	163
Plessow P.N.	27	Schürmann M.	31
Polley C.M.	151		

Schwarz F.	35	Vazquez-Miranda S.	143
Schwarzer M.	55, 111, 137	Volkov S.	91
Seitz C.	53	von Allmen K.	53
Sellschopp K.	45	Vonbun-Feldbauer G.B.	45
Setvín M.	113, 185	Vonk V.	27, 53, 91
Shahsavari A.	121	Wagner M.	107
Šikola T.	51, 139	Wall D.S.	135
Sirotti F.	139	Walz A.	41
Slater T.	201	Weber F.	31
Smerieri M.	193	Weichselbaum D.	161
Sokolović I.	113, 185	Weng X.	79
Soler D.	99	Werl M.	145
Springholz G.	75	Westphal M.	31
Starke U.	151	Wibowo R.A.	189
Steiner C.	37	Wiell T.	67
Steiner D.	159	Wieser V.	73
Stempel T.	69	Wilhelm R.A.	145, 161
Sterr M.	35	Winkler J.	189
Stierle A.	27, 53, 91	Wodtke A.M.	55, 111, 137
Stilp F.	29	Wolf M.	147
Stoiber K.	41	Wortmann M.	31
Sudhoff H.	31	Wrana D.	185
Surnev S.	181	Würger T.	169
Švec M.	43	Wurz P.	81, 101
Szabo P.S.	81, 101	Xu H.	41
Tegenkamp C.	151	Yakimova R.	151
Thaler M.	159	Yamaguchi S.	155
Troglia A.	191	Yang H.J.	135
Uhlíř V.	139	Yang Z.	135
Valtiner M.	73, 125, 131, 165, 167, 189	Yokota M.	65
van Vliet S.	191	Zahradnik M.	71, 105, 109
Vartanyants I.A.	27	Zakharov A.A.	151
Vattuone L.	193	Zetterberg J.	61

RoyalFlush

DO NOT GAMBLE – TAKE ADVANTAGE OF
THE WINNING ARPES SOLUTION FROM A SINGLE SOURCE



KEY FEATURES

- Unsurpassed data quality
- Small Spot μ ARPES
- Ultralow temperatures
- Highly flexible and versatile system
- Ultimate reliability and usability
- Fully integrated k-space data analysis

SPECS Surface Nano Analysis GmbH

T +49 30 46 78 24-0

E info@specs.com

H www.specs.com

SPECSTM
A member of SPECSGROUP

Advanced Ion Beam Technology for Surface Analysis

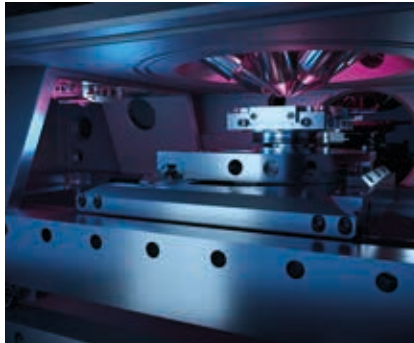
M6



Superior SIMS Performance

The M6 is the latest generation of high-end TOF-SIMS instruments developed by IONTOF. Its design guarantees superior performance in all fields of SIMS applications.

M6 Plus



TOF-SIMS and SPM in situ

The M6 Plus is the tool for nano characterisation. Combining high-end performance SIMS and SPM, true in situ 3D chemical imaging becomes possible.

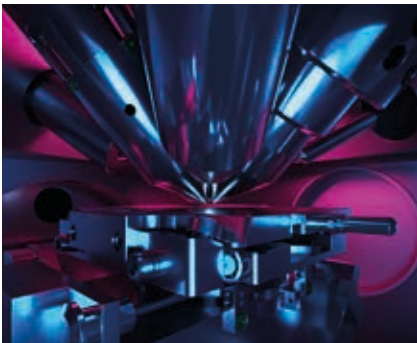
M6 Hybrid SIMS



High-end Mass Spectrometry

With the new Q Exactive™ extension, IONTOF introduces the first commercial SIMS instrument combining highest mass resolution and mass accuracy with high resolution cluster SIMS imaging.

TOF.SIMS 5



Field proven and efficient

With the TOF.SIMS 5 IONTOF offers a field proven and efficient TOF-SIMS tool which outperforms most of its competitors. Its design guarantees optimum performance in all fields of SIMS applications.

Qtac



Top Atomic Layer Analysis

The Qtac is a high sensitivity low energy ion scattering (LEIS) instrument. It is extremely surface sensitive, providing elemental characterisation of the top atomic layer.

VLS-80



Vacuum SPM Technology

The VLS-80 is a high vacuum scanning probe microscope developed by NanoScan. Its Dual-PLL MFM mode allows straight forward real-world sample magnetic domain characterisation.

IONTOF

Heisenbergstraße 15
48149 Münster
Germany

Phone +49 251 1622-100
Email sales@iontof.com
Internet www.iontof.com

3S'22

SYMPOSIUM ON SURFACE SCIENCE 2022 St. Christoph am Arlberg, Austria March 13 - 19, 2022

Friedrich Aumayr, Ulrike Diebold and Markus Valtiner, organizers
Institute of Applied Physics, TU Wien, Vienna, Austria

Sunday, 13 Mar. 2022

16:00 - 18:30	REGISTRATION
18:30 - 19:30	DINNER
20:00 - 20:20	OPENING <i>chair: AUMAVR</i>
20:25 - 20:45	STIERLE
20:45 - 21:05	GIESSIBL
21:05 - 21:25	GÖLZHAUSER

Monday, 14 Mar. 2022

07:15 - 08:00	BREAKFAST
08:00 - 08:20	STERRER <i>chair: SIKOLA</i>
08:20 - 08:40	MAIER
09:15 - 12:00	SKIING INSTRUCTIONS LUNCH
12:00 - 13:00	LUNCH
13:30 - 15:30	SKIING INSTRUCTIONS
16:40 - 17:00	MORGENSTERN <i>chair: SCHNEIDER W D</i>
17:00 - 17:20	BARTH
17:20 - 17:40	DOLEZAL
17:40 - 18:00	VONBUN-FELDBAUER
18:00 - 18:20	ERNST

Tuesday, 15 Mar. 2022

07:15 - 08:00	BREAKFAST
08:00 - 08:20	LUNDGREN <i>chair: BERGER</i>
08:20 - 08:40	JELINEK
09:15 - 12:00	SKIING INSTRUCTIONS LUNCH
12:00 - 13:00	LUNCH
13:30 - 15:30	SKIING INSTRUCTIONS
16:40 - 17:00	BERGHAUS <i>chair: DIEBOLD</i>
17:00 - 17:20	AMANN
17:20 - 17:40	STEMPEL
17:40 - 18:00	REBARZ
18:00 - 18:20	VALTNER

Wednesday, 16 Mar. 2022

07:15 - 08:00	BREAKFAST
08:00 - 08:20	REUTER <i>chair: PAVLEC</i>
08:20 - 08:40	KUNZE-LIEBHÄUSER
09:15 - 12:00	SKIING INSTRUCTIONS LUNCH
12:00 - 13:00	LUNCH
13:30 - 15:30	SKIING INSTRUCTIONS
16:40 - 17:00	LJBUDA <i>chair: BALAIKA</i>
17:00 - 17:20	VONK
<i>chair: KUNZE-LIEBHÄUSER</i>	
17:25 - 18:25	POSTER INTRODUCTION

Thursday, 17 Mar. 2022

07:15 - 08:00	BREAKFAST
08:00 - 08:20	STARKE <i>chair: MÜLLER</i>
08:20 - 08:40	BRUNE
09:15 - 12:00	SKIING INSTRUCTIONS LUNCH
12:00 - 13:00	LUNCH
13:30 - 15:30	SKIING INSTRUCTIONS
16:40 - 17:00	SANCHEZ-PORTAL <i>chair: WILHELM</i>
17:00 - 17:20	IBANEZ-AZPIROZ
17:20 - 17:40	MITTENDORFER
17:40 - 18:00	NIGGAS
18:00 - 18:20	OSTERMANN

Friday, 18 Mar. 2022

07:15 - 08:00	BREAKFAST
08:00 - 08:20	ARNAU <i>chair: JAKUB</i>
08:20 - 08:40	NOVOTNY
09:15 - 12:00	GIANT SLALOM RACE LUNCH
12:00 - 13:00	LUNCH
13:30 - 15:30	SKIING INSTRUCTIONS
16:30 - 16:50	NETZER <i>chair: HAMMER</i>
16:50 - 17:10	HAAGER
17:10 - 17:30	KOCANI
17:30 - 17:50	RIVA
17:50 - 18:10	GOETZ
18:30 - 18:50	BLIEM <i>chair: CUPAK</i>
18:50 - 19:10	FOCCA
19:10 - 19:40	GIANT SLALOM RACE AWARD CEREMONY
19:30 - 19:50	RAMMACH <i>chair: SILKIN</i>
19:50 - 20:10	BILOTTO
20:10 - 20:30	MEISSNER
20:30 - 20:50	HOSTER
20:00	CONFERENCE DINNER